Role of stromal MMP14 and MMP3 in skin homeostasis

Inaugural-Dissertation

zur

Erlangung des Doktorgrades

der Mathematisch-Naturwissenschaftlichen Fakultät

der Universität zu Köln

vorgelegt von

Maike Kümper

Aus Düsseldorf

Cologne 2022

Berichterstatter: Prof. Dr. Ulrich Baumann

                      Prof. Dr. Gerhard Sengle

Vorsitzender: Prof. Dr. Matthias Hammerschmidt

Tag der mündlichen Prüfung: 20.04.2023 ....

Table of Content

List of Tables

List of Figures

Abbreviations

4-OHT	4-hydroxy-tamoxifen
A. dest	Aqua distilled
Aa	Amino acid
Arg	Arginine
Asn	Asparagine
BSA	Bovine serum albumin
BM	Basement membrane
CCL2	Chemokine (C-C motif) ligand 2
CD31	Cluster of differentiation 31 (PECAM1)
CD45	Cluster of differentiation 45
cDNA	Complementary deoxyribonucleic acid
Cys	Cysteine
CO_2	Carbon dioxide
CXCL4	C-X-C motif chemokine 4 (Platelet factor 4)
Dll4	Delta-like ligand 4
DMEM	Dulbeccos's modified eagle medium
DNA	Deoxyribonucleic acid
dNTP	2'-Deoxynucleosine-5'-triphosphate
EC	Endothelial cell
EDTA	Ethylenediamine tetraacetic acid
EGF-R	Epidermal growth factor receptor
EndoMT	Endothelial-to mesenchymal transition
EMT	Epithelial-to mesenchymal transition
ERK	Extracellular signal-regulated kinase
EtOH	Ethanol
FACIT	Fibril-associated collagen with interrupted triple helices
FCS	Fetal calf serum
FGF2	Fibroblast growth factor 2
FITC	Fluorescein isothiocyanate
g	Gram
GFP	Green fluorescence protein
Gly	Glycine

H&E	Hematoxylin and eosin
HGF	Hepatocyte growth factor
HHL	Histidinohydroxylysinonorleucine
HPRT	Hypoxanthine-guanine phosphoribosyltransferase
HUVEC	Human umbilical vein endothelial cell
IA	Intussusceptive Angiogenesis
IF	Immunofluorescence
IFN-α	Interferon alpha
IGF-1	Insulin-like growth factor 1
IHC	Immunohistochemistry
IL	Interleukin
ITPP	Myo-inositol trispyrophosphate
kDa	kilo Dalton
KGF	Keratinocyte growth factor
l	Liter
LAP	Latency-associated peptide
LTBP1	Latent-transforming growth factor beta-binding protein 1
LysM	Lysozyme M
LYVE-1	Lymphatic vessel endothelial hyaluronan receptor 1
MACS	Magnetic-activated cell sorting
m	Meter
M	Molar
MAPK	Mitogen activated protein kinases
min	Minute(s)
mg	Milligramm
ml	Milliliter
mM	Millimolar
mm	Millimeter
MMP	Matrix metalloproteinase
NaCl	Sodium chloride
NEAA	Non-essential amino acids
NF-κB	Nuclear factor kappa B
NG2	Neuron glial 2
NGS	Normal goat serum

nm	Nanometer
Nox1	NADPH oxidase 1
o/n	Overnight
OTC	Optimal-cutting temperature
PAGE	Polyacrylamide gel electrophoresis
PAK	p21-activated kinase
PBS	Phosphate buffered saline
PCR	Polymerase chain reaction
PDGF	Platelet-derived growth factor
PDGFRβ	Platelet-derived growth factor receptor beta
PFA	Paraformaldehyde
PGK	3-phosphoglycerate kinase
PI3K	Phosphatidylinositol 3-kinase
PIP3	Phosphatidylinositol-3,4,5-trisphosphate
PM	Plasma membrane
PMA	Phorbol 12-myristate 13-acetate
PLC	Phospholipase C
PTEN	Phosphatase and tensin homolog deleted on chromosome 10
RNA	Ribonucleic acid
ROS	Reactive oxygen species
rpm	Revolutions per minute
RT	Room temperature
SB	Sample buffer
Scx	Scleraxis BHLH transcription factor
SD	Standard deviation
SDS-PAGE	Sodium dodecyl sulfate PAGE
SEM	Standard error mean
SSC	Systemic Scleroderma
TAF	Tumor angiogenesis factor
TAM	Tumor-associated macrophage
TAZ	Transcriptional co-activator with PDZ binding motif
TBS	Tris-buffered saline
TCA	Trichloroacetic acid
TIMP	Tissue inhibitor of metalloproteinase

TGFβ1	Transforming growth factor 1
TME	Tumor microenvironment
TNF-α	Tumor necrosis factor alpha
Tris	Tri (hydroxymethyl)-aminomethane
TSP1	Thrombospondin 1
U	Unit
v/v	Volume/volume
VE-cadherin	Vascular endothelial cadherin
VEGF	Vascular endothelial growth factor
VEGFR1	Vascular endothelial growth factor receptor 1
w/v	Weight/volume
WB	Western blot
WT	Wildtype
YAP	Yes-associated protein 1
μl	Microliter
μm	Micrometer
°C	Degrees Celsius

Summary

The transmembrane matrix metalloproteinase (MMP) 14 is a zinc-dependent endopeptidase with diverse functions in skin physiology and pathologies. Its pleiotropic functions were underscored in mice with global deletion which suffered from multiple defects ultimately leading to death within three weeks after birth. However, *in vivo*, the function of the protease in specific cells was only limitedly understood. Although global deletion of MMP14 displayed several defects as consequence of altered angiogenesis, whether the defects were due to altered activity of the protease in endothelial cells or in vascular associated cells remained unclear. To address the functional relevance of EC-derived MMP14 *in vivo* in development and pathology, mice with constitutive MMP14 deletion in endothelial cells (ECs) were generated (MMP14$^{EC-/-}$). These MMP14$^{EC-/-}$ mice developed and bred normal and showed no obvious phenotype, including a normal tissue vascularization. In the present work we extended these investigations and focused on the mechanisms mediated by MMP14 in endothelial cells during pathological induced angiogenesis. As model we used *in vivo* grafting of murine melanoma cells, which is widely used to study melanoma cells growth and metastasis. Analysis of B16F1 melanoma growth in MMP14$^{EC-/-}$ mice displayed reduced tumor growth and lung metastasis compared to controls. Formation and density of the vascular network was normal, but vessels were less permeable in the MMP14$^{EC-/-}$ tumors. Among the vessel stabilizing factors, pericytes covering tumor vessels were increased MMP14$^{EC-/-}$ melanoma, but vascular basement membranes densities and homogeneity appeared comparable to controls. In addition, the EC-specific junction protein VE-cadherin was upregulated in MMP14-deficient tumor vessels as result of enhanced transcription. To further contribute to vessel stabilization, we found reduced eNOS transcription, and as consequence, decreased nitric oxide (NO) production in EC-MMP14-deficient cells. *In vitro* siRNA-mediated knockout of MMP14 in HUVECs also decreased eNOS mRNA expression and in human melanoma specimens, expression of eNOS correlated with MMP14 intensities. The importance of this study lies in the demonstration that targeting of MMP14 activity specifically in endothelial cells may be effective in reducing melanoma metastasis and enhance vessel stabilization. This latter could, as suggested by the literature, potentially be exploited to improve drug delivery to tumors.

In further investigations we set to understand the functional role of the regulation of MMP3 in fibroblasts carrying the MMP14 deletion (MMP14$^{Sf-/-}$). MMP14$^{Sf-/-}$ mice were shown to develop a fibrosis-like phenotype due to impaired collagen type I degradation, however cutaneous repair was normal in these mice. Protein and RNA analysis of the skin and isolated fibroblasts

identified upregulated MMP3 expression in MMP14$^{Sf-/-}$ mice. To address *in vivo* the functional significance for MMP3 in that context, we generated by crossings, mice with the MMP3 deletion in addition to fibroblast-specific loss of MMP14 (MMP3$^{-/-}$/MMP14$^{Sf-/-}$ mice). These mice displayed a phenotype resembling mice with the single MMP14 deletion in fibroblasts, with fibrosis of skin and tendons.

In contrast, skin repair, investigated with a model of excisional wounding, displayed a delayed wound closure and enhanced granulation tissue formation in double deficient mice. Single and double MMP3$^{-/-}$/MMP14$^{Sf-/-}$ knockout mice developed a myofibroblast phenotype. In single and double knockout mice, early wound myofibroblast population of the wound tissue was reduced. But in later wounds, myofibroblasts persisted longer in all knockouts compared to wild type mice. However, myofibroblasts in scars were most significantly higher in wounds from double MMP3$^{-/-}$/MMP14$^{Sf-/-}$ knockouts compared to all other mice genotypes. Although we did not find altered TGFβ1 in wound tissue, and isolated skin fibroblasts from all mice genotypes were functionally able to respond to TGFβ1 and to mechanical stimuli, we cannot exclude that *in vivo* release of ECM-bound TGFβ1 in single and double MMP3$^{-/-}$/MMP14$^{Sf-/-}$ knockout mice is altered, this needs further investigations. Reduced myofibroblast clearance from later wounds was accompanied by reduced apoptosis in all knockouts, while in MMP3$^{-/-}$/MMP14$^{Sf-/-}$ mice wounds we additionally detected enhanced myofibroblast proliferation possibly contributing to the higher numbers of myofibroblasts detected later on in scar tissue. These studies provide new cell type-specific regulatory functions of MMP14 and MMP3 in mediating skin repair through the regulation of myofibroblasts homeostasis in wounds.

Zusammenfassung

Die transmembrane Matrix Metalloproteinase (MMP) 14 ist eine Zink-abhängige Endopeptidase mit diversen Funktionen in Physiologie und Pathologien der Haut. Die pleiotropischen Aufgaben der Protease wurden besonders in Mäusen mit globaler Deletion deutlich, die aufgrund verschiedener Defekte innerhalb von drei Wochen nach der Geburt starben. Dennoch war das Wissen über die zellspezifischen MMP14 Funktionen weiterhin limitiert. Zwar wurden in den Mäusen mit globaler MMP14 Deletion Defekte bezügliche angiogener Prozesse deutlich, doch blieb offen, ob dies auf das Fehlen in Endothelzellen (EC) oder Blutgefäß-assoziierter Zellen zurück zu führen ist. Um die funktionale Relevanz von EC-spezifischem MMP14 *in vivo* in Entwicklung und Pathologien zu untersuchen, wurden Mäuse mit konditioneller Deletion von MMP14 in Endothelzellen generiert (MMP14$^{EC-/-}$). Die Tiere entwickeln sich normal, haben eine normale Lebensdauer und Zuchtverhalten. Darüber hinaus wurde kein deutlicher Phänotyp beobachtet, auch Vaskularisierung der Haut war vergleichbar. In der vorliegenden Arbeit wurden diese Untersuchen erweitert, wobei der Fokus auf der Identifikation von Mechanismen in pathologisch-induzierter Angiogenese unter der Kontrolle von MMP14 in Endothelzellen lag. Dafür wurde ein *in vivo* Melanom-Modell genutzt, bei dem B16F1 Melanom-Zellen in Mäuse injiziert wurde, um Melanomwachstum und Metastasierung zu untersuchen. Dabei wurde im Vergleich zu Kontrolltieren ein reduziertes Melanomwachstum in MMP14$^{EC-/-}$ Mäusen beobachtet. Auch Metastasierung zur Lunge war reduziert, während die Lymphknoten-Metastasierung unverändert blieb. Trotz MMP14-Deletion in Endothelzellen waren auch Formation und Dichte des Blutnetzwerkes in den Tumoren normal, doch diese zeigten eine reduzierte Permeabilität in MMP14$^{EC-/-}$ Mäusen. Verschiedene Faktoren regulieren Gefäß-Permeabilität, darunter auch Ummantelung mit Pericyten, die in Tumoren aus MMP14$^{EC-/-}$ Mäusen erhöht war, während die Gefäß-umfassende Basalmembran unverändert blieb. Darüber hinaus wurde auch eine erhöhte Expression des Endothelzell-spezifischen Junction Proteins VE-cadherin detektiert. Dies war eine Konsequenz hochregulierter Expression. Stabilisierung der Tumor Blutgefäße wurde zusätzlich durch eine verringerte Expression von eNOS erreicht, was zu einer reduzierten Produktion von Stickoxid führte, die ebenfalls in Endothelzellen aus MMP14$^{EC-/-}$ beobachtet wurde. Knockout von MMP14 durch siRNA *in vitro* in HUVECs führte zu einer reduzierten mRNA Expression von eNOS. Darüber hinaus wurde in humanen Melanomen eine Korrelation von eNOS und MMP14 in Blutgefäßen observiert. Daher liefert diese Studie wichtige Information über die Rolle von Endothelzell-spezifischem MMP14 und dem Potential, dieses als Target in Krebstherapien zu

nutzen, um möglicherweise Metastasierung von Melanomen zu reduzieren, resultierend aus einer erhöhten Stabilisierung der Tumor Blutgefäße. Basierend auf den Ergebnissen vorangegangener Studien könnte dies zudem einen positiven Effekt auf den Transport von Medikamenten zu den Tumorzellen haben.

Weitere Untersuchungen wurden durchgeführt, um ein besseres Verständnis der Funktion des hochregulierten MMP3 in MMP14-defizienten Fibroblasten zu erhalten. Mäuse mit Fibroblasten-spezifischer Deletion (MMP14$^{Sf-/-}$) entwickelten einen Fibrose-ähnlichen Phänotyp, der aus einer gestörten Degradierung von Kollagen Typ I resultierte. Allerdings zeigten diese Tiere eine normale Wundheilung. Protein und RNA Analyse der Haut und isolierter Fibroblasten zeigten eine erhöhte MMP3 Expression in MMP14$^{Sf-/-}$ Mäusen. Um die *in vivo* Bedeutung von MMP3 in diesem Zusammenhang zu ergründen, wurden Tiere mit Deletion von MMP3 zusätzlich zum Fibroblasten-spezifischen MMP14 Knockout generiert (MMP3$^{-/-}$/MMP14$^{Sf-/-}$). Diese spiegelten den zuvor in MMP14$^{Sf-/-}$ Mäusen observierten Phänotyp wieder und entwickelten Fibrose in Haut und Sehnen.

Allerdings wurde in doppelt defizienten Mäusen eine verzögerte Wundheilung von Exzisionsbiopsien beobachtet, was von einem vergrößerten Granulationsgewebe begleitet wurde. Mäuse mit Einzel- und Doppelknockout von MMP3 und MMP14 zeigten zudem einen Myofibroblasten-bezogenen Phänotyp. Dabei wurde, im Vergleich zu gefloxten Kontrollen, in frühen Wunden dieser Tiere eine geringere Myofibroblasten Population identifiziert, während diese Zellen in späteren Wunden bestehen blieben. Dieser Unterschied war dabei im Narbengewebe in doppelt-defizienten Tieren am signifikantesten. Zwar wurde in Wundgewebe kein Unterschied für TGFβ1 Mengen gefunden und die Zellen behielten ihre Fähigkeit auf TGFβ1 und mechanische Reize zu reagieren, dennoch kann nicht ausgeschlossen werden, dass die Freisetzung von Matrix-gebundenem TGFβ1 durch den Verlust von MMP3 und/oder Fibroblasten-spezifischem MMP14 beeinflusst wird. Dies benötigt weitere Untersuchungen in der Zukunft. Erhöhte Präsenz von Myofibroblasten in späten MMP3$^{-/-}$/MMP14$^{Sf-/-}$ und Einzel-Knockout Wunden resultiert vermutlich aus reduziertem Zelltod durch Apoptose. Darüber hinaus wurde in MMP3$^{-/-}$/MMP14$^{Sf-/-}$ Wunden eine höhere Proliferation von Myofibroblasten beobachtet, was zu der erhöhten Präsenz in Narben beitragen könnte. Somit demonstrieren die präsentierte Studie neue Zelltyp-spezifischen Funktionen von MMP3 und MMP14 in der Regulation von Wundheilung durch die Kontrolle von Myofibroblasten in Wunden.

1. Introduction

1.1. Skin

The skin is the largest organ of our body with multiple roles. Primarily functioning as a protective barrier, it is divided into three main layers: epidermis, dermis, and hypodermis. The epidermis is mainly formed by layers of differentiated keratinocytes, becoming at last corneocytes in the outmost layer. In addition, melanocytes and Merkel cells reside in the epidermal layer, whose composition is finalized by Langerhans cells [1-3], γδ T cells [4] and resident macrophages [5]. Hemidesmosomes connect the epidermal keratinocytes to the underlying basement membrane (BM), a 50-100 nm thick layer of extracellular matrix (ECM) containing laminins, nidogens, collagen type IV and heparin sulfates, among other proteins, and separates epidermis from dermis [6-14]. The BM functions as barrier between the epidermis and dermis while simultaneously connecting these two layers. Underneath the BM lies the dermis composed of a loose network of ECM in the papillary layer right below the BM and a denser structure in the deeper reticular layer. The ECM mediates mechanical strength and flexibility aside from providing structure and stability [15] while it undergoes constant remodeling [16]. Fibroblasts deriving from fibroblast progenitors reside in the upper papillary and the bottom reticular dermal layer and are the primary producer of dermal ECM proteins [15]. In the dermis a variety of specialized structures are embedded including sebaceous and sweat glands, hair follicles, muscles, sensory neurons, macrophages, adipocytes, stem cells, mast cells, blood and lymphatic vessels [17].

The main component of the dermal ECM are collagens. This family of matrix proteins contains 29 members, divided into five subfamilies [18]: fibrillar collagens (e.g. types I and III), fibril-associated collagens with interrupted triple helices, short FACITs (e.g. types XII and XIV), network forming collagens (types IV, VIII, X), anchoring fibrils (type VII) and transmembrane collagens (types XVII, XXV) [19]. Generally, collagens have a characteristic triple-helical organization that defines their physical and mechanical properties. They build α-chains of repeating Gly-X-Y sequences with X and Y representing proline and hydroxyproline [20, 21]. In addition, two non-helical structures form the end of a collagen protein [18]. If three α-chains of the same type form a collagen bundle the homotrimer is left-handed, which is the case for collagens type II and III. Heterotrimers like collagen type I, V, IX on the other hand are right-handed [22]. All collagen bundles are kept together by hydrogen bonds that form between the single chains and cross-links [23-25] like histidinohydroxylysinonorleucine (HHL) which is suggested to be the main form of skin cross-link between collagens [26]. These different

collagen structures also enable regulation of multiple cellular processes, including proliferation, apoptosis, differentiation, adhesion, migration and invasion [27, 28].

The predominant collagen in adult skin is collagen type I, making up to 80% [29]. However, collagen type I only makes up about 20% in the skin during embryonic development, while collagen type III is the main collagen in embryos with 70%. Latter is then drastically reduced to 10-15% in adulthood [29, 30]. This inversion of collagen type I/type III amount from development to adulthood is a perfect example for the dynamic remodeling of dermal ECM that can occur to meet new requirements like during repair of injuries or to form the tumor microenvironment (TME). Skin collagens have a long half-life with that of collagen type I in human skin being estimated to 15 years [31]. In mice and rat collagen type I has a 74-80 day half-life [32, 33].

These ECM proteins build the core matrisome, which incorporates multiple cytokines and growth factors bound to the ECM [30, 34]. This storage enables proteins like FGF2, HGF or TGFβ1 [35] to be readily available when needed [36].

1.2. Cutaneous wound healing

Wound healing is a multi-phased process necessary to restore tissue homeostasis after injury, consisting of 4 main stages: hemostasis, inflammation, proliferation and remodeling [37, 38]. In the first stage, platelets enter the damaged site from the injured vessels [39], and release fibrin, fibronectin, collagen, and thrombin to form the fibrin clot to close the open wound [39, 40]. Besides, the clot also serves as a source for cytokines and growth factors [39, 41] and a scaffold for invading cells [42]. The released cytokines including TGFβ and PDGF induce neutrophil and macrophage infiltration [43], whose first task is the removal of pathogens and debris [41, 44] apart from further releasing additional cytokines and growth factors [45]. MMPs expressed by neutrophils and macrophages support clearance of the wound site by degrading damaged ECM [46]. Cytokine secretion leads to the attraction of ECs, keratinocytes and fibroblasts in order to initiate the second phase, formation of the granulation tissue [41].

Keratinocytes from the epithelial borders migrate across the wound bed. They use the underlying fibrin network as scaffold in a mechanism involving multiple proteases [43]. Cleavage of collagen type I by MMP1 or syndecan-1 by MMP7 break the migration restraining activity of $\alpha_2\beta_1$ integrin in keratinocytes [40, 47-49], which accumulates at the wound edges, bound to collagen type I [48, 50]. Both proteases were described as essential for keratinocyte migration in restoration of the epithelial integrity [40]. Moreover, BM proteins are processed

during re-epithelialization, by the activity of MMP2, MMP9, and MMP14 from keratinocytes [40]. Growth factors secreted by neighboring fibroblasts like KGF and IL-6 support keratinocyte migration and proliferation [51]. VEGF secreted by keratinocytes at the wound edge promotes EC proliferation and angiogenesis. This is further boosted by the macrophage-mediated release of VEGF, FGF, and TNFα to attract ECs [41].
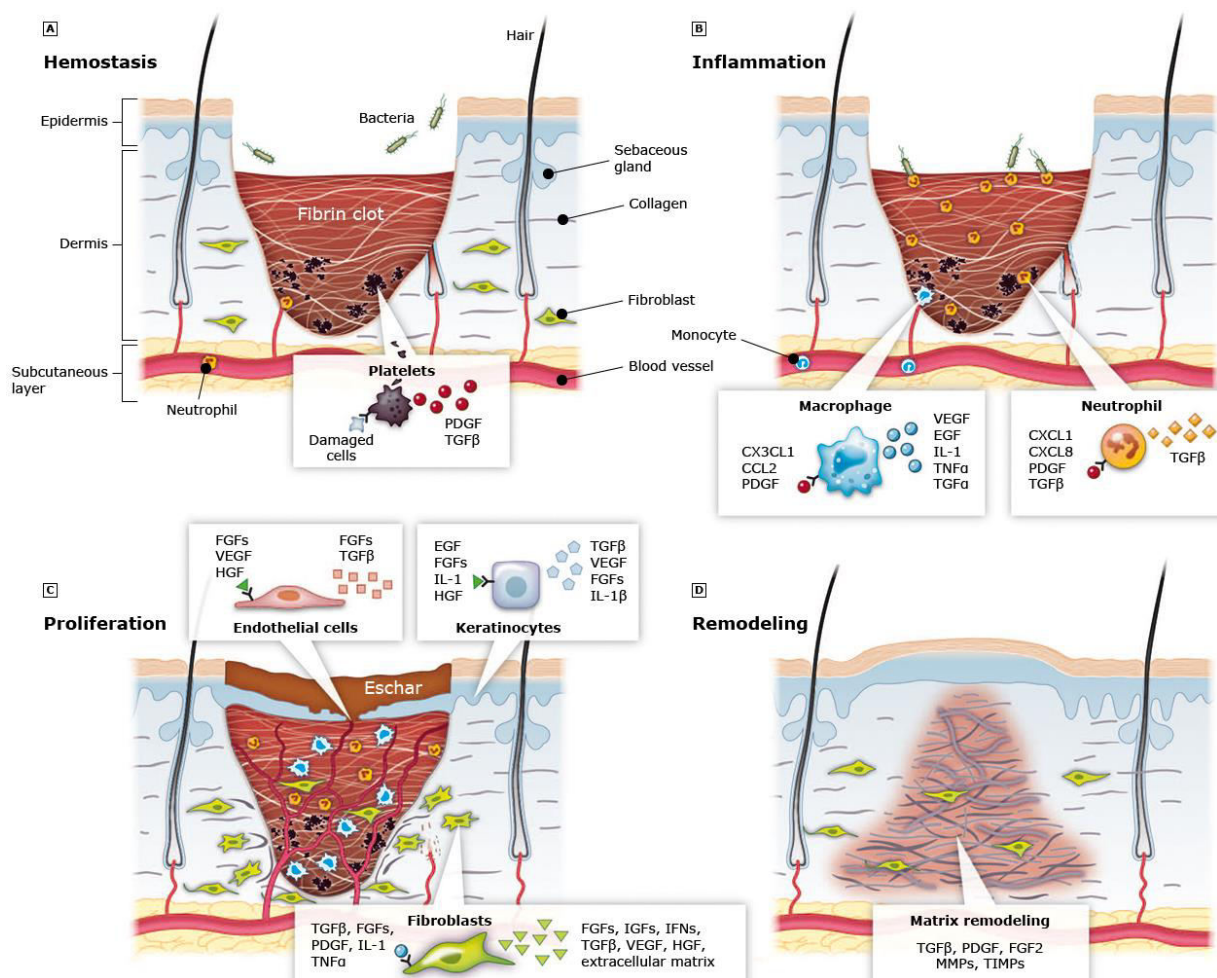
Figure 1: The 4 phases of wound healing: a) Hemostasis, **b)** Inflammation, **c)** Proliferation and **d)** Remodeling. For each phase key regulatory cells and factors involved are displayed. From [37]

The last cell type of the granulation tissue is fibroblasts that mainly enter from the surrounding tissue [52, 53]. In the second stage of tissue repair, the proliferation phase, fibroblasts are activated and transform into myofibroblasts, the major cellular component of the granulation tissue [54, 55]. This conversion is characterized by the formation of stress fiber actin filaments [56] and expression of αSMA [57, 58] that is incorporated into the actin cytoskeleton [59]. It enhances fibronexus or 'super mature' adhesion of the filaments to the ECM [52, 60, 61]. These specialized structures then orchestrate contractile activities leading to wound closure and ECM secretion [41, 62]. The primary inducer of fibroblast differentiation is TGFβ1 [63]. This growth

18

factor is secreted as inactive protein in complex with the latency-associated peptide (LAP) [64, 65]. LAP binding to the latent TGFβ binding protein 1 (LTBP1) [66] enhances secretion of the growth factor [67] and enables its binding to the ECM [68-70]. In the ECM TGFβ1 remains in this latent complex, ready to be released when necessary. In wound myofibroblasts, signaling of activated TGFβ1 is associated with two main functions: mediation of wound contraction [71] and induction of enhanced ECM protein synthesis, especially collagen type I [71, 72].

In the last stage, the remodeling phase, the ECM is degraded by matrix metalloproteinases (MMPs) and the previously cell-dense granulation tissue is cleared [55]. During earlier stages of tissue repair cells mainly secrete ECM molecules typically found during development, like EDA fibronectin and collagen type III [43]. Degradation of these and secretion of collagen type I leads to a more homeostatic ECM consisting of mainly collagen type I and 10-20% collagen type III [41]. At the end of repair, myofibroblasts and ECs are mainly cleared via apoptosis [73], but can also become senescent or function as scar-resolving fibroblasts upon deactivation [55]. However, hair follicles are usually not restored [43], and the dermis often contains a richer ECM than its uninjured counterparts, the scar tissue. This likely results from fibrosis and scar formation caused by the cytokines and growth factors active during tissue repair [74, 75].

1.3. Melanoma

1.3.1. Melanoma origin, development and metastasis

Melanoma is the deadliest type of skin cancer, and in 2021 5.6% of new US cancer cases and 1.2% of cancer death were accounted to melanoma (NIH Site Search 2021: https://seer.cancer.gov/statfacts/html/melan.html.) [76, 77]. Melanoma rise primarily from the transformation of melanocytes [78, 79]. Melanocytes, the melanin-producing cells, originate embryonal from neural crest cells [79] that migrate into the skin. These express specific adherence proteins, namely E-cadherin, P-cadherin and desmoglein, which mediate cell-cell communication with keratinocytes [78, 80]. This communication enables keratinocytes to control division, migration and BM-reattachment of melanocytes. In human skin melanocytes distribute in a ration 1:10 to keratinocytes [80, 81] and maintain skin pigmentation as a protection against ultraviolet radiation [82]. For this, melanin expressed by melanocytes is translocated to keratinocytes, which internalize the protein [81]. One melanocyte delivers melanin to 36 to 40 keratinocytes, an entity known as epidermal melanin unit [83, 84]. However, enhanced melanocyte proliferation leads to increased melanin production and to the formation of naevi [80].
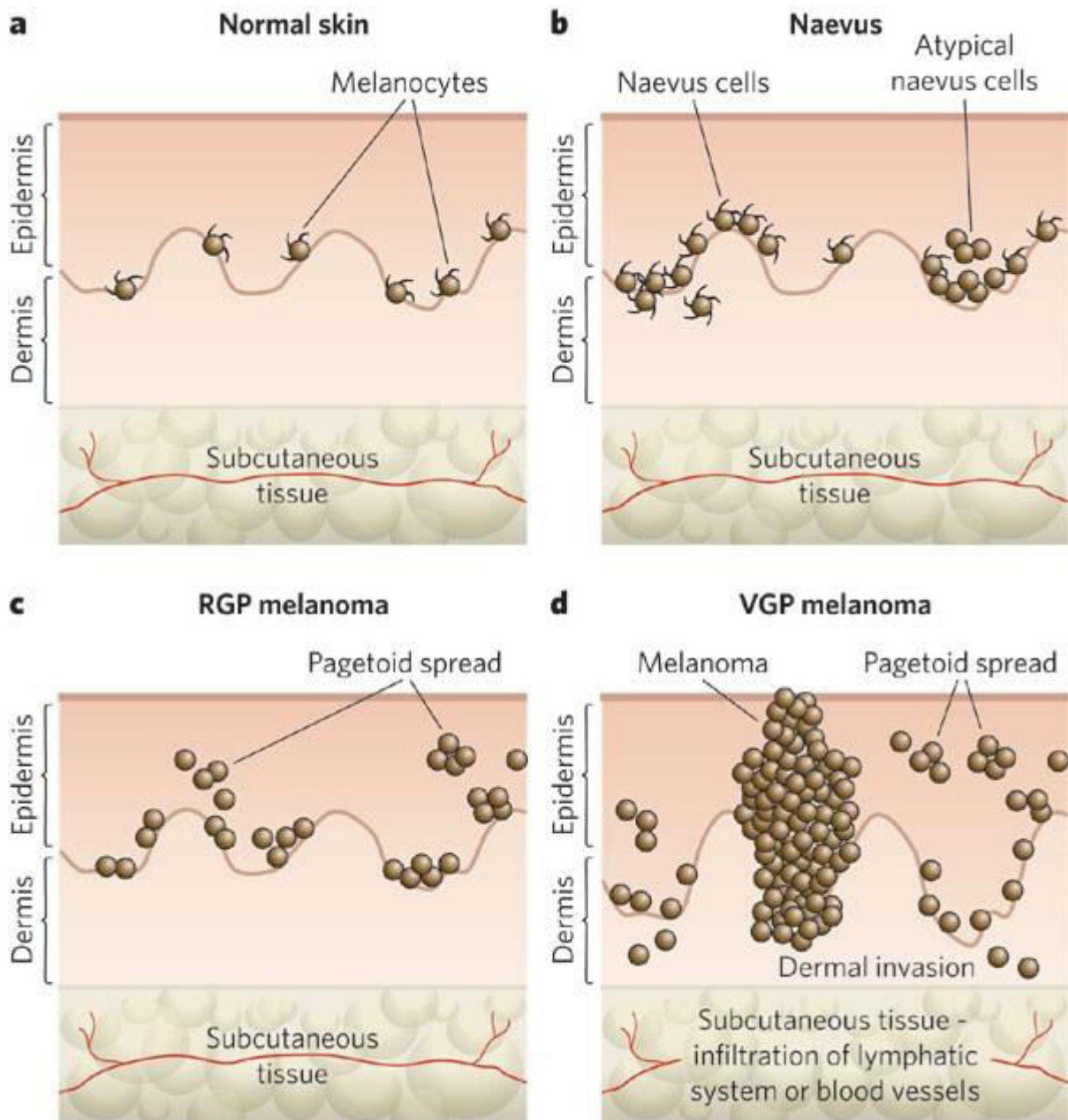
Figure 2: Formation of melanoma from melanocytes. a) Normal skin epidermis contains keratinocytes and melanocytes. **b)** Melanocyte number increases and (benign) naevi are formed. **c)** Radial-growth-phase (RGP) of melanoma from benign naevi as first malignant stage. **d)** Acquiring malignant potential melanoma enter the vertical-growth-phase (VGP). Tumors become metastatic and gain high invasive potential. [85]

Multiple mechanisms can drive the development of melanoma either from nevi or also from a single melanocyte. Genetic predisposition and phenotypical features like light skin, hair and blue eyes can increase the risk of developing melanoma [86]. Mechanistically, genetic mutation accumulation is the leading cause of irregular melanocyte proliferation and transformation [87]. Some of the best known mutations are in the BRAF gene, e.g. BRAF^{V600E}, where glutamic acid is substituted by valine [88] leading to constitutive ERK phosphorylation, thus enhanced cell

proliferation among others [89]. Another affected gene, especially in older people, is NRAS [90] impairing GTPase activity [91], hence continuous NRAS activity. Common mutations include NRAS^{Q61R}, NRAS^{Q61L}, NRAS^{Q61K} or NRAS^{G12D} [92]. In addition to these changes, tumor suppressor genes p16INK4 and p14ARF are often altered, mediated by mutations in the CDKN2a gene [93]. Examples of the multiple CDKN2a mutations found in melanoma patients are insertions into the 5' end coding sequence of 24 bp, missense mutations (CDKN2a^{R24P}, CDKN2a^{M53I} and CDKN2a^{S56I}) and a deletion of a 2-bp fragment causing a protein truncation [94]. However, it is noteworthy that both NRAS and BRAF are MAPKs, and mutations occur in an exclusive manner, thus never in both at the same time [95-97]. Besides MAPK-related mutations, cell cycle-related abnormalities make up to 13% of melanoma mutations [98]. Also, the PI3K pathway is commonly altered [97]. For example PIP3-mdiated AKT inhibition occurs in 50% of melanoma cells through downregulation of the tumor suppressor PTEN, which is completely abolished in about 5-15% of melanoma [99, 100]. Altogether, genetic alterations, altered growth factors and loss of microenvironmental control lead to melanoma development. For instance, melanocytes expressing E-cadherin are still in contact and under control from adjacent keratinocytes. Transformation of melanocytes into melanoma cells leads to loss of E-cadherin expression, thus of keratinocytes control, and to exponential growth within the epidermis, a process known as radial growth phase [80, 85]. In the following phase, the vertical growth phase, melanoma cells start expressing proteolytic enzymes, including metalloproteinases, which degrade the BM and allow their invasion into the dermis [80, 85]. While the E-cadherin expression is lost in melanoma cells, movinh into the dermis, these cells start to express N-cadherin, which enables melanoma cells to communicate to ECs and dermal fibroblasts [101]. This mechanism is known as 'cadherin switch'.

Further, melanoma invasion in the dermis, and beyond is enhanced by the expression of ECM degrading proteases like MMPs [102, 103]. These increase melanoma cell migration, and generate the paths leading to metastasis by single cells entering the blood vascular network [104].

1.3.2. Tumor angiogenesis

The formation of an intratumoral vascular network is a crucial element of tumor progression, as the lack of such restricts tumor growth [105, 106]. This blood system ensures the survival of the tumor cells as it delivers nutrients and oxygen [107, 108]. Indeed, it was shown that tumor cells distant to blood vessels proliferate less and are prone to cell death through apoptosis or

necrosis [109-111]. The first indicator that tumors can induce angiogenic processes to gain access to the blood vasculature came from studies in corneas. Tumors implanted in corneas in proximity to vessels could grow, while the ones that were not connected to the vasculature did not [112]. When close to the vasculature, tumors attracted capillaries, thus entering a growth state once they had access to the blood system [112]. Analysis in multiple mouse models cemented the correlation of the formation of a vascular network and its influence on the progression of tumor growth. For example, transgenic mice expressing the oncogene SV40 T antigen under the control of the insulin promotor in β-cells developed tumors scattered in nodules across the pancreas [113]. These started as dysplastic cell clusters that partly became hyperproliferative [114], and those forming a vascular network (1-2 %) developed into solid tumors, demonstrating the importance of tumor angiogenesis for cancer progression [115].

Comparable to development, tumor-induced angiogenesis is the formation of new vessels from existing ones initiated by the secretion of pro-angiogenic factors by tumor cells [108]. The first factor identified was VEGF-A, initially described as tumor angiogenesis factor (TAF) [116-118]. VEGF-A is expressed in multiple tumor types including adenocarcinoma [119], bile duct carcinomas [120] and melanoma [121]. Other pro-angiogenic factors that can initiate tumor angiogenesis are VEGF-B [122] or VEGF-C, although this is more involved in lymph angiogenesis [123-125], aFGF and bFGF [126, 127]. VEGF-A and bFGF are considered the most potent inducers, demonstrated by lethality of VEGF-A knockout mice due to impaired angiogenesis [128, 129]. Moreover, *in vitro* studies showed that combined treatment with VEGF-A and bFGF lead to EC invasion of three-dimensional collagen gels and tube formation, but also stimulation with only one of these was sufficient in bovine-derived cells [130, 131]. Important to note is that VEGF-A is specifically acting towards ECs [132].

Upregulated secretion of these pro-angiogenic factors leads to an increased ratio over anti-angiogenic signals coming from factors like IFN-α [133, 134], CXCL4 [135] and angiostatin [136]. This excess of pro-angiogenic factors is commonly known as angiogenic switch. This switch then initiates vessel formation in a 3 step process. First, tip cell selection occurs, which is determined by relative VEGFR1 and VEGFR2 levels, with higher VEGFR2 levels being favored for selection as tip cells [137]. These receptors mediate VEGF-A signaling and deletion caused vascular overgrowth and prenatal death in mice [138, 139]. Although VEGF-A binds to VEGFR1 with higher affinity than to VEGFR2 [140], the latter plays a crucial role in tip cell selection [137] and hypoxia-induced angiogenesis via dimeric VEGF-A [141]. Hypoxia is recognized by tumor-associated macrophages (TAMs), which possibly induce the angiogenic

switch through VEGF-A release from the matrix via MMP9-mediated ECM degradation [142, 143].

After selection of the migratory leading cell surrounding cells are blocked from taking this role by lateral inhibition mediated by a downstream actor of VEGF signaling: Dll4 (Delta-like ligand 4)/Notch signaling [144-147]. Among the regulators of this signaling pathway is MMP14 (more in section 1.5.1) [148]. This negative regulation mechanism ensures a balanced distribution of tip and stack cells and restricts the number of newly formed sprouts [147]. During sprout extension the tip cell develops multiple filopodia to support cell motility and invasion [137], and follows a chemotactic path, dependent on a VEGF-A gradient, trailed by the stalk cells whose proliferation is regulated by VEGF-A concentration [149, 150]. The highly proliferative stalk cells extend less filopodia, regulated by the ankyrin repeat protein that is controlled by Notch signaling [151]. In the last step formation of a new vessel is completed by connecting the luminal space of parent and sprouting vessel [108, 152]. However, multiple mechanisms are proposed and there is still an ongoing discussion [152].

1.3.1.1. Vessel structure in physiology and tumors

Blood vessels are a multi-level structure, that in healthy tissues is "tight and only very little permeable [153], conversely in tumors they are highly permeable to provide tumor access to nutrients and oxygen [107].

The core structure of a vessel is built by ECs that form the vascular tube/capillary wall sitting on a basement membrane covered by a sheet of pericytes and smooth vascular cells [108, 154, 155]. Pericytes are recruited by multiple mechanisms. For example, pericyte-expressed angiopoietin [156] signals through the receptor-like tyrosine kinase Tie2 [157] expressed on ECs [158-160]. Deletion or mutation of Tie2 [161, 162] or angiopoietin-1 (Ang-1) [158, 163] caused impaired pericyte recruitment to the vascular wall demonstrated through impaired vascular integrity which lead to oedema, hemorrhage or even embryonal lethality. On the other hand, Ang-1 overexpression enhanced vascularization in mice [164], paralleled by increased vessel stability and reduced permeability [165, 166]. Mechanistically, interaction of Ang-1 with Tie2 leads to the kinase's phosphorylation [157], downstream activation of PI3-kinase [167] [168], and Akt and Survivin signaling [169, 170]. Akt phosphorylates the transcription factor FOXO1 [171] driving expression of vessel destabilizing genes [172]. These functions identified Ang-1 as Tie2 agonistic ligand, while Ang-2 functions as antagonist [173]. In addition, PDGF-B/PDGFRβ signaling also mediates pericytes coverage of blood vessels [174-176] which was

impaired in PDGF-B or PGDFRβ knockout mice [177, 178]. EC-expressed PDGF-B [179] binds to PDGFRβ localized in the pericyte membrane [180], which activates multiple signaling pathways whose additive effect is the deciding factor on the power of the response, thus pericyte recruitment [181, 182]. Once recruited, pericytes support production and assembly of the BM surrounding vessels [183]. *In vitro* experiments showed that only in pericyte-EC co-cultures but not mono-cultures secreted and assembled fibronectin, nidogen-1, perlecan and laminin isoforms together with collagen type IV to a matrix structure [183].
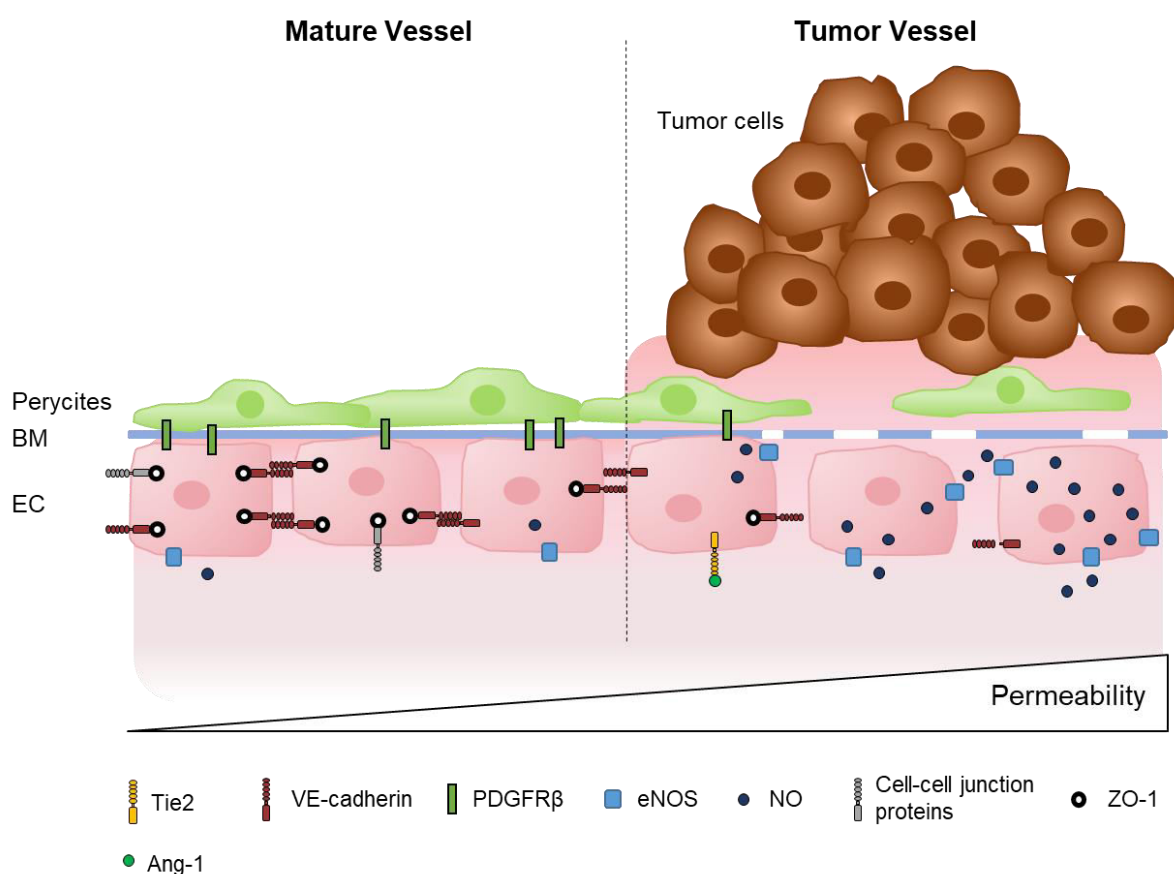
Figure 3: Blood vessels in physiology and tumors consisting of endothelial cells (EC), basement membrane (BM), pericytes and regulatory proteins.

Conversely, tumor vessels are torturous, irregularly shaped and leaky displaying poor pericyte coverage and abnormal basement membrane [184, 185]. Among the factors responsible for such abnormal structure is the excessive signaling of pro-angiogenic factors [186, 187]. Studies showed that extended VEGF signaling correlates with enhanced vessel permeability [166]. Altered pericyte coverage, reduced numbers and loose attachment to the vascular wall [188, 189] promotes leakiness [188, 190] and EC proliferation during angiogenesis [191]. For example, VEGF signaling in tumors mediates reduction of pericyte recruitment by enhancing

Ang-2 expression in ECs, which then inhibits Tie2 phosphorylation, thus interfering with the recruitment signaling [192-194]. Analysis of pericytes relies on the use of multiple markers as some are either not exclusively expressed by pericytes, e.g. PDGFRβ also identifies smooth muscle cells [174] or only expressed in specific organs, like desmin which is not expressed in heart [195, 196]. Suitable for tumor-associated pericytes are NG2 and PDGFRβ, which are known to be expressed in multiple cancer types including melanoma [197-200]. Between pericytes and endothelial cells is a basement membrane layer which in tumor vessels may be irregular with heterogeneous distribution, multiple holes of under 2.5 μm diameter and varieties in thickness [186]. This is primarily consisting of collagen type IV as observed in RIP-Tag2 pancreatic islet tumors, MCa-IC mammary carcinomas and Lewis lung carcinomas [186]. In addition, also laminin, nidogen and fibronectin were identified in this layer [201]. The attachment of ECs or pericytes to the BM was described as rather loose [186].

Early studies showed that density of intercellular junctions influence vessel permeability [202]. Those junctions are formed in ECs [203-205] by VE-cadherins (vascular endothelial cadherin) that was shown to be essential for vessel assembly and angiogenesis [206-208]. VE-cadherin is a transmembrane glycoprotein that is Ca^{2+}-dependent [209, 210], consisting of a cytoplasmic tail, a transmembrane domain and five extracellular domains [211, 212]. Binding of the extracellular domains of two VE-cadherin proteins connects two adjacent cells [211]. The intracellular domain is linked to α- and β-catenins [213-215] which form the connection to the actin cytoskeleton [216, 217]. In the case of β-catenin, the connection to the cytoskeleton is provided by ZO-1 [218-220]. Cleavage of this cytoplasmic tail leads to dissociation of the VE-cadherin/catenin complex [221], which in turn destabilizes the cell-cell junction, eventually leading to increased permeability of the vascular tube [222]. Further, VE-cadherin deletion in embryonic stem cells leads to inhibition of vascular structures formation in embryoid bodies [206]. Moreover, VE-cadherin knockout in mice impaired vessel maturation during embryonic development, leading to lethality around E9.5 [207]. This process was accompanied by EC apoptosis, suggested to be due to the lack of VEGF-A mediated survival signaling via Akt and Bcl2 [207].

In tumor vessels, formation of the EC-EC junctions is impaired and characterized by poor connectivity between ECs with average gaps between single cells of 1.7 μm and transcellular holes of 0.6 μm in average [223]. This reduces the 'gatekeeper' function of ECs and enhances plasma, leukocyte, erythrocyte and tumor cell passaging across the vessel wall [186, 224]. One mechanism leading to reduction of VE-cadherin junctions in vessels is mediated by VEGF [225]. In melanoma, binding to VEGFR-2 activates the Scr-kinase activity that phosphorylates

VE-cadherin [224], and leads to disassembly of the VE-cadherin/β-catenin adherence complex [226-228]. That ultimately causes enhanced vessel permeability and subsequent growth, aggressiveness and metastasis [228-230]. Moreover, Scr-dependent phosphorylation of Vav2 leads to signaling of the small GTPase Rac and p21-activated kinase (PAK) activation. PAK then phosphorylates the cytoplasmic tail of VE-cadherin resulting in VE-cadherin internalization into clathrin-coated vesicle, and disassembly of the junction [225]. In melanoma, EC-EC junctions were also shown to be disrupted via signaling of the phospholipase C (PLC) in Ca^{2+}-dependency which seems to be important for maintenance of VE-cadherin complex assembly [231].

Expression and function of VE-cadherin is regulated by nitric oxide (NO) produced by the endothelial nitric oxide synthase (eNOS) [232]. NO mediates VE-cadherin detachment through β-catenin S-nitrosylation induced by VEGF which leads to enhanced EC permeability [233]. Further, in HUVECs endothelial permeability was enhanced by NO upregulation leading to downregulation of VE-cadherin expression [234], thus demonstrating a correlation of the expression of VE-cadherin and NO/eNOS.

1.4. MMPs

The metalloproteinase superfamily of metzincins comprises multiple subfamilies, including astacins, serralysins, pappalysins, adamalysins and MMPs [235]. The catalytic functions of matrix metalloproteinases require a zinc-ion in their catalytic center [236]. MMPs are proteolytic active in several cells and thereby can control ECM homeostasis and cell behavior such as migration, chemotaxis and proliferation [236, 237].

1.4.1. MMP structure

Besides the common catalytic zinc MMPs also have a similar domain structure whose basic components are: signal peptide, pro-peptide domain, catalytic domain, hinge region and hemopexin domain [238]. Depending on the family member the 17-19 amino acid (aa) long, N-terminal signal peptide regulates early localization. The pro-peptides (77-87 aa) contain a conserved PRCGXPD sequence, known as cysteine-switch sequence, that binds to the catalytic Zn^{2+}, thus maintaining MMPs in their inactive pro-form [239]. Main element of MMPs is the 170 aa long catalytic domain. This highly homologous domain contains a HEBGHXLGLXHSBMXP zinc-binding consensus sequence that binds the catalytic Zn^{2+} [240] and contains a methionine that forms the 'Met-turn' supporting the structure around the

catalytic Zn^{2+}. [241]. The basic MMP structure is completed by the proline-rich hinge region which conciliates protein flexibility, and the hemopexin domain controlling protein binding [238].

MMPs, 23 family members in human [242], are divided according to structural and functional differences [243]. The matrilysins MMP7 and MMP26 have a minimal structures lacking the hemopexin domain [244] and their substrates include fibronectin, proteoglycans, gelatin and collagens [243, 245]. Fibronectin type II modules in the catalytic domain characterize the gelatinases MMP2 and MMP9 and enable further processing of denatured and cleaved collagens in the extracellular environment [235, 246], and possibly intracellular [247]. Interstitial collagens type I, II and III are substrate to collagenases (MMP1, MMP8 and MMP13). Collagenases bind to the target proteins via their hemopexin domain, which is essential for this activity, cleave collagen between Gly775 and Ile776 of the α1 chain and in between Gly775 and Leu776 in α2 chains of collagen type I generating the characteristic ¼ (C-terminal) and ¾ (N-terminal) fragments [241, 248]. In humans MMP1 was the first identified collagenase [249], but of the mouse homologues MMP1a and MMP1b only the first has collagenolytic activity. However, mice with MMP1a deletion did not develop obvious phenotypes indicating MMP1a collagenolytic activity is of less importance in mice [250]. This particular processing is also achieved by the transmembrane MMP14 which is an important collagenase in mice [251-253]. MMP14 belongs to the transmembrane MMPs together with MMP15, MMP16, MMP17, MMP24 and MMP25. While most have a transmembrane domain, MMP17 and MMP25 are attached to the plasma membrane (PM) via a GPI anchor [244, 254-256]. These transmembrane MMPs are further equipped with a cytoplasmic tail, that mediates intracellular signaling independent of their proteolytic activity as for example observed in breast cancer cells for MMP14 where the cytoplasmic domain activates ERK1/2 resulting in cell proliferation and cell migration [257]. Additional MMP subfamilies are stromelysins comprising of MMP3, MMP10 and MMP11, elastases (MMP12) [243] and the rest is unspecified [241].
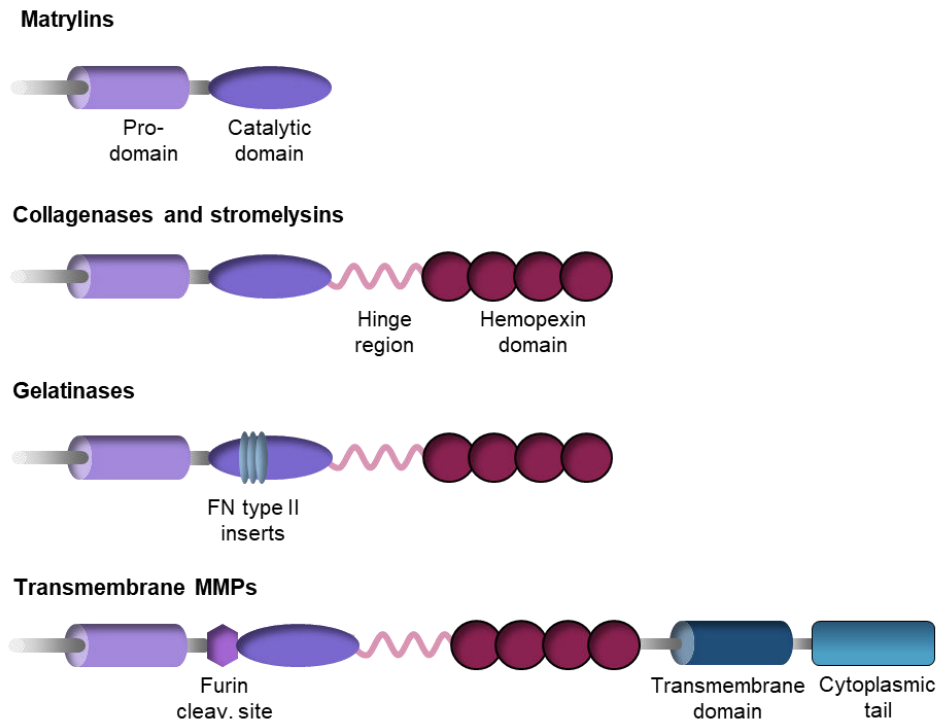
Figure 4: Metalloproteinase structure. Domain structure of the different MMP subfamilies (matrylins, collagenases, stromelysins, gelatinases and transmembrane MMPs).

1.4.2. Regulation of MMP activity

Expression and activity of MMPs underlie strong regulation by transcriptional and several post-transcriptional mechanisms including pro-enzyme activation, enzyme inhibition and compartmentalization [258, 259].

First layer of MMP control is regulation of transcription. While during homeostasis expression is maintained in basal levels, upon stimuli like cytokines or growth factors, MMP expression is upregulated. Thereby a common feature are *cis* elements in MMP promotor regions, which are suggested to be localized downstream of common signaling pathways [260]. Common MMP transcription inducing factors are NF-κB, MAPK, members of the Smad family and the AP-1 response element [260]. Some of these are shared transcriptional elements that can cause co-expression of multiple MMPs at once, while some are distinct to a smaller group of MMPs. For example, E-cadherin specifically enhances MMP14 expression in lung cancer cells [261], while MMP9 and MMP13 gene expression can be induced by the chondrocyte and osteoblast-specific transcription factor Runx-2 [262, 263].

Being expressed as inactive pro-enzymes MMPs become activated during the transport to the plasma membrane or once they are secreted out of the cell. Thereby the pro-domain secures inactivity by a free cysteine protein, whose thiol group binds the catalytic Zn^{2+}, preventing

binding of potential substrates [235, 239]. During MMP activation this interaction is interrupted through the so-called 'cysteine-switch' and can be induced for example, by ROS (reactive oxygen species) and alkylating agents like heavy metal ions or disulfides that can reduce the thiol group thus leading to auto proteolytic removal of the pro domain [238, 259]. Alternatively, other proteases like the type I membrane subtilisin-like serine protease furin [264] disrupt the thiol-zinc interaction by cleavage of the RXKR or RRKR sequence between the catalytic and pro-domain [239, 259]. This mechanism applies to approximately 1/3 of all MMPs that are substrate to furin-mediated activation during Golgi transport prior incorporation into the plasma membrane or secretion [256, 264, 265]. MMPs can mutually activate members of the family. Examples are MMP14 activating MMP2 [266, 267] and MMP13 [268, 269] or MMP3 activating MMP1, MMP7 and MMP13 [270, 271].

Function of MMPs is strongly influenced by their site of action, activation and mode of trafficking, thus compartmentalization is another way to control protease activity. While several MMPs reach their final localization in their active form, others are secreted inactive. In the case of MMP14, after furin-mediated activation during Golgi transport it can be localized to the PM in two main mechanisms. During clathrin-dependent trafficking MMP14 interacts with the AP2 protein upon palmitoylation of the C574 in the proteases intracellular domain [272-274]. On the other hand, internalization of MMP14 with Caveolin-1 is independent from clathrin [274]. Final localization of MMPs then controls substrate preferences. For example, MMPs secretion to the extracellular space primarily leads to binding to integrins and ECM processing. But when remaining intracellular or being transported to the nucleus MMPs are involved in the regulation of chromosome stability, cell invasion, apoptosis and gene transcription [275, 276].

Last instance in MMP regulation is their inhibition by endogenous inhibitors, the tissue inhibitors of matrix metalloproteinases (TIMPs) [277]. While also involved in the activation process of some MMPs, as seen for MMP2, their main function in inhibition of MMP activity by blocking the catalytic center of MMPs. There are different types of TIMPs, 4 of them being (multi-functional) active towards MMPs (TIMP 1-4) [278-283]. Although TIMPs are the most known, also other molecules exert inhibitory activity towards MMPs, such as RECK which inhibits MMP2, MMP9 and MMP14 [284, 285], α2-macroglobulin with inhibitory activity towards most MMPs [286] or the tissue factor pathway inhibitor II against MMP1 and MMP2 [287].

1.4.3. MMP dysregulation and function in pathologies

Tissue remodeling occurring in homeostatic conditions ensures continuous renewal and requires a strict control of MMP activity thus dysregulation of the proteases is strongly associated with multiple pathologies [276]. Common processes under MMP control during pathologies include cancer development, angiogenesis, arthritis, repair and immune responses which have been nicely demonstrated in knockout models [46, 252, 288-292]. In these, MMP activity towards regulatory proteins like growth factors and receptors is the main source for the observed effects, in addition to altered ECM processing. For example, in tissue repair, activation and release of growth factors is also regulated by MMPs and multiple proteases like MMP2, MMP3, MMP9, MMP12 or MMP14 are upregulated and active in all phases of wound healing [46]. However, dysregulation is strongly associated with chronic wounds and scarring due to persistent inflammation, altered re-epithelialization or remodeling [293].

Altered MMP levels, like downregulation of MMP1, and enhanced matrix deposition are characteristics of fibrotic disease like Systemic Scleroderma (SSc) [294]. Also MMP13 appears to be downregulated in SSc patient sera, which might further contribute to collagen accumulation during fibrosis [295, 296]. Lastly, MMP3 was also decreased in SSc fibroblasts which lead to enhanced ECM deposition [297]. On the other hand, pro-fibrotic function of MMP2 and MMP9 was suggested upon upregulated levels were detected in blood sera from SSc patients [298]. MMP2 and MMP13 are essential for the formation of aortic aneurysms [299] where their upregulation possibly mediates enhanced matrix degradation [300, 301]. Moreover, MMP2 depletion in knockout mice or via treatment with the MMP2-specific inhibitor TISAM was shown to be protective against cardiac rupture upon myocardial infarction, by reducing ECM degradation and subsequent macrophage infiltration [302]. Myocardial infarction can be promoted by destabilization of atherosclerotic plaques. This can be mediated by MMPs-mediated collagen type I and collagen type II degradation [303]. However, MMP3 and MMP9 were identified to have plaque-protective functions while MMP12 promotes their destabilization [304].

Last, MMPs are active in multiple cancer types with functions ranging from ECM processing to bioactive fragment release and growth factor activation [276, 305, 306]. Multiple MMPs are associated with poor prognosis in cancer, as it has been described for MMP9 in skin, breast, lung, colon, gastric, pancreatic and prostate cancer [307-311]. Moreover, MMP9 and MMP14 are connected to increased cancer cell invasion [312, 313]. Also in breast cancer metastasis

correlated with upregulation of MMPs like MMP1, MMP2, MMP7, MMP9, MMP11 and MMP13 [314].

1.5. MMP14

MMP14, also known as MT1-MMP was discovered as the first transmembrane matrix metalloproteinase [315]. It is functional in several processes involving its proteolytic activity including tissue development and remodeling, inflammation and cancer progression [316]. Structurally, MMP14 has a transmembrane domain and a cytoplasmic tail and is furin-activated during Golgi transport. MMP14 is activated in a two-step process, after the first cut in the RRKR recognition site (see 1.4.2), a second cleavage occurs at the pro-domain's PGDL or PQSL sequence within a ''bait' region linking the first two helices of a three-helix bundle structure [317]. The second cleavage is furin-independent and mediated by other MMPs (MMP2, MMP9, MMP14, MMP15, MMP24, MMP25 or MMP26) [318]. *In vitro* full removal of the pro-domain has also been demonstrated to occur via trypsin [319]. Via the Golgi MMP14 is transported in vesicles and integrated into the PM [320, 321]. In addition, MMP14 can undergo autocatalysis which results in a 44 kDa fragment that is also localized at the cell membrane [322]. Apart from Golgi-mediated transport to the plasma membrane, MMP14 can also be trafficked in microvesicular exosomes, leading to exosomal secretion and activity at sites distant from the protease-expressing cell [323].

When MMP14 was identified, it was first suggested to be a cellular receptor needed for the activation of proMMP2 [266]. Later studies unraveled the complexity of this process, which requires homodimerization of MMP14 at the cell membrane [266, 324-326]. This dimeric MMP14 forms a complex with proMMP2 and TIMP2 in a 1:1:1 ratio where the C-terminal TIMP2 domain binds to the C-terminal hemopexin domain of proMMP2 [266, 324]. The inhibitory N-terminal part of TIMP2 binds to the catalytic domain of one MMP14 protein, whereas the other on remains active and is oriented in a way that allows removal of the MMP2 pro-domain [242, 279]. Considering TIMP2 is an MMP inhibitor, balance of its concentration is an essential factor determining whether proMMP2 activation can occur or whether TIMP2 is only inhibitory towards MMP14 [327].

Further studies identified multiple other proteins processed by MMP14, many of them being part of the ECM. The most prominent is collagen type I, whose processing is also enabled by the transmembrane and hemopexin domain [328], but also other ECM proteins like fibronectin [329, 330], vitronectin [330], laminins 1, 2/4 and 5 [330, 331], perlecan [329], nidogens [329]

and fibrinogen [332, 333]. Also other proenzymes like proMMP13 [269] and ADAM9 are activated by MMP14 [334]. Moreover, the substrate palette of MMP14 further expands to cytokines (IL-8, SDF-1, MCP-3) [335-337], receptors (CD44, EphA2) [338, 339] and growth factors (Cyr61, TGFβ1) [340-342].

TGFβ1 can be released by MMP14 through cleavage of LTBP1 [342] which binds latent TGFβ1 to the ECM [68, 69]. However, this MMP14-mediated processing and for instance also that of CD44 have been only shown in *in vitro* studies so far, so the importance for *in vivo* processes is not clear yet. Still, due to this diverse set of substrates MMP14 is a manifold of cellular processes, including proliferation, migration, invasion, differentiation [343]. Most of these functions rely on MMP14's proteolytic activity in the extracellular space, however, intracellular functions of MMP14 were also identified and are independent of its enzyme activity. For example, nuclear localization initiates MMP14 activity in transcription regulation as observed for VEGF-A [344], IL-6, IL-12 and IL-33 [345]. Moreover, in breast cancer cells cytoplasmic MMP14 localization leads to activation of ERK1/2 by the proteases cytoplasmic tail when in complex with TIMP-1 eventually initiates cell proliferation and migration [346]. In hypoxic tumors the MMP14 cytoplasmic domain further induces expression of HIF-1 which promotes tumor [347].

1.5.1. MMP14 in skin tumors

MMP14 is highly active in multiple cancer types including those of the skin like melanoma, where its expression often correlates with poor prognosis [348-350]. In melanoma MMP14 expression is highly upregulated starting from the nevus-to-primary melanoma transition [351]. In growing melanoma the protease is then highly expressed in the cells forming the invasive front [352]. Here collagenolytic activity towards collagen type I and type IV is one of the driving factors as seen *in vitro*, where silencing of MMP14 in melanoma cells impaired invasion of matrigel [353]. Also processing of other ECM molecules like laminin drives melanoma cell migration and invasiveness [354, 355]. Cleavage of laminin has further been shown to mediate formation of tumor vessels via vascular mimicry [356]. In epithelial tumors cleavage of the laminin-332 γ chain by MMP14 mediates tumor cell migration and invasion, possibly through interaction of the resulting fragment with the epidermal growth factor receptor (EGF-R) [357]. Aside from ECM proteolysis MMP14 drives melanoma growth by processing of growth factors [358]. Cleavage of Notch1 by MMP14 is sufficient to induce melanoma cell proliferation [148].

Besides progression of the primary tumor, MMP14 also induces metastasis to distant organs like lung [359]. For example, cleavage of lymphatic endothelial cell-Notch3 by MMP14 activates β1-integrin and subsequently induces formation of invasive sprouts and, eventually, metastasis [360].

1.5.2. MMP14 in angiogenesis

Multiple studies over the year further highlighted MMP14 activity in angiogenic processes.

First indications of MMP14 functions in angiogenesis came from full knockout mice, were angiogenesis was among the observed defects angiogenesis [252, 361] as seen for example in the defective vascularization of bones [252]. Moreover, a corneal micropocket assay demonstrated impaired angiogenic sprouting upon FGF2 treatment [361]. Further analysis then revealed MMP14 involvement in EC migration, capillary tube formation and recruitment of accessory cells [362].

For example, rat aortic ECs without transmembrane localization of MMP14 failed to invade fibrin-rich matrix, despite maintained fibrinolytic activity, indicating importance of MMP14 localization in the EC membrane during migratory processes [363]. Moreover, *in vitro* ECs treated with LEM-2/63, an anti-MMP14 antibody, failed to migrate into matrigel, thus tube formation by these cells was defective [364]. They further showed that this is likely a result of impaired CCL2 activation upon MMP14 inhibition [364]. Lung ECs derived from MMP14 knockout mice also failed to invade 3D matrigel matrices, independent from MMP2 activation, as MMP2-deficient ECs successfully migrated into the matrix [289]. Similar sprouting defects were also observed in aortic ring explants placed in collagen gels [365]. Aortic rings from mice with global MMP14 deletion did not form sprouts, while deletion of MMP2 or MMP9 did not affect neovessel formation indicating dependency of migrating ECs on the collagenolytic activity of MMP14 [365]. Use of the aortic ring assay as *ex vivo* model further indicated MMP14 function in vessel stabilization [366]. Aortas treated with MMP14 neutralizing antibodies or TIMP-2, TIMP-3 or TIMP-4 showed inhibited angiogenesis while vessels became more stable [366]. Analysis of corneal sprouting demonstrated that MMP14 regulates sprouting through interaction with VEGFR1 in order to enable VEGF signaling [367]. Thereon, tumor angiogenesis was inhibited upon treatment with the MMP14 inhibitory antibody DX-2400 [368].

Use of lacZ controlled by the endogenous MMP14 promotor in reporter mice showed strong expression of MMP14 in the tip cells of newly developing sprouts indicating an important role

of EC-derived MMP14 during angiogenesis [369]. Low MMP14 expression in quiescent ECs and strong upregulation upon the cells activation was observed [370].

Prior sprout formation small sub-cellular structures called podosome rosettes form in VEGF-activated ECs at branching points that are characterized by a high degradative activity. Here, the degradative activity in mainly dependent on MMP14, which further underscores the proteases importance for angiogenic sprouting [371]. Moreover, MMP14 regulates formation of the vascular tube which was abrogated in ECs seeded in 3D collagen matrices upon application of MMP14-directed inhibitors due to loss of collagenolytic activity of the cells [372].

Activity of MMP14 in angiogenesis doesn't end with formation of the vascular tube and the protease is functional in the recruitment of vessel-associated cells which is part of the process of vessel maturation. Association of MMP14 with PDGFRβ in vascular smooth muscle cells (VSMCs) is required for PDGF-B signaling that mediates VSMC recruitment to vessel [373]. All together, these studies demonstrate MMP14 involvement in various steps from angiogenesis to vessel maturation.

1.5.3. MMP14 in wound healing

MMP14 is active during multiple phases of cutaneous wound healing, especially during the proliferation phase. In early wounds, MMP14 is expressed by macrophages mediating their infiltration to the injured site by BM degradation [374]. Through activation of MMP2 and induction of EC migration MMP14 promotes wound angiogenesis [364, 365]. This MMP2 activation function might also be important for re-epithelialization. Here, keratinocyte proliferation and migration is induced by laminin-322 cleavage, which has been shown to be mediated by MMP2 [375], but also MMP14 itself [331, 376, 377]. The resulting fragment induces syndecan-1 and CD44 that subsequently activate MMP9 and MMP14 in podosomes. This further promoted keratinocyte migration [378]. Function of MMP14 in Keratinocyte migration dependent on BM processing was also indicated in *ex vivo* skin explants from MMP14 knockout mice, which demonstrated normal closure after excisional wounding, but impaired re-epithelialization on membrane substratum [379]. However, keratinocyte expression of MMP14 does not appear to be the driving factor as keratinocyte-specific deletion of the protease has no effect on the overall tissue repair [380]. Instead, MMP14 loss in keratinocytes caused altered generation of a collagen type XVIII-derived endostatin-like fragment that has anti-angiogenic function, which resulted in impaired vascular clearance [380].

1.6. Mouse models of MMP14 deficiency

1.6.1. Global deletion of MMP14

Around the same time two different mouse lines with global MMP14 deletion were generated [252, 361]. The first, a PGK controlled HPRT minigene replaced parts of the MMP14 gene, namely the section between exon 3's first half (3' end) and the 3' end of exon 5 which removes amino acids 6-274, thus parts of the pro- and catalytic domain leading to an inactive protein [252]. The second model utilizes a neomycin cassette under control of a pgk1 promotor partially replacing exon 4 of the MMP14 gene, again producing an inactive protease [361]. Both studies identified similar defects resulting from the loss of MMP14 activity which culminated in early lethality of the mice within three weeks after birth [252, 361]. The described defects were visible postnatal and spanned from skeletal, to angiogenic and soft tissue defects leading to early death within the first three weeks of birth [252, 361]. However, abnormalities only became visible a few days after birth, around P5 [252] or after 10 days [361] with knockout mice remaining smaller and lighter than heterozygous and wildtype littermates [252]. Moreover, versatile skeletal defects occurred, including skeletal dysplasia, defective long bone formation, altered growth of unmineralized epiphyseal cartilage due to impaired ossification and vascularization, deformed skulls with altered suture closure and defective removal of cranial cartilage that caused cranial dysmorphism. In addition, in regions connecting bones and soft tissues such as joints, ligaments, tendons, synovial capsules and articular cartilage MMP14 knockout mice developed arthritis and osteopenia while signs of fibrosis developed in a few mice exceeding the age of three month [252, 361].

More recent MMP14 knockout models also demonstrated the proteases role in the cardiac system and metabolism [253, 381]. Gutierrez-Fernandez and colleagues obtained deletion by removal of exon 4 and 5 of the MMP14 gene, thus exclusion of the proteases catalytic domain [253]. These mice displayed a thickened muscular wall of the right heart ventricle, ventricular septum hypertrophy and accumulation of collagen type I in heart tissue. This was accompanied by increased expression of p16 and p21 in heart, kidney and adipose tissue, thus senescence [253]. In addition to altered ECM proteolysis, cell connections via the cytoskeleton to the ECM were impaired [253]. Moreover, analysis of the mammary gland proteome from MMP14 knockout mice showed reduced glycogen in tissue, lipid levels in blood and IGF-1 in the circulation and in the blood plasma triglyceride was decreased, while growth hormone circulation was enhanced [381].

1.6.2. Cell type-specific MMP14 deletion models

Global deletion of MMP14 in mice highlighted the proteases pleiotropic functions, predominantly during embryonal and postnatal development. However, these mouse models could not address *in vivo*, first the cell specific protease function and secondly, due to early lethality, the function of MMP14 in adulthood. Therefore, mice with cell-type specific deletion of MMP14 were generated. Deletion in keratinocytes was performed using the keratin 14 promotor to delete the lox P enclosed exons 2-4 of the MMP14 gene [380]. During development and adulthood these MMP14$^{ep-/-}$ mice did not display any phenotype. However, when investigating skin repair, a subtle phenotype with delayed vascular regression in later wound was detected and consequence of decreased endostatin release from collagen type XVII [380]. Crossing MMP14 floxed mice with mice carrying the Cre-recombinase expression under LysM control, led to MMP14 deletion in macrophages [382]. These mice developed and repaired skin normally, but croton oil-induced contact dermatitis resulted in an altered immune response in the absence of MMP14 in macrophage, despite ear swelling being comparable to controls [382]. In these mice, decreased infiltration of monocyte, macrophage and T-cell was detected in the irritated skin, and the reduced monocytes/macrophages influx in the tissue likely resulted from altered macrophage cell migration in the absence of MMP14 [382].

However, a beneficial effect of MMP14 loss in macrophages using a LysM-Cre recombinase deletion model was observed by Alonso-Herranz and colleagues [383]. They found mitigated fibrosis and a preserved cardiac capillary network in tissue upon a post-myocardial infarction that was alleviated in these mice [383]. Mechanistically, they ascribed the protective effect of macrophage-specific MMP14 loss to reduced EndoMT, thus less ECs transforming into myofibroblast and fibrosis formation, highlighting the proteases role in this process [383].

Another model was generated to investigate the functional significance of MMP14 in lung epithelial cells, here a doxycycline-induced Cre-recombinase controlled by the SPC gene and floxed exon 4 and 5 of the MMP14 gene were used [384, 385]. Treatment of the lung with bleomycin resulted in an increased fibrotic reaction, demonstrating the anti-fibrotic role of epithelial cell-derived MMP14 [385].

Similar to the observations made in the full knockouts, tendon-specific deletion of MMP14 driven by the Cre recombinase under the control of the Scx promotor lead to several skeletal defects [386]. In addition, these mice developed a limb phenotype with paw dorsiflexion, altered tail and Achilles tendon sizes, and accumulated fibronectin. However, collagen type I was comparable between knockouts and wild types. Further analysis suggested impaired

collagen fibril release due to lack of FN processing in fibropositors as cause for the impaired tendon development [386].

In order to further analyze the skeletal defects observed in full knockouts, mice with conditional deletion of MMP14 in mesenchymal progenitors were generated using the Dermo (Twist2)-driven Cre recombinase [387]. In these mice, involvement of MMP14 in the regulation of skeletal stem cell fate was observed as these cells underwent adipo- and chondrogenesis rather than osteogenesis. The mechanism for the regulation of stem cell fate involved the MMP14 remodeling of the microenvironment as regulator of integrin receptors and intracellularly of the YAP/TAZ signaling, describing another signaling pathway that is controlled by MMP14 [387].

1.6.2.1. Endothelial cell-specific MMP14 deletion

Although MMP14 regulatory functions in angiogenic processes have been described, the importance of EC-derived MMP14 *in vivo* remains unclear. To help identify these functions, multiple mouse models with Cre-recombinase expression controlled by different promotors leading to EC-specific MMP14 deletion were generated.

For example, 4-hydroxy-tamoxifen (4-OHT)-inducible deletion specific in ECs was achieved by Cre^{ERT2}-recombinase driven by the cdh5 promotor [388]. This deletion led to the identification of EC-derived MMP14 as important player in progression of intussusceptive angiogenesis (IA) in a colitis model. Further analysis showed that loss of EC-MMP14 impaired IA by impairing cleavage of TSP1, which lead to reduced NO production [388]. Another model used the Cre-recombinase expression under control of the Tie1 promotor [389]. This study focused on the effect of the deletion of EC-derived MMP14 on the lymphatic vasculature and identified LYVE-1 as new substrate [389].

Lastly, we used our floxed mice and paired them with Tie2-Cre mice where Cre expression underlies the control of the Tie2 promotor [390, 391]. In these MMP14$^{EC-/-}$ mice, Tie2-driven Cre expression of the recombinase starts at E13 leading to knockout of MMP14 in all ECs [391, 392]. MMP14$^{EC-/-}$ were found to breed and develop normal without effects on the mice' life span. Only minor defects regarding the bone development were identified with mild cranial dysmorphia and delayed suture closure but long bone development and ossification as well as skin development were normal [390].
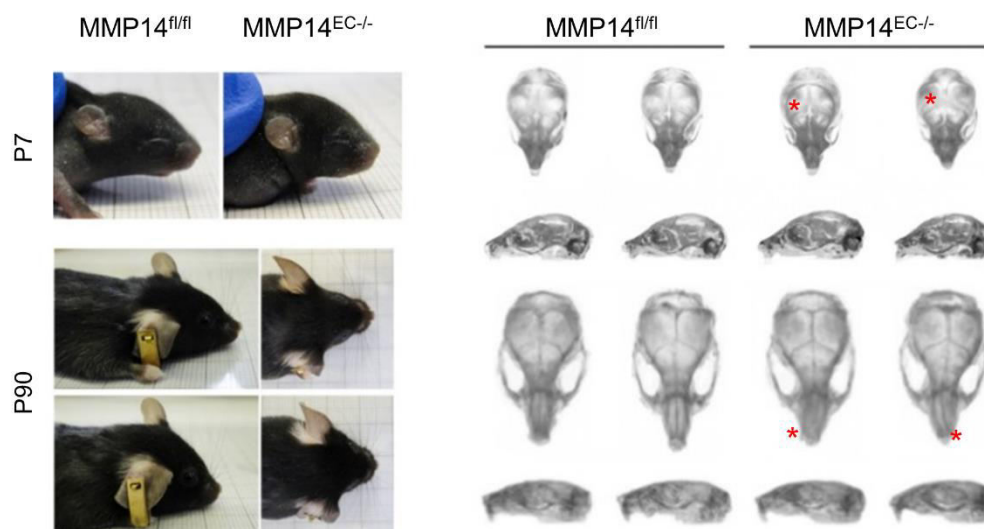
Figure 5: Skull phenotype in MMP14$^{EC-/-}$ mice. Analyzed at P7 and P90, skulls of MMP14$^{EC-/-}$ mice were slightly deformed (bulkier, deviation of snout) and suture closure was delayed. Red stars indicate the incomplete suture closure at P7 and the distorted snout at P90. Modified from [390].
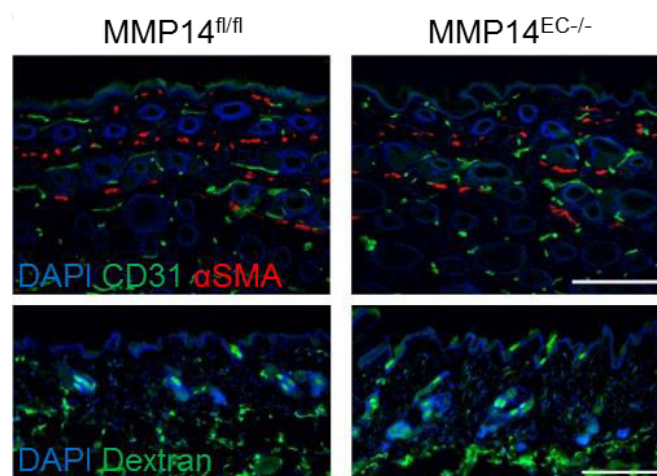
Figure 6: Skin vascularization of MMP14$^{EC-/-}$ mice was comparable to controls. Modified from [390].

1.6.2.2. Fibroblast-specific MMP14 knockout

A cell type-specific knockout model generated by our group was in dermal fibroblasts. Using the tamoxifen-inducible CRE^{ERT} recombinase under the control of the collagen-α2 type I promotor that specifically leads to deletion in stromal fibroblasts we have generated a MMP14-fibroblasts specific line [251, 393, 394]. Deletion was obtained by tamoxifen feeding for a period of 4 weeks to enable Cre-localization to the cells' nucleus and obtain an efficient deletion of MMP14 in dermal fibroblasts, 1 week later the feeding protocol was terminated we detected a skin and tendon phenotype [251]. These MMP14$^{Sf-/-}$ mice displayed a fibrosis-like phenotype

due to collagen type I accumulation in the skin as result of impaired collagen degradation [251]. Additionally, grafting melanoma cells in the flank of these MMP14$^{Sf-/-}$ mice resulted in reduction of tumor growth [395]. The stiff and matrix-dense TME negatively influenced tumor vascularization and melanoma cell proliferation [395]. Moreover, proteome analysis of matrix derived from MMP14$^{Sf-/-}$ fibroblasts lead to the identification of collagen type XIV as new MMP14 substrate [396]. It's accumulation in the TME of MMP14$^{Sf-/-}$ further contributed to reduce melanoma growth, thus identifying another function of fibroblast-derived MMP14 [396].

1.7. MMP3

Other than MMP14, MMP3, also known as stromelysin 1, is a soluble MMP encoded on chromosome 11 and secreted into the extracellular space [397, 398]. It was first described as a "proteoglycanase" due to its activity towards proteoglycans isolated from cartilage [399]. Structurally similar to collagenases, MMP3 consists of pro-, catalytic and hemopexin domain and a hinge region [242].

The catalytic domain exerts its enzymatic activity in a Ca^{2+}-dependent manner with optimal efficiency obtained at pH 7.5-7.8 [397]. Among the main substrates of this protease are multiple ECM proteins, including those of the BM like collagen type IV and laminin, as well as fibronectin, gelatin and proteoglycans like aggrecan [397, 400, 401]. MMP3 does not cleave interstitial collagens, but can still bind to them, possibly having an influence on interstitial collagen processing [402-405]. Moreover, it is a known activator of pro-collagenases (MMP13) which indirectly implicates it in the regulation of interstitial collagens [268, 406, 407]. Besides ECM proteins, MMP3 processes cell surface proteins like E-cadherin [408], or is involved in growth factor activation, e.g. of TGFβ1 [409]. MMP3 derived from matrix vesicles secreted from chondrocytes is able to activate latent recombinant TGFβ1 from the matrix via LTBP1 cleavage [409].

Activity of MMP3 is inhibited by TIMP1 [410] and TIMP2 [411]. One of the main regulators of MMP3 expression is AP-1. In the MMP3 promotor region, binding of AP-1 to the conserved phorbol ester response element (TRE) [412] is essential to induce and maintain the proteases' expression [413, 414]. However, further studies showed that AP-1 binding is not necessarily sufficient and activation of NFκB seems to be essential [415].

While in physiology, expression and activity of MMP3 is limited and its function is not fully understood, multiple roles of MMP3 in disease were identified. In atherosclerosis MMP3 was

ascribed a protective function and upregulated expression inhibited growth and stability of plaques [304]. On the other hand, it was shown to be upregulated in the cartilage in rheumatoid arthritis [416, 417] as well as in osteoarthritis where its activity is associated with cartilage damage [418].

MMP3 is one of the multiple proteases upregulated during cutaneous tissue repair. Studies identified multiple function of the protease during wound healing which defer depending on the phase and localization [46]. One of the most important functions for MMP3 in skin repair is likely to mediate wound contraction [419, 420]. In addition, MMP3 expression in keratinocytes likely mediates restoring of the epidermal integrity as its keratinocyte expression was upregulated during re-epithelialization but declined thereafter [421-423]. Upregulation of MMP3 may promote chronic wounds as it was upregulated in human ulcers. Upon compression therapy, MMP3 was one of the downregulated proteases, along with MMP1 and MMP2, but the regulatory mechanisms were not identified [424].

1.7.1. MMP3 global knockout

In order to analyze MMP3 *in vivo* functions a mouse model with global deletion was generated [425]. Using a pS1-RV1.1 replacement vector parts of exon 3 and exon 4 that encode for the MMP3 Zn^{2+}-binding site were replaced by a neomycin expression cassette with antisense direction [425]. Despite deletion of MMP3, mice developed normal and no phenotype was detected when analyzing tissue histology, serum chemistry and hematologic characteristics indicating the proteases dispensability or compensation in development and homeostasis [425]. In support of the latter, analysis of mRNA levels in the MMP3$^{-/-}$ mice revealed increased expression of MMP7 and MMP10, likely taking over functions of MMP3 [426]. However, multiple pathological conditions suggested MMP3 involvement and functions. For example, loss of the protease had a protective effect against lung injury induced by LPS or hydrochloride acid due to a reduced inflammatory response [427]. A similar beneficial effect was observed towards contact hypersensitivity [428]. MMP3 has also been associated with the ROS-induced activation of Nox1 (NADPH oxidase 1) leading to death of dopaminergic neurons. Using MMP3 knockout mice revealed that induction of Nox1 is MMP3-dependent, thus the proteases activity death of the dopaminergic neurons [429]. Also, increased osteoarthritis was observed in the knockout animals [418]. However, collagen-induced arthritis was unaltered in MMP3$^{-/-}$ mice, despite upregulated MMP3 levels in patient sera [425]. Moreover, wounding of MMP3$^{-/-}$

mice resulted in delayed wound closure. Analysis showed, that loss of MMP3 impaired wound contraction, likely due to defective formation of the fibroblast actin network [419].

1.8. Aim

MMPs are multi-functional players in health and disease, contributing to maintaining tissue homeostasis or, when deregulated, promoting and sustaining the development of pathologies like cancer. Among the MMPs, a pivotal role in development was shown for MMP14 as its global deletion led to early postnatal death [252, 253, 361]. MMP14 enhanced expression also strongly correlates with tumor progression and is highly upregulated during wound healing, events that share many biological and molecular features [331, 348-350, 364, 365, 376, 377, 430].

To study the function and cellular source of MMP14 in the skin, our group generated mice with MMP14 deletion specific to various cells, including dermal fibroblasts and endothelial cells. Deletion of MMP14 in fibroblasts caused a fibrotic skin phenotype, thus identifying the protease as the main collagenase in the skin of mice [251]. The skin from the MMP14$^{Sf-/-}$ mice analyzed by transcript and protein-based assays displayed upregulated MMP3 expression. However, the function of this protease in the absence of fibroblasts-MMP14 needed further investigations.

In addition, another mouse line where MMP14 was deleted in endothelial cells MMP14^{ECKO} was generated. Preliminary data revealed that endothelial cells-specific MMP14 deletion results in almost no apparent developmental alterations in any organ including the skin. In contrast, growth and metastasis of grafted melanomas were reduced thus identifying a function of EC-MMP14 in tumor growth and metastasis, but the underlying mechanisms were unknown.

The aims of this study were to identify the molecular events mediated by the MMP14 in endothelial cells during the growth of melanoma and, secondly, to unravel the function of MMP3 upregulated in mice skin carrying the MMP14 deletion in dermal fibroblasts for skin development and repair.

To address the first part of the project mice (controls and MMP14$^{EC-/-}$) were grafted with murine melanoma to follow melanoma development. Tumor growth was monitored as a function of time, and tumor size, structure, vascularization, and vessel permeability were analyzed and measured at different time points. *In vitro* culture systems using endothelial cells isolated from MMP14$^{EC-/-}$ and control mice were used to examine at a molecular level how the expression of MMP14 affected the endothelial cell function.

In the second part of the studies, to investigate the function of MMP3 upregulation in fibroblast-derived MMP14 mice, we generated mice with a double deficiency of both proteases, MMP14 in fibroblasts and MMP3 as global deletion. Double-deficient mice were generated. The skin tissue from the MMP3$^{-/-}$/MMP14$^{Sf-/-}$ mice was characterized by morphology, structure, and collagen composition. The effects of loss of both proteases were investigated in a tissue repair model, where wound closure was studied. In this process, several crucial parameters were investigated over time: inflammatory cell composition, vascularization, myofibroblast population of the wounds, and re-epithelialization. Last, *in vitro* assays using primary fibroblasts extracted from MMP3$^{-/-}$/MMP14$^{Sf-/-}$, single knockout, and control mice were performed to examine whether protease loss affects fibroblasts differentiation in response to mechanical and growth factor (TGFβ1) stimuli.

2. Materials and Methods

2.1. Materials

2.1.1. General Chemicals & Reagents

All standard chemicals were purchased in analytical grade from Carl Roth (Karlsruhe, Germany), Sigma-Aldrich (Taufkirchen, Germany), Serva (Heidelberg, Germany), Walter-CMP (Kiel, Germany) Chemsolute (Renningen, Germany) or Merck (Darmstadt, Germany).

2.1.2. Consumable Materials

General plastic materials including for tissue culture, were purchased from Corning (Karlsruhe, Germany), Greiner Bio-One (Frickenhausen, Germany), Sarstedt (Nürnbrecht, Germany), Eppendorf (Hamburg, Germany), Thermo Scientific (Darmstadt, Germany), Life Technologies (Darmstadt, Germany), Becton Dickinson GmbH (Heidelberg, Germany) and VWR (Darmstadt, Germany).Whatman® chromatography paper (3 MM) was from Whatman (Dassel, Germany). Cryomolds and biopsy cassettes for tissue preparation were obtained from Sakura Finetek (Umkirch, Germany).

2.1.3. Buffers and Solutions

PBS: 136 mM NaCl, 2.6 mM KCl, 10 nM Na_2HPO_4, 1.5 mM KH_2PO_4, pH 7.4

RIPA buffer: 50 mM Tris, 150 mM NaCl, 0.5% DOC, 2% SDS, 1 % , NP40, pH 7.4

TBS (10x): 50 mM Tris-HCl, 20 mM Tris-Base, 150 mM NaCl, pH 7.6

TBE (10x): 500 mM Tris-Base, 10 mM EDTA, 500 mM boric acid, pH 8.1

Separation gel buffer: 1.5 M Tris-HCl, 0.4% SDS, pH 8.8

Stacking gel buffer: 0.5 M Tris-HCl, 0.4% SDS, pH 6.8

Running buffer: 250 mM Trizma® base, 0.2 M Glycin, 1% SDS, pH 8.3

Anode I buffer: 0.3 M Trizma® base, 20% (v/v) Methanol, pH 10.4

Anode II buffer: 25 mM Trizma® base, 20% (v/v) Methanol, pH 10.4

Cathode buffer: 40 mM 6- Aminocaproic acid, 20% (v/v) Methanol, pH 7.6

2.1.4. Equipment

Blotting systems	Semi Dry Electroblotting Unit SV20-SDB (Sigma-Aldrich)
Centrifuges:	Eppendorf® Microcentrifuge 5415 R
	Megafuge ST Plus Series Centrifuge: Thermo Fisher Scientific
Cryostat and Microtome	RM2255 microtome (Leica, Wetzlar, Germany)
	Microm HM 560 Cryostat: Thermo Fisher Scientific
Euthanasia station	GasDocUnit® ATNG/XJ M (Medres – medical research GmbH, Köln, Germany)
Gel Systems	Hoefer™ Mighty Small™ II Vertical Electrophoresis System (Hoefer Inc, Holliston, MA, United States)
	PerfectBlue™ horizontal gel system (VWR)
Incubators	Heracell™ 150i CO2 incubator (Thermo Fisher Scientific)
Magnetic stirrer	IKA®-combimag RCO (IKA Labortechnik, Staufen, Germany)
Microscopes	Nikon Digital Sight (Nikon, Amsterdam, Netherlands)
	Nikon Eclipse TS100
	Nikon Eclipse TS2
	Nikon SMZ800
	Stereoscopic microscope (Nikon)
	Light source PHOTONIC PL 2000: Photonic (Vienna, Austria)
Paraffin station	Cooling Plate COP 30 (Medite, Burgdorf, Germany)
	TES 99 Paraffin Embedding Center (Medite)
pH Meter:	Multi-parameter MU 6100 L (VWR)
Power Supplies	Power Supply PowerPac™ 300 (Bio-RAD, Feldkirchen, Germany)
	Power Source PS2001-2 (Sigma-Aldrich)
Shakers	Eppendorf ThermoMixer® 5437
	KS250 basic shaker (IKA Labortechnik)
	Roller mixer SRT6 (Stuart, Staffordshire, United Kingdom)
	Rotator SB2 (Stuart)
Sterile Hood	Thermo Scientific™ Safe 2020 Class II Biological Safety Cabinets (Thermo Scientific)
Vortex	Vortex Genie 2™ (Bender & Hobein, Zürich, Switzerland)
Water Bath	Julabo® SW-20C Water Bath (Julabo, Seelbach, Germany)

| Western Blot detection | Curix 60 Processor Developer for Western Blot (AGFA, Düsseldorf, Germany) |
| | Dupont Cronex Quanta III Intensifying Screens (Heinrich Faust GmbH, Köln, Germany) |

2.2. Methods

<u>2.2.1. Cell Culture</u>

2.2.1.1. Cell lines

B16F1 melanoma cells (CRL-6323 ATCC®, Wesel, Germany) [431] and human umbilical vein endothelial cells (HUVECs) (PromoCell) were cultured in melanoma cell medium and EC growth medium on gelatin coated tissue culture plates, respectively. All cells were cultured at 37 °C and 5% CO_2. Cells were passaged every 2-3 days by washing with PBS (Gibco, Karlsruhe, Germany) detaching them from plates with 1% (v/v) trypsin/2% (v/v) EDTA at 37°C. Trypsin reactivity was stopped by addition of FCS containing medium and cells collected in a 15 ml falcon tube, centrifuged (320 x g, RT, 5 min,) and seeded on new plates with new complete medium. B16F1 melanoma cells were split weekly in a 1:10 ratio, HUVECs were split in a 1:3 ratio.

Melanoma cell medium:
DMEM (Dulbecco's Modified Eagle's Medium, +4.5 g/l D-Glucose, L-Glutamine; Gibco)
100 U/ml penicillin/ 100 µg/ml streptavidin (Sigma-Aldrich)
10% (v/v) fetal calf serum (FCS, Gibco)
2 mM glutamine (Sigma-Aldrich)

EC growth medium:
DMEM (+4.5 g/l D-Glucose, L-Glutamine)
20% (v/v) FCS,
100 U/ml penicillin/ 100 µg/ml streptavidin (Sigma-Aldrich)
1% (v/v) non-essential amino acids (NEAA, Gibco)
1% (v/v) Na-pyruvat (Sigma-Aldrich)
 0.2% (v/v) EC growth supplements with heparin (PromoCell)

***Gelatin coating*:**

1% (v/v) gelatin (Sigma-Aldrich) in PBS

For coating tissue culture plates were incubated with the 1% gelatin at 37 °C for 30 min. Remaining liquid was removed before seeding the cells.

2.2.1.2. Isolation of mouse lung endothelial cells

To isolate lung endothelial cells mice were sacrificed via cervical dislocation at the age of 5 weeks. The chest was opened and the rib cage was removed. All five lung lobes were carefully removed and stored in sterile PBS on ice. Under a sterile hood lungs were dissected into small pieces for 5 min using scalpels (20x blade). Minced lungs were incubated with 400 U/ml collagenase I at 37 °C for 30 min. The resulting lung suspension was filtered through an EASYstainer^{TM} 40 µm nylon mesh (Greiner Bio-One) into a 50 ml falcon tube carefully triturating the mass through the filter. Cells were washed with 10 ml DMEM with 10% (v/v) FCS and filtered a second time to remove cell clumps. Centrifugation (320 x g, RT, 7 min) followed before suspending the cells in 90 µl MACS buffer per 10^7 cells. 10 µl CD31 microbeads (130-097-418, Miltenyi Biotec, Bergisch Gladbach, Germany) were added to 10^7 cells and incubated at 4 °C (fridge) for 12 min. After addition of 1 ml MACS buffer, cells were centrifuged (320 x g, 10 min), suspended in 500 µl ice cold MACS buffer and loaded onto an equilibrated MACS® MS column (130-042-201, Miltenyi Biotec). The flow through was collected as negative fraction containing mainly fibroblasts. Columns were washed with ice cold MACS buffer and cells were eluted with 1 ml ice cold MACS buffer by removing the column from the OctoMACS® (130-042-108, Miltenyi Biotec) and pushing through with a plunger. Eluted cells and negative collection were centrifuged (320 x g, 10 min). Cell were suspended in EC growth medium and seeded on gelatin coated tissue culture plates. If necessary, fibroblast contamination in EC cultures were removed by a second sorting after a few days of culture. Cells were cultured at 37 °C and 5% CO_2 and passaged in a 1:3 ratio.

MACS buffer:

0.5% (v/v) FCS

2 mM EDTA

pH 7.2, in PBS

Collagenase I:

400 U/ml Collagenase I (Worthington, Lakewood, NJ, United States)

130 mM NaCl

10 mM Ca-Acetate

20 mM HEPES

0.5% (v/v) BSA

2.2.1.3. Isolation of primary fibroblasts

Dermal fibroblasts were isolated from the back skin of mice as described previously [251]. Shortly, after sacrificing via cervical dislocation back skin was shaved, dissected and maintained in PBS on ice. The skin was disinfected 2 min in 0.1 g/ml betaisodona iodine (Mundipharma, Frankfurt am Main, Germany), 1 min in 70% (v/v) ethanol and washed twice for 1 min in PBS before carefully mincing it into small pieces for several minutes. To release cells from the ECM the skin fragments were incubated in 400 U/ml collagenase I (see chapter 2.2.1.2) in PBS at 37 °C for 1-2 h. When the solution appeared turbid to block collagenase activity 5 ml DMEM with 20% (v/v) FCS and 100 U/ml penicillin, 100 μg/ml streptavidin were added. Cells were centrifuged (320 x g, RT, 5 min) to remove debris and suspended in 10 ml complete DMEM with 20% (v/v) FCS before seeding on a P10 dish. Cells were cultured in fibroblast growth medium at 37 °C and 5% CO_2 and passaged in a 1:3 ratio.

Fibroblast growth medium:

DMEM (+4.5 g/l D-Glucose, L-Glutamine)

10% FCS

100 U/ml penicillin/100 μg/ml streptavidin

2 mM glutamine

0.05 g/l L-ascorbic acid

2.2.1.4. Analysis of nitric oxide production

Nitric oxide production in ECs was analyzed using the cell-permeable fluorescent component DAF-FM [432-434]. When reacting with NO, DAF-FM transforms into a fluorescent compound, with fluorescence intensity at 495 nm being directly proportional to NO levels [432-434]. Therefore, primary ECs were seeded in 96 well plates with 6.25 x 10^4 cells/cm^2 and cultured for 24 h. Then, 20 mM DAF-FM diacetate (D23844, Thermo Fisher Scientific) in Opti-

MEM (Gibco) were added to the cells and further incubated at 37 °C for 1 h. After incubation the mix was replaced by fresh Opti-MEM before measuring fluorescence intensity at 495 nm 1, 2, 4 and 24 h post-treatment using the Victor³ 1420 Multilabel Counter (Perkin Elmer, Turku, Finland).

2.2.1.5. siRNA transfections

Silencing of MMP14 and eNOS gene expression was performed by transient transfections of mouse ECs and HUVECs with small interfering RNA (siRNA). Therefore, 8×10^3 cells/cm^2 were seeded per well in a 24 multiwell plate and transfected using Lipofectamine^{TM} RNAiMAX (13778100, Thermo Fisher Scientific) in Opti-MEM (10 µl in 500 µl transfection mix). Human Mmp14 was silenced in HUVECs using siRNA and mouse ECs with mouse eNOS siRNA. Scrambled control siRNA transfection was used as control. Concentrations of siRNAs used for transfections are listed in Table 1. Medium was replaced after 24 h. Samples were collected after 48 h for protein or RNA analysis.

Table 1: List of used siRNA including concentration, company and order number.

Product	Concentration	Company	Order Number
Human MMP14 siRNA	10 nM	Ambion, Darmstadt, Germany	4390824
Mouse NOS3 siRNA	100 µM	Santa Cruz, Heidelberg, Germany	Sc-36094
Negative Control siRNA	100 µM	Ambion	4611G

2.2.1.6. Fibroblast activation

Primary fibroblasts were seeded as monolayers (2.6×10^4 cells/cm^2 in 6 multiwell plates) and cultured at 37 °C O/N. After 8 h starvation in serum free growth medium cells were treated with 40 ng/ml TGFβ1 (5231LF, Cell Signaling, Frankfurt am Main, Germany) in serum free media for 24 h. Proteins and RNA were isolated and analyzed by immunoblot and real-time PCR. Alternatively, fibroblasts were cultured in 3D-cultures of collagen, 300.000 fibroblasts/ml were seeded in 1 mg/ml collagen gel solution (see Table 2). Tethered collagen gels were prepared in normal tissue culture plates, while free-floating gels were in bacterial dishes. Upon polymerization 500 µl medium were added and free-floating gels were carefully detached from the dish walls and gel size was measured over time. To obtain cell extracts, after 24 h culture cells were extracted from the collagen gel by digestion with 2 ml 400 U/ml collagenase I

(Worthington) ~20 min. To ensure proper dissolution of the gels, samples were inverted every few minutes. Extracted cells were centrifuged (320 x g, RT, 5 min), washed twice with PBS and lysed in RIPA buffer with protease inhibitor at 4 °C O/N.

Table 2: Collagen gels.

Substance stock concentration	Final concentration
3 mg/ml bovine collagen type I (IBFB GmbH, Leipzig, Germany	1 mg/ml
5x DMEM	1x
0.1 M NaOH	5 mM
FCS	10 %
Cell suspension	0.1 ml per 1 ml gel
H_2O	

5x DMEM:

10x DMEM (Gibco)

2% (w/v) $NaHCO_3$

H_2O

2.2.2. Protein Analysis

2.2.2.1. Protein preparation

Proteins were isolated from cells and tissues. For cell lysates, cells were washed with PBS and either directly scraped from the plate or suspended in RIPA buffer containing protease inhibitors (200-664-3, Sigma-Aldrich). After O/N lysis at 4 °C lysates were centrifuged (16000 x g, 4 °C, 10 min). Supernatants were transferred to a new tube and protein concentration was detected via Pierce® BCA™ Protein assay (23227, Thermo Fisher Scientific). For concentration determination a BSA standard curve with defined protein concentrations (0.1-10 µg/µl) was used and extinction was measured at 595 nm in the Victor^3 1420 Multilabel Counter (Perkin Elmer). For protein isolation from whole skin and day 5 wounds, biopsies (8 mm diameter) were carefully cut into small pieces on ice. 400 µl PBS containing protease inhibitor (1 ml inhibitor/ 0.2 g lysates; P2714, Sigma-Aldrich) were added. Day 14 wound lysates were prepared from 2x 50 µm cryosections in 200 µl extraction buffer I with protease inhibitors. Metal beads (FR0120, Retsch, Haan, Germany) were added and all tissues were homogenized in the Mixer Mill MM300 (Retsch) at 30 Hz for 3 min. Triton X-100 was added to final concentration of 1% (v/v). Day 5 samples were frozen at -80 °C for 2 h and carefully thawed on ice. Day 14 samples were incubated at 4 °C O/N, rotating. Lysates were

centrifuged (16000 x g, 4 °C, 10 min), supernatants were transferred to a new tube and protein concentrations determined using Pierce® BCA™.

Proteins were concentrated using the trichloroacetic acid (TCA) method. Triton X-100 was added to samples to final concentration of 1% (v/v) and 55% (w/v) TCA was added to final concentration of 10%. Samples were vortexed and incubated on ice. After centrifugation (16000 x g, 4 °C, 10 min) pellets were washed three times with ice cold acetone. Pellets were air dried for 5 min at RT and suspended in 20 µl 1 x Sample Buffer (SB) (with β-mercaptoethanol if reduction was required). Reduced protein samples were heated at 95 °C for 5 min, centrifuged and kept on ice before use.

5x sample buffer:

60 mM Tris-HCl

25% (v/v) Glycerol

2% (w/v) SDS

0.1% (v/v) bromphenol blue

5% (v/v) β-mercaptoethanol)

Extraction buffer I:

150 mM NaCl

50 mM Tris-Base

pH 7.4

2.2.2.2. SDS-PAGE and Western Blot

Proteins in supernatants, cell and tissue lysates were resolved by SDS-PAGE and analyzed by immunoblot. Equal amounts of protein under reducing conditions were loaded onto an 8 or 10% SDS-PAGE and separated with 30-40 mA per gel (midi gel). Molecular weight markers for proteins PageRuler™ Plus prestained Protein Ladder (26620) and PageRuler™ Unstained Protein Ladder (26614) were from Thermo Fisher Scientific (Darmstadt, Germany).

Afterwards, proteins were transferred onto a 0.45 µm Hyperbond-C Super™ nitrocellulose membrane (GE Healthcare, Darmstadt, Germany) in a semi-dry blotting system (30 V, 2 h). Ponceau S staining (Sigma-Aldrich) was used to control transfer efficiency. After blocking in 5% (w/v) skimmed milk powder in 0.5% (v/v) PBS-Tween® for 1 h membranes were incubated in primary antibody in blocking buffer O/N at 4 °C. All antibodies used for immunoblot detection are listed in table 3. Membranes were washed with 0.5% (v/v) PBS-Tween® three times for 10 min before incubation with secondary HRP-conjugated antibodies (listed in table 3) in blocking buffer at RT for 1 h. After washing, bound antibodies were detected by CL-Xposure™ Films (34091, Thermo Fisher Scientific) using Pierce™ ECL Western Blotting Substrate (32106, Thermo Fisher Scientific).

Table 3: List of primary and secondary antibodies used for detection on immunoblot including dilution, company and order number

Antibody	Dilution	Company	Order Number
Mouse anti-Actin	1:2000	MP Biomedicals, Eschwege, Germany	2928H
Rabbit anti- mou/hum αSMA	1:2000	Abcam, Berlin, Germany	ab5694
Mouse anti-eNOS	1:500	BD Bioscience, Heidelberg, Germany	610297
Rabbit anti-MMP3	1:1000	Abcam	ab52915
Goat anti-VE-cadherin	1:1000	R&D Systems	AF1002
Rabbit anti-Mouse HRP	1:2000	Dako/Agilent, Waldbronn, Germany	P0260
Swine anti-Rab HRP	1:2000	Dako/Agilent	P0217
Rabbit anti-Goat HRP	1:2000	Dako/Agilent	P0449

2.2.2.3. In vitro enzymatic assays

Cleavage of VE-cadherin by MMP14 and MMP2 was tested *in vitro*. To this end, 50 ng/µl recombinant human MMP2 (902-MPN, R&D Systems) were previously activated by incubation with 1 mM APMA (A9563, Sigma-Aldrich) in MMP2 activation buffer at 37 °C for 1 h. Recombinant human MMP14 (100 ng/µl) (918-MPN, R&D Systems) was activated with 0.1 µg/ml trypsin in MMP14 activation buffer for 1 h at 37 °C followed by trypsin inactivation with 1 mM pefablock (31682.01, Serva) for 15 min at RT. Active recombinant MMP14 was diluted to a working concentration of 50 ng/µl by adding MMP14 assay buffer. Then, 1 µg recombinant VE-cadherin (1002-VE , R&D Systems) was incubated with 100 ng active MMP2 or MMP14 in the respective assay buffer for 2 h at 37 °C. Samples were separated by SDS-PAGE and visualized by Pierce^{TM} Silver Stain Kit (24612, Thermo Fisher Scientific) according to the Kits manual.

MMP2 activation buffer:

100 mM Tris

10 mM CaCl$_2$

150 mM NaCl

0.05% (w/v) Brij-35

pH 8

MMP2 assay buffer:

50 mM Tris

10 mM CaCl$_2$

150 mM NaCl

0.05% (v/v) Brij-35

pH 7.5

MMP14 activation buffer:

50 mM Tris

0.15 M NaCl

10 mM CaCl$_2$

5 µM ZnCl$_2$,

0.05% (w/v) Brij-35

pH 7.5

MMP14 assay buffer:

50 mM Tris

3 mM CaCl$_2$

1 µM ZnCl$_2$

pH 8.5

2.2.2.4. TGFβ1 Quantikine ELISA Kit

Protein lysates (isolation was described in section 2.2.2.1) were analyzed using the TGFβ1 Quantikine ELISA Kit (MB100B, R&D Systems). For each sample, 50 µg protein were used to a final volume of 50 µl with H$_2$O. All TGFβ1 was activated by adding 10 µl 1 N HCl and incubation at RT for 10 min. The acid was neutralized with 10 µl 1.2 N NaOH/0.5 M HEPES before starting the assay and samples were prepared according to the assay's manual. The ELISA signals, detected by the optical density of the HRP reaction were measured at 450 nm and 570 nm for background corrections using the Victor[3] 1420 Multilabel Counter (Perkin Elmer).

2.2.2.5. Proteome Profiler™ Mouse Angiogenesis Array Kit

Tissue lysates (section 2.2.2.1) were analyzed using the Proteome Profiler™ Mouse Angiogenesis Array Kit (ARY015, R&D Systems). The Array was performed according to the assay manual using 100 µg protein of each animal and pooling lysates from three animals per genotype per membrane. Membrane signals were detected on CL-Xposure™ Films using the Pierce™ ECL Western Blotting Substrate.

2.2.2.6. Immunodetection on tissue and cells

Tissue preparation

Mouse tissue from tumors, wounds and back skin was previously prepared and either embedded in optimal-cutting-temperature (OCT) compound (Sakura Finetek) and frozen on dry ice for cryosections or fixed in 4% PFA at 4 °C O/N and embedded in paraffin. Formalin fixed tissues were kept in PBS afterwards and dehydrated and stored in liquid paraffin in an automated tissue-processing machine (Autotechnikon, Shandon, Pittsburgh, PA, United States) in the

Histology Laboratory of the Dermatology Department. Cryosections were cut at 8 mm on poly lysine glass slides (Thermo Scientific), paraffin sections were 6 mm.

Human material was provided by the Central Project (Z4) of the SFB829. Human material was collected according to the study protocol conformed to the ethical guidelines of the 1975 Declaration of Helsinki and was approved by the Ethics Committee of the Medical Faculty of the University of Cologne (Registration No. 08-144). Informed consent has been obtained.

Immunohistochemistry

Paraffin sections were fixed with ice cold acetone (8 min), blocked with 5% (w/v) BSA in TBS-Tween® (0.05% v/v) and incubated with the primary antibodies at 4 °C O/N. Afterwards, sections were washed with TBS, incubated with a biotinylated secondary antibody (polyLink, DCS Innovative Diagnostik-Systeme, Hamburg, Germany) for 20 min at RT. Sections were washed before incubation with an Alkaline Phosphatase polymer conjugate (DCS Innovative Diagnostik-Systeme) for 20 min at RT. After extensive washes, the phosphatase substrate Fast Red Substrate chromogene (HK182-5KE, XBioGenex, Fremont, CA, United States) was added. The reaction was stopped with A. dest. nuclei were stained with hematoxylin and 'blued' in lukewarm water. Sections were covered with glass cover slides using Shandon™ Immu-Mount™. Immunohistochemistry stainings were analyzed using the Leica DM4000 B microscope (Leica) equipped with the Diskus software (version 4.50.1638, Diskus, Königswinter, Germany).

Immunofluorescence

Cryosections were fixed with ice cold acetone (8 min) or PFA (for 10 min). Cells grown on coverslips were fixed with ice cold acetone for 5 min (ECs) or ice cold acetone/MeOH (1:1) for 10 min (fibroblasts). After fixing with PFA, sections were permeabilized with 0.05% (v/v) PBS-Triton X-100 at RT for 15 min. Samples were blocked with 10% (v/v) NGS (X0907, Dako/Agilent) or 10% (w/v) BSA in 0.05% (v/v) PBS-Tween® at RT for 1 h before adding primary antibodies (table 4) diluted in 1% blocking solution. Incubation followed at 4 °C O/N in a humidified chamber. Sections or coverslips were washed with PBS and incubated with fluorescence-labeled secondary antibodies (table 4) in 1% blocking solution at RT for 1 h. 4,6-diamidino-2-phenylinodole (DAPI, 1 mg/ml, D9542, Sigma-Aldrich) was used for nuclei visualization. Sections were washed, covered with glass slides (Thermo Scientific) using Shandon™ Immu-Mount™ (9990412, Thermo Fisher Scientific) and stored in the dark at 4 °C. Coverslips were washed and mounted onto microscopy slides with Shandon™ Immu-Mount™.

Microscopic analysis was performed using the Keyence Microscope BZ-9000 (Keyence, Neu-Isenburg, Germany) equipped with the BZ-II Analyzer and BZ-II Viewer software (version 2.2, Keyence) and quantitative analysis followed using the ImageJ software (version 1.53e, Java/Oracle, Munich, Germany).

Cornea stainings

For staining of corneas mice were sacrificed via cervical dislocation and eyes were removed by gentle pulling using bent tweezers. Eyes were fixed in ice cold acetone (20 min) and washed several times with PBS. The cornea was isolated by carefully cutting along the circumference of the limbus with a microscissor upon punching a small whole into the posterior limbus with a 20 G cannula. The isolated cornea was permeabilized for 10 min with 0.5% (w/v) saponin/10% (v/v) NGS in PBS^{T++} before blocking in 2% (w/v) BSA in PBS^{T++} for 2 h. Incubation with primary antibodies or the DyLight® 594 *lycopersicon esculemtum* (tomato) Lectin (20 µg/µl, Vector Laboratories, Burlingame, CA, United States) was performed in PBS^{T++} at 4 °C O/N. The cornea was washed 3x with PBS^{T++} and incubated with the secondary antibody at RT for 1 h. Afterwards three washes in PBS, cornea were placed on a glass slide and flattened by making 3 incisions and mounted with Immu-Mount.

Table 4: List of primary and secondary antibodies used for immunofluorescence detection including dilution and fixative (Ac or PFA), company and order number. Ac: acetone fixation

Antibody	Dilution (Fixative)	Company	Order Number
αSMA Cy3	1:200 (Ac, 1% PFA)	Sigma-Aldrich	C6198
Rabbit anti-CD31	1:1000 (Ac)	Abcam	ab28364
Rat anti-CD31	1:1000 (Ac)	BD Bioscience	557355
Rat anti-CD31	1:150 (cornea, Ac)	BD Bioscience	550274
Rabbit anti-c-kit	1:100 (Ac)	Cell Signaling	D13A2
Rabbit anti-cleaved Caspase 3	1:100 (1% PFA)	Cell Signaling	9661-S
Rabbit anti-Collagen type IV	1:200 (Ac)	Cedarlane, BIOZOL Diagnostica Vertrieb GmbH, Eching, Germany	CL50451AP
Mouse anti-eNOS	1:100 (Ac)	BD Bioscience	610297
Rat anti-F4/80	1:100 (Ac)	Serotec/Bio-Rad	MCA497R
Rabbit anti-HSP47	1:100 (Ac)	Abcam	ab109117

Rabbit anti-K14	1:1000 (Ac)	Covence/Biolegends, London, United Kingdom	PRB-155P
Rabbit anti-Ki67	1:100 (PFA)	Abcam	ab15580
Rabbit anti-LYVE-1	1:1000 (sections); 1:150 (cornea) (Ac)	Abcam	ab14917
Rabbit anti-MMP3 AF488	1:100 (Ac)	Abcam	ab194980
Mouse anti-MMP14 LEM-2	1:200 (Ac)	Chemicon, Merck	MAB3328
Rabbit anti-NG2	1:200 (Ac)	Millipore/Merck	AB5320
Rabbit anti-nidogen-1	1:1000 (Ac)	Kindly provided by AG Nischt	
Rat anti-PDGFRβ	1:100 (Ac)	eBioscience, Darmstadt, Germany	14-1402
Rabbit anti-Perlecan	1:600 (Ac)	Kindly provided by AG Nischt	
Rabbit anti-pSmad2	1:200 (PFA)	Invitrogen	44-244G
Rat anti-VE-cadherin/ CD144	1:100 (Ac)	BD Bioscience	555289
Rat anti-ZO-1	1:2 (Ac)	Hybridoma, kindly provided from AG Niessen	
Alexa Goat anti-Rab 594	1:1000	Invitrogen, Darmstadt, Germany	A11037
Alexa Goat anti-Rat 488	1:1000	Invitrogen	A11006
Alexa Goat anti-Rab 488	1:1000	Invitrogen	A11034
Alexa Goat anti-Rat 594	1:1000	Invitrogen	A11007
Alexa Donkey anti-Goat 594	1:1000	Invitrogen	A11058
Alexa Goat anti-Mouse 594	1:1000	Invitrogen	A11032

PBS^{T++}:
0.2% (v/v) Triton X-100
0.1 mM $CaCl_2$
1 mM $MgCl_2$
in PBS

2.2.2.7. Histochemical stainings

H&E

For analysis of tissue structure and morphology paraffin embedded or cryosections were stained with hematoxylin and eosin (H&E). Prior staining paraffin sections were dewaxed in xylol for 20 min and rehydrated in a decreasing alcohol row (100% EtOH, 95% (v/v) EtOH and 70% (v/v) EtOH, 1 min each). Both cryo- and paraffin sections were incubated in Meyers haematoxylin (3801582E, Leica) for 5 min. Sections were washed 3x with lukewarm tab water and incubated in eosin (3801590BBE, Leica) for 5 sec. After dehydration in an ascending alcohol row (70% (v/v) EtOH, 95% (v/v) EtOH, 100% EtOH and 2x xylol for 1 min each) sections were mounted with GLC^{TM} mounting medium (1408, Sakura Finetek).

Picrosirius red staining

Collagens were visualized by Picrosirius red staining. Therefore, dewaxed paraffin sections were stained with hematoxylin for 5 min for nuclei visualization. After washing with lukewarm tab water sections were stained for 1 h in a Picrosirius red solution. Sections were washed twice with 0.5% (v/v) acetic acid and dehydrated in an ascending alcohol. Sections were mounted in the xylol-based GLC^{TM} medium. Microscopy was performed using the Leica DM4000 B microscope. The Picrosirius Red staining was documented by light microscopy and under polarized light. Image analysis of overall and fibrillary collagen was performed using the ImageJ software. Courtoy *et al*., described a quantitative analysis method that was used for analysis of fibrillary collagen in images taken with polarized light [435]. Therefore, picture were converted into a binary format and percent area was determined.

Picrosirius red solution:
0.1% Direct Red 80 (Sigma-Aldrich, 365548-5G)
in picric acid solution (Sigma-Aldrich, 197378-100G)

2.2.3. Nucleic acid analysis

2.2.3.1 RNA isolation

RNA was isolated from primary cells or skin tissue. Cells were washed with PBS, RNAzol^{TM} B (18 µl/cm^2, WAK-Chemie, Steinbach, Germany) was added and incubated on ice for 5 min. Cells were scraped, homogenized and DNA sheared through a 26 Gauges needle and transferred to a tube. RNA was further purified by adding chloroform (1/5 volume), shortly shaking and

incubating on ice for 3 min followed by centrifugation (16000 x g, 4 °C for 15 min). The aqueous phase was transferred to a fresh tube, the same volume ice cold isopropanol was added to precipitate RNA at -20 °C O/N. Precipitated RNA was centrifuged (16000 x g, 4 °C for 10 min), the pellet washed three times with ice cold 70% (v/v) EtOH, air dried on ice and suspended in nuclease free H_2O.

For RNA isolation from mouse tissues, skin, lungs and lymph nodes were stored in RNA Later[TM] RNA stabilization Reagent (Qiagen, Hilden, Germany) at -20 °C. For RNA isolation from mouse skin the Qiagen RNeasy® Fibrous Tissue Mini Kit (74704, Qiagen) was used. Skins were cut into small pieces using scalpels, transferred into a 2 ml tube and supplemented with 300 µl RLT buffer from the kit with 0.15 M β-mercaptoethanol and a sterile metal bead. Tissue was homogenized in the MixerMill (30 Hz, 3 min), 590 µl RNase free H_2O and 10 µl proteinase K were added, mixed and incubated at 55 °C for 10 min. After centrifugation to remove cell debris (10.000 x g, 3 min) the supernatant was transferred to a fresh tube and supplemented with 0.5 volumes 100% EtOH for clearance of the mix. The whole volume was added to an RNeasy Mini column and further processed according to the Kit's manual. RNA from organs was prepared by mincing the tissue with scalpel blades and homogenizing in RNAzol[TM] (1 ml/2 ml tube) using the Mixer Mill MM 300 (30 Hz, 3 min). Following extraction was via chloroform precipitation as performed for cells.

Quality of the RNA was controlled by electrophoretic analysis on a 1% (w/v) agarose-TBE gel with RedSafe[TM] and concentration was measured using the NanoDrop[TM] 2000 Spectrometer (Thermo Scientific) equipped with the NanoDrop 2000 software (version 1.6.198, Thermo Scientific).

2.2.3.2. Reverse transcription and semi-quantitative PCR

Reverse transcription of RNA into cDNA was performed using the iScript[TM] cDNA Synthesis Kit (1708891, Bio-Rad). Reactions were performed using in 20 µl volumes with 1 µg RNA, 4 µl 5x iScript Reaction Mix and 1 µl iScript Reverse Transcriptase. Transcription was performed using the following protocol: 25 °C for 5 min, 46 °C for 20 min, 95 °C for 1 min. Quality of cDNA was controlled by amplification of the house keeping gene S26 [436] by semi-quantitative PCR using 1 µl cDNA. Further, expression of GFP in lung and lymph nodes was analyzed by semi-quantitative PCR using the T3000 Thermocycler (Biometra, Göttingen, Germany). Primers and PCR reaction protocols are listed in table 5 and 6, respectively. PCR products were analyzed by electrophoresis in a 1.8% (w/v) agarose-gel in TBE buffer

containing RedSafe^{TM} and visualized using Eagle eye UV transillumination. The DNA marker (100 bp DNA ladder, N3231S) was from New England Biolabs GmbH (Frankfurt am Main, Germany).

Table 5: List of primers used for semi-quantitative PCR including sequences, annealing temperature, required PCR cycles and product size.

Gene	Primer (forward/reverse)	Product size (bp)
mS26	5' AATGTGCAGCCCATTCGCTG 3' 5' CTTCCGTCCTTACAAAACGG 3'	324
hS26	5′ CCGGTCCGTGCCTCCAAGATGACAA 3′ 5′ CCTTGGGCACGCATCGGGCA 3′	115
GFP	5' ACC CCG ACC ACA TGA AGC 3' 5' CGT TGG GGT CTT TGC TCA GGG 3'	417

Table 6: PCR programs used for semi-quantitative PCR.

	mS26	hS26	GFP
Initial denaturation	94 °C, 2 min	94 °C, 2 min	94 °C, 2 min
Denaturation	94 °C, 45 sec	94 °C, 45 sec	94 °C, 1 min
Primer annealing	56 °C, 45 sec	67 °C, 45 sec	68 °C, 1 min
Elongation	72 °C, 45 sec	72 °C, 45 sec	72 °C, 1 min
Cycle number	30	30	38
Elongation	72 °C, 5 min	72 °C, 5 min	72 °C, 5 min

2.2.3.3. Quantitative real-time polymerase chain reaction (qPCR)

Expression of various genes was analyzed by quantitative PCR. Each gene (primers and sequences are listed in table 7) was measured in triplicates per sample including a water control and S26 as housekeeping gene. Quantification by the comparative $2^{-\Delta\Delta Ct}$ method [437] was performed using a QuantStudio™ 5 Real-Time PCR System equipped with the QuantStudio^{TM} Design & Analysis software (version vl.1.4.3, Applied Biosystems distributed by Thermo Scientific).

Table 7: List of primer used for qPCR including sequence and product size.

Gene	Protein	Primer sequence (forward/reverse)

Human *MMP14*	MMP14	5' ACCGACAAGATTGATGCTGC 3' 5' CATCGCTGCCCATGAATGAC 3'
Human *CDH5*	VE-cadherin	5' AAGCGTGAGTCGCAAGAATG 3' 5' TCTCCAGGTTTTCGCCAGTG 3'
Human *S26*	S26	5′ CCGGTCCGTGCCTCCAAGATGACAA 3′ 5′ CCTTGGGCACGCATCGGGCA 3′
Mouse *Nos3*	eNOS	5' CCTTCCGCTACCAGCCAGA 3' 5' CAGAGATCTTCACTGCATTGGCTA 3'
Mouse *Acta2*	αSMA	5' CAGCGGGCATCCACGAA 3' 5' CCCACCGATCCAGACAGA 3'
Mouse *Mmp3*	MMP3	5' TCCCAGGAAGATAGCTGAGG 3' 5' CAACTGCGAAGATCCACTGA 3'
Mouse *S26*	S26	5' AATGTGCAGCCCATTCGCTG 3' 5' CTTCCGTCCTTACAAAACGG 3'
Mouse *Tgfb1*	TGFβ1	5' CAACGCCATCTATGAGAAAACC 3' 5' AAGCCCTGTATTCCGTCTCC 3'
Mouse *TgfbR1*	TGFβR1	5' ATCGGCAATAGCTGGTTTT 3' 5' GCCATAACCGCACTGTC 3'
Mouse *Cdh5*	VE-cadherin	5' ACGGACAAGATCAGCTCCTC 3' 5' TCTCTTCATCGATGTGCATT 3'

qPCR mix per reaction:

1 µl cDNA

1 µl forward primer

1 µl reverse primer

10 µl GoTaq® qPCR master mix (A600A, Promega)

0.2 µl C&R Reference Dye (C541A, Promega)

6.8 µl H_2O

2.2.3.4. DNA isolation and genotyping PCR
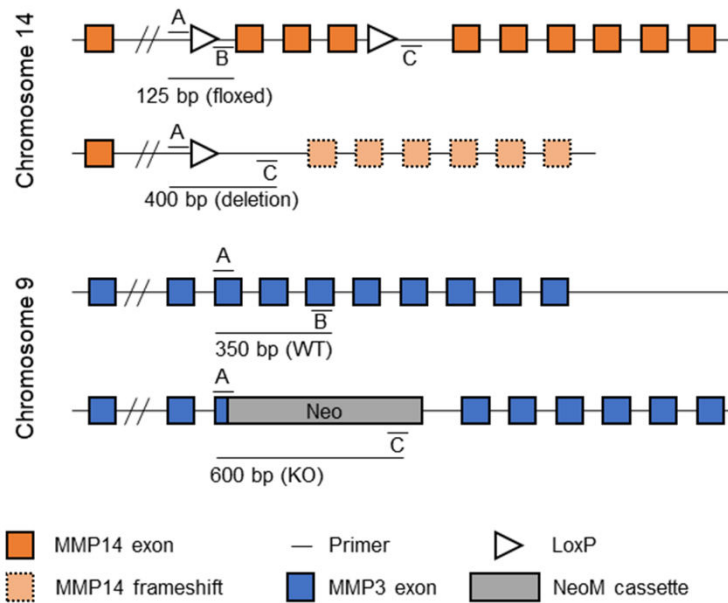
Figure 7: Schematic representation of the genotyping used to detect deletion of MMP14 and MMP3. Schematics show gene exons, primer binding sites, inserted LoxP sites in the MMP14 gene and the NeoM cassette inserted in the MMP3 gene. Primers were used to detect the LoxP sequence (MMP14 primers A & B), the MMP14 deletion (MMP14 primers A & C), the wildtype MMP3 (MMP3 primers A & B) and the MMP3 knockout (MMP3 primers A & C).

Genomic DNA was isolated from tail or ear biopsies by lysis in 300 µl DNA lysis buffer with 1 µl proteinase K (20 mg/ml, AM2548, Ambion) at 56 °C, shaking at 600 rpm O/N. After centrifugation (16000 x g, RT, 10 min) supernatants were transferred to a new tube and DNA precipitated by addition of 500 µl 100% EtOH. DNA was pelleted by centrifugation (16000 x g, RT, 10 min) and washed twice with 70% (v/v) EtOH, Air dried DNA was suspended in 50 µl TE (Tris-EDTA) buffer. Genotyping PCR was performed in 25 µl reaction volume using a REDtag® ReadyMix™ PCR reaction mix (12.5 µl) (R2523-100RXN, Sigma-Aldrich), forward and reverse primers (0.5 µl each, 100 ng/µl), H_2O and genomic DNA (0.5-1 µl). Primers are listed in table 8. Tie2-Cre PCR required additional 0.1 mM dNTPs for successful elongation (Roche, Karlsruhe, Germany). MMP3 genotyping PCR was performed with Promega Master Mix (2x) (M7502, Promega).

PCR products were analyzed on 1.8% agarose gels (Bio-Budget Technologies GmbH, Krefeld, Germany) with RedSafe™ (21141, iNtRON, Burlington, MA, United States) in TBE buffer. Signals were visualized using an Eagle Eye UV transilluminator (Bio-Budget).

Table 8: Primers used for PCR.

Gene	Primer (forward/reverse)	Product size (bp)
MMP14 fl/wt PCR	5' GAGGCAGAGGCAGAACAAGC 3'	WT: 165
	5' GAGCATCAGAAAGTTGAGAGG 3'	KO: 285
Tie2Cre	5' TAGCGCCGTAAATCAAT 3'	400
	5' GACCAGGTTCGTTCACTCA 3'	
MMP14Del	5' GAGGCAGAGGCAGAACAAGC 3'	400
	5' CCACCAAGAAGATGTCATTCC 3'	
MMP3	5' TTGCCAAGACAGAGTGTGGATTC 3'	WT: 350
	5' TTCCTCGTGCTTTACGGTATCG 3'	KO: 600
	5' GTCCATCGTTCATCATCGTCAA 3'	
α2Cre	5' GTCCAATTTACTGACCGTACAC 3'	350
	5' CTGTCACTTGGTCGTGGCAGC 3'	

Table 9: PCR programs.

	MMP14 fl/wt	Tie2Cre	α2Cre	MMP14Del	MMP3
Initial denaturation	94 °C, 5 min	94 °C, 3 min	94 °C, 5 min	94 °C, 5 min	94 °C, 5 min
Denaturation	94 °C, 1 min	94 °C, 1 min	94 °C, 1 min	94 °C, 30 sec	94 °C, 1 min
Annealing	60 °C, 1 min	50 °C, 1 min	60 °C, 1 min	60 °C, 30 sec	65 °C, 1 min
Elongation	72 °C, 1 min	65 °C, 1 min	72 °C, 1 min	72 °C, 1 min	72 °C, 1 min
Cycle number	35	30	35	35	35
Final Elongation	72 °C, 10 min	65 °C, 5 min	72 °C, 5 min	72 °C, 5 min	72 °C, 10 min

DNA lysis buffer:

0.2% (w/v) SDS

0.1 M Tris/HCl

0.005 M EDTA

0.2 M NaCl

pH 7.5

Tris-EDTA (TE) buffer:

1 mM EDTA

10 mM Tris

2.2.4. Animal work

2.2.4.1. Mouse lines and cell type specific MMP14 deletion

All mouse lines used were on C57BL/6N background and floxed MMP14 gene (MMP14$^{fl/fl}$) allowing Cre-recombinase mediated deletion of MMP14 exon 2-4 [380]. Tissue specific inactivation of MMP14 was obtained by crossing mice with the floxed MMP14 gene and mice carrying the Cre recombinase under the control of cell-specific promoters.

For endothelial cell-specific deletion we used mice in which the Cre-recombinase is expressed under the control of the Tie2 promotor (Figure 8) [390-392]. For dermal fibroblasts specific MMP14 inactivation we crossed MMP14 floxed mice with mice carrying the tamoxifen-inducible Cre–ERT fusion transgene under the control of a minimal collagen a2 type I promoter and enhancer driving fibroblast-specific and inducible Cre expression (MMP14$^{Sf-/-}$) [251, 393, 394] (see section 2.2.4.2).

Double deficiency of MMP3 in addition to fibroblast-specific loss of MMP14 was attained by crossing MMP14$^{Sf-/-}$ mice with MMP3$^{-/-}$ mice (described by Mudgett *et al.* [425]*,* kindly provided by Barbara Fingleton, Vanderbilt University). MMP3 single knockouts were crossed back to a C57BL/6N background until F7 before generating MMP3$^{-/-}$/MMP14$^{Sf-/-}$ double deficient mice.
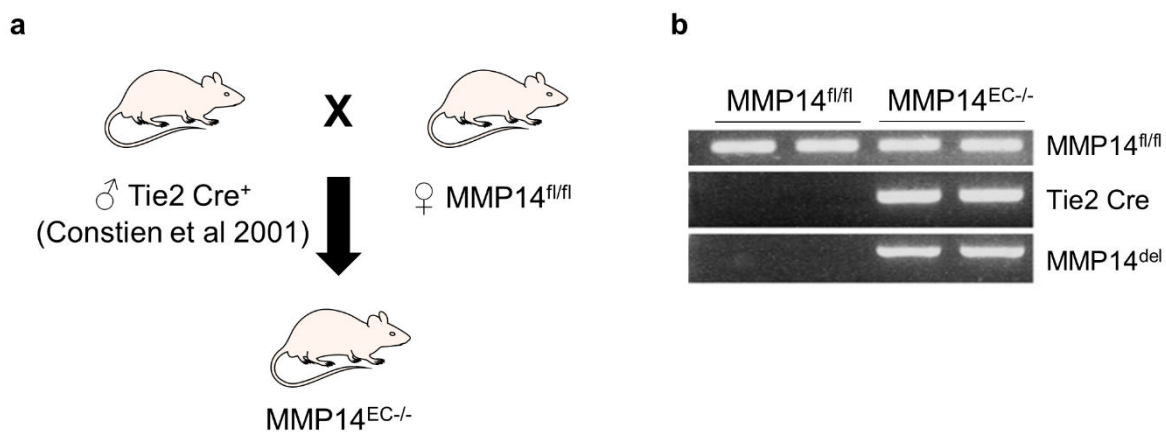
Figure 8: Generation of MMP14$^{EC-/-}$ mice. a) Breeding scheme for MMP14$^{EC-/-}$ mice. Tie2-Cre positive males were paired with MMP14$^{fl/fl}$ females. **b)** Genotyping PCR of MMP14$^{fl/fl}$ and MMP14$^{EC-/-}$ mice detecting floxed MMP14 genes, Tie2-Cre and deletion of MMP14 (MMP14^{del}).

Animals were housed under specific pathogen-free conditions in a 12-/12-h light/dark cycle with free access to food and fresh water ad libitum. All animal experiments were performed in compliance with German Regulations for Welfare of Laboratory Animals and were approved by the Regierungspräsidium Köln, Germany (NRW authorization AZ84-02.04.2016.A013,

AZ84-02.04.2016.A012, AZ84-02.05.40.17.073 and AZ 84-02.05.40.16.039). Male and female animals were kept separately with 2-5 animals per cage unless in breeding cages. Pups are weaned, ear marked three weeks after birth.

2.2.4.2. Tamoxifen treatment

Cre-recombinase positive animals and controls were fed with 400 mg/mg tamoxifen pellets (Haarlan, Venray, Netherlands) starting at P28 for a period of 5 weeks. Additional 5 weeks were given for full development of a fibrosis-like phenotype [251]. This time point is defined as T2 and is the starting point for further experiments. The time course of tamoxifen treatment is shown in Figure 9.

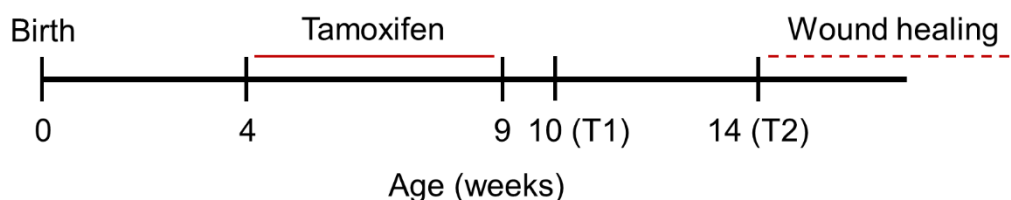**Figure 9: Time points of tamoxifen treatment for Col 1α2 Cre^{ERT} animals.** Mice were fed with tamoxifen pellets from week 4 to week 9 of age. Time point T1 is defined as 1 week after tamoxifen treatment (10 week old mice). At T2 (14 weeks) mice developed the complete phenotype and had a complete deletion of MMP14 in isolated fibroblasts [251]. The T2 marked the start of wound healing experiments.

2.2.4.3. B16F1 melanoma grafting and cisplatin treatment

To analyze the function of endothelial cell-derived MMP14 in tumor growth melanoma were grafted in the right flank of MMP14$^{EC-/-}$ and MMP14$^{fl/fl}$ mice. Mice were used at the age of 8-10 weeks. Prior melanoma cell injection the right flank was shaved with the Contura HS61 razor (Wella Professionals, Darmstadt, Germany), and 0.5 x 10^6 B16F1 GFP melanoma cells [431] in 20 µl PBS were injected intradermal using a G27 (0.45 x 28 mm) cannula. For treatment with cisplatin [438-440], when first tumors were visible, mice received one-time dose with 1 mg/100g body weight cisplatin (Sigma-Aldrich) or 0.9% NaCl (2.5 mg/ml stock solution, Berlin-Chemie AG, Berlin, Germany) as control on day 5 via intra-peritoneal injection. Tumor growth was followed over time and tumor size measured every other day using a Caliper (Mitutoyo Corporation, Neuss, Germany). The experiment was terminated when first tumors appeared to be close to rupturing (Day 11) and 15 min prior death mice received an intravenous injection of 0.1 ml FITC-dextran (20 kDa) (Fluorescein isothiocyanate-dextran mol wt 20000, Sigma-Aldrich). Tumors, lung and lymph nodes were isolated, bisected and either

directly frozen in optimal-cutting-temperature (OCT) compound (Sakura Finetek) on dry ice or fixed in 4% formalin at 4 °C O/N and later embedded in paraffin.

2.2.4.4. Wound healing

Prior wounding, mice were anesthetized by intra-peritoneal injection with 100 µl/10 g body weight of Ketavet®/rompun. Eyes were treated with bepanthen crème (Veet, Heidelberg, Germany) to avoid drying. Backs were shaved and hair completely removed using Veet depilation crème (Veet). Before wounding the skin was cleaned with PBS. Two 6 mm full-thickness excision wounds were generated using disposable biopsy punches (6 mm, Pfm medical AG, Köln, Germany), removing skin and *panniculus carnosus*. Wound closure was recorded over time with camera for analysis of wound closure kinetics. Mice were sacrificed at different time points using CO_2. Wounds were isolated including the epithelial margin, bisected in caudocranial direction and tissues either fixed in formalin and embedded in paraffin or embedded in OCT compound and frozen.

Ketavet/rompun:
10% Ketavet® (v/w) (100 mg/ml, Pfizer, Berlin, Germany)
5% (v/w) rompun (2%, Bayer Vital GmbH, Leverkusen, Germany) in
0.9% NaCl

2.2.5. Statistical analysis

All statistical analysis were performed using GraphPad Prism 7 (GraphPad Software, version 7.05, La Jolla, CA, United States). Multiple comparisons were performed using ANOVA, two-tailed Student t-test was used for other statistical analysis. Significance was regarded for $p < 0.05$.

3. Results

3.1. Role of EC-MMP14 in tumor vessels

3.1.1. Corneal vascularization is unaffected by MMP14 loss

Multiple studies including in mice with global MMP14 knockout demonstrated MMP14 function in angiogenic processes [252, 361]. In order to identify the specific role of the protease in ECs, transgenic mice with MMP14 deletion in ECs were generated. These developed and bred normally and only minor defects regarding skull shape and suture closure were observed [390].
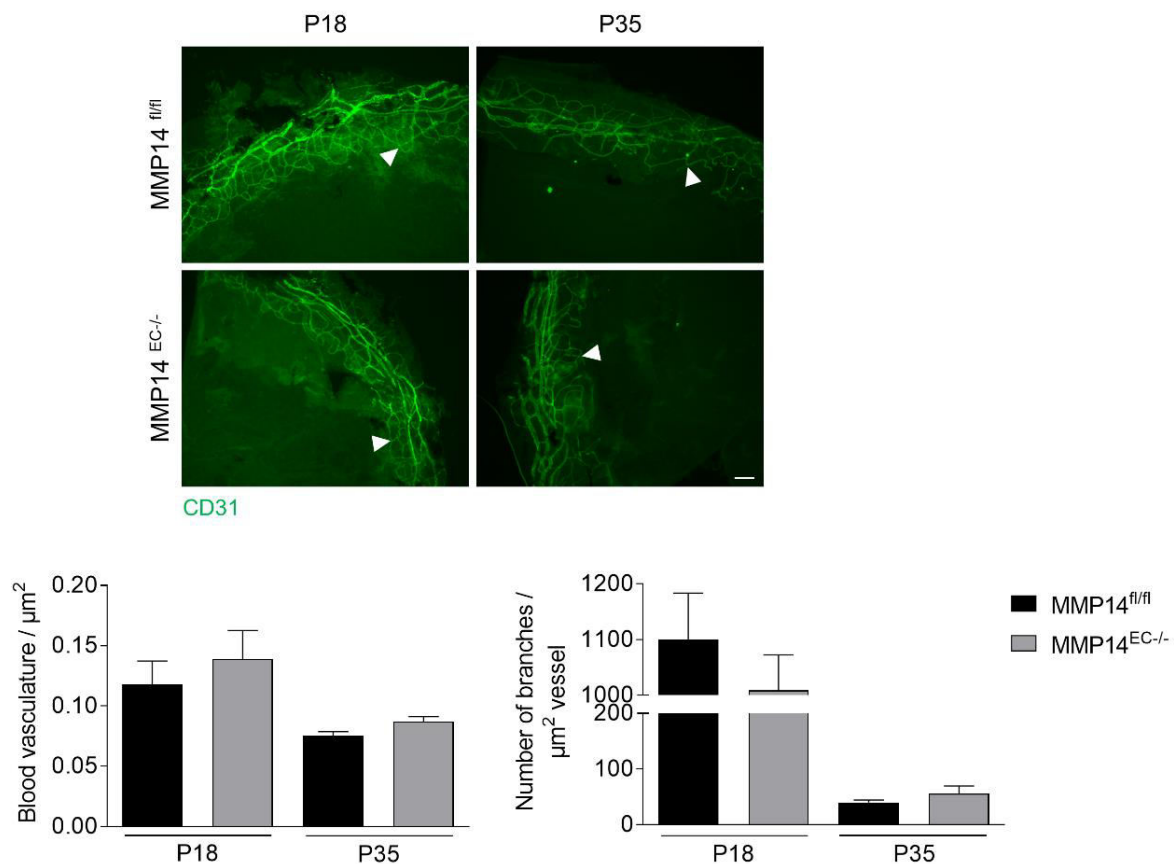
Figure 10: Corneal blood vasculature is normal in MMP14$^{EC-/-}$ mice. Immunofluorescence staining for the blood vessel marker CD31 (green) in P18 and P35 corneas of MMP14$^{EC-/-}$ and control mice. Vascular density and number of branching points were quantitatively analyzed. White arrows indicate branching points. Mean ± SD; n=3; Scale: 200 μm.

However, the vascular network in the skin was not affected in MMP14$^{EC-/-}$ mice. But, skin vasculature was analyzed in adulthood and possible early defects could have been compensated over time. Indeed, mice with global MMP14 deletion showed angiogenic defects in development [361]. Aiming to identify EC-MMP14 involvement in development, a study using a Tie1-Cre-driven deletion model identified defects in corneal blood and lymph vessel

angiogenesis [389]. Here they identified MMP14 as regulator of lymphatic vasculature through its proteolytic functions towards LYVE-1 [389].

To investigate whether these alterations also occurred in our Tie2-Cre-driven model, corneas were isolated from MMP14$^{EC-/-}$ and control mice at P18 and P35, as in the study by Wong and colleagues [389], and stained for the blood vessel marker CD31 (Figure 10). Blood vessel density (left graph) and number of branching points (right graph) were analyzed, but both were similar in the two genotypes at both time points. Comparing the two time points showed a reduction in density and branching points at P35 compared to P18, indicating regression of vessels as previously described [441, 442]. Thus, loss of EC-derived MMP14 does not affect corneal blood vessel angiogenesis.

Figure 11: Lymph vessel density and sprouting in P18 corneas. Immunofluorescence staining for lymphatic vessels (LYVE-1, green) and nuclei (DAPI, blue) in cornea of P18 mice. Lymphatic density (left graph), branching points and sprouts (right graph) were analyzed. White arrows indicate branching points (middle panel) and sprouts (right panel). Mean ± SD; n=4; Scale: 200 μm (left pictures), 50 μm (middle), 20 μm (right).

Additionally, we also analyzed whether lymphatic angiogenesis might be affected in MMP14$^{EC-/-}$ mice similar to the observations made in the Tie1-Cre-driven model [389], as Tie2 is also expressed in lymphatic ECs [443]. Again, P18 and P35 corneas were immunofluorescence stained for the lymphatic vessel marker LYVE-1. Analysis of P18 eyes showed no difference

in lymphatic vessel density (Figure 11, left graph) and number of branching points (Figure 11, right graph). However, although not significant, number of lymphatic sprouts appeared slightly increased in MMP14$^{EC-/-}$ sprouts (Figure 11, right graph).

When analyzing P35 corneas no differences in lymphatic vessel density or number of branching points were observed (Figure 12). These data indicate there might be a minor developmental phenotype compensated over time.
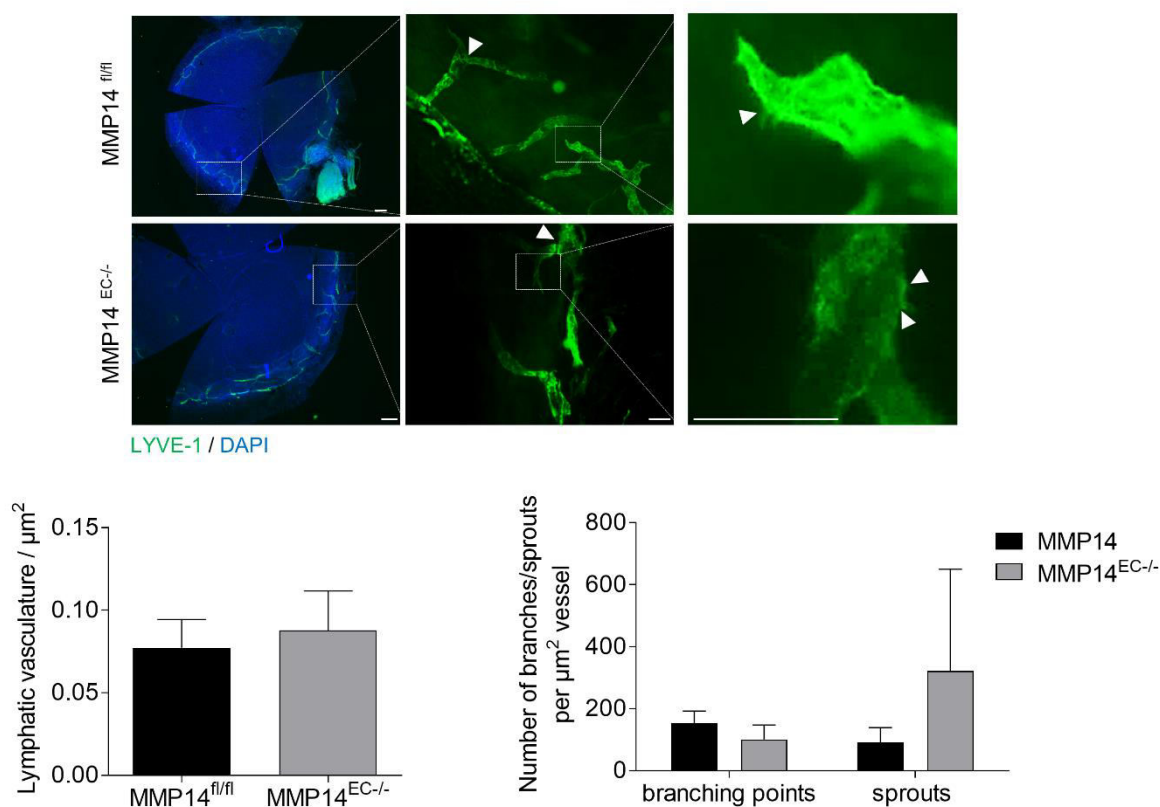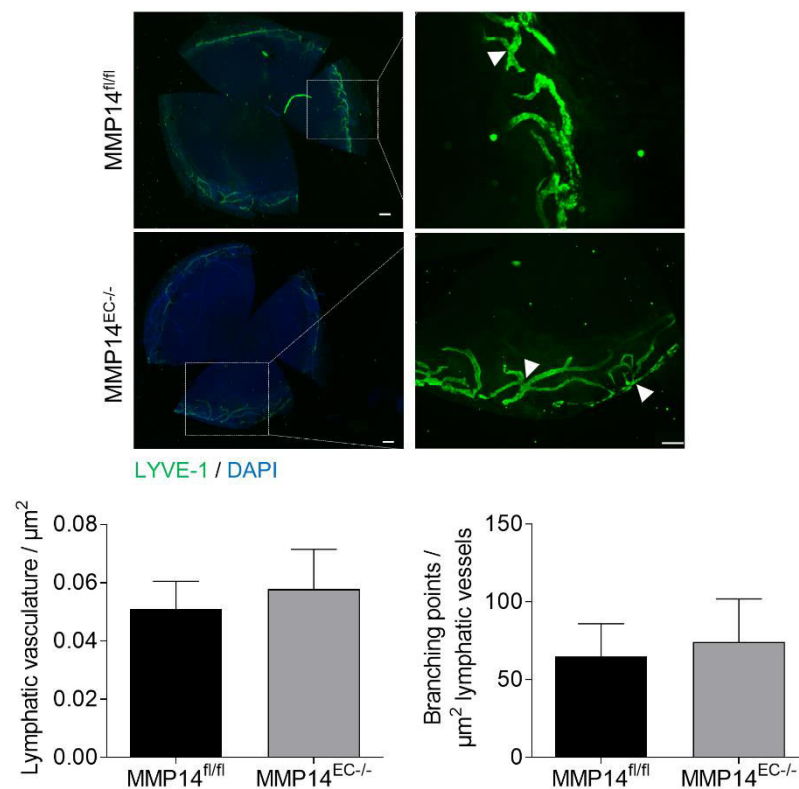

Figure 12: Lymph vessel density and sprouting in P35 corneas. Immunofluorescence staining for lymphatic vessels (LYVE-1, green) and nuclei (DAPI, blue) in cornea of P35 mice. Lymphatic density (left graph) and branching points (right graph) were analyzed. The white arrows indicate branching points. Mean ± SD; MMP14$^{fl/fl}$ n=8, MMP14$^{EC-/-}$ n=6; Scale: 200 μm.

3.1.2. Loss of endothelial MMP14 reduces melanoma growth

After development, tumor progression is one of the major events in adulthood where angiogenesis is essential and required to establish cell survival and invasion [107, 108]. Even though developmental angiogenesis is not prominently altered by loss of MMP14, previous studies showed that blocking MMP14 activity using humanized antibodies resulted in reduced breast cancer development accompanied by impaired tumor-induced angiogenesis [368]. These suggest that MMP14 may mediate preferentially pathological angiogenesis. To directly address

this, we used an *in vivo* model of melanoma where B16F1 GFP melanoma cells are grafted by intradermal injection into the flank of MMP14$^{EC-/-}$ and MMP14$^{fl/fl}$ control mice.
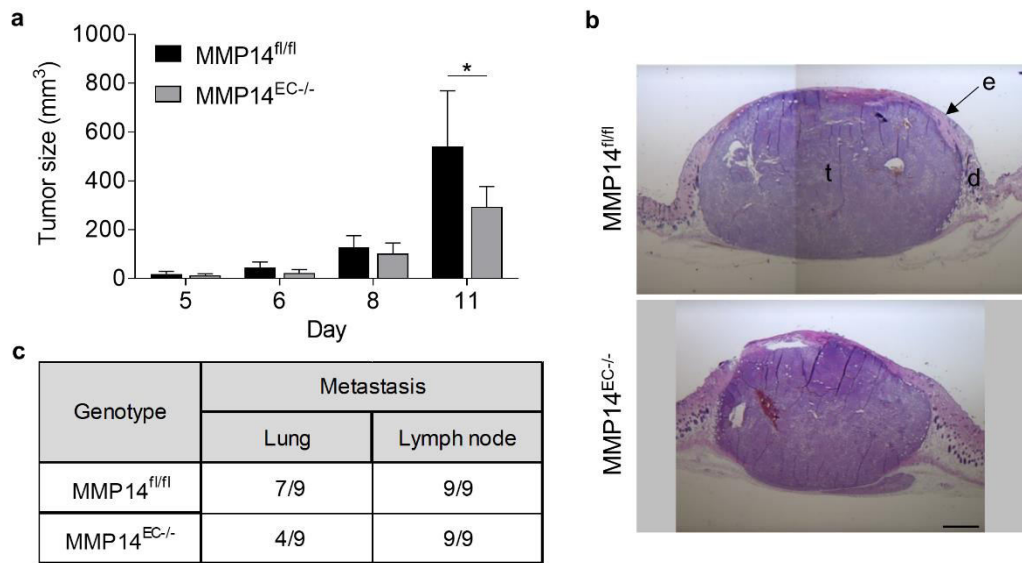
Figure 13: B16F1 melanoma growth and lung metastasis are reduced in MMP14$^{EC-/-}$ mice. a) Analysis of tumor size over time in MMP14$^{fl/fl}$ and MMP14$^{EC-/-}$ mice. Mean ± SD; *p<0.05; MMP14$^{fl/fl}$ n=6; MMP14$^{EC-/-}$ n=7. **b)** H&E staining of day 11 tumor sections. t: tumor; e: epidermis, d: dermis. Scale: 1000 μm. **c)** B16F1 GFP melanoma cell metastasis to lung and lymph nodes was analyzed by RNA isolation from the organs, followed by RT-PCR. Number of GFP-positive organs out of the total number are shown (n=9).

Tumor growth was observed over time with first tumors visible at day 5 (Figure 13a). Until day eight tumor size was comparable between MMP14$^{EC-/-}$ and control mice. However, while tumors in floxed controls continued to grow rapidly reaching an average size of 491.92 mm^3 at day 11, tumors in MMP14$^{EC-/-}$ knockouts remained significantly smaller (293.33 mm^3). Day 11 post-injection marked the end-date of the growth as several tumors reached the maximal ethical accepted size for this type of experiment. Despite size variations, H&E staining of tissue sections displayed a comparable morphology of tumors and surrounding stroma in MMP14$^{EC-/-}$ and MMP14$^{fl/fl}$ control (Figure 13b). However, proliferation analyzed by Ki67 staining was reduced in MMP14$^{EC-/-}$ tumors while apoptosis remained comparable [390].

To further investigate whether tumor cells spread to distant organs, lungs and lymph nodes were isolated from mice at day 11 post-injection, RNA was isolated and reverse transcribed. PCR amplification of GFP that is expressed by the used B16F1 melanoma cells showed GFP positivity for all analyzed lymph nodes of both genotypes (Figure 13c). However, metastasis to lungs was reduced in MMP14$^{EC-/-}$ mice with only 4 out of 9 lungs being positive for GFP, while 7 out of 9 MMP14$^{fl/fl}$ lungs were GFP positive. Therefore, loss of EC-MMP14 leads to reduced B16F1 growth and metastasis to the lungs melanoma.

<u>3.1.3. Vascular density is not altered in MMP14$^{EC-/-}$ tumors, but permeability is</u>

Blocking of MMP14 using the human inhibitory antibody DX-2400 resulted in reduced tumor growth and lung metastasis, both likely due to impaired tumor angiogenesis [368]. Therefore, we asked whether reduced melanoma growth and metastasis in the MMP14$^{EC-/-}$ mice could result from altered neovascularization of the tumors. However, when analyzing blood vessel density by CD31 staining in tumor cryosections no difference was found in vascular structure formed within (t) and outside (p) the melanomas (Figure 14a). These data indicate that loss of EC-MMP14 does not alter tumor neoangiogenesis.
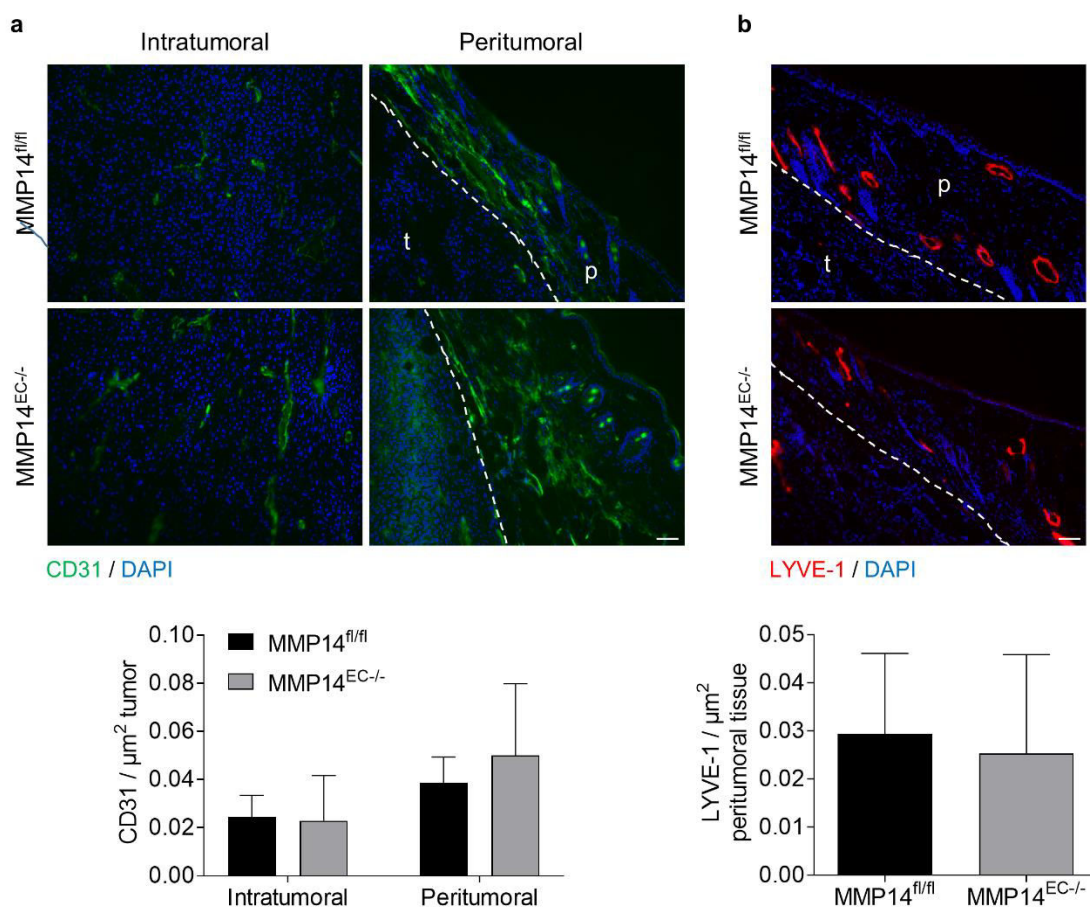
Figure 14: Loss of endothelial MMP14 does not alter vascular density. **a)** Blood vasculature in tumor sections was analyzed by immunofluorescence staining for the endothelial marker CD31 (green) and DAPI (blue) to visualize the nuclei. Analysis of fluorescence intensity per tumor area was used for quantification. The dotted line indicates the border between tumor (t) and peritumoral tissue (p). Mean ± SD; intratumoral: MMP14$^{fl/fl}$ n=6, MMP14$^{EC-/-}$ n=7; peritumoral: MMP14$^{fl/fl}$ n=5, MMP14$^{EC-/-}$ n=6; Scale: 50 µm. **b)** Analysis of lymphatic vasculature in tumor sections using the marker LYVE-1 (red) and DAPI (blue) to visualize the nuclei. Fluorescence intensity was analyzed per tumor area. Mean ± SD; MMP14$^{fl/fl}$ n=5, MMP14$^{EC-/-}$ n=4; Scale: 50 µm.

While blood vasculature mainly regulates ventilation and nutrition of the tumor [107, 108], fluid homeostasis and immune response regulation are mainly mediated by the lymphatic vasculature [444]. In addition, lymphatic vasculature is the route taken for metastasis to lymph

nodes [444]. Thus, we asked whether EC-specific MMP14 loss affects lymphangiogenesis in tumors. Therefore, MMP14$^{EC-/-}$ tumor cryosections were stained for the lymphatic vascular marker LYVE-1, a hyaluronan receptor [445]. Lymph vessel were found primarily around the tumors and their density was comparable in both mice genotypes (Figure 14b) indicating that EC-derived MMP14 does not influence lymphatic angiogenesis in melanoma. This is in line with the unaltered lymph node metastasis detected in MMP14$^{EC-/-}$ mice.
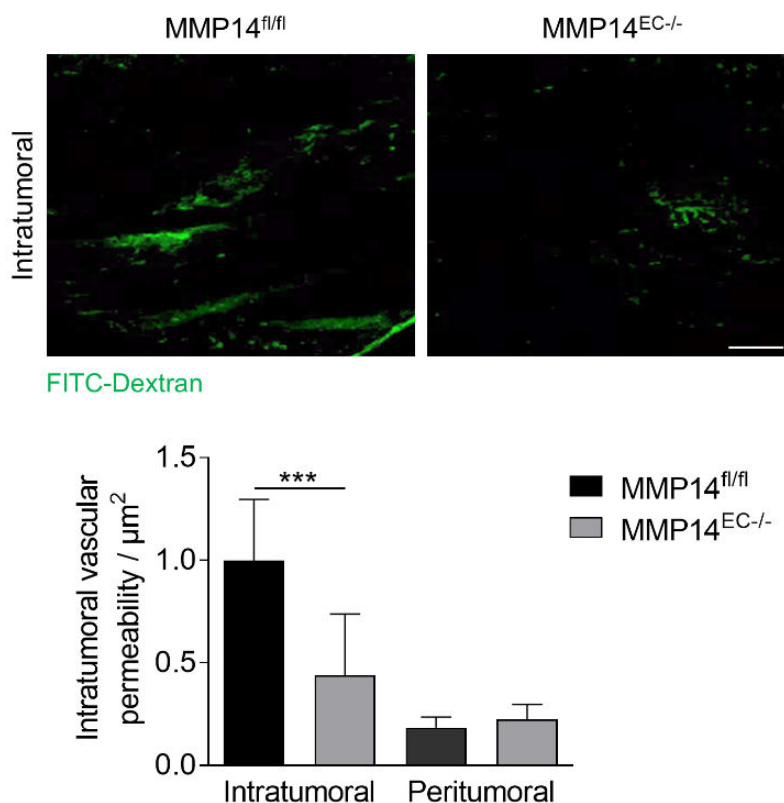
Figure 15: Reduced permeability in MMP14$^{EC-/-}$ tumor vessels. Pictures of FITC-Dextran (15 mg/ml; 20 kDa) leaked from the intra- and peritumoral vessels. Analysis of fluorescence intensity was performed for quantification. Mean ± SD; ***p<0.0005; intratumoral n=8, peritumoral n=6; Scale: 500 μm.

Characteristic of tumor vessels is their tortuosity and hyperpermeablity [185, 446] resulting from reduced pericyte attachment [188, 190], aberrant basement membrane [186] and loose/disorganized endothelial connections [223]. All together these vascular properties support tumor growth and metastasis [447].

To address whether loss of EC-MMP14 influences vessel permeability, mice were intravenously injected with small molecular weight FITC-Dextran (20 kDa) 30 min prior death. Spread into the tissue of the fluorescent dextran was analyzed by microscopy of cryosections and the amount of permeated dextran was analyzed by quantifying signal intensities in the tumor tissue (Figure 15). While the amount of peritumoral labelled dextran was comparable between MMP14$^{EC-/-}$ and MMP14$^{fl/fl}$ peritumoral tissue, a significant decrease was detected

intratumoral in knockouts mice. This indicates that loss of EC-MMP14 reduces intratumoral permeability of vessels.

3.1.4. Alterations in intratumoral vessel structure in MMP14$^{EC-/-}$ tumors

Vessel permeability is regulated by several factors, external and internal. Pericytes are often detached from tumor vessels compared to physiological conditions where their attachment is essential for vessel maturation and thus stabilization [188, 190]. To analyze pericyte coverage of tumor vessels in MMP14$^{EC-/-}$ and controls, in tumor sections we used two pericyte markers since no single markers can distinctly identify pericytes [448]. Thus, we used NG2 and PDGFRβ, both known to be expressed in tumor-associated pericytes [197-200] and performed co-stainings with the blood vessel marker CD31. Analyzing the percentage of pericyte marker signals per CD31 positive area in a vessel [449-451] we showed a tendential but not significant increase for PDGFRβ in MMP14$^{EC-/-}$ tumors (Figure 16a). For NG2, this increase was significant (Figure 16b) in mice without EC-derived MMP14 compared to floxed controls, indicating enhanced pericytes intratumoral vessel coverage.
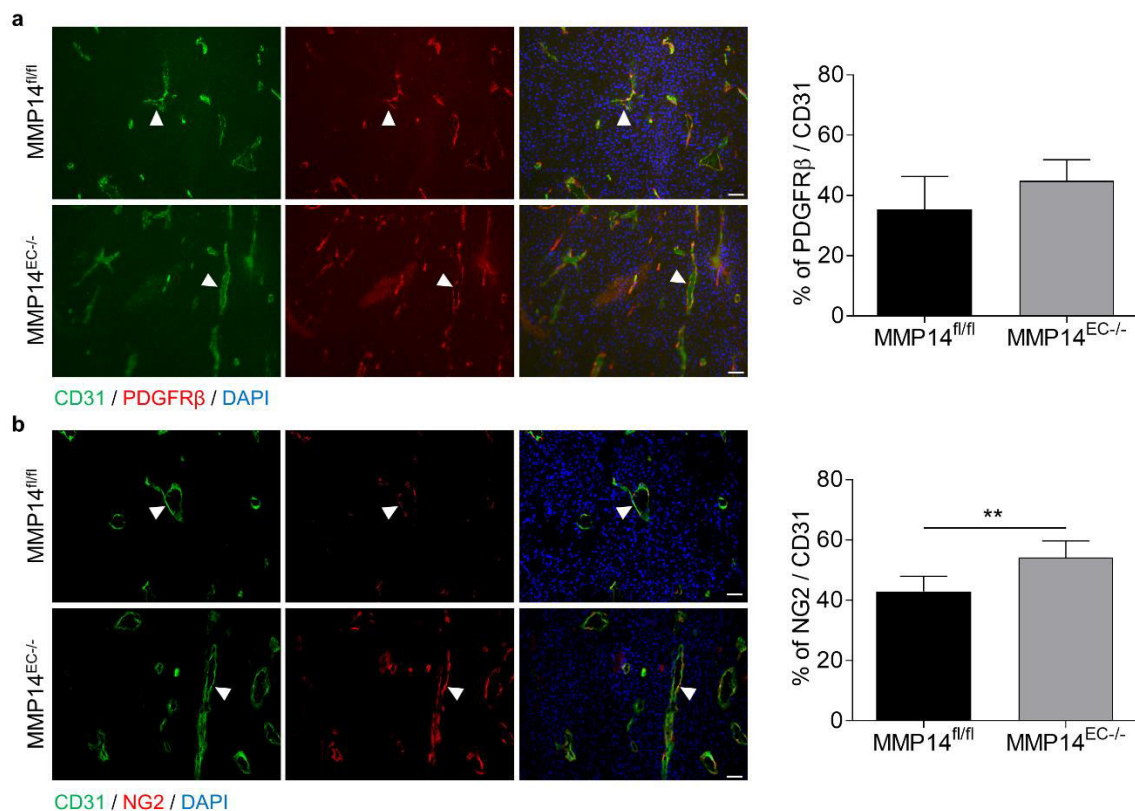

Figure 16: Increased pericyte coverage of intratumoral MMP14$^{EC-/-}$ vessels. a) For analysis of pericyte coverage tumor sections were co-stained for tumor vessels (CD31, green) and the pericyte marker PDGFRβ (red) or **b)** NG2 (red). DAPI (blue) was used for nuclei visualization. For quantification, the percent PDGFRβ and NG2 positive per CD31 positive area was calculated. White

arrowheads indicate vessels. Mean ± SD; **p<0.005; PDGFRβ: MMP14$^{fl/fl}$ n=3, MMP14$^{EC-/-}$ n=4; NG2: MMP14$^{fl/fl}$ n=7; MMP14$^{EC-/-}$ n=6, Scale: 50 μm.

Besides pericyte coverage, structural stability of vessels is also provided by EC attachment to basement membrane proteins. Several BM proteins are substrate to MMP14 or MMP2 [316, 452]. Therefore, their proteolytic activity might modulate tumor vessel leakiness, which is known to be influenced by the BM [186]. However, staining and quantification of relative intensities of collagen type IV, nidogen-1 and perlecan in tissue sections from MMP14$^{EC-/-}$ and control tumors displayed no significant differences in the amount and distribution of any of the analyzed BM proteins (Figure 17). These data suggest that BM arrangement and composition in mouse melanoma are independent of EC-MMP14.
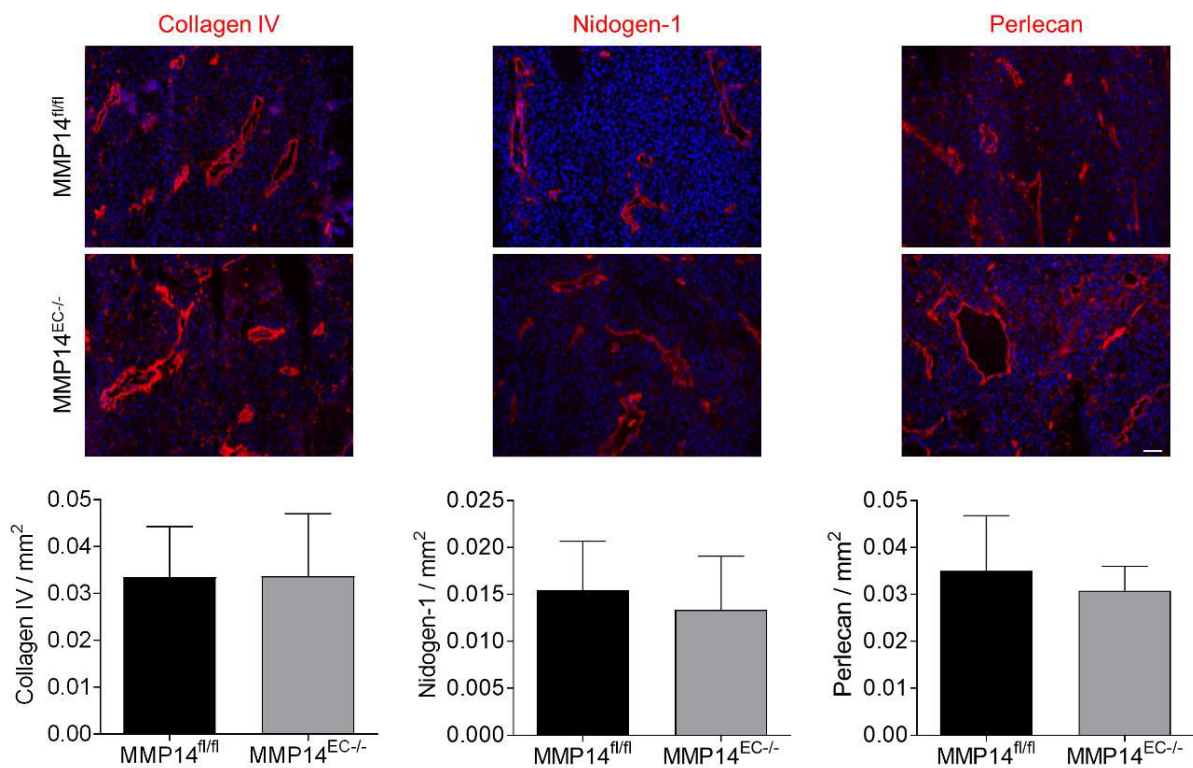
Figure 17: Unaltered basement membrane proteins in MMP14$^{EC-/-}$ tumors. B16F1 tumor sections were stained for collagen type IV, nidogen-1 or perlecan (red) and DAPI (blue) for nuclei visualization. Fluorescence intensity was analyzed and normalized to tumor area. Mean ± SD; collagen IV and perlecan: MMP14$^{fl/fl}$ n=10, MMP14$^{EC-/-}$ n=12; nidogen-1: MMP14$^{fl/fl}$ n=11, MMP14$^{EC-/-}$ n=13; Scale: 100 μm.

3.1.5. EC-derived MMP14 regulates expression of junctional proteins

Apart from adherence to an intact BM and vessel coverage, vessel tightness also requires intact intercellular connections mediated by the endothelial cells junction proteins as VE-cadherin [204, 205, 225, 453, 454]. One of the intracellular mediators of VE-cadherin junction

functionality is ZO-1 which connects to VE-cadherin intracellularly and mediates VE-cadherin recruitment and assembly [455]. Thus, to analyze, whether loss of EC-MMP14 alters expression of these two tight junction proteins in tumor associated vessels *in vivo* we first co-stained tumor sections for ZO-1 and ECs (CD31) (Figure 18a). The percentage of ZO-1 expression intensity per CD31 positive area showed a significant increase in MMP14$^{EC-/-}$ tumors as compared to floxed controls. Comparably, co-staining and quantification of VE-cadherin per CD31 positive vessel area also revealed enhanced expression in tumor sections derived from mice lacking EC-MMP14 compared to controls (Figure 18b). These data indicate that EC-derived MMP14 is a regulator of ZO-1 and VE-cadherin expression.
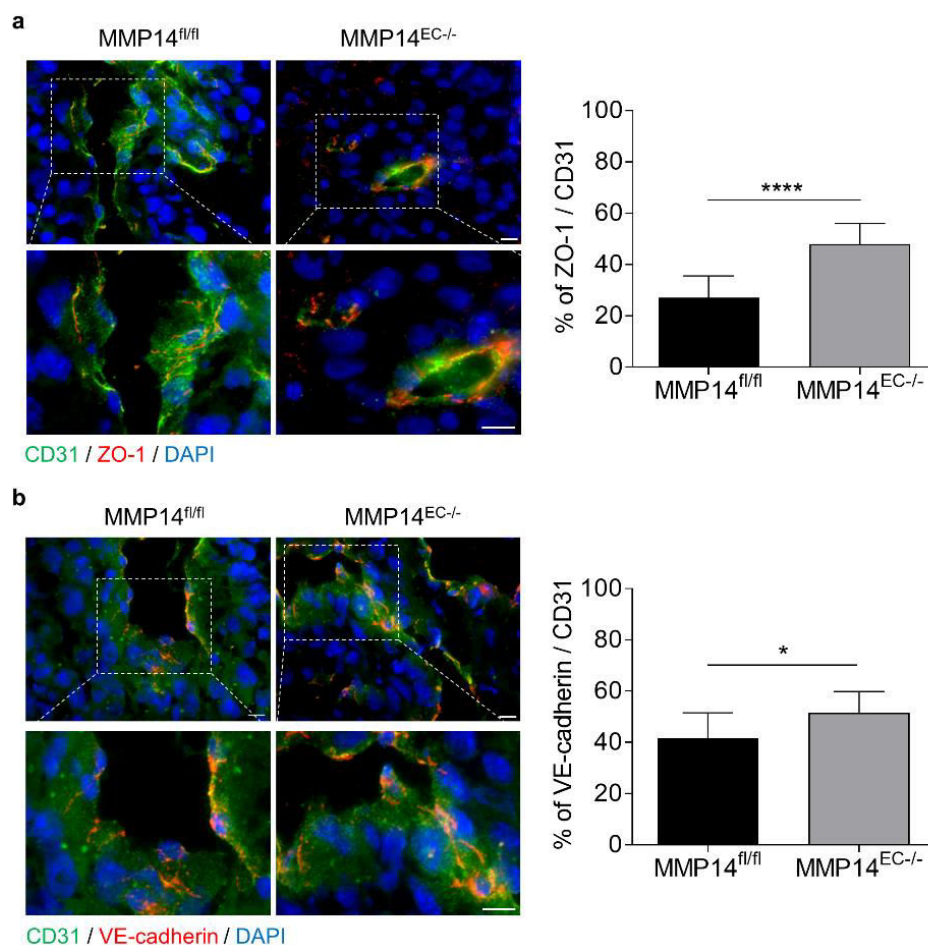
Figure 18: Association of ZO-1 and VE-cadherin with vessels is increased in MMP14$^{EC-/-}$ tumors. **a)** Tumor sections were co-stained for CD31 (vessels, green) and the junction protein ZO-1 (red). DAPI (blue) was used for nuclei visualization. The amount of ZO-1 positive was normalized to CD31 positive area. Mean ± SD; ****$p<0.0001$; n=9; Scale: 10 μm. **b)** Co-staining of VE-cadherin (red) and CD31 (green) and analysis of VE-cadherin positive area per CD31 (green) positive area on tumor sections. Mean ± SD; *$p<0.05$; MMP14$^{fl/fl}$ n=9, MMP14$^{EC-/-}$ n=8; Scale: 10 μm.

To further analyze the EC-intrinsic defect due to MMP14 loss we performed *in vitro* experiments using primary ECs isolated from MMP14$^{EC-/-}$ and MMP14$^{fl/fl}$. Cell were grown as monolayer to confluence to allow establishment of tight cell-cell contacts and VE-cadherin

expression and localization was investigated by immunofluorescence analysis. These investigations showed strong increase in VE-cadherin expression in cells derived from MMP14$^{EC-/-}$ mice compared to controls (Figure 19a, left panel). Although not significant, VE-cadherin expression at cell-cell interphases was enhanced (Figure 19a, right panel).

The increased VE-cadherin protein in ECs was accompanied by a significantly increased transcription in MMP14$^{EC-/-}$ ECs as compared to controls (Figure 19b).
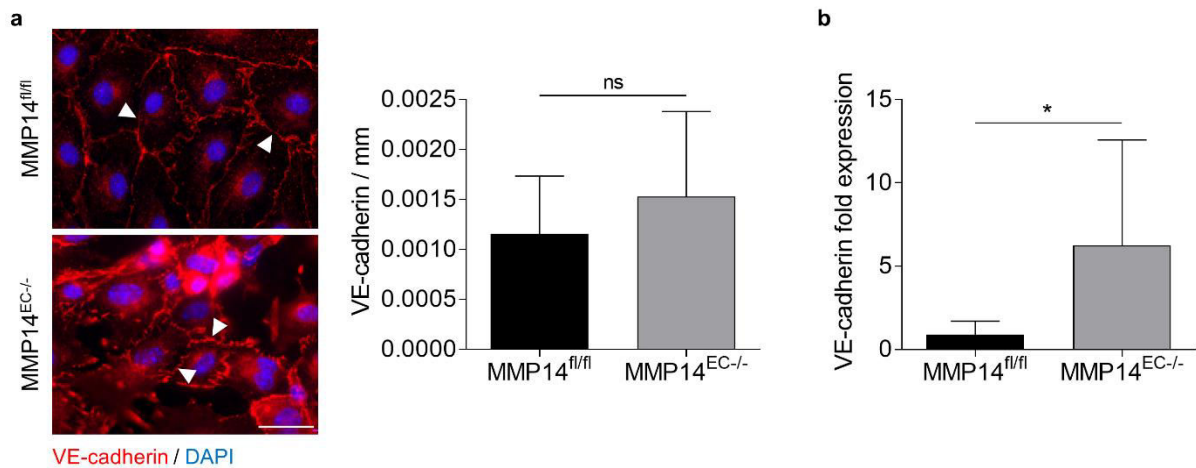
VE-cadherin / DAPI

Figure 19: VE-cadherin expression is increased in isolated endothelial cells. a) Primary ECs from MMP$^{EC-/-}$ mice and controls were grown as monolayer and stained to detect VE-cadherin (red) and nuclei (DAPI, blue). Fluorescence intensity was analyzed. White arrowheads indicate analyzed VE-cadherin at cell-cell intersections. Mean ± SD; n=3 mice pooled; Scale: 20 μm. **b)** VE-cadherin transcripts were quantified from primary ECs grown to tightness in monolayer. S26 was used as control. Mean ± SD; *p<0.05; MMP14$^{fl/fl}$ n=11, MMP14$^{EC-/-}$ n=9.

However, to further investigate whether reduced MMP14's proteolytic function leads to VE-cadherin increase in ECs lacking the protease, we studied VE-cadherin in primary MMP14$^{EC-/-}$ and control ECs in protein lysates and serum free supernatants by immunoblot. VE-cadherin was found as surface bound (in lysates) and as soluble protein (in supernatants) in ECs of both genotypes. A reduction in the released soluble protein was detected by MMP14$^{EC-/-}$, but that did not result in a relative increase of the cell membrane form. (Figure 20a).
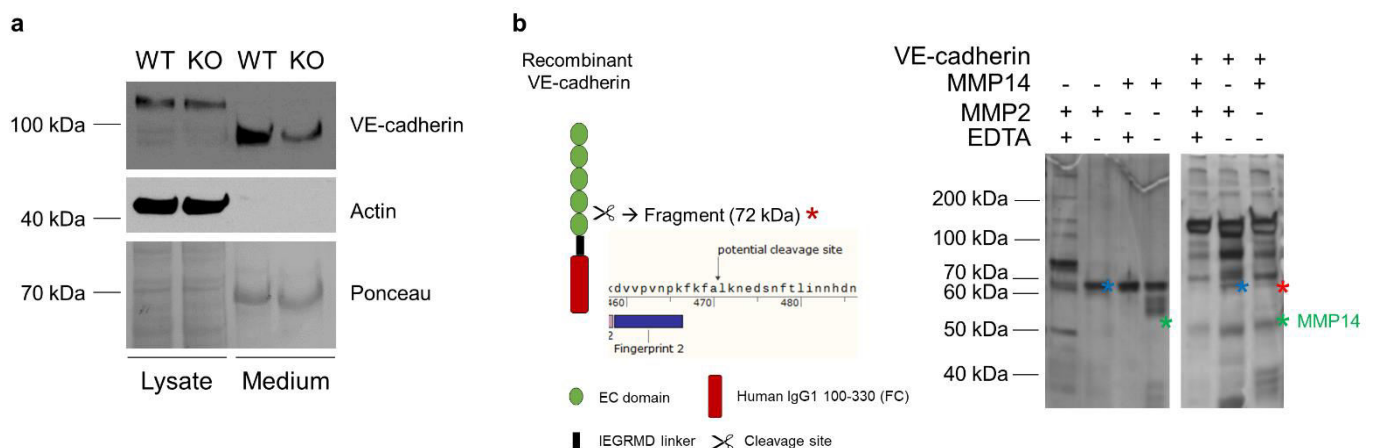
Figure 20: MMP14 processes VE-cadherin. a) Immunoblot analysis of MMP14^fl/fl (WT) and MMP14^EC-/- (KO) EC cell lysates and supernatants detecting VE-cadherin (full length: 130 kDa, soluble: 90 kDa). Actin (42 kDa) and Ponceau staining were used as loading control. **b)** *In vitro* processing of recombinant VE-cadherin by active and EDTA-inactivated recombinant human MMP14 and MMP2. Proteins resolved by SDS-PAGE were visualized by silver staining of the gel. VE-cadherin fragments generated by MMP14 are indicated by red stars. Blue stars indicate active MMP2, green stars indicate active MMP14. Based on fingerprint analysis the potential cleavage site (indicated by scissor symbol) was located in the first extracellular domain of VE-cadherin as shown in the scheme.

As MMP14 often acts indirectly through MMP2 activation, the question remained open, whether VE-cadherin processing is directly or indirectly mediated by MMP14. Therefore, recombinant VE-cadherin was incubated with active and inactive recombinant MMP2 and MMP14 *in vitro*. The proteins and possible degradation fragments were analyzed by SDS-PAGE and silver staining. These analysis showed an additional low molecular weight band of VE-cadherin when processed by active MMP14 but not MMP2, demonstrating that MMP14 directly cleaves VE-cadherin (Figure 20b, left panel). The newly identified fragment is 72 kDa and was further identified by fingerprint analysis. Previous studies showed that MMPs have no specific sequence but favor leucine at the P1' position [456]. In accordance, a potential cleavage site could be located in the first extracellular domain of VE-cadherin between amino acids 470 (alanine, P1) and 471 (leucine, P1') right after the last fingerprinted fragment (Figure 20b, schematic view of the cleavage site).

3.1.6. EC-derived MMP14 regulates eNOS and NO production

Although MMP14 has proteolytic activity towards VE-cadherin, most of its increased expression in MMP14^EC-/- cells is likely derived from enhanced transcriptional activity (Figure 19b). This may result either from a direct or an indirect MMP14-mediated effect. One potential

candidate known to be involved in regulating VE-cadherin expression and vascular stability is NO [233, 234], that is produced by the endothelial nitric oxide synthase (eNOS) [232]. MMP14 in turn has been shown to regulate eNOS and NO in an intussusceptive model [388].
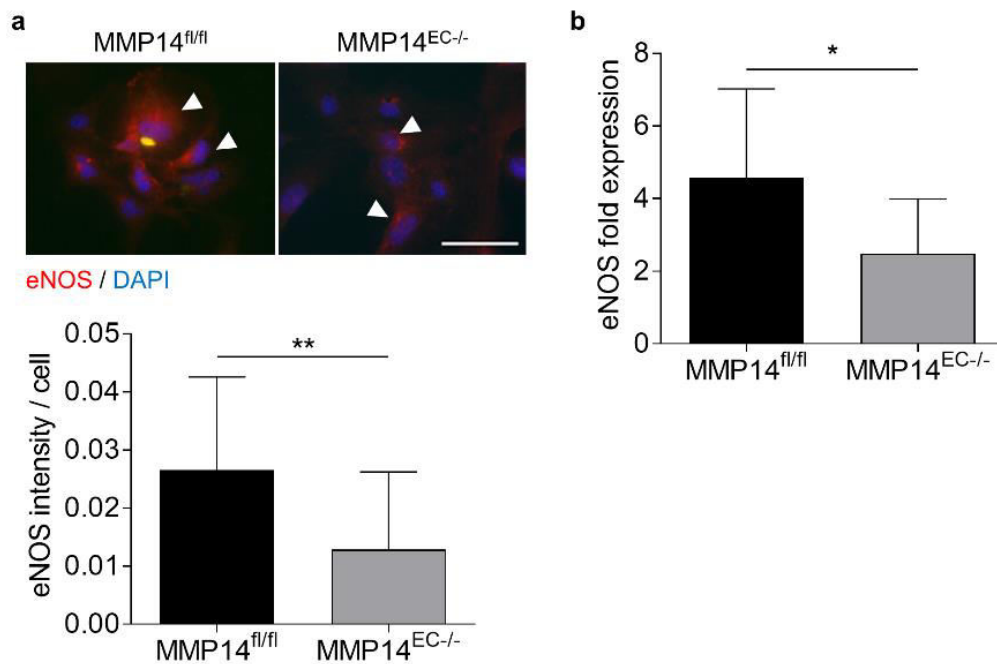
Figure 21: eNOS expression is decreased upon MMP14 loss in ECs. a) Immunofluorescence staining of ECs isolated from MMP14$^{fl/fl}$ and MMP14$^{EC-/-}$ mice for eNOS (red) and DAPI (blue) visualizing nuclei. Fluorescence intensity was analyzed per cell. White arrowheads indicate eNOS expression in analyzed cells. Mean $\pm$ SD; **p<0.005; n=4; Scale: 50 nm. **b)** Transcript analysis of eNOS expression in MMP14$^{fl/fl}$ and MMP14$^{EC-/-}$ ECs. S26 was used as control. Mean $\pm$ SD; *p<0.05; MMP14$^{fl/fl}$ n=8, MMP14$^{EC-/-}$ n=9.

In order to address, whether loss of EC-MMP14 affects eNOS production primary ECs from MMP14$^{EC-/-}$ mice and controls were cultured, and stained by immunofluorescence for eNOS (Figure 21a). eNOS expression in MMP14$^{EC-/-}$ ECs was significantly decreased. In these cells, reduced protein expression was paralleled by significant downregulation of eNOS transcripts as detected by real time quantification of transcripts thus suggesting that EC-derived MMP14 regulates expression of eNOS (Figure 21b).

eNOS, using L-arginine as source, is the main producer of nitric oxide (NO) in endothelial cells [457-459]. To assess, whether altered eNOS expression also affects enzyme activity and thus NO production, we used DAF-FM (4-Amino-5-Methylamino-2',7'-Difluorofluorescein) diacetate. That is a weakly-fluorescent reagent that reacts upon contact with NO and produces a green fluorescent triazolofluorescein, whose intensity is directly proportional to the NO concentration (Figure 22a) [432-434]. Therefore, primary ECs were treated with DAF-FM diacetate.
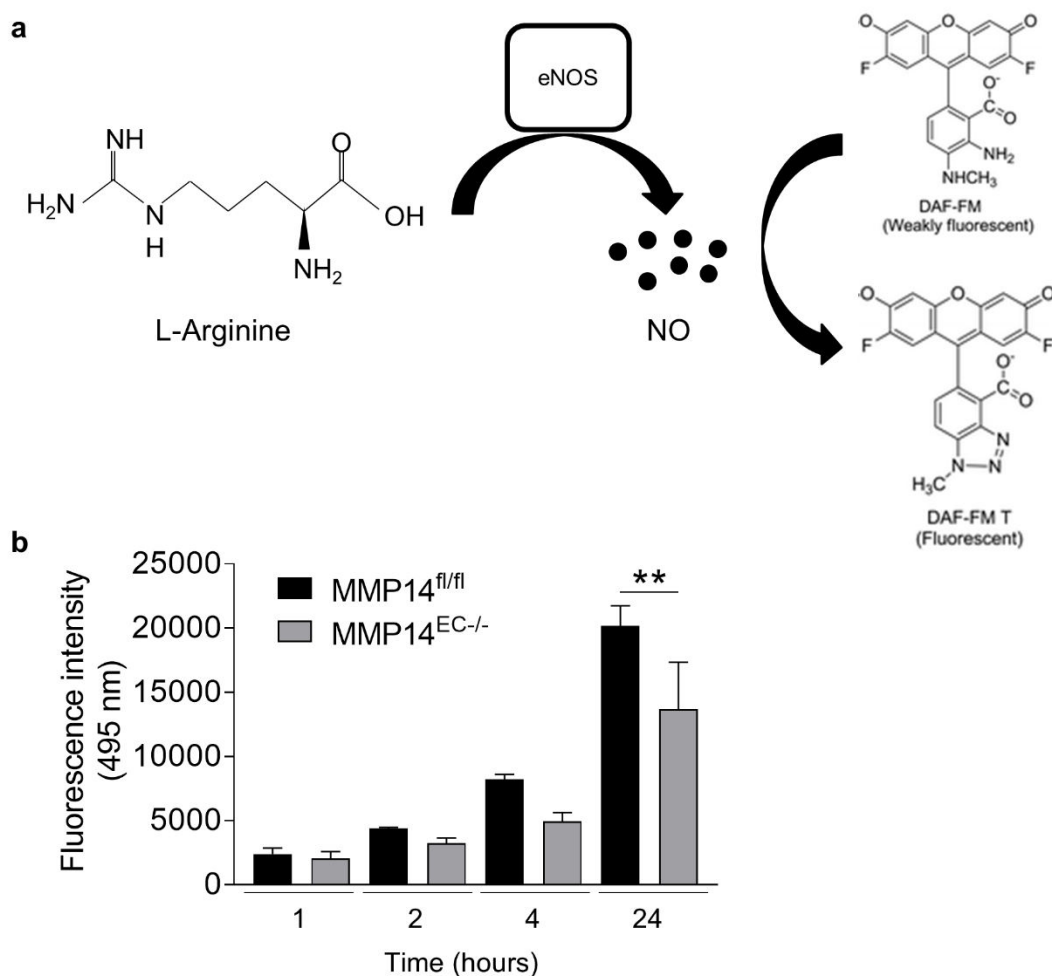
Figure 22: Reduced nitric oxide production in MMP14$^{EC-/-}$ ECs. a) Schematic overview of NO production by eNOS from L-arginine. Weakly fluorescent DAF-FM reacts with NO and is transformed into fluorescent DAF-FM T (measured at 495nm). **b)** Production of nitric oxide in MMP14$^{fl/fl}$ and MMP14$^{EC-/-}$ endothelial cells was measured at several time points. The experiment was repeated three times in triplicates. Mean ± SD; **p<0.005.

The amount of NO in MMP14$^{EC-/-}$ ECs was significantly reduced as compared to controls indicating reduced activity of eNOS (Figure 22b). This likely results from the decreased eNOS expression.

To address whether VE-cadherin upregulation in ECs lacking MMP14 expression is mediated directly by MMP14 or indirectly through eNOS downregulation, primary EC were transfected with eNOS siRNA. Downregulation of eNOS by approximately 70% was confirmed by real-time PCR (Figure 23, left panel) and immunoblot analysis (Figure 23, right panel). Despite the significant downregulation of eNOS, VE-cadherin expression appeared unaltered on either mRNA (Figure 23, middle panel) or protein levels (Figure 23, right panel). Thus increased VE-cadherin expression in cells from MMP14$^{EC-/-}$ mice is independent of eNOS regulation.
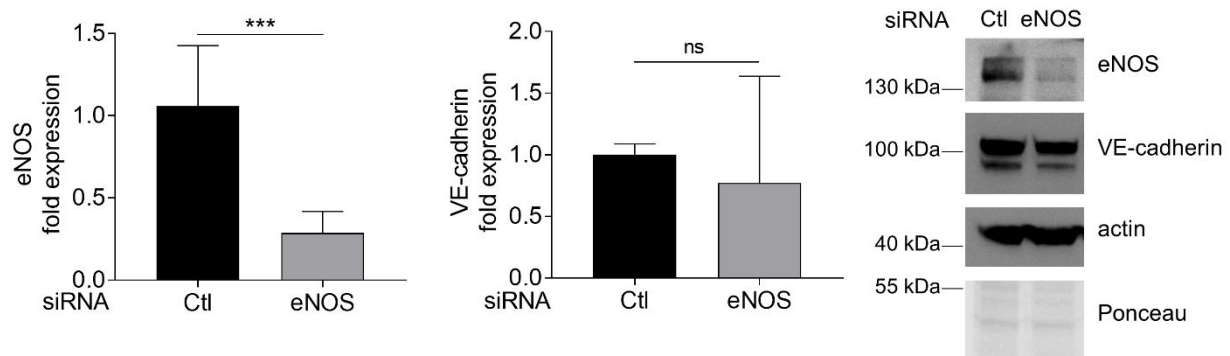
Figure 23: eNOS siRNA mediated downregulation MMP14$^{fl/fl}$ ECs. Transcript (graphs, left) and immunoblot (right picture) analysis of eNOS and VE-cadherin of MMP14$^{fl/fl}$ ECs transfected with eNOS siRNA and scramble siRNA as control (Ctl). S26 transcripts were used as control in RNA analysis, actin and Ponceau staining as loading and transfer control, respectively, of the blot. Mean ± SD; ***p<0.0005; n=3.

3.1.7. In human ECs MMP14 regulates eNOS but not VE-cadherin

Although often applicable, not all mechanisms identified in rodents can be translated to the human system [460]. To analyze whether VE-cadherin and eNOS are regulated by MMP14 in human endothelial cells, we undertook a silencing approach and transfected HUVECs with MMP14 siRNA. This led to downregulation of MMP14 transcripts by approximately 60% (Figure 24a, left panel), but no differences in human VE-cadherin expression accompanied this reduction (Figure 24a, middle panel) indicating that in human ECs VE-cadherin regulation is independent of MMP14. eNOS protein in HUVECs transfected with hMMP14 siRNA was reduced as compared to control cells (Figure 24a, right panel). Thus, similar to mouse ECs eNOS appears to be dependent on MMP14 expression, but VE-cadherin is not.

To investigate whether expression of MMP14 and eNOS correlate in in human melanoma, sections from specimens of grade T3-T4 (TNM staging [461]) melanomas were stained for MMP14 and eNOS (Figure 24b). Expression intensities specifically in visible blood vessels were qualitatively analyzed by arbitrary categorization in low (+), medium (++) and high (+++) expression. This investigation showed that eNOS levels in tumor vessels correlated with those of MMP14, thus being eNOS low in vessels with low MMP14 expression and conversely high when MMP14 was also highly expressed.
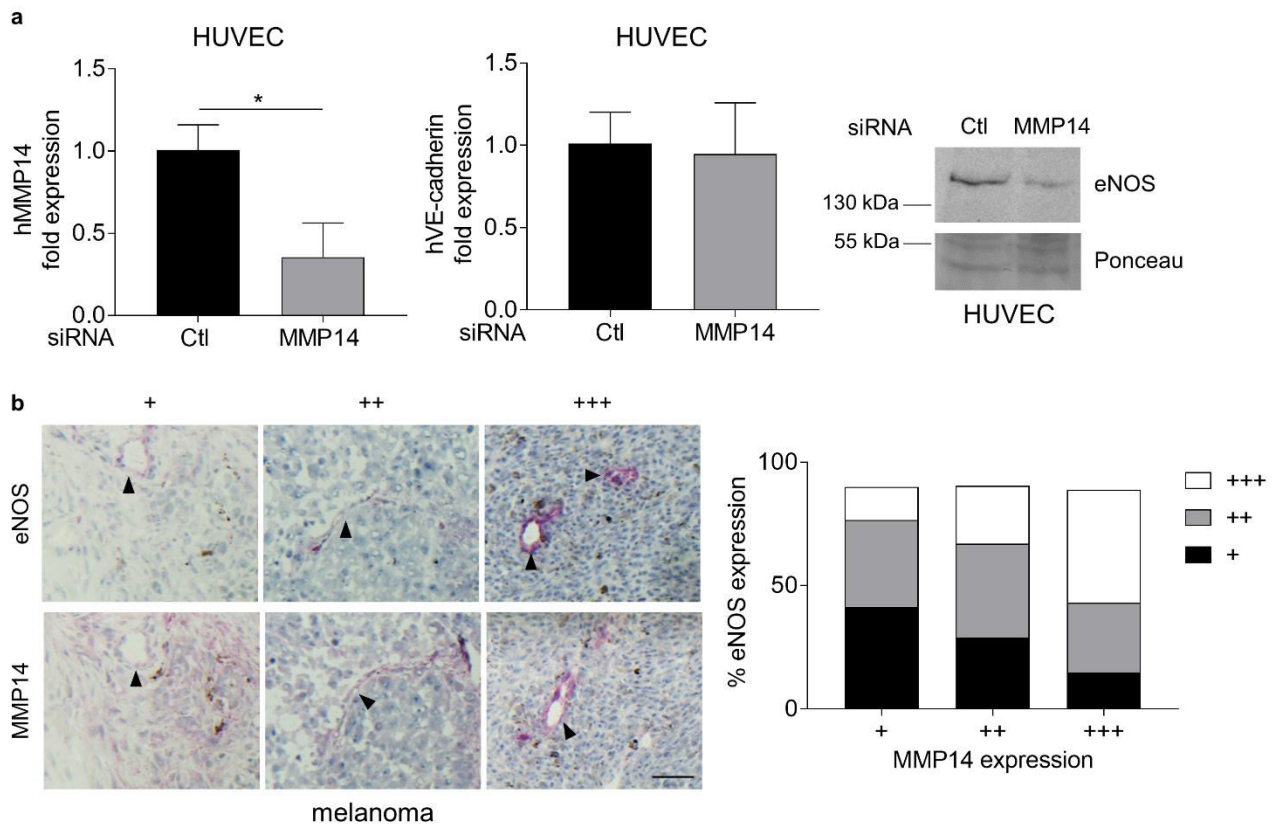
Figure 24: MMP14 downregulates eNOS, but not VE-cadherin in human EC. a) siRNA mediated MMP14 downregulation in HUVECs is analyzed by transcript analysis (left graph). Scrambled siRNA was used as control (Ctl). Expression of VE-cadherin was examined by real time PCR (graph on the right) and eNOS via immunoblot. S26 transcripts were used as control in RNA analysis, ponceau staining of the membrane was used as loading control for the immunoblot. Mean ± SD; *p<0.05; n=3. **b)** Immunohistochemical staining of eNOS and MMP14 was used to quantify the expression in human melanomas. Expression intensities for both proteins were arbitrarily set as: + low; ++ moderate; +++ high; representative pictures are shown and stained vessels are indicated by arrowheads. Percentage of eNOS expression in low, moderate, or high MMP14 expressing vessels is shown in the graph. n=21; Scale: 125 μm.

3.1.8. Loss of EC-MMP14 has no additional effect on therapeutic treatment of melanoma

Enhancing vessel maturation can also limit therapeutic efficiency [191]. Therefore, we questioned whether stabilization of tumor vessels by deletion of MMP14 in ECs may affect efficacy of cisplatin as a widely used antineoplastic drugs [462]. To address this, B16F1 melanoma cells were intradermal injected into MMP14$^{EC-/-}$ and control mice. When tumors became visible, at day 4, mice received a one-time treatment with cisplatin (1 mg/100 g body weight) (schematic overview in Figure 25a). Tumor growth was followed over time (Figure 25b).
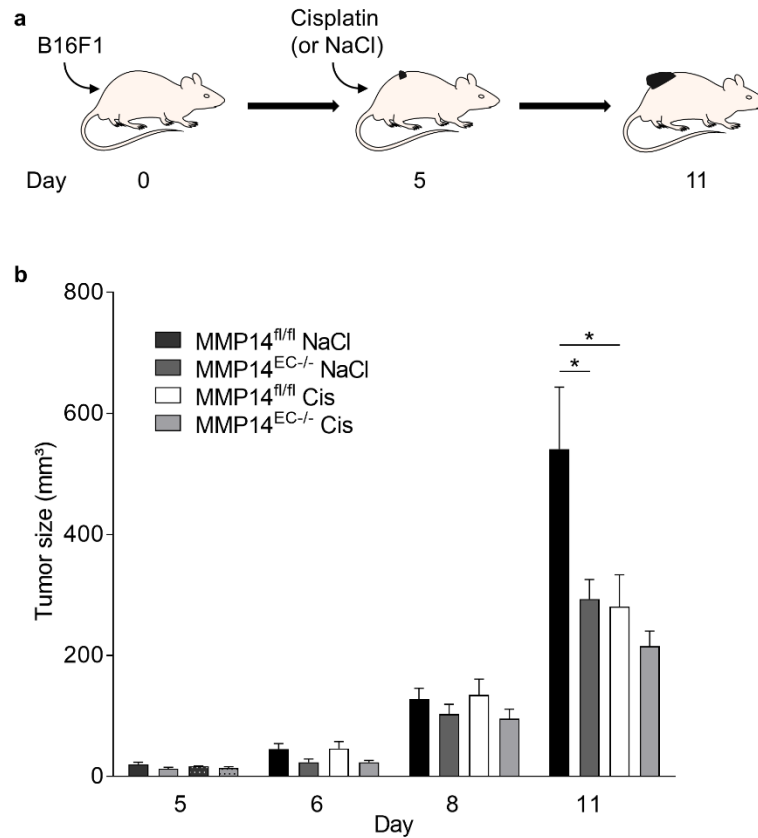
Figure 25: Cisplatin has less impact on B16F1 tumor growth in MMP14^EC-/- mice. a) Schematic representation of experimental procedure for B16F1 and Cisplatin or sodium chloride (NaCl) control injections in mice. **b)** Tumor size analysis in MMP14^fl/fl and MMP14^EC-/- mice treated with cisplatin (Cis) or NaCl as control. Mean ± SEM; *p<0.05; n=7.

As previously observed, up until day 8 only a minor reduction in tumor growth was observed in MMP14^EC-/- compared to MMP14^fl/fl, and treatment with cisplatin or NaCl did not alter tumor growth. At day 11, when growth of melanoma was significantly reduced in MMP14^EC-/- as compared to MMP14^fl/fl, cisplatin treatment strongly reduced melanoma growth in MMP14^fl/fl to an average of 280.72 mm^2 versus 491.92 mm^2 in NaCl treated tumors. In melanomas grown in MMP14^EC-/- mice cisplatin treatment only slightly, but not significantly, reduced growth (from 291.92 mm^2 in NaCl treated to 215.45 mm^2). These data show that loss of EC-derived MMP14 did not synergize with cisplatin treatment in inhibiting tumor growth.
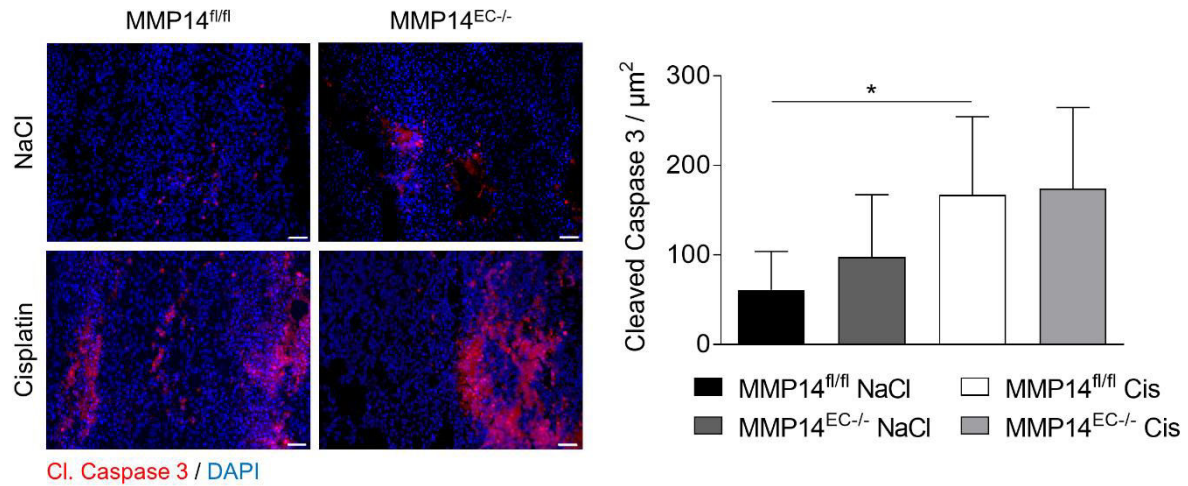
Figure 26: Cisplatin treatment increases apoptosis in B16F1 tumors. Immunofluorescence staining of tumor sections treated with NaCl or cisplatin (Cis) for cleaved (cl.) caspase 3 (red) and DAPI (nuclei, blue). Positive signals were quantified per tumor area. Mean ± SD; $*p<0.05$; MMP14$^{fl/fl}$ NaCl n=6, MMP14$^{fl/fl}$ Cis, MMP14$^{EC-/-}$ NaCl/Cis n=7; Scale: 50 μm.

One of the main effects of cisplatin on tumor cells including melanoma is programmed cell death [463] induced by caspase 3 and caspase 7 cleavage and subsequent signaling [464]. Thus, to further proof efficacy of cisplatin treatment in tumors, we analyzed cell death by immunofluorescence staining of cleaved caspase 3 (Figure 26). Quantitative analysis showed a significant increase in apoptosis in MMP14$^{fl/fl}$, but not MMP14$^{EC-/-}$, in cisplatin treated tumors as compared to NaCl controls. However, lack of significance may be due to the higher numbers of apoptotic cells already present in NaCl treated MMP14$^{EC-/-}$ mice melanomas.

3.2. MMP3 is upregulated in skin upon loss of fibroblast MMP14

Deletion of MMP14 specific to fibroblasts using a tamoxifen-induced model identified fibroblast-derived MMP14 as the main processor of collagen type I in the skin as loss lead to a fibrosis-like phenotype as a result from collagen accumulation [251]. However, wound healing in these MMP14$^{Sf-/-}$ mice was similar to controls [251]. Considering the multiple skin-related functions of MMP14, including involvement in multiple processes during tissue repair, comparable wound closure indicated compensation by other proteases, or dispensability of fibroblast-derived MMP14.

Analysis of whole skin tissue lysates from MMP14$^{Sf-/-}$ and floxed controls was performed using a Proteome Antibody Array$^{®}$ (Figure 27a) that detected multiple enzymes and factors involved in tissue repair, including ADAMTS1, MMP3, MMP8, MMP9, TIMP1 and 2, basic and acidic FGF, PDGF, angiopoietin-1 and 2, VEGF, thrombospondin and more.
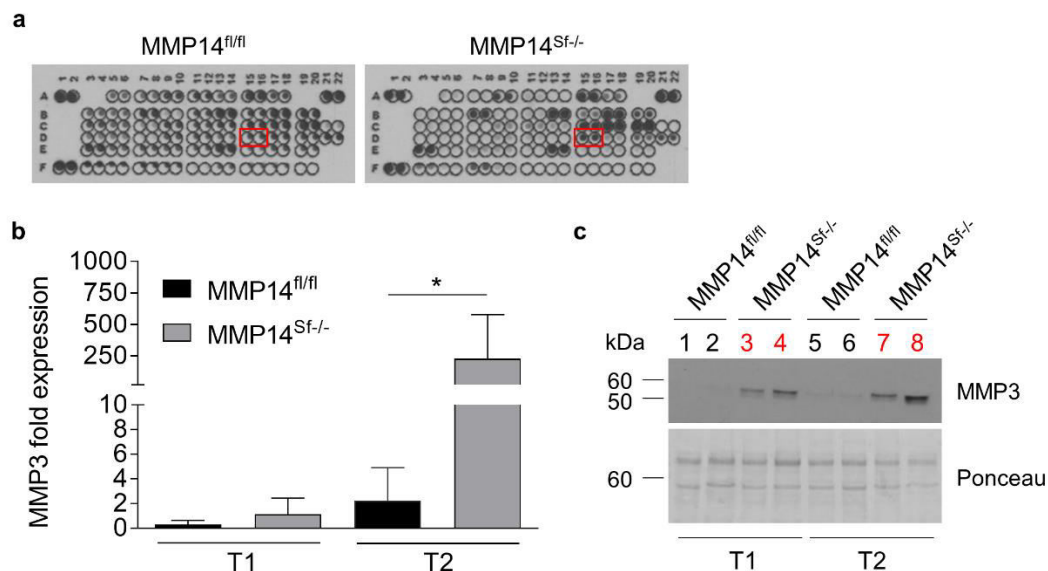
Figure 27: MMP3 expression is upregulated in MMP14$^{Sf-/-}$ skin. a) Proteome Profiler^{TM} Angiogenesis Array of whole skin tissue lysates from MMP14$^{Sf-/-}$ mice and floxed controls. Red squares indicate the MMP3 signals. **b)** Transcript analysis of MMP3 in MMP14$^{Sf-/-}$ and MMP14$^{fl/fl}$ skin at T1 and T2. S26 was used as transcript control. Mean ± SD; *p<0.05; T1: n=6, T2: MMP14$^{fl/fl}$ n=6, T2 MMP14$^{Sf-/-}$ n=7. **c)** Immunoblot analysis of MMP3 protein levels in whole skin tissue lysates of MMP14$^{fl/fl}$ and MMP14$^{Sf-/-}$ mice at T1 and T2. Ponceau staining was used as loading control. Red numbers indicate samples from MMP14$^{Sf-/-}$ mice.

Analysis of signal intensities of the single spots on the membrane (Antibody array) showed increased signals for platelet factor 4, IGFBP1 and 2 in tissue derived from MMP14$^{Sf-/-}$ mice, while serpin 1 and CCN3 were reduced. However, most striking was the increase in MMP3 in lysates derived from MMP14$^{Sf-/-}$ skin compared to controls (Figure 27a). To further verify these results, we isolated RNA from whole skin biopsies and analyzed it by qPCR (Figure 27b).

Furthermore, MMP3 protein was analyzed in tissue extracts by immunoblot (Figure 27c). In both assays, MMP3 levels were enhanced in skin from MMP14[Sf-/-] mice one week (T1) after tamoxifen feeding was completed (4 weeks feeding schedule), and were even further increased in skin after further 4 weeks (T2). Thus, loss of fibroblast-derived MMP14 leads to upregulation of MMP3 expression in skin.

3.2.1. MMP3 upregulation is in MMP14[Sf-/-] skin fibroblasts

Although we detected increased MMP3 in the skin of MMP14[Sf-/-] mice, the cellular source for this protease was unknown. To identify the cells responsible for the enhanced expression of MMP3, co-stainings for MMP3 and cellular markers for mast cells (c-kit) [465], macrophages (F4/80) [466] and fibroblasts (HSP47) [467] were performed in skin sections from MMP14[Sf-/-] and control mice (Figure 28 and 29).
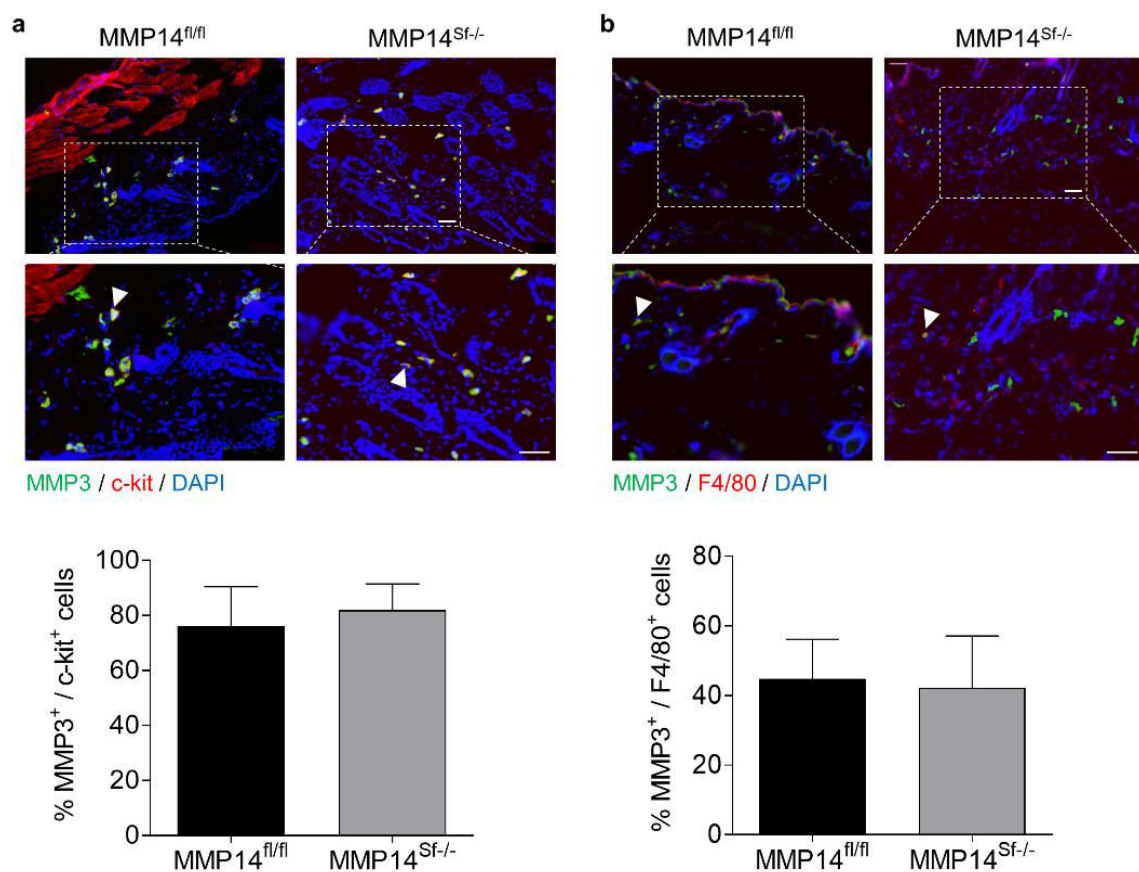
Figure 28: MMP3 expression is unaltered in mast cells and macrophages. a) MMP14^{fl/fl} and MMP14[Sf-/-] skin sections were co-stained for MMP3 (green) and markers for mast cells (c-Kit, red) or **b)** macrophages (F4/80, red). Nuclei were visualized by DAPI (blue). Percentage of double positive (white arrowheads) MMP3 and c-kit or F4/80 cells was calculated. Mean ± SD; mast cells: MMP14^{fl/fl} n=9, MMP14[Sf-/-] n=10; macrophages: MMP14^{fl/fl} n=5, MMP14[Sf-/-] n=7; Scale: 50 µm.

Analysis of the percentage of MMP3 positive mast cells (Figure 28a) and macrophages (Figure 28b) showed comparable levels of MMP3 expression in these cell types in the skin of MMP14$^{Sf-/-}$ and control mice. Conversely, the percentage of MMP3 positive fibroblasts was significantly increased in MMP14$^{Sf-/-}$ skin (Figure 29a) indicating these cells as the source for the enhanced MMP3 expression MMP14$^{Sf-/-}$ mice. To confirm these findings, supernatants of cultured primary skin fibroblasts from MMP14$^{fl/fl}$ and MMP14$^{Sf-/-}$ mice were analyzed by immunoblot (Figure 29b). In these samples enhanced expression of the 54 kDa molecular weight band corresponding to proMMP3 was detected in MMP14$^{Sf-/-}$ supernatants, further confirming that fibroblasts carrying the deletion of MMP14 enhance MMP3 secretion.
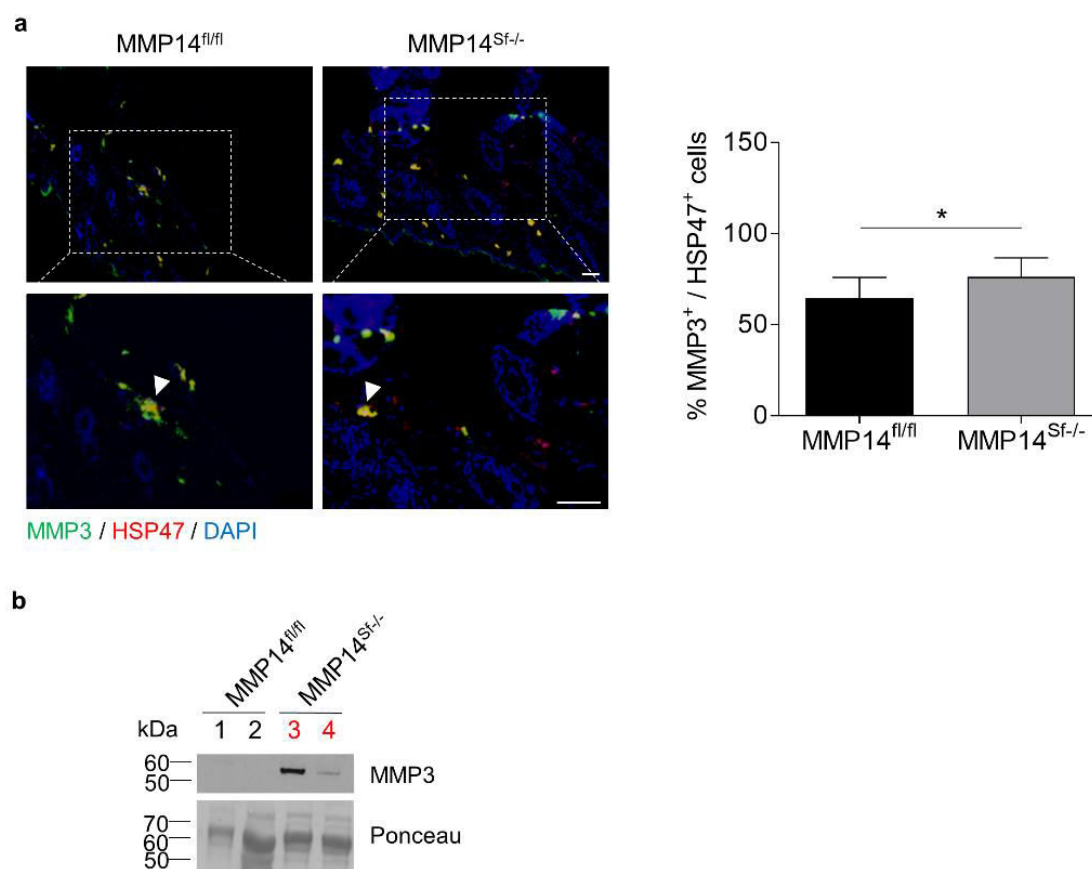
Figure 29: Fibroblast upregulate MMP3 upon loss of MMP14. a) Immunofluorescence staining of skin sections for MMP3 (green) and the fibroblast marker HSP47 (red). DAPI (blue) was used for nuclei visualization. Percentage of MMP3 and HSP47 double positive cells was calculated. Mean ± SD; *p<0.05; MMP14$^{fl/fl}$ n=14, MMP14$^{EC-/-}$ n=10; Scale: 50 µm. **b)** Immunoblot analysis of MMP14$^{fl/fl}$ (1 & 2) and MMP14$^{Sf-/-}$ (3 & 4) fibroblast supernatants detecting MMP3 (54 kDa). Ponceau was used as loading control.

3.2.2. Generation of MMP3$^{-/-}$/MMP14$^{Sf-/-}$ mice

Different MMPs share substrates specificities, which enables compensation for cell functions by loss of most MMPs [258]. Also, MMP3 and MMP14 share several substrates in the ECM [242] and although MMP3 has no collagenolytic activity, it is suggested to be involved in proteolysis of collagen indirectly through the activation of MMP13 [270, 406]. Moreover, MMP3 was recognized as driver of wound closure [419]. To identify which functions MMP3 might compensate for upon loss of MMP14 in fibroblast in adulthood in steady state conditions and during skin repair, double deficient mice were generated by pairing MMP3$^{-/-}$ knockouts [425] with the tamoxifen inducible MMP14$^{Sf-/-}$ mice [251].
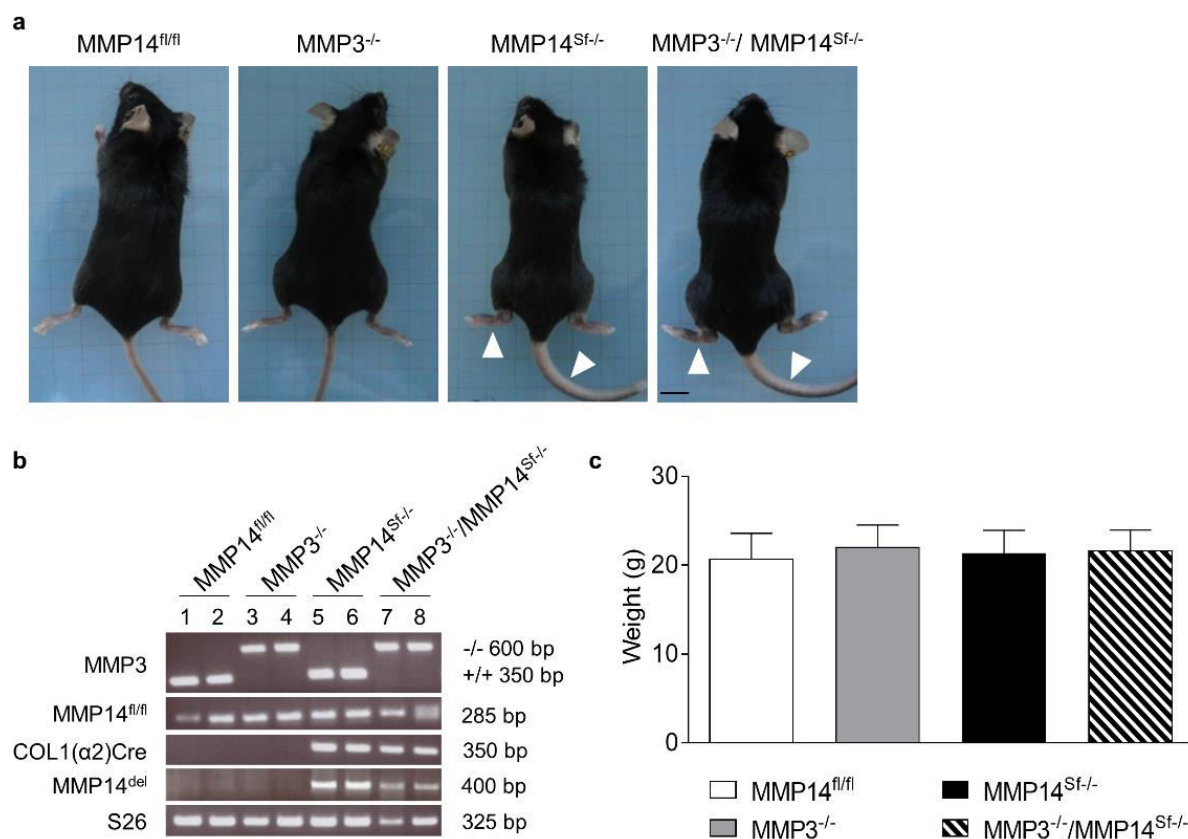
Figure 30: Generation of MMP3$^{-/-}$/MMP14$^{Sf-/-}$ double deficient mice. a) 14 week old MMP14$^{fl/fl}$, MMP3$^{-/-}$, MMP14$^{Sf-/-}$ and MMP3$^{-/-}$/MMP14$^{Sf-/-}$ mice after tamoxifen treatment White arrowheads indicate thickened paws and tails. Scale: 1 cm. **b)** Semi-quantitative genotyping PCR images showing amplification products for MMP3, floxed MMP14 exons 2-4 (MMP14$^{fl/fl}$), Collagen α2 Cre^{ERT} recombinase (Col1(α2)Cre), a specific PCR product resulting from the deletion of MMP14 exons 2-4 (MMP14^{del}) upon LoxP recombination and S26 as control. Length of amplification products is shown in base pairs. **c)** Analysis of weight at time point T2. Mean ± SD; n=7.

When MMP14$^{Sf-/-}$ mice reached the age of 13-14 weeks after tamoxifen feeding, MMP3$^{-/-}$/MMP14$^{Sf-/-}$ mice's weight and overall appearance was indistinguishable from MMP14 single knockouts (Figure 30a and c). As previously described for MMP14$^{Sf-/-}$ animals [251], MMP3$^{-/-}$

/MMP14$^{Sf-/-}$ mice also displayed at stiffening of skin, visible tail and paws thickening (Figure 30 white arrow heads), while floxed controls and MMP3$^{-/-}$ mice (that were also fed with tamoxifen) showed no phenotypical alterations. Genotyping PCR confirmed floxed MMP14 exons in all mice, deletion of MMP3 in MMP3$^{-/-}$ knockouts and double deficient mice as well as expression of the Cre recombinase. Detection of MMP14 was confirmed by amplification of a specific PCR fragment detectable only after LoxP recombination and deletion of exons 2-4 (Figure 30b).
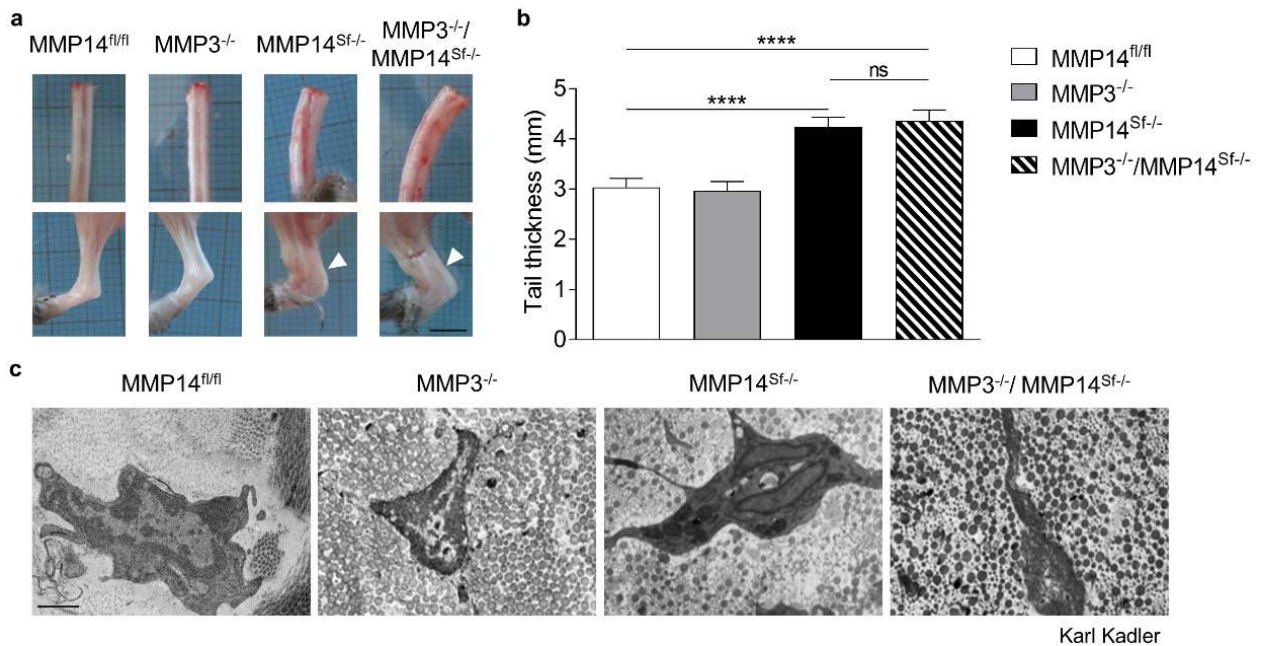
Figure 31: Double deficient mice recapitulate the MMP14$^{Sf-/-}$ tendon phenotype. a) Tail and Achilles tendons MMP3$^{-/-}$/MMP14$^{Sf-/-}$ and control mice. White arrowheads indicate the Achilles tendon. Scale: 1 cm. **b)** Analysis of tail thickness of MMP14$^{fl/fl}$, MMP3$^{-/-}$, MMP14$^{Sf-/-}$ and MMP3$^{-/-}$/MMP14$^{Sf-/-}$ mice at time point T2. Mean ± SD; ****$p<0.0001$; ns: not significant; n=7. **c)** Electron microscopy of tail tendons visualizing collagen fibril structure in the different mouse genotypes. These investigations were performed by the group of Karl Kadler (University of Manchester). Scale: 1 µm.

As shown in the MMP14$^{Sf-/-}$ mice [251], the fibrotic phenotype in MMP3$^{-/-}$/MMP14$^{Sf-/-}$ was detected, apart from skin, also in tail and Achilles tendons (Figure 31a). Macroscopic quantification of tendon further confirmed the phenotype (Figure 31b). Cooperation with Karl Kadler at the University of Manchester allowed a more detailed analysis of tail tendon structure by electron microscopy. At this magnification, tendons showed in MMP14$^{Sf-/-}$ and MMP3$^{-/-}$/MMP14$^{Sf-/-}$ mice accumulation of multiple thinner collagen fibers in addition to the thick collagen bundles (Figure 31c), but no additional alterations were observed that could account for the deletion of MMP3 in addition to MMP14. MMP3$^{-/-}$ tail tendons were comparable to controls.

In skin, microscopical analysis of tissue sections and relative quantification of dermal thickness revealed significant increased dermal depth in MMP3^{-/-}/MMP14[Sf-/-] as observed in MMP14[Sf-/-] skin (Figure 32). Collagen content analyzed by Picrosirius Red staining followed by polarized light observation [468, 469] showed enhanced collagen in MMP14[Sf-/-] and MMP3^{-/-}/MMP14[Sf-/-] mice (Figure 33a). Quantitative analysis demonstrated that both overall (Figure 33b) and fibrillar (Figure 33c) collagen were enhanced in MMP14 double and single knockout mice. Taken together, these findings show that deletion of MMP3 in addition to loss of fibroblast-MMP14 has no further effect on the skin and tendon fibrosis-like phenotype previously described in MMP14[Sf-/-] mice [251].
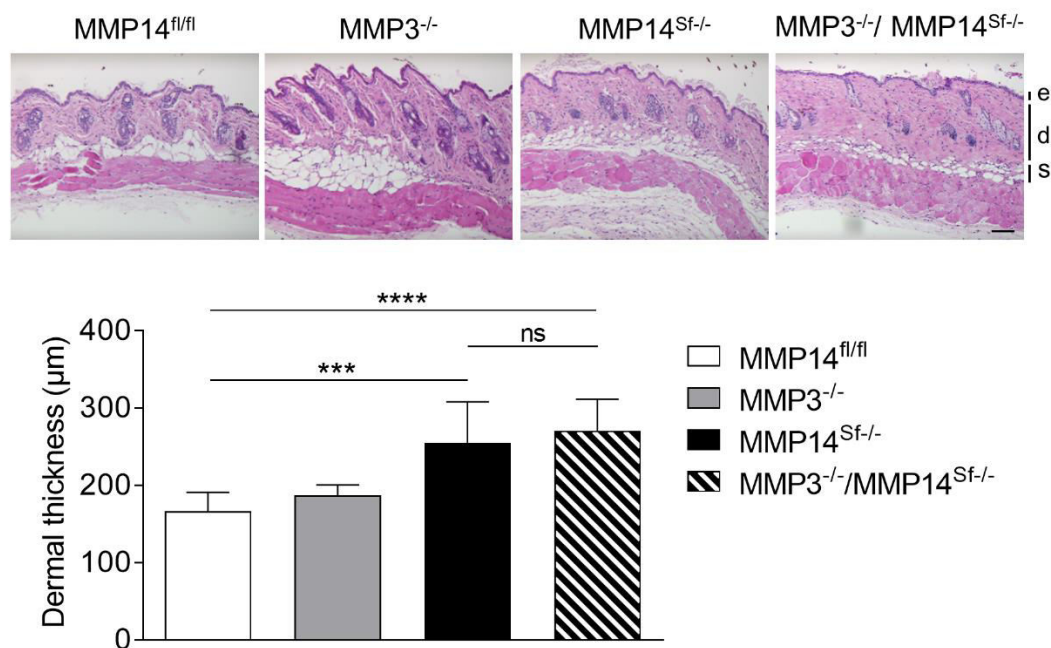
Figure 32: Loss of fibroblast-MMP14 increases dermal thickness in single and double knockout skin. Skin sections of MMP3^{-/-}/MMP14[Sf-/-] and control mice were stained for H&E. Analysis of dermal thickness in MMP3^{-/-}/MMP14[Sf-/-] mice and controls was performed. Mean ± SD; ***$p < 0.0005$, ****$p < 0.0001$, ns: not significant, n=7; Scale: 500 μm; e: epidermis; d: dermis; s: subcutaneous fat layer.
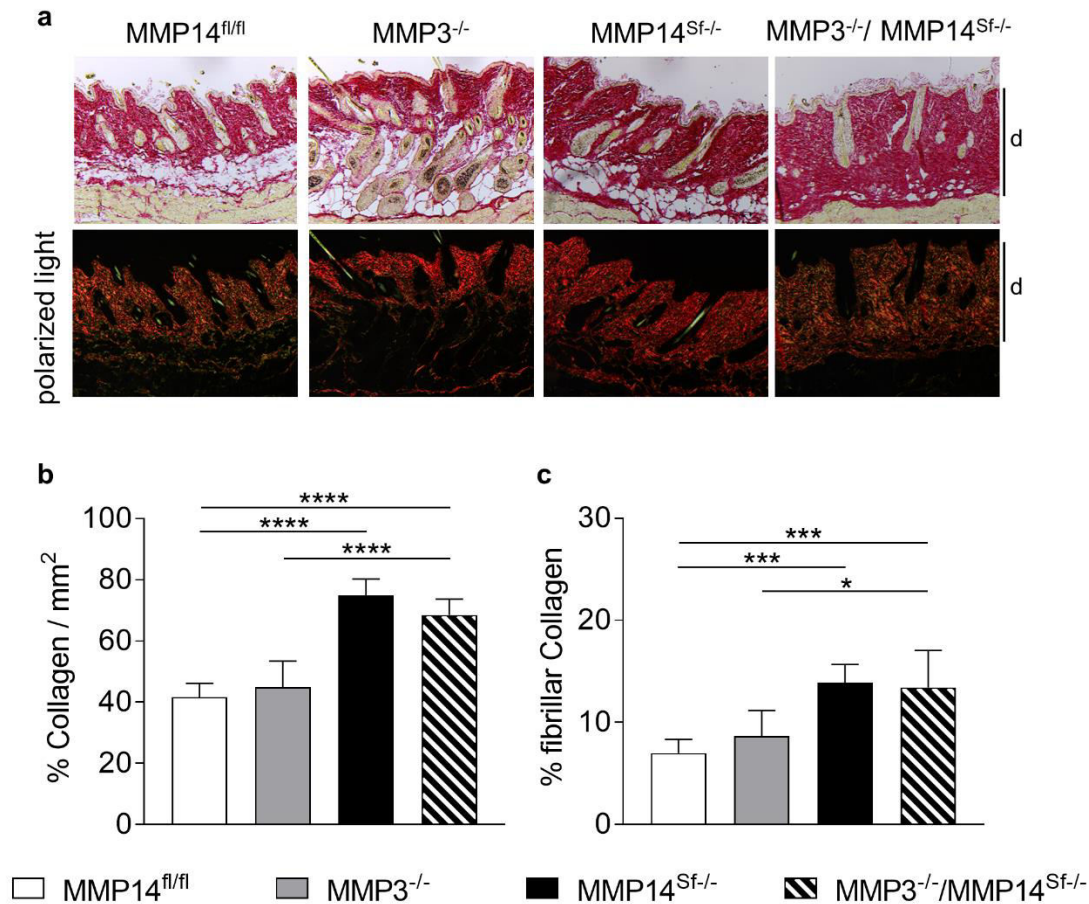
Figure 33: Enhanced collagen in the skin of MMP3$^{-/-}$/MMP14$^{Sf-/-}$ mice. a) Picrosirius red staining of skin section from MMP3$^{-/-}$/MMP14$^{Sf-/-}$ and control mice analyzed by brightfield microscopy (top panel) and under polarized light. Scale: 100 μm; d: dermis. **b)** Analysis of overall collagen analyzed as percentage collagen per area using pictures taken with brightfield microscopy. Mean ± SD; ****p < 0.0001; n = 6–7. **c)** Determination of percentage fibrillary collagen per area using images obtained with polarized light. Mean ± SD; *p < 0.05, ***p < 0.001; n = 6–7.

3.2.3. Double deficiency affects wound closure

In physiological conditions activity of MMPs is very low and as we showed for MMP14 [251], required only in low amount to ensure skin homeostasis. However, during skin wound healing in adulthood, several MMPs are upregulated in a very timely and controlled manner to ensure correct tissue repair [46]. Among these proteases are also MMP3 and MMP14 [46, 419, 430, 470]. Although in the MMP14$^{Sf-/-}$ mice skin repair was overall unaltered despite the fibrosis-like phenotype [251] we asked the question whether there are functions during this process that are compensated through the activity of the upregulated MMP3.
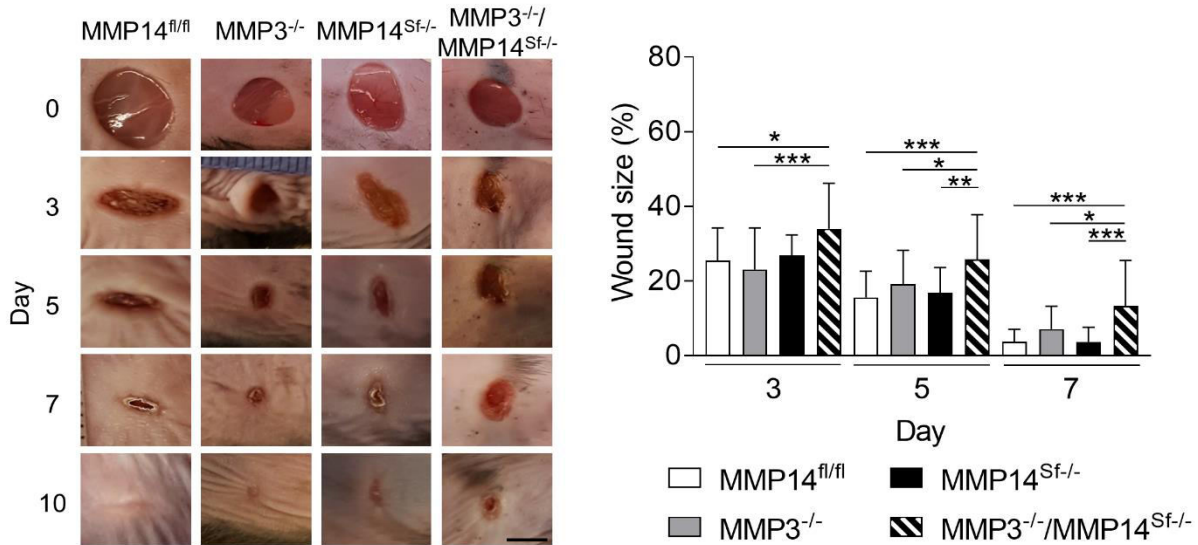
Figure 34: Wound closure is delayed in MMP3$^{-/-}$/MMP14$^{Sf-/-}$ mice. Excisional wound closure was macroscopically analyzed over time by measuring wound size at different time point. Closure was presented as percentage of initial wound area. Mean ± SEM; *p<0.05, **p<0.005, ***p<0.0005, other comparisons are not significant; for all time points: MMP14$^{fl/fl}$ n=12, MMP3$^{-/-}$ n=17, MMP14$^{Sf-/-}$ n=10, MMP3$^{-/-}$/MMP14$^{Sf-/-}$ n=13; Scale: 500 mm.

To address this question, excisional wounds of 6 mm diameter were made to the back skin of all investigated mice. Pictures of the wounds were taken and wound size measured macroscopically over time. The percentage of the free wound area from the initial wound size at day 3, 5, 7, 10 and 12 post-wounding is shown in the graph (Figure 34). As previously observed [419], wounds of MMP3$^{-/-}$ showed a delay in closure which was significant at day 7 post-wounding when compared to floxed controls. Macroscopical analysis further showed a significant increase in wound size in MMP3$^{-/-}$/MMP14$^{Sf-/-}$ mice compared to MMP14$^{fl/fl}$ wounds at days 3 to 10 post-wounding.
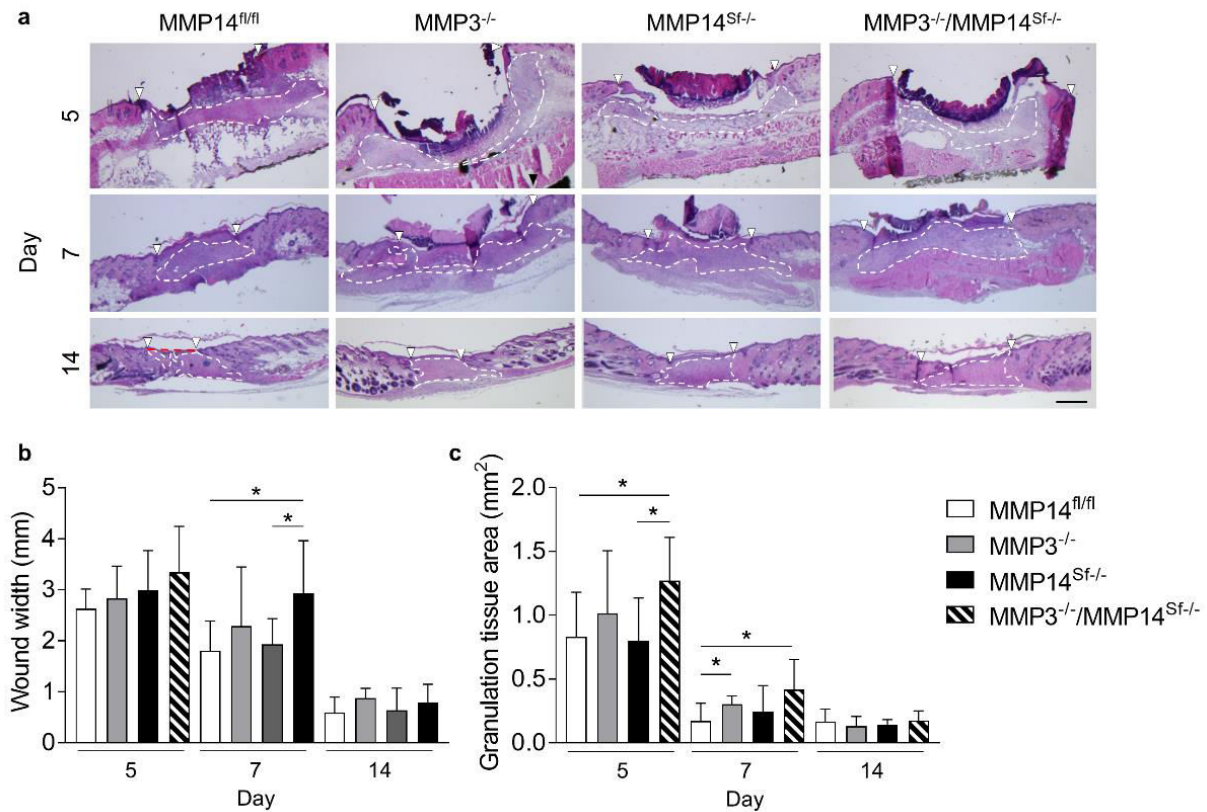
Figure 35: Histochemical analysis reveals delay in MMP3$^{-/-}$/MMP14$^{Sf-/-}$ wound closure. a) H&E staining of day 5, 7 and 14 wound sections from MMP3$^{-/-}$/MMP14$^{Sf-/-}$ and control mice. Dotted white lines mark the granulation tissue area. Wound edges are indicated by arrowheads. Scale: 500 μm. **b)** Wound width was calculated by measuring the distance of the wound edges at day 5, 7 and 14. Dotted red line represents measured wound width. Mean ± SD; *p<0.05, other comparisons are not significant; for all time points: MMP14$^{fl/fl}$ n=6–7, MMP3$^{-/-}$ n=6–9, MMP14$^{Sf-/-}$ n=8–7, MMP3$^{-/-}$/MMP14$^{Sf-/-}$ n=7–8. **c)** Granulation tissue area analysis in H&E sections. Mean ± SD; *p<0.05, other comparisons are not significant; for all time points: MMP14$^{fl/fl}$ n=7–8, MMP3$^{-/-}$ n=3–9, MMP14$^{Sf-/-}$ n=8, MMP3$^{-/-}$/MMP14$^{Sf-/-}$ n=5–8.

The delay in wound closure in MMP3$^{-/-}$/MMP14$^{Sf-/-}$ was even more striking by microscopical analysis of wound sections stained for H&E (Figure 35a). After staining, wounds width in sections of day 5, 7 and 14 wounds (Figure 35b) and granulation tissue area were measured (Figure 35c). Contrary to the macroscopical analysis, wound width at day 5 was comparable among all genotypes, but at day 7 sections in MMP3$^{-/-}$/MMP14$^{Sf-/-}$ mice that was significantly larger as compared to floxed controls and MMP14$^{Sf-/-}$ mice. The measured granulation tissue area was significantly increased in MMP3$^{-/-}$ at day 7 in agreement with a delay in wound closure here observed macroscopically and previously shown [419]. Granulation tissue was significantly enlarged in day 5 and 7 wounds of double deficient mice, whereas, in line with the previous publication [251] MMP14$^{Sf-/-}$ wounds were comparable to floxed controls regarding width and granulation area at all time points.
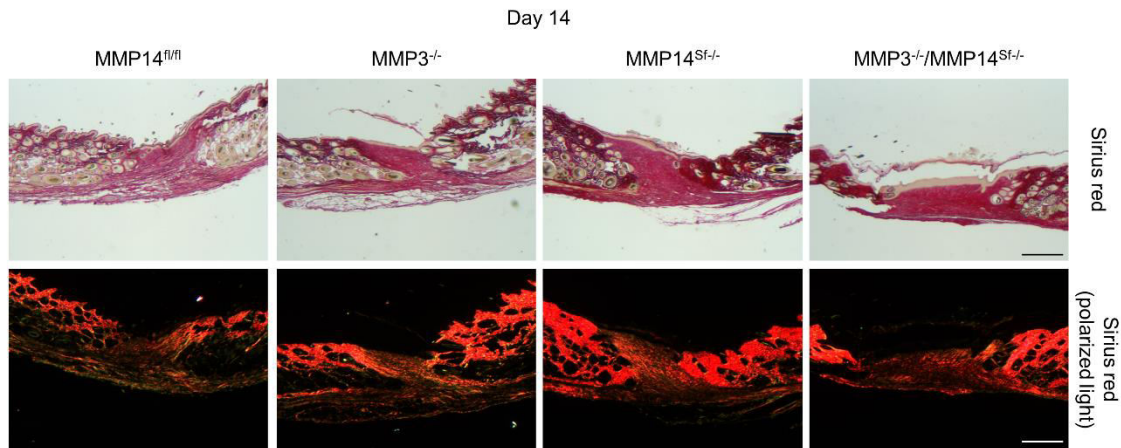
Figure 36: Fibrillar collagen is comparable in day 14 granulation tissue. Picrosirius Red staining of day 14 wound sections from MMP3$^{-/-}$/MMP14$^{Sf-/-}$ mice and controls. Tissues were analyzed under bright field and polarized light. Scale: 500 μm.

Although loss of fibroblast-derived MMP14 caused development of a fibrosis-like phenotype, collagen content in MMP14$^{Sf-/-}$ late stage wounds and scars was comparable to controls [251]. Staining of tissue sections of day 14 wounds with Picrosirius Red and following analysis under polarized light (Figure 36), showed that double deficiency of MMP14 and 3 had no striking effect on fibrillar collagens in the granulation tissue and collagen content appeared comparable among all genotypes.

Moreover, regardless of delayed wound closure, skin repair seemed unaffected by the individual and combined loss of MMP3 and MMP14 as observed in macroscopical analysis, where all wounds appeared closed at day 14 post wounding. Furthermore, as detected by immunostaining of the epithelial marker Keratin 14 (K14) (Figure 37), at day 14, all genotypes showed a restored epithelial layer.

Therefore, loss of MMP3 affects early wound closure, but overall wound repair is comparable and completed at day 14 in all genotypes.

Day 14

MMP14^{fl/fl}

MMP3^{-/-}

MMP14^{Sf-/-}

MMP3^{-/-}/
MMP14^{Sf-/-}

K14 / DAPI
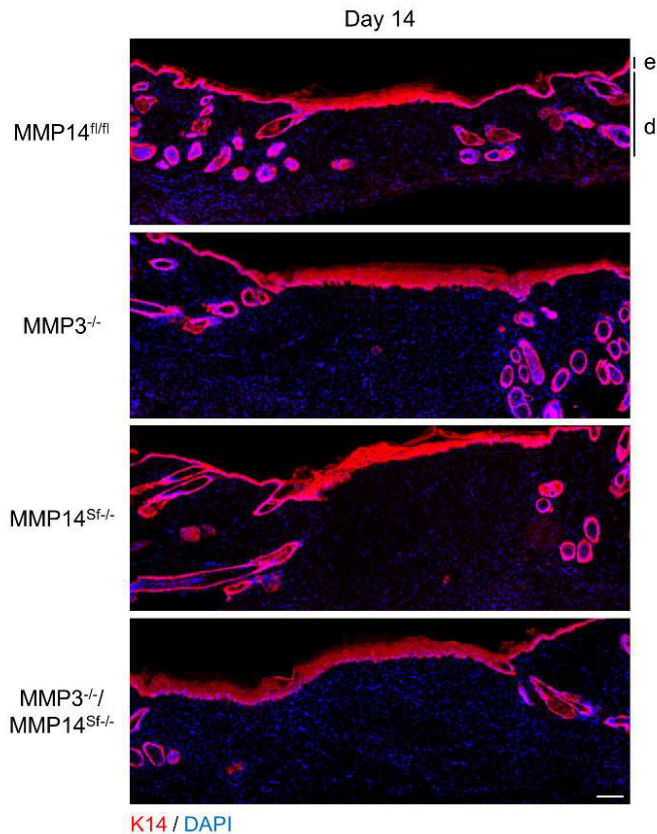
Figure 37: Epidermal integrity is restored at day 14 in all mice. Immunofluorescence staining for the keratinocyte marker keratin 14 (K14, red) and nuclei (DAPI, blue) in day 14 wound sections. e: epidermis, d: dermis. Scale: 100 µm.

3.2.4. Loss of MMP3 and fibroblast-MMP14 does not affect wound immune infiltrate and vascularization but alters myofibroblast density

The early delayed wound healing in MMP3$^{-/-}$/MMP14$^{Sf-/-}$ mice could result from different defects. In early tissue repair the granulation tissue is formed over the wound. This consists of a mass of vascularized connective tissue hosting several inflammatory cells including homed and resident macrophages [471]. As changes in these cells lead to alterations in tissue repair, we addressed whether they are present in the injured site despite loss of MMP3 and fibroblast-MMP14. To this end, wound sections (day 5 and 7) were stained for the EC marker CD31 (Figure 38a) and the macrophage marker F4/80 (Figure 38b). Quantitative analysis of macrophage and vascular density showed no difference between all genotypes, although an assessment of the macrophage phenotype and vascular functionality was not further performed. Thus, migration of ECs and macrophages to the granulation tissue is independent of MMP3 and MMP14.
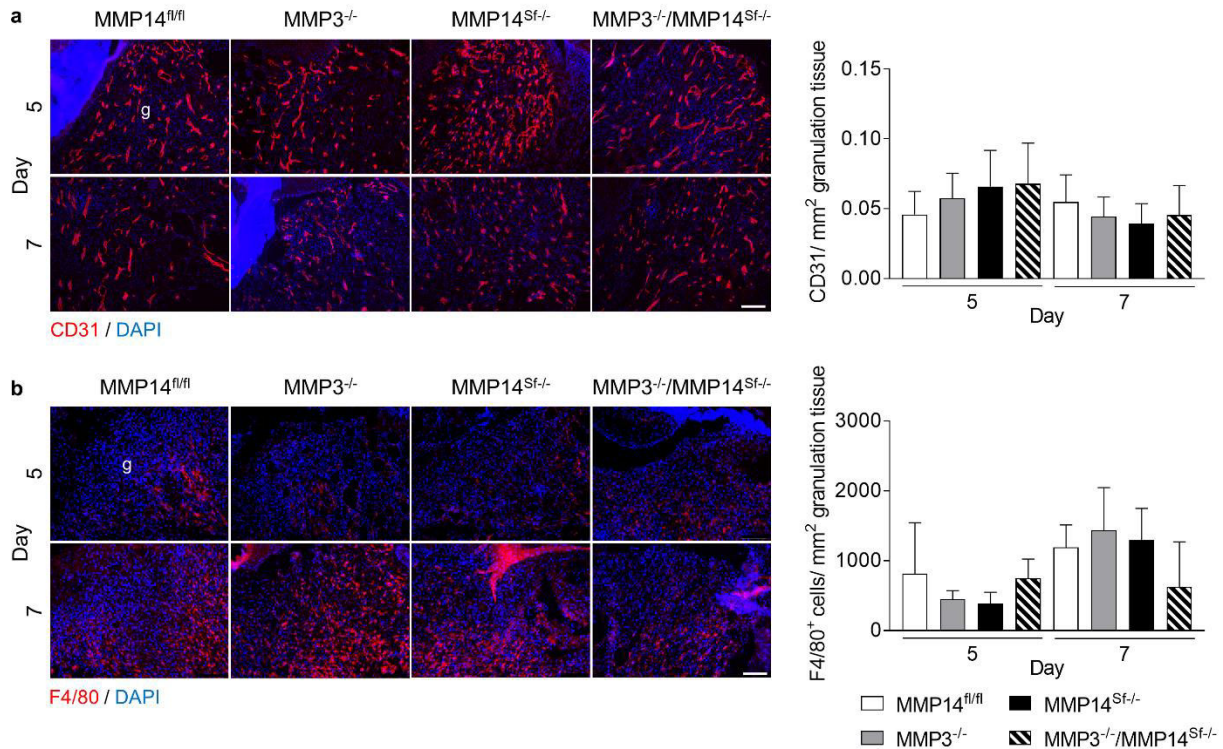
Figure 38: Comparable macrophages and vascularization in MMP3$^{-/-}$ and MMP14$^{Sf-/-}$ wounds. a) Immunofluorescences staining of day 5 and 7 wound sections for blood vessels (CD31) and **b)** macrophages (F4/80). Quantitative analysis of vascular density and macrophage numbers is represented shown in the graphs, with each dot representing one mouse/specimen. Mean ± SD; MMP14$^{fl/fl}$ n=6-8, MMP3$^{-/-}$ n=5-7, MMP14$^{Sf-/-}$ n=6-7, MMP3$^{-/-}$/MMP14$^{Sf-/-}$ n=8; Scale: 100 mm; g: granulation tissue.

After the granulation tissue is formed, wounds start to contract to restore tissue integrity. One of the main drivers of wound contraction are myofibroblasts residing in the granulation tissue [54]. Reduced wound closure and enhanced granulation in MMP3$^{-/-}$/MMP14$^{Sf-/-}$ and MMP3$^{-/-}$ wounds may point to a defective tissue remodeling and contraction of the wound, thus possibly implicating alterations in myofibroblasts in these processes. To further investigate this, myofibroblasts were immune-stained in tissue sections of day 5, 7 and 14 wounds and day 28 scar tissue using the marker αSMA [57].

Following quantitative analysis of αSMA signal intensity per granulation tissue area (Figure 39, pictures), all genotypes showed low αSMA intensities in early wounds (day 5), but increase in day 7 wounds. However, wounds from single and double deficient mice demonstrated significantly less αSMA compared to floxed controls. At day 14, in wounds of floxed control only a few αSMA positive cells remained in the granulation tissue, but in MMP3$^{-/-}$ and MMP14$^{Sf-/-}$ wounds they were significantly higher. In double deficient mice, the increase in αSMA was even more striking and significantly higher than in floxed controls and single knockouts (Figure 39, left graph). In scar tissue (day 28) αSMA signal intensities were overall very low, but remained significantly elevated in MMP3$^{-/-}$/MMP14$^{Sf-/-}$ mice compared to

MMP14$^{Sf-/-}$ animal, while comparable in the other three genotypes (Figure 39, right graph). Thus, loss of MMP3 and MMP14 leads to reduced presence of myofibroblasts in wounds, but these cells persist longer in the granulation tissue.
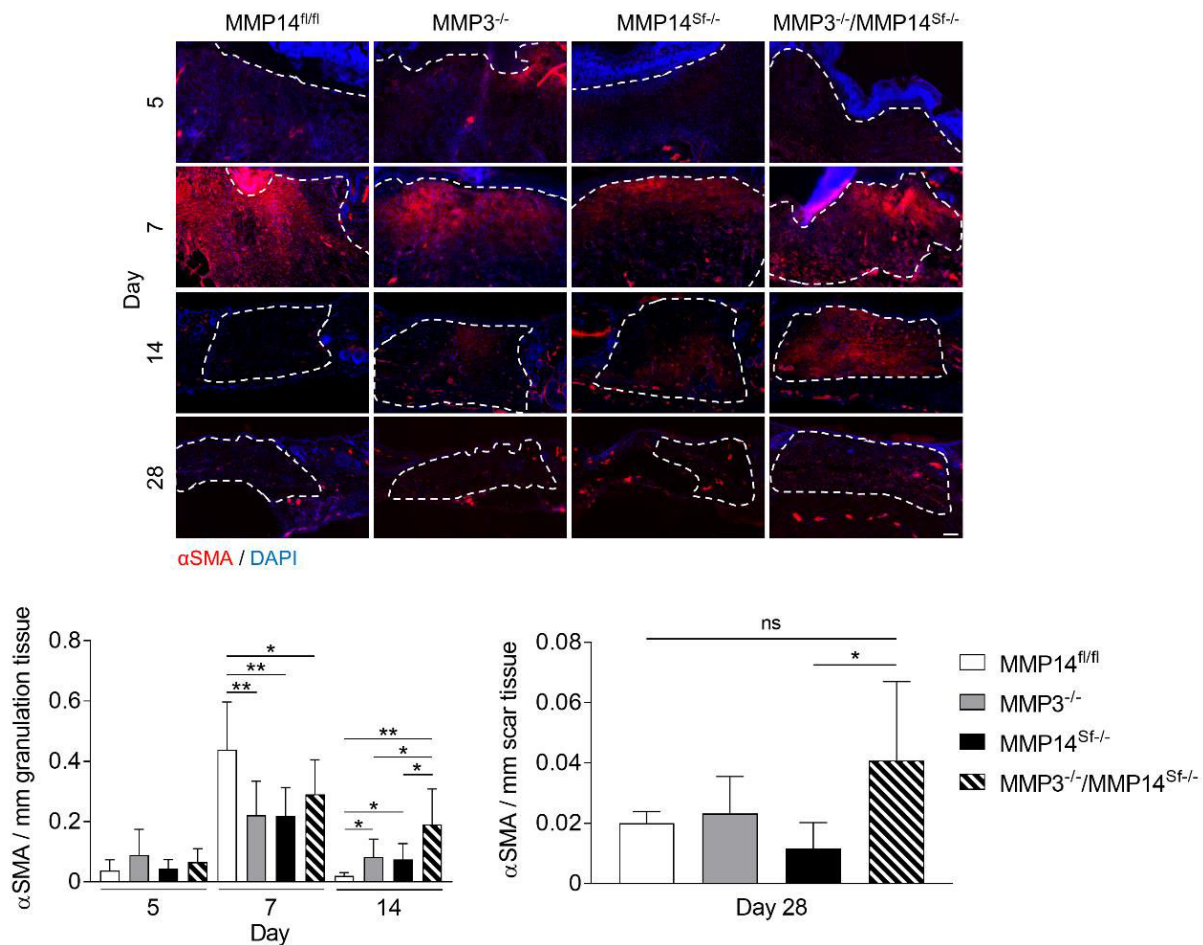
Figure 39: Myofibroblast formation and resolution is affected by loss of MMP3 and MMP14. Sections of day 5, 7 and 14 wounds, and day 28 scars were immunofluorescence stained for myofibroblasts (αSMA, red) and nuclei (DAPI, blue). αSMA was analyzed as fluorescence intensity per granulation tissue (left graph) and scar tissue area (day 28, right graph). Dotted line indicates analyzed area. Mean ± SD; *p<0.05, **p<0.005; for all time points: MMP14$^{fl/fl}$ n=5–8, MMP3$^{-/-}$ n=3–9, MMP14$^{Sf-/-}$ n=6–9, MMP3$^{-/-}$/MMP14$^{Sf-/-}$ n=5–8; Scale: 100 μm.

During granulation tissue formation, cell numbers are strongly increased through recruitment of endothelial cells, macrophages and fibroblasts to the site of injury [472, 473]. To return to homeostatic conditions, granulation tissue is resolved and cells are cleared from the site through apoptosis [73]. For myofibroblasts several molecular paths lead to cell apoptosis and clearance [474]. Thus, one hypothesis we put forward is that in the absence of the investigated MMPs, higher number of myofibroblasts in day 14 wound are due to reduced apoptosis rather than enhanced proliferation. To address this, tissue sections of day 7 and 14 wounds were stained by immunofluorescence for the apoptosis marker cleaved caspase 3 (Figure 40a). Quantitative analysis of positive cell numbers showed low numbers of apoptotic cells in day 7 wounds

without differences among the genotypes. However, while the number of cleaved caspase 3 positive cells strongly increased in floxed controls at day 14 post-wounding, wounds from MMP14$^{Sf-/-}$ and MMP3$^{-/-}$/MMP14$^{Sf-/-}$ demonstrated significantly less positive cells, indicating decreased apoptosis in the granulation tissue of these mice. When tissue staining were performed using both, cleaved caspase 3 and αSMA antibodies, the percentage of double positive myofibroblasts was significantly lower in single and double deficient mice lacking fibroblast-derived MMP14 compared to floxed controls (Figure 40b). Also MMP3$^{-/-}$ mice showed reduced numbers of cleaved caspase 3 positive myofibroblasts, but this difference was not significant.
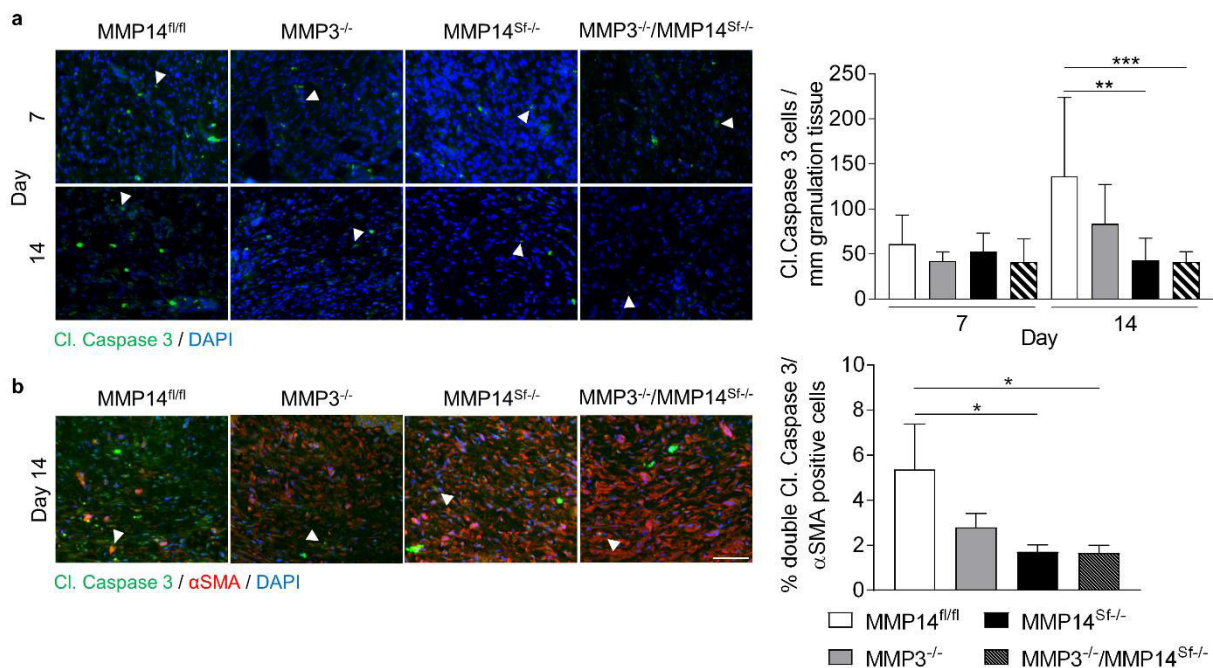
Figure 40: Reduced cell death of myofibroblasts in MMP3$^{-/-}$/MMP14$^{Sf-/-}$ day 14 wounds. a) Day 7 and 14 wound sections were stained for the cell death marker cleaved (cl.) Caspase 3 (green) and DAPI (blue) for nuclei visualization. The number of cl. Caspase 3 positive cells were analyzed per granulation tissue area. White arrowheads indicate cl. Caspase 3 positive cells. Mean ± SD; **p<0.005, ***p<0.0005; Day 7: MMP14$^{fl/fl}$ n=13, MMP3$^{-/-}$ n=11, MMP14$^{Sf-/-}$ n=13, MMP3$^{-/-}$/MMP14$^{Sf-/-}$ n=16; Day 14: MMP14$^{fl/fl}$ n=8, MMP3$^{-/-}$ n=18, MMP14$^{Sf-/-}$ n=6, MMP3$^{-/-}$/MMP14$^{Sf-/-}$ n=12. **b)** Immunofluorescence staining of day 14 wound sections for cl. Caspase 3 (green) and myofibroblasts (αSMA, red). Nuclei are visualized by DAPI (blue). Number of double positive cl. Caspase 3 and αSMA positive myofibroblasts was calculated. Mean ± SEM; *p<0.05; MMP14$^{fl/fl}$ n=7, MMP3$^{-/-}$ n=8, MMP14$^{Sf-/-}$ n=9, MMP3$^{-/-}$/MMP14$^{Sf-/-}$ n=7; Scale: 100 μm.

In addition, also proliferation of myofibroblasts was analyzed in late wounds (day 14). Co-staining of the proliferation marker Ki67 with α-SMA identifying myofibroblasts and quantification of percentage of double positive α-SMA cells revealed increased myofibroblast proliferation in MMP3$^{-/-}$/MMP14$^{Sf-/-}$ mice (Figure 41). These results demonstrate that in addition to the above shown reduction of myofibroblasts that undergo apoptosis in late wounds

(day 14) of mice lacking MMP3 and MMP14, enhanced proliferation leads to myofibroblast persistence in these mice.
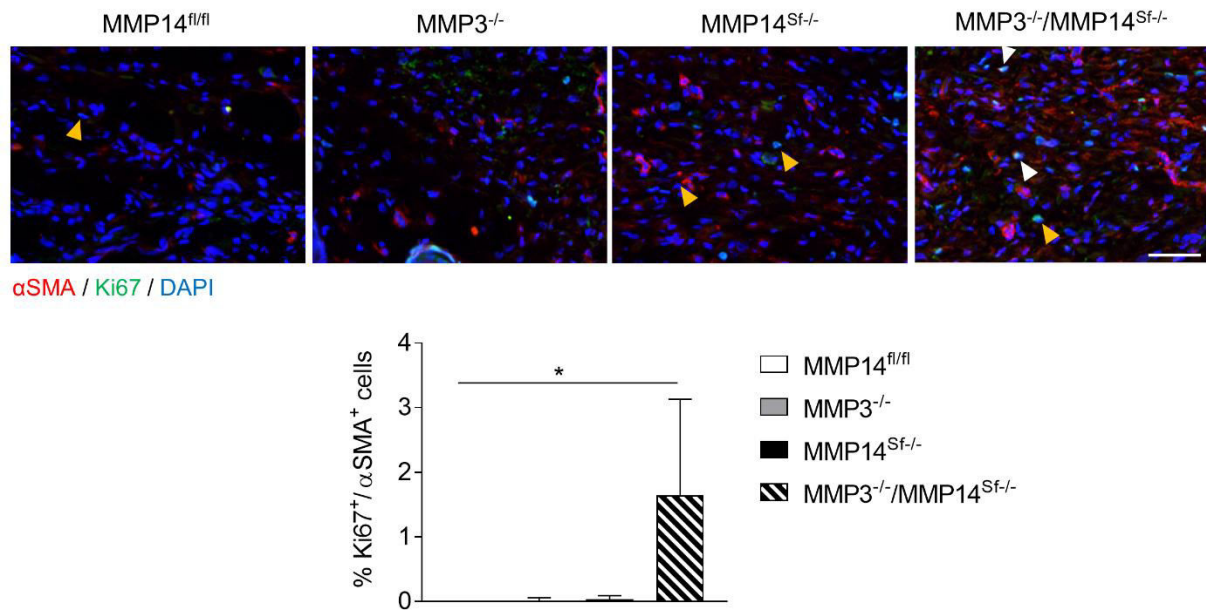
Figure 41: Increased proliferation in myofibroblasts of day 14 wounds. Immunofluorescence staining of day 14 wounds for the proliferation marker Ki67 (green) and myofibroblasts (αSMA, red). Nuclei were visualized with DAPI (blue). Percent of Ki67 positive myofibroblasts was determined. Mean ± SD; *p<0.05; MMP14$^{fl/fl}$ n=4, MMP3$^{-/-}$ n=9, MMP14$^{Sf-/-}$ n=3, MMP3$^{-/-}$/MMP14$^{Sf-/-}$ n=5; Scale: 50 μm

3.2.5. Does loss of MMP3 and MMP14 affect TGFβ signaling?

Apart from the myofibroblasts persistence, overall the numbers of myofibroblasts earlier in wounds at day 7 is reduced as compared to controls. That can be the result of altered fibroblasts activation by growth factors that is the main source of myofibroblasts [475-477], with TGFβ1 being the most prominent activator [63, 478, 479].
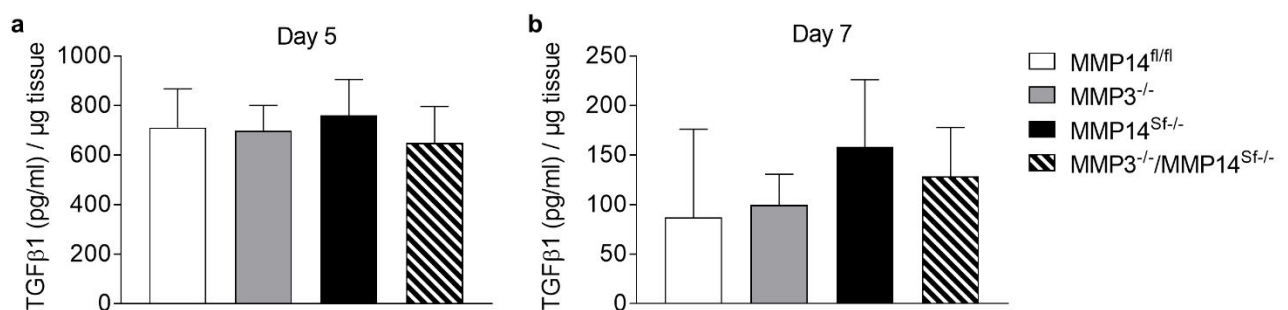
Figure 42: Comparable TGFβ1 levels in wounds. a) Analysis of TGFβ1 concentration in day 5 and **b)** day 7 wound lysates by TGFβ1 ELISA. Mean ± SD; n=4.

To determine whether TGFβ1 levels are altered upon loss of MMP3 and MMP14, tissue lysates prepared from day 5 and 7 wounds were analyzed by the TGFβ1 Quantikine ELISA Kit (Figure 42). For the analysis, since active TGFβ1 in tissue was barely detected, we quantified total HCl-activated TGFβ1 in the tissue lysates. Overall the concentrations detected in day 5 wound lysates were around 600-800 pg/ml (Figure 42a), and in day 7 wound lysates around 80-160 pg/ml (Figure 42b). At both time points TGFβ1 concentration was comparable among all genotypes. Since despite differences in myofibroblasts the total amount of TGFβ1 was not altered in wound tissue, it remained to be investigated whether the amount the amount of total TGFβ1 only in fibroblasts was comparable. TGFβ1 secreted by primary fibroblasts, as analyzed by ELISA, showed no differences between single and double deficient cells, and floxed controls (Figure 43c). Furthermore, as detected by qPCR analysis, TGFβ1 (Figure 43a) and TGFβR1 (Figure 43b) transcripts in primary fibroblasts were comparable among all genotypes. Thus, loss of MMP3 and MMP14 has no effect on expression of TGFβ1 and of the cellular receptor TGFβR1.
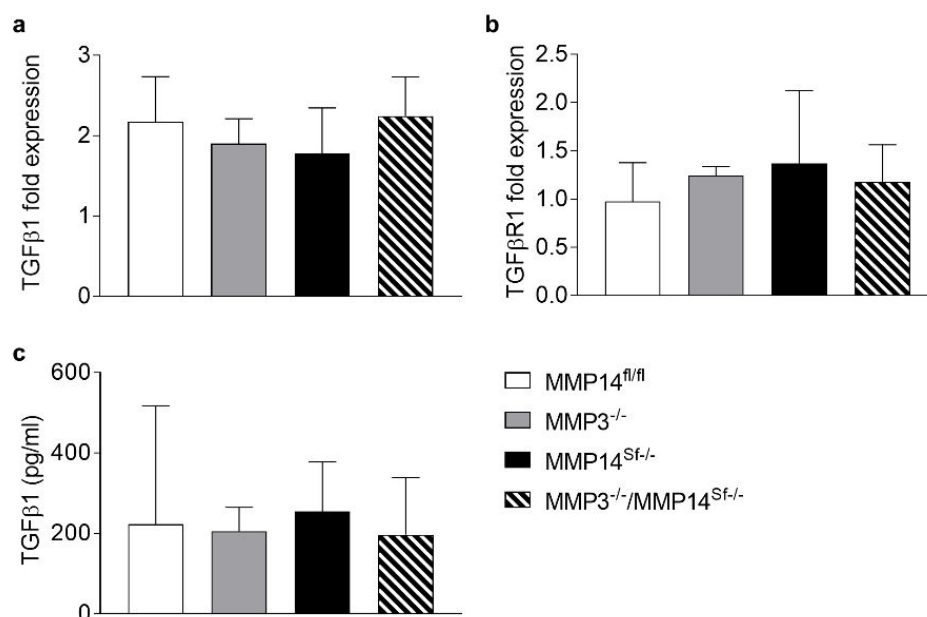
Figure 43: TGFβ1 and TGFβR1 expression are comparable in primary fibroblasts. a) TGFβ1 ELISA detecting TGFβ1 concentration in supernatants of MMP3^{-/-}/MMP14[Sf-/-] and control fibroblasts. Mean ± SD; n=3. **b)** Transcript analysis of TGFβ1 and **c)** TGFβR1 expression in MMP3^{-/-}/MMP14[Sf-/-] and control fibroblasts. S26 was used as control. Mean ± SD; n=3.

Although TGFβ1 and cell receptors expression were unaltered, we wanted to address whether the TGFβ1-mediated signaling pathway was still active upon stimulation. Therefore, cultured fibroblasts isolated from MMP3^{-/-}/MMP14[Sf-/-] and control mice were treated with 40 ng/ml recombinant TGFβ1. The readout for fibroblasts activation was the αSMA expression (Figure

44). Stimulation with TGFβ1 resulted in induction of αSMA expression, detected by RNA (Figure 44a) and in immunoblot analysis (Figure 44b), in all cells independently of the genotypes thus the transduction of signals through the receptor was efficient.

However, besides TGFβ1 signaling, fibroblast differentiation can also be induced by mechanical cues [53, 480, 481]. One model to mimic the effect of mechanical tension on fibroblasts is culturing them in tethered 3D-collagen gels [482]. Cells were cultured in the gels and as monolayer for 24 h and after extracting cells from the gel cultures, αSMA expression was analyzed in lysates by immunoblot. αSMA was detected at a low level in all cells cultured as monolayer, and found enhanced upon cell culture in 3D collagen gels, with no differences in intensity in all cell genotypes (Figure 44c). Taken together, these experiments showed that loss of MMP3 and MMP14 in fibroblasts does not impact fibroblast activation into myofibroblasts either by TGFβ1 induction or mechanical stress.
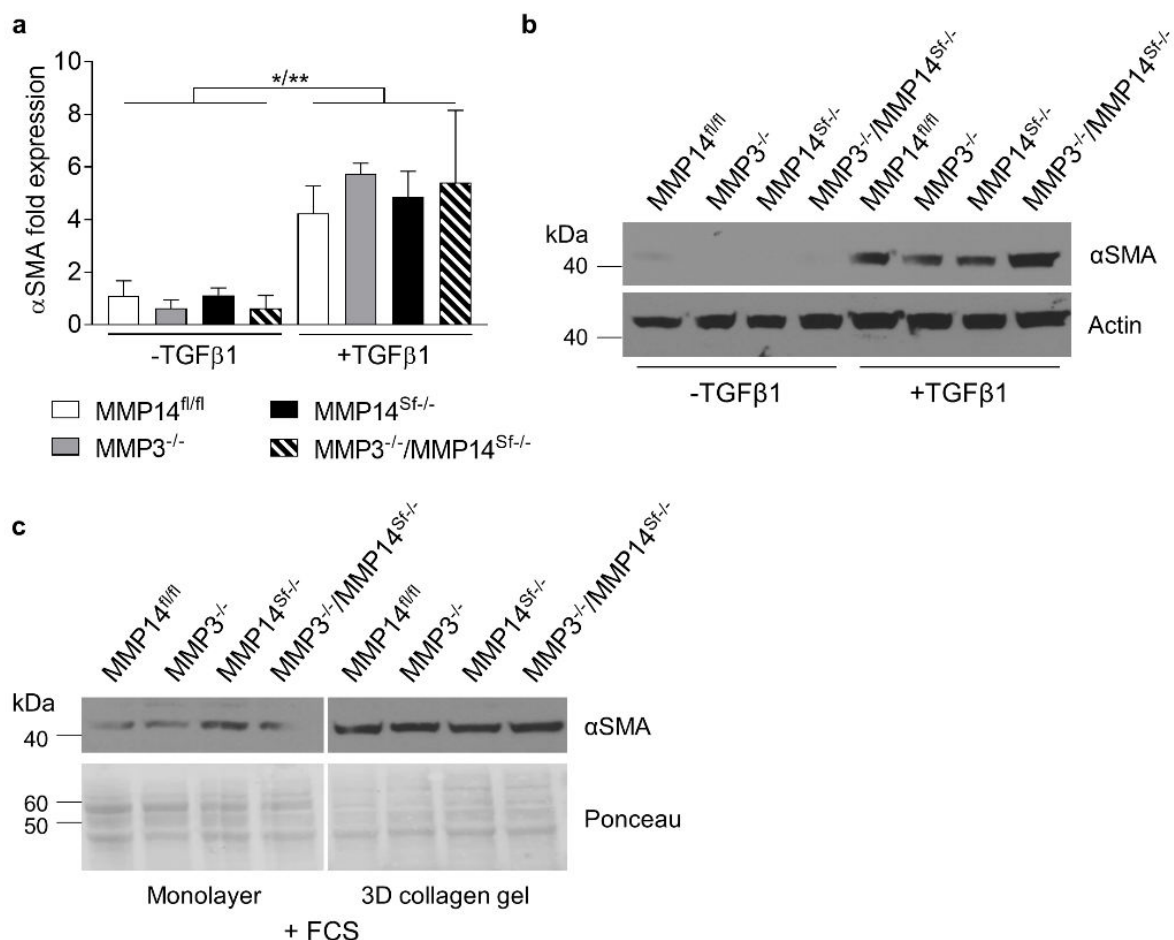
Figure 44: Loss of MMP3 and MMP14 has no effect in intrinsic sensitivity of fibroblasts towards TGFβ1 signaling and mechanical stress. a) Analysis of fibroblast activation upon TGFβ1 treatment by detecting αSMA expression on transcript level and b) via immunoblot. S26 was used as control in

transcript analysis, actin as loading control in immunoblot. Mean ± SD; *p<0.05, **p<0.005; n=3. c) Immunoblot analysis of αSMA expression in fibroblasts cultured as monolayer and in 3D tethered collagen gels. Ponceau was used as loading control.

The question remaining open was: is TGFβ1 signaling altered upon the loss of MMP3 and MMP14? One of the main intracellular mediators of TGFβ1 signaling in myofibroblasts is pSmad2 [483-485]. Therefore, co-staining for pSmad2 and αSMA was performed in sections from early wounds (day 5) (Figure 45). Percentage of double positive cells was determined and revealed significantly less nuclear pSmad2 staining in αSMA positive cells in mice lacking fibroblast-derived MMP14 (Figure 45). This number also seems to be reduced in MMP3-deficient mice, but this reduction is not significant. Thus, downstream signaling of TGFβ1 might be impaired by the loss of MMP3 and fibroblast-derived MMP14.
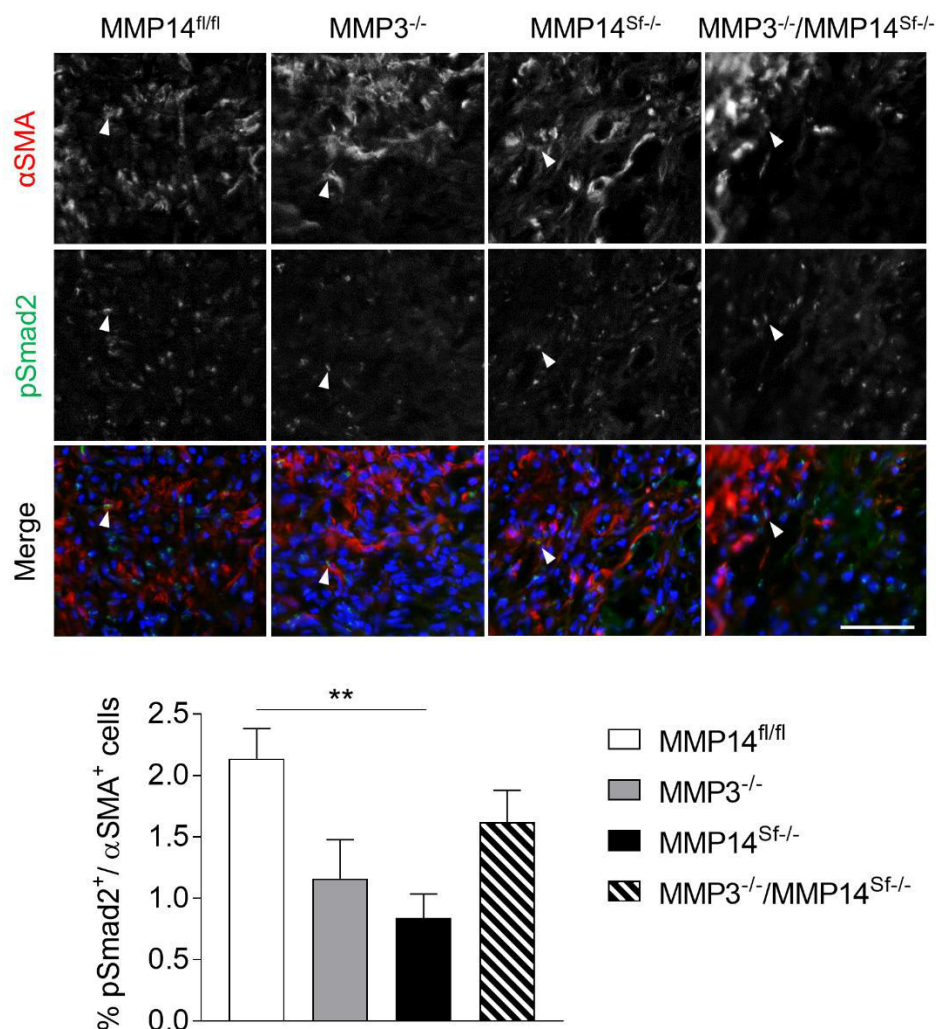
Figure 45: Loss of fibroblast MMP14 reduces pSmad2. Day 5 wound sections were stained for pSmad2 (green) and myofibroblasts (αSMA, red). Nuclei are visualized by DAPI (blue). Percent of double positive pSmad2 and αSMA positive myofibroblasts was calculated. Mean ± SEM; **p<0.01; MMP14$^{fl/fl}$ n=7, MMP3$^{-/-}$ n=6, MMP14$^{Sf-/-}$ n=7, MMP3$^{-/-}$/MMP14$^{Sf-/-}$ n=8; Scale: 50 μm.

3.2.6. Loss of MMP3 but not MMP14 affects contractile activity of fibroblasts

Delayed wound contraction in MMP3 knockout mice was identified to likely result from impaired fibroblast contractile activity [420]. When comparing the observed phenotypes in single and double deficient mice in regards to wound closure and myofibroblasts one thing that is standing out is that the delay in wound closure on microscopical level only occurred in mice lacking MMP3, whereas all single and double deficient mice showed a myofibroblast phenotype. This could indicate that altered myofibroblast formation is not the only factor contributing towards impaired wound contraction. Therefore, to further analyze the contractile activity of fibroblasts, cells isolated from MMP3^{-/-}/MMP14[Sf-/-] and control mice were seeded in free floating 3D-collagen gels. Collagen gel size was measured over time and the percent size reported as average in the graph (Figure 46). As visible in the graph and in the photographs of the gel (Figure 46), while gels with fibroblasts from floxed controls and MMP14[Sf-/-] mice were rapidly reduced in size, those with embedded cells from mice lacking MMP3 remained significantly larger. Thus, MMP3 appears to be the main factor causing reduced wound contraction, possibly leading to the observed delay in wound closure in MMP3^{-/-} and MMP3^{-/-}/MMP14[Sf-/-] mice.
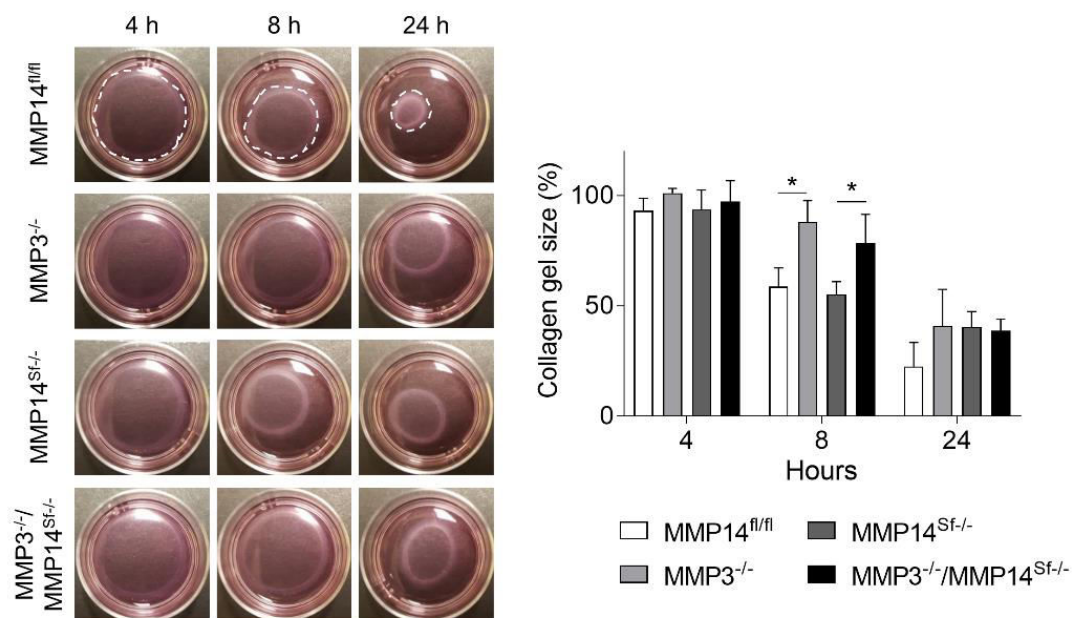
Figure 46: Reduced collagen gel contraction by fibroblasts lacking MMP3. Primary fibroblasts from MMP3^{-/-}/MMP14[Sf-/-] and control mice were seeded in 3D free floating collagen gels and gel size was measured over time. Mean $\pm$ SD; *$p<0.05$; n=3.

3.2.7. Soluble factors altered in wound at day 5 in knockout mice.

Although TGFβ1 is considered the main driver of myofibroblast formation, other factors have been identified to successfully induce fibroblast differentiation, as for example PDGF-B [476] and TNFα [475]. These and many other factors could be investigated by proteome profile analysis based on antibody arrays. This array was used to analyze factors in day 5 wound lysates from MMP3$^{-/-}$/MMP14$^{-/-}$ and control mice. Signal intensities detected for each analyzed factor were compared to MMP14$^{fl/fl}$ intensities and considered to be significant at a ratio of 2 and higher (or under 0.5 and lower). Multiple factors were significantly altered in single and double deficient wounds and are listed in table 10. As previously detected (Figure 24), MMP3 was upregulated in MMP14$^{Sf-/-}$ and, as expected, is not detected in MMP3$^{-/-}$ and MMP3$^{-/-}$/MMP14$^{Sf-/-}$ wound lysates. Among the regulated factors is ADAMTS1 that was downregulated in wounds of single and double deficient mice. Significantly upregulated in all knockouts were angiogenin, endoglin, leptin and PDGF-AA. In MMP14$^{Sf-/-}$ and MMP3$^{-/-}$/MMP14$^{Sf-/-}$ wounds there was an increase in endothelin-1, whereas PIGF-2 was only significantly enhanced in wound lysates from double deficient mice. On the other hand, amphiregulin was upregulated in MMP14$^{Sf-/-}$ wounds but not in the other lysates. These data indicate that several factors other than TGFβ1 could contribute to altering myofibroblast formation in knockout wounds. Their impact on the phenotype will require further analysis.

Table 10: Factors identified as significantly altered in Proteome Profiler^{TM} analysis of day 5 wound lysates. Values were normalized to MMP14$^{fl/fl}$ controls and per genotype three different lysates were pooled.

Protein	MMP14$^{fl/fl}$	MMP3$^{-/-}$	MMP14$^{Sf-/-}$	MMP3$^{-/-}$/MMP14$^{Sf-/-}$
ADAMTS1	1.0	0.5	0.3	0.3
Amphiregulin	1.0	1.0	5.2	1.0
Angiogenin	1.0	7.4	8.0	5.6
Endoglin	1.0	3.4	8.3	5.6
Endothelin-1	1.0	1.0	5771.8	2866.7
Leptin	1.0	3733.6	3863.4	1940.5
MMP-3 (pro and mature form)	1.0	0.0	11.7	0.0
PDGF-AA	1.0	65.5	70.7	27.3
PIGF-2	1.0	1.1	1.9	2.2

4. Discussion

4.1. EC-specific deletion of MMP14

4.1.1. Skin vascularization and sprouting are unaffected by MMP14 deletion

Despite multiple angiogenic defects resulting from the complete deletion of MMP14 in mice [252, 361, 364], we did not detect significant developmental abnormalities in mice with EC-specific deletion of MMP14. A few alterations were observed in the skull with delayed suture closure at day seven post-birth and a slight deviation of the snout, most prominent three months after birth [390]. This was surprising, as although suture closure was also defective in mice with global MMP14 deletion, these skeletal defects were associated with MMP14 loss impacting the membranous cranial bone formation and the impaired removal of cartilage primordia [252]. These data now suggest that in addition to MMP14 derived from skeletal stem cells, whose deletion caused skeletal defects similar to the complete knockout [387], also EC-MMP14 participates in skull development.

Corneal vascularization that is highly plastic shortly after birth [441, 442] was found normal in MMP14$^{EC-/-}$, but aortic explants from MMP14$^{EC-/-}$ mice embedded in collagen gels, although formed, sprouts were reduced in length, and ticker than controls. Also, using a Tie1-driven model for EC-specific MMP14 deletion, no alterations in cornea blood vessels vascularization were detected [389], but these authors identified EC-derived MMP14 as a protease for LYVE-1, whose shedding enhanced postnatal sprouting of lymphatic vessels [389]. However, we did not detect differences in lymph angiogenesis in the cornea of the MMP14$^{EC-/-}$ mice. A possible explanation is that our mouse model is different than that of Wong and colleagues [389], who used Cre-recombinase under the control of the Tie1 promotor. Cre activity in these mice could already be detected at E8-9 when using the β-Galactosidase reporter gene activity staining [486]. On the contrary, Tie2-driven Cre-recombinase is active in ECs starting at E13 [392]. Since development is a rapid process, the difference in time in MMP14 deletion might result in a less pronounced phenotype in the lymphatic vasculature.

However, the above data indicate that EC-derived MMP14 has no essential role during developmental angiogenesis or that other proteases or alternative pathways can compensate for its loss. A possibility is that expression of MMP14 in cells surrounding the endothelium, e.g., vascular smooth muscle cells or pericytes, is sufficient to enable sprouting and vessel elongation. In support of this theory, the complete deletion of MMP14 caused the failure of neoangiogenesis in response to FGF-2 in a corneas micropocket angiogenesis assay [361]. Moreover, aortic ring assays using aortas from MMP14 null mice, but not from our EC-specific

MMP14, showed impaired sprouting [365]. Taken together, these studies indicate that MMP14 expression by perivascular cells might support angiogenic sprouting. However, MMP14 expression in perivascular cells is relatively low [369], but we do not know whether MMP14 expression or that of enzymes with comparable functions, is upregulated in these cells in the MMP14$^{EC-/-}$ mice, and this issue still needs further investigations. Collagenolysis required for endothelial cell migration during elongation, although partly affected by lack of MMP14, could be sustained by MMP13, which was shown to regulate tumor blood vessel angiogenesis during melanoma growth [487]. Transcription of MMP15 and MMP16 is increased during tube formation [488], and MMP15 overexpression in MMP14$^{-/-}$ ECs rescued collagen proteolysis when cells were seeded in collagen gels [365]. Also, the activation of alternative mechanisms may compensate for the lack of MMP14. For example, during endochondral ossification, vascular canals that enter the epiphysis by invading the uncalcified hyaline cartilage are absent in the MMP14 deleted mice. Here ossification occurs in the absence of vascular canals and starts from the mineralized cartilage matrix via the perichondrium [252]. Thus, in MMP14$^{EC-/-}$ compensatory mechanisms cannot be excluded. Concerning the cornea, later time points may be necessary to identify alternative paths activated by the lack of MMP14 in the ECs.

10.1.2. Reduced tumor growth and intratumoral vascular permeability

Besides development, angiogenic processes in adulthood occur in multiple pathological conditions, such as, for example, in cancer [107]. As observed during development, in MMP14$^{EC-/-}$ mice, despite reduced melanoma growth, intra and peritumoral vascular density, generated by pathologically-induced angiogenetic processes, was not affected. As discussed above, also during these processes compensation of EC-MMP14 might be due to protease expression in surrounding cells, one of the most prominent being the tumor cells. Melanoma cells have enhanced expression of MMP14 [350, 489] where the protease mediates invasion and metastatic dissemination [349, 490]. Thus, MMP14 located on the B16F1 tumor cells might be sufficient for degrading the matrix and generate the path for blood vessel cells to elongate and expand vascular structures into the tissue. Another source of active MMP14 are pericytes and smooth vascular cells [373, 491]. Covering the vascular tube of endothelial cells, these cell types are close and actively involved in EC migration. The presence and activity of MMP14 in these cells, would explain why complete MMP14 knockout led to impaired vascular sprouting from aorta explant [365], but that was not altered, as we observed, by specific deletion in ECs.

During tumor growth and metastasis, the tumor vasculature acquires unique functional features, most strikingly it is hyperpermeable [185, 446, 492]. However, tumors in MMP14$^{EC-/-}$ mice displayed reduced intratumoral permeability. High vessel leakiness around tumors causes decreased blood flow into the tumor mass [492], and leads to hypoxia [493-495]. Hypoxia in turn induces HIF-1α [496], an activator of pro-angiogenic factors like VEGF [497-499] and bFGF [500, 501], thus angiogenesis and continuous formation of new vessels. However, despite being less permeable, this did not alter the numbers of intra and peritumoral vessels in the MMP14$^{EC-/-}$ mice. The increased vessel stability might though have affected the metastatic process since metastasis to distant organs was reduced in the MMP14$^{EC-/-}$ animals. Indeed, metastasis is supported by permeable vessels [502-504] and several studies showed, that vessel maturation is an effective way to prevent metastasis [505, 506].

Thus, the question arose which mechanisms could be altered from loss of EC-MMP14 and lead to the observed permeability phenotype. Regulation of vessel stability, and thus permeability, is a complex process mediated by multiple factors. In tumor vessels pericyte detachment enables EC proliferation [191] and promotes vessel leakiness [188, 190]. MMP14 in endothelial cells is in close proximity to surrounding cells, pericytes and vascular smooth muscle cells, and can thereby influence in several ways their attachment to the vessel. Indeed, in MMP14$^{EC-/-}$ mice pericytes association to the tumor vessels was increased.

Activity of MMP14 mediates several pathways that may modulate vessel coverage by those cells. Among them is the PDFG/PDGFR axis with EC-expressed PDGF-B binding PDGFRβ on pericytes [180, 507]. Also the angiopoietin/Tie2 [508] and TGFβ [509-511] signaling in ECs are modulated by MMP14 activity [341, 512, 513].

Pericytes recruitment is regulated by the Ang-1/Tie2 signaling [158, 161-163]. Besides Ang-1 having to compete with the antagonistic Ang-2 [192-194], also MMP14 was shown to interfere with Ang-1-mediated pericyte recruitment. Although MMP14 was shown to mediate Tie2 shedding [514, 515], we were not able to detect constitutively processed Tie2 in control cells in the same conditions previously used. However, we cannot exclude that technical issues, e.g. low sensitivity of the used antibodies, may have impaired these studies. In support of a role for MMP14-mediated Tie2 processing is however a previous study conducted with a mouse hind limb ischemia model. In that system, soluble Tie2 (cleaved Tie2), was reduced in HUVECs upon MMP14 siRNA silencing and led to preservation of full length Tie2 and active Ang-1 signaling [513].

Moreover, MMP14 has been also shown to be involved in PDGF-B/PDGFRβ mediated pericytes recruitment. It associates with PDGFRβ at the plasma membrane and loss of the

protease caused defects in mural cell chemotaxis and proliferation [373]. Pointing towards MMP14 regulation of pericytes recruitment by receptor shedding, are data we obtained by analysis of tumor lysates by proteome angiogenesis array, where neither Ang-1 nor PDGF-B were altered in melanoma tissue (unpublished data from our lab), thus excluding effect on the expression of these factors resulting from EC-MMP14 loss.

Enhanced vessel permeability was detected in the MMP14 complete knockout and by inhibition of proteolytic activities by GM6001 in mustard oil treated ears [516]. Mechanistically, this effect was attributed to impaired activation of TGFβ1 by MMP14, and subsequent inhibition of Alk5 signaling [516]. Differences with our system may rely in the fact that firstly, MMP14 was deleted in all cells, and secondly, inhibition by GM6001 is not specific only to MMP14 [517]. Furthermore, TGF β1 was shown to have both pro- and anti-angiogenic properties mediated by its capability to activate both Alk5 and Alk1 that are normally in balance. When Alk5 is activated, Smad2 and 3 signaling is induced and EC migration and proliferation are constrained thus promoting vessel maturation [509]. On the other hand, when TGFβ1 activates Alk1, Alk1 initiates activation of Smad1 and 5 leading to EC proliferation and migration that results in pro-angiogenic activities [509]. Possibly the fact that in our system MMP14 is deleted only in ECs, does not exclude that MMP14 expression in other cells may keep the balance in TGFb1 signaling. In contrast, in the previous work from Sounni and coworkers [516] with MMP14 loss in the entire organism skews completely the balance. That possibly leads to the alteration of the dominant path, Alk5, although Alk1 was not analyzed.

However, loss of EC-MMP14 could affect TGFβ1-mediated pericyte regulation in an alternative fashion. Endoglin, a dimeric glycoprotein predominantly expressed by ECs acts as transmembrane accessory receptor for TGFβ1 essential for Alk1 activation [510, 511, 518, 519]. High levels of soluble endoglin produced by shedding correlated with reduced neovascularization *in vitro* and MMP14 was demonstrated to be the processing enzyme for endoglin in tumors and preeclamptic placentas [520, 521]. Hypothetically, without EC-MMP14 endoglin shedding may be impaired and thereby the Alk1 mediated pro-angiogenic state of the vessels would be maintained, this needs further proof.

When recruited, pericytes align with the vascular tube and support BM assembly [183, 522], that further contributes to vessel stabilization [523]. Pericyte also provide an additional source for BM proteins [524, 525]. Reduction and discontinuity of capillary BM detected in cancer enhances vessel leakiness. This may require MMPs activity. In fact, MMP14 directly processes nidogen, perlecan, aggrecan [329] and laminin-332 [331], while it is indirectly involved in collagen type IV cleavage through activation of MMP2 [266, 290]. However, despite loss of

EC-MMP14 and enhanced pericytes coverage, density and continuity of BM proteins were comparable in MMP14[EC-/-] and control tumors. This is surprising, when considering that interaction of ECs and pericytes increases BM deposition and their dissociation in cancer is thought to contribute to the alterations observed in tumor vessels [183, 522]. Likely, pericyte coverage not only contribute to deposition of BM proteins, but also compensate for remodeling of this matrices in the absence of ECs derived MMP14.

Moreover, although MMP14 can cleave BM proteins, soluble proteases like MMP2 and MMP9 are more important in the remodeling of the BM as deletion of the gelatinases in mice increased collagen type IV which led to reduced metastasis [290, 526]. Additionally, MMP14, MMP15 and MMP16 expressed in tumor cells can process the BM [527] providing another source of proteases.

VE-cadherin and ZO-1 (VE-cadherin's intracellular cytoskeleton binding partner [218-220]), were upregulated in MMP14[EC-/-] tumor vessels, possibly further stabilizing the tumor vasculature. This could suggest that EC-MMP14 is another regulator of VE-cadherin assembly and expression in tumor cells [224, 226]. Supportive of this blocking the metalloproteinases use of the inhibitor TAPI in HUVECs prevented VE-cadherin shedding, and retaining structural and signaling properties of adherence junctions [528]. Moreover, VE-cadherin shedding, involving a c-Met/ETS-1/MMP14 pathway, was prevented by knockout of the tyrosine-protein kinase c-Met [529]. However, although these studies show that MMP14 might have cleavage activity towards VE-cadherin, here we did not find significant alterations in VE-cadherin cleavage in primary ECs from MMP14[EC-/-] mice, but we detected upregulation of VE-cadherin transcription. Also ZO-1 is upregulated upon MMP14 loss in ECs.

Although not demonstrated with VE-cadherin and ZO-1, MMP14 can also directly regulate transcription of other proteins as demonstrated for PI3Kγ [530]. Further indirect regulators cannot also be excluded.

4.1.3. EC-MMP14 regulates eNOS and NO in mouse and human, but VE-cadherin is differently regulated in these two systems

A recent study identified eNOS to be regulated by MMP14 [388]. Mice with tamoxifen-induced deletion of MMP14 in endothelial cells, driven by the cadherin 5 promotor, showed reduced expression of eNOS and decreased NO production in an intussusception model [388], where intussusceptive angiogenesis is a mechanism by which the microvasculature expands [531].

We also found reduced eNOS expression in MMP14[EC-/-] ECs, which further led to decreased NO. NO, besides driving EC migration and tube formation [532-534], is a regulator of vascular permeability, as for example by promoting VEGF-mediated hyperpermeability [535, 536]. In turn, VEGF also induces eNOS expression [537, 538]. As MMP14 is a known activator of VEGF during angiogenesis [367, 539], reduced VEGF activation upon MMP14 loss in ECs might indirectly alter eNOS expression. Although we did not detect altered VEGF expression in MMP14[EC-/-] ECs (data from our laboratory), we have not addressed whether VEGFR signaling was active. MMP14 may possibly regulate eNOS expression through its transcriptional regulatory functions, as previously described for other proteins [530, 540]. Moreover, MMP14 can control eNOS synthesis via thrombospondin 1 (TSP1) [388] cleavage and binding to CD47/$\alpha v \beta 3$ [541, 542]. However, this mechanism underlied intussusception in a colitis model. Transferability to tumor vasculature needs to be further tested in the future, especially in regards to the observed increased vessel permeability upon EC-MMP14 loss in both systems.

In HUVECs increased eNOS expression and NO production caused downregulation of VE-cadherin [234]. Studies in eNOS knockout mice showed that eNOS/NO induces VEGF-mediated S-nitrosylation of β-catenin, causing dissociation from VE-cadherin that ultimately leads to the collapse of the adherence junctions [233]. In leukocytes NO has an inhibitory effect towards integrins and intercellular adhesion molecules such as VCAM-1 [543-546]. However, despite the described regulatory function of eNOS and NO on VE-cadherin, when we silenced eNOS in mouse ECs we did not detect altered VE-cadherin expression. Since eNOS knockdown was not 100 % efficient (we used siRNA), the remaining eNOS might be sufficient to maintain the normal VE-cadherin expression levels in these cells. Alternatively, increase of VE-cadherin expression in MMP14[EC-/-] ECs rather than indirectly mediated through eNOS and NO reduction, could be a direct effect of MMP14 loss, but further investigations may be necessary to clarify this issue.

It cannot be excluded that the observed effect could be species-specific as MMP14 knockdown in HUVECs whereas had no effect on VE-cadherin expression, downregulated eNOS similarly as in MMP14[EC-/-] ECs. eNOS and MMP14 are known to co-localize and NO has been identified as a regulator of MMP14 expression and clustering in migrating ECs [547]. Taking these findings together, these two proteins might form a positive feedback loop enhancing each other. In support of a specie specificity of VE-cadherin expression, mouse VE-cadherin proximal promoter regions contain Alu sequences and a CpG island, elements known to influence gene expression dependent on methylation [548-550]. However, these elements are missing in the

human VE-cadherin promotor [551]. Moreover, although Sp1 sites are present in both species, binding affinity of different promotors to these sequences vary in mouse and human, as observed for the luteinizing hormone beta (LHbeta) promoter [552] and the PIT1 phosphate transporter gene [553].

4.1.4. Potential of EC-MMP14 blocking in therapy

Vascular permeability and vessel maturation are crucial factors in regulating cancer growth and metastasis. Although not addressed directly, this study indicates that enhanced vessel stability might be beneficial towards reducing not only melanoma growth, but also metastasis. Combination of EC-specific MMP14 loss and chemotherapeutic treatment with cisplatin, a well-known chemotherapeutic drug [554], slightly, but not significantly, reduced tumor growth in comparison to untreated MMP14$^{EC-/-}$. As the inhibition in melanoma growth detected in control mice treated with this drug was similar to that obtained by deleting MMP14 in ECs alone, the extent of inhibition in the MMP14$^{EC-/-}$ was likely the maximal obtainable in that system. However, the further growth reduction observed in treated melanomas in the MMP14$^{EC-/-}$, although slight, suggest that cisplatin and the additional tumor vessel stabilization might be beneficial in cancer treatment. In the past, multiple treatments aiming at stabilization of hyperpermeable tumor vessels were developed and demonstrated to be promising therapeutic approaches [108]. One of the first observation in support of that was the treatment of lung carcinoma with the cytostatic cancer drug ICRF 159 [555] that significantly reduced metastasis and showed stabilization of vessels [556]. Based on these and other data, until today several strategies combining approaches that normalize the tumor vasculature in combination with other therapies were developed. Vessel maturation is achieved by targeting different components of the vascular structure. For example in melanoma, inositol trispyrophosphate (ITPP) treatment was found to enhance oxygen tension and blood flow, leading to reduced hypoxia and vessel normalization [557]. Reduction of tumor growth and enhanced survival upon immunotherapy was obtained combining ITPP with NGR-TNF (a Cys-Asn-Gly-Arg-Cys peptide-TNF fusion product) treatment [558]. Here, vessel normalization was attained by increasing cell adhesion molecules. In an approach using the oligonucleotide based inhibitor CD5-2 the VE-cadherin/miR-27a interaction was disrupted, leading to enhanced VE-cadherin expression. This resulted in vessel maturation which ultimately led to improved efficacy of anti-PD-1 blockers [559].

Since current therapy strategies usually target one vessel stabilizing mechanism, EC-MMP14 might provide a target that, due to regulating multiple factors regulating vessel functionality, leads to a stronger effect in therapy. Indeed, MMP14 has a long history of being targeted in cancer therapy and new specific approaches appear very promising. One of these is the humanized DX-2400 antibody that targets MMP14 and proven effective in reducing tumor growth and metastasis in breast cancer and melanoma metastasis models [368, 560].

4.2. Role of MMP3 and fibroblast-MMP14 in skin

4.2.1. MMP3 upregulation in MMP14-deficient fibroblast

MMP14 expression and activity in skin is low in homeostatic conditions, but can be induced in various cell types for example during skin repair and melanoma development [276]. Previously, work from our laboratory demonstrated that mice with inducible MMP14 deletion in stromal fibroblasts (MMP14$^{Sf-/-}$) developed a fibrosis-like phenotype as a result from impaired collagen degradation, *in vitro* and *in vivo* [251]. However, these mice display a normal skin repair process upon injury [251], but growth melanoma in the skin of these mice is reduced [395].

It was surprising that skin repair was not affected by deletion of MMP14 in fibroblasts as during wound healing MMP14 is upregulated in several cells including fibroblasts and it was involved in collagen remodeling [251, 561]. Moreover, MMP14 was implicated in the activation of TGFβ1 [341, 342, 512], which is an essential signaling factor orchestrating multiple activities during wound healing [562]. As observed for other MMPs knockout models [258], the cell specific function of MMP14 in fibroblasts during skin development and repair can be compensated by other proteases. In the skin and fibroblasts of the MMP14$^{Sf-/-}$ mice, we found a strong upregulation of MMP3. The increase in MMP3 expression was at a transcriptional level, and likely caused by MMP14 acting either as repressor, directly (transcriptional regulation) or indirectly by the modulation of regulatory factors. The first proof of nuclear localization of MMP14 was found in macrophages where it regulated PI3K expression, thus the inflammatory program and its deletion led to an enhanced inflammatory state in cells and tissue [530, 540]. Another protein transcriptionally regulated by MMP14 is VEGFA, shown in adenocarcinoma cells (MCF-7 cells) [563]. The inhibitory activity of MMP14 towards transcription was previously shown for Dickkopf-3, whose expression was indeed increased in MMP14 knockout cells [564].

Prominent pathways mediating MMP3 expression that could be affected and should be analyzed in the future are MMP3 transcription regulation via NFκB [415, 565] or IL-6/STAT-1 [566].

But, how exactly MMP14 might regulate MMP3 transcription remains unknown and requires further analysis in the future.

Although structurally different, MMP3 and MMP14 share some of their substrates. For example, MMP3 actively remodels the ECM by processing of collagen type IV, fibronectin, decorin and nidogen [242, 405] but not collagen type I. However, through activation of pro-MMP13, a substrate shared with MMP14 [268-270], MMP3 may indirectly mediate collagenolysis. In addition, both proteases have been shown to activate TGFβ1 [341, 342, 409, 512]. MMP3 and MMP14 are also highly active in similar pathologies, for example overexpression of both induce mammary carcinogenesis [567, 568], and during tissue repair [421, 423, 569].

Thus, based on the literature it was unclear what specific function of fibroblast-derived MMP14 could be compensated by MMP3.

4.2.2. MMP3 does not compensate for physiological fibroblast-MMP14 functions

To address that issue we undertook a genetic approach and generated mice carrying the double deletion, MMP3^{-/-} in all body and MMP14[Sf-/-] in fibroblasts. The double deficient mice were phenotypically indistinguishable from MMP14[Sf-/-] mice and developed the fibrosis-like tendon and skin phenotype previously described in the MMP14[Sf-/-] mice [251] with no additional defects. The latter further suggested that activity of MMP3's in proMMP13 activation [268, 270] is dispensable for collagen homeostasis in adult skin.

Although low expressed in physiology, MMPs including MMP3 and MMP14 are highly upregulated during skin repair that requires major remodeling of the matrix [46]. However, their function during repair is tightly regulated and their alterations is associated with pathological conditions. For example, MMP3 is upregulated in human ulcer tissue [424] and MMP14 is strongly increased in fibroblasts from chronic wound beds [379]. In normal conditions, multiple MMPs are important drivers of healing processes and MMP3 was identified as significant player of wound contraction in mice [419, 420]. However, when depleted both MMP14[Sf-/-] and MMP3^{-/-}, although overall wound repair was comparable, wound closure was initially delayed in single and double deficient mice. Mice lacking MMP3 showed enlarged wound width and granulation tissue size in earlier wounds. Overall, the observed phenotypes were most pronounced in the double deficient mice, indicating that some activities in the MMP14[Sf-/-] repair process were performed by MMP3. The previous studies by Bullard and colleagues ascribed the delayed closure in MMP3 knockout mice to impaired fibroblast contractile activity, as

collagen gel contraction by fibroblasts from MMP3 knockout mice was reduced owing to altered actin stress fibers organization [419, 420]. Fibroblasts from MMP3 single and double MMP3$^{-/-}$/MMP14$^{Sf-/-}$ mice, displayed a similar impairment of gel contraction, suggesting no further contribution to this process by MMP14.

In the MMP3 knockout mice [419] myofibroblasts were detected in day 7 wounds, but no quantification was provided. In our studies, the numbers of myofibroblasts were reduced early in all knockout mice compared to controls, suggesting a contribution of each protease to the population of granulation tissue by these cells. These specialized fibroblasts are considered main drivers of wound contraction [62] and multiple studies demonstrated that alterations in their numbers [53] or depletion of αSMA^{+} myofibroblasts [570, 571] significantly affects wound healing.

Fibroblasts are considered the main source of myofibroblasts in wound healing [62]. Although MMP3 drives by unknown mechanisms the formation of the cells cytoskeleton in fibroblasts [419, 420], so far neither MMP3 nor MMP14 were directly implicated in mediating fibroblast activation leading to myofibroblasts formation.

However, both proteases are known to activate TGFβ1, by cleavage of LAP or LTBP1 [341, 342, 409], the main inducer of myofibroblast formation from fibroblasts during tissue repair [63, 478]. Once active, TGFβ1 induces downstream pSmad2 signaling and mediates myofibroblast formation [483-485]. Since in early wound of single and double deletion MMP3$^{-/-}$/MMP14$^{Sf-/-}$ mice pSmad2 was reduced, we hypothesized that loss of proteolytic activity of MMP3 and MMP14 might reduce TGFβ1 activity, activation or expression. TGFβ1 expression in wounds and isolated fibroblasts in MMP3$^{-/-}$/MMP14$^{Sf-/-}$ and single knockout controls was not changed. Moreover, the intrinsic sensitivity of fibroblasts from all mice genotypes to TGFβ1 signaling was not altered.

Although TGFβ1 is considered the main inducer of myofibroblast formation during wound healing [63, 478, 479], also other growth factors can mediate fibroblast activation. For example, also PDGF-B [476] and FGF [477] promoted myofibroblast formation. While MMP14 has been association with regulation of both these factors [373, 572], no studies are known that showed MMP3 being involved in their control. However, both factors PDGF-B and FGF, remained unaltered in MMP3$^{-/-}$/MMP14$^{Sf-/-}$ and control wounds (data from the laboratory). Thus, it is unlikely, that altered PDGF-B or FGF signaling causes the observed myofibroblast phenotype in mice lacking MMP3 and/or fibroblast-MMP14, further pointing towards impaired TGFβ1 matrix release and activation as underlying mechanism. However, we cannot exclude that loss

of MMP3 and MMP14 also affects the growth factor release from the matrix where the latent TGFβ1 is stored [573].

Besides fibroblasts, other cellular sources were identified to transform into myofibroblasts. During wound healing epithelial and endothelial cells can transition into myofibroblasts in a process known as EMT (epithelial-to-) or EndoMT (endothelial-to-mesenchymal transition), respectively [574, 575]. For example, MMP3 is upregulated in epithelial cells during wound healing [421] and has been shown to induce EMT via E-cadherin cleavage [408, 576, 577]. For induction of EndoMT, MMP3 likely activates MMP9 which in turn mediates signaling of Notch1 and TGFβ1 [578]. MMP14 was shown to mediate EndoMT via TGFβ1 and subsequent Smad2 signaling in ECs in the context of myocardial infarction [383]. However, this study solely showed the impact of macrophage-derived MMP14 in the heart on activation of the latent LAP-bound TGFβ1 in the case of cardiac infarction, the role of fibroblast-MMP14 has not yet been analyzed in the context of EndoMT. Moreover, these studies also demonstrate that although originating from other cellular sources, myofibroblast formation is TGFβ1-dependent [579]. Therefore, if TGFβ1 activation is impacted by the loss of MMP3 and MMP14 in fibroblasts, it is likely that EMT and EndoMT are also impaired. Moreover, EMT has been mainly studied in a fibrosis context and its importance for tissue repair requires more attention. While the numbers of wound myofibroblasts was reduced in single and double MMP3$^{-/-}$/MMP14$^{Sf-/-}$ mice, they persisted longer. We guessed that through endurance of the myofibroblasts in the granulation tissue, their reduced formation in early wound might be compensated, and ultimately lead to the completed repair. In double deficient mice this effect was the strongest, likely due to the contemporarily enhanced myofibroblast proliferation. The enhanced cell proliferation could be an effect of simultaneous deletion of MMP3 and MMP14, as single knockouts showed myofibroblast proliferation comparable to the wildtypes, and so far neither of the proteases has been identified to mediate myofibroblast proliferation. On the other hand, the elevated numbers of myofibroblast in day 14 wounds of MMP3 and MMP14 single knockout mice, was likely the result of decreased apoptosis. Usually, this last phase of wound healing is characterized by heavy remodeling and cells, including myofibroblasts [58, 73] are cleared by apoptosis from the packed granulation when returning to the homeostatic condition [474].

Although not shown during tissue repair, both MMP3 and MMP14 may have a function in apoptosis. In CHO cells, apoptosis was increased when overexpressing MMP3 [580] that localized into the nucleus and cleaved PARP, thus inhibiting DNA repair mechanisms and ultimately leading to apoptosis [580]. Moreover, mitochondrial ROS production was increased

by MMP3 and induced apoptosis in mammary tumor cells [581]. While these studies clearly indicate a pro-apoptotic function of MMP3, MMP14 has been suggested to be protective against apoptosis. In breast cancer cells MMP14 was shown to be protective against apoptosis induced by collagen type I [582]. Mechanistically, this might occur by inhibiting BCL-2 and BIK expression [583]. Assuming these functions would be translated to a wound healing context and fibroblasts, loss of MMP3 could indeed be involved in directly downregulating myofibroblast apoptosis. However, loss of MMP14 would have the opposite effect, although, possibly, lack of MMP3 could compensate it and also reduced it. However, the described roles of MMP3 and MMP14 towards apoptosis may be specific to these cell types and do not occur in fibroblasts. For instance, MMP3 may also be anti-apoptotic in cardiomyocytes. Here, apoptosis of AngII-treated fibrotic cells was enhanced upon siRNA-mediated MMP3 knockdown [584]. Moreover, the effect of MMP3 and MMP14 loss on apoptosis might be indirectly mediated via altered growth factor or cytokine signaling. An example would be TGFβ1, who is an inducer of apoptosis via multiple signaling pathways including Smad, p38 and AP-1 [585]. Thus, possible reduction of TGFβ1 activation upon loss of MMP3 and fibroblast-derived MMP14 could also affect induction of myofibroblast apoptosis in late wounds.

Increasing evidence indicates, that removal of growth factors, thus pro-survival stimuli, induces myofibroblast apoptosis in late wounds [474]. For example, death of lung myofibroblasts can be prevented by treatment with PDGF-A [586]. Also, TGFβ1, whose withdrawal leads to cell apoptosis in the granulation tissue, has a pro-survival effect when applied to lung myofibroblasts [587]. Mechanistically, this resulted from TGFβ1-induced p38/MAPK and PI3K/AKT signaling [588]. This downstream signaling pathway is activated by endothelin-1, leading to a prolonged myofibroblast lifetime in pulmonary fibrosis [588]. Since we have shown, that loss of MMP3 and/or MMP14 leads to reduced pSmad2 signaling during early wound healing phases, the overall level of available TGFβ1 as result from release from the matrix, rather than production that we found not altered, may be lower and more difficult to detect in experimental systems.

4.3. Conclusion and perspectives

Taken together, the presented data demonstrate that endothelial cell-derived MMP14 orchestrates multiple events involved in the regulation of tumor vessel functionality, where the protease is a driver of vascular permeability due to the regulation of pericyte recruitment, EC-EC junctions' density and nitric oxide production. Therefore, the observed vessel stabilization

resulting from deletion of EC-MMP14 further highlights the potential of targeting MMP14 in therapies. However, as the effect of classic chemotherapeutics such as cisplatin appeared to be limited in our model, it would be important to address whether a synergistic treatment of MMP14 targeting and other drugs, for instance immune-modulators or targeted therapeutics would displayed improved efficacy.

Besides cancer, enhanced vascular stability resulting from EC-MMP14 loss might also have a beneficial effects in other pathological conditions. One example would be dermal fibrosis. Vascular damage is one of the initial events in skin fibrosis enhancing inflammatory reactions [589] and causing chronic hypoxia which further promotes fibrosis [590]. Thus, it could be possible that enhanced vessel stability in MMP14$^{EC-/-}$ mice is protective against dermal fibrosis. Indeed, first analysis in our group using a bleomycin-induced fibrosis model showed a reduced fibrotic reaction in the knockout mice (unpublished date), but the underlying mechanisms require further investigation. Still, this shows that EC-derived MMP14 might present, if approached in a cell specific manner, a powerful target in treating multiple pathological conditions.

The data of the second part of the thesis project, show that although strongly upregulated in skin of MMP14$^{Sf-/-}$ mice, MMP3 has no compensatory function in skin steady-state homeostasis. However, in wound healing, double deficiency causes a significant delay in wound closure which is likely a cumulative effect of altered myofibroblast formation, resolution and contractility upon single or combined MMP3 and MMP14 loss. The current results especially point towards MMP3 and MMP14 regulatory function in TGFβ1 activation by matrix release. However, future experiments should address the relevance of other growth factors like PDGF-B and FGF, substrates or regulated by these MMPs, in the system. Furthermore, analysis of the ECM structure and composition, complemented by degradomics, in the absence of MMP3 and/or MMP14 could improve our understanding of the *in vivo* substrates for these proteases. Moreover, addressing the possibility of regulation of processes like EMT and EndoMT by MMP14 would open new research venues and a possible targeting approaches in fibrotic diseases. For this, lineage tracing could provide the right system for these investigations, which was used to identify myofibroblast origins in multiple studies (reviewed in Pakshir *et al.,* 2020 [591]).

5. Literature

1.   Langerhans, P., *Über die Nerven der menschlichen Haut*. Vol. 44. 1868: Archiv f. pathol. Anat. .

2.   Otsuka, M., G. Egawa, and K. Kabashima, *Uncovering the Mysteries of Langerhans Cells, Inflammatory Dendritic Epidermal Cells, and Monocyte-Derived Langerhans Cell-Like Cells in the Epidermis.* Front Immunol, 2018. **9**: p. 1768.

3.   Rowden, G., *Immuno-electron microscopic studies of surface receptors and antigens of human Langerhans cells.* Br J Dermatol, 1977. **97**(6): p. 593-608.

4.   Cruz, M.S., et al., *Human αβ and γδ T Cells in Skin Immunity and Disease.* Front Immunol, 2018. **9**: p. 1304.

5.   Yanez, D.A., et al., *The role of macrophages in skin homeostasis.* Pflugers Arch, 2017. **469**(3-4): p. 455-463.

6.   Smyth, N., et al., *Absence of basement membranes after targeting the LAMC1 gene results in embryonic lethality due to failure of endoderm differentiation.* J Cell Biol, 1999. **144**(1): p. 151-60.

7.   Timpl, R., et al., *A network model for the organization of type IV collagen molecules in basement membranes.* Eur J Biochem, 1981. **120**(2): p. 203-11.

8.   Timpl, R., et al., *Nature of the collagenous protein in a tumor basement membrane.* Eur J Biochem, 1978. **84**(1): p. 43-52.

9.   Timpl, R., et al., *Laminin--a glycoprotein from basement membranes.* J Biol Chem, 1979. **254**(19): p. 9933-7.

10.   Chung, A.E., et al., *Properties of a basement membrane-related glycoprotein synthesized in culture by a mouse embryonal carcinoma-derived cell line.* Cell, 1979. **16**(2): p. 277-87.

11.   Carlin, B., et al., *Entactin, a novel basal lamina-associated sulfated glycoprotein.* J Biol Chem, 1981. **256**(10): p. 5209-14.

12.   Kanwar, Y.S. and M.G. Farquhar, *Presence of heparan sulfate in the glomerular basement membrane.* Proc Natl Acad Sci U S A, 1979. **76**(3): p. 1303-7.

13.   Kanwar, Y.S. and M.G. Farquhar, *Isolation of glycosaminoglycans (heparan sulfate) from glomerular basement membranes.* Proc Natl Acad Sci U S A, 1979. **76**(9): p. 4493-7.

14.   Breitkreutz, D., et al., *Skin basement membrane: the foundation of epidermal integrity--BM functions and diverse roles of bridging molecules nidogen and perlecan.* Biomed Res Int, 2013. **2013**: p. 179784.

15.   Sorrell, J.M. and A.I. Caplan, *Fibroblast heterogeneity: more than skin deep.* J Cell Sci, 2004. **117**(Pt 5): p. 667-75.

16.   Frantz, C., K.M. Stewart, and V.M. Weaver, *The extracellular matrix at a glance.* J Cell Sci, 2010. **123**(Pt 24): p. 4195-200.

17.   Brown, T.M. and K. Krishnamurthy, *Histology, Dermis*, in *StatPearls*. 2022, StatPearls Publishing Copyright © 2022, StatPearls Publishing LLC.: Treasure Island (FL).

18.   Sorushanova, A., et al., *The Collagen Suprafamily: From Biosynthesis to Advanced Biomaterial Development.* Adv Mater, 2019. **31**(1): p. e1801651.

19.   Gordon, M.K. and R.A. Hahn, *Collagens.* Cell Tissue Res, 2010. **339**(1): p. 247-57.

20.   Traub, W. and K.A. Piez, *The chemistry and structure of collagen.* Adv Protein Chem, 1971. **25**: p. 243-352.

21.   Ramshaw, J.A., N.K. Shah, and B. Brodsky, *Gly-X-Y tripeptide frequencies in collagen: a context for host-guest triple-helical peptides.* J Struct Biol, 1998. **122**(1-2): p. 86-91.

22.   Ricard-Blum, S., *The collagen family.* Cold Spring Harb Perspect Biol, 2011. **3**(1): p. a004978.

23.   Housley, T., et al., *Collagen crosslinking: isolation of hydroxyaldol-histidine, a naturally-occurring crosslink.* Biochem Biophys Res Commun, 1975. **67**(2): p. 824-30.

24.   Fujimoto, D., *Isolation and characterization of a fluorescent material in bovine achilles tendon collagen.* Biochem Biophys Res Commun, 1977. **76**(4): p. 1124-9.

25.   Tanzer, M.L. and J.H. Waite, *Collagen cross-linking.* Coll Relat Res, 1982. **2**(2): p. 177-80.

26.   Yamauchi, M., D.T. Woodley, and G.L. Mechanic, *Aging and cross-linking of skin collagen.* Biochem Biophys Res Commun, 1988. **152**(2): p. 898-903.

27.   Xu, S., et al., *The role of collagen in cancer: from bench to bedside.* J Transl Med, 2019. **17**(1): p. 309.

28.   Pickering, J.G., *Regulation of vascular cell behavior by collagen : form is function.* Circ Res, 2001. **88**(5): p. 458-9.

29.   Epstein, E.H., Jr., *(Alpha1(3))3 human skin collagen. Release by pepsin digestion and preponderance in fetal life.* J Biol Chem, 1974. **249**(10): p. 3225-31.

30.   Hu, M.S., et al., *Embryonic skin development and repair.* Organogenesis, 2018. **14**(1): p. 46-63.

31.   Verzijl, N., et al., *Effect of collagen turnover on the accumulation of advanced glycation end products.* J Biol Chem, 2000. **275**(50): p. 39027-31.

32. Ohuchi, K. and S. Tsurufuji, *Degradation and turnover of collagen in the mouse skin and the effect of whole body x-irradiation.* Biochim Biophys Acta, 1970. **208**(3): p. 475-81.

33. Rucklidge, G.J., et al., *Turnover rates of different collagen types measured by isotope ratio mass spectrometry.* Biochim Biophys Acta, 1992. **1156**(1): p. 57-61.

34. Naba, A., et al., *The extracellular matrix: Tools and insights for the "omics" era.* Matrix Biol, 2016. **49**: p. 10-24.

35. Taipale, J. and J. Keski-Oja, *Growth factors in the extracellular matrix.* Faseb j, 1997. **11**(1): p. 51-9.

36. Schönherr, E. and H.J. Hausser, *Extracellular matrix and cytokines: a functional unit.* Dev Immunol, 2000. **7**(2-4): p. 89-101.

37. Sun, B.K., Z. Siprashvili, and P.A. Khavari, *Advances in skin grafting and treatment of cutaneous wounds.* Science, 2014. **346**(6212): p. 941-5.

38. Shaw, T.J. and P. Martin, *Wound repair: a showcase for cell plasticity and migration.* Curr Opin Cell Biol, 2016. **42**: p. 29-37.

39. Rivera, J., et al., *Platelet receptors and signaling in the dynamics of thrombus formation.* Haematologica, 2009. **94**(5): p. 700-11.

40. Rohani, M.G. and W.C. Parks, *Matrix remodeling by MMPs during wound repair.* Matrix Biol, 2015. **44-46**: p. 113-21.

41. Broughton, G., 2nd, J.E. Janis, and C.E. Attinger, *The basic science of wound healing.* Plast Reconstr Surg, 2006. **117**(7 Suppl): p. 12s-34s.

42. Kurkinen, M., et al., *Sequential appearance of fibronectin and collagen in experimental granulation tissue.* Lab Invest, 1980. **43**(1): p. 47-51.

43. Bielefeld, K.A., S. Amini-Nik, and B.A. Alman, *Cutaneous wound healing: recruiting developmental pathways for regeneration.* Cell Mol Life Sci, 2013. **70**(12): p. 2059-81.

44. Leibovich, S.J. and R. Ross, *The role of the macrophage in wound repair. A study with hydrocortisone and antimacrophage serum.* Am J Pathol, 1975. **78**(1): p. 71-100.

45. Guo, S. and L.A. Dipietro, *Factors affecting wound healing.* J Dent Res, 2010. **89**(3): p. 219-29.

46. Caley, M.P., V.L. Martins, and E.A. O'Toole, *Metalloproteinases and Wound Healing.* Adv Wound Care (New Rochelle), 2015. **4**(4): p. 225-234.

47. Koivisto, L., et al., *Integrins in Wound Healing.* Adv Wound Care (New Rochelle), 2014. **3**(12): p. 762-783.

48. Pilcher, B.K., et al., *The activity of collagenase-1 is required for keratinocyte migration on a type I collagen matrix.* J Cell Biol, 1997. **137**(6): p. 1445-57.

49. Saarialho-Kere, U.K., et al., *Cell-matrix interactions modulate interstitial collagenase expression by human keratinocytes actively involved in wound healing.* J Clin Invest, 1993. **92**(6): p. 2858-66.

50. Dumin, J.A., et al., *Pro-collagenase-1 (matrix metalloproteinase-1) binds the alpha(2)beta(1) integrin upon release from keratinocytes migrating on type I collagen.* J Biol Chem, 2001. **276**(31): p. 29368-74.

51. Smola, H., G. Thiekötter, and N.E. Fusenig, *Mutual induction of growth factor gene expression by epidermal-dermal cell interaction.* J Cell Biol, 1993. **122**(2): p. 417-29.

52. Hinz, B., *The myofibroblast: paradigm for a mechanically active cell.* J Biomech, 2010. **43**(1): p. 146-55.

53. Darby, I.A., et al., *Fibroblasts and myofibroblasts in wound healing.* Clin Cosmet Investig Dermatol, 2014. **7**: p. 301-11.

54. Gabbiani, G., G.B. Ryan, and G. Majne, *Presence of modified fibroblasts in granulation tissue and their possible role in wound contraction.* Experientia, 1971. **27**(5): p. 549-50.

55. Hinz, B., C.A. McCulloch, and N.M. Coelho, *Mechanical regulation of myofibroblast phenoconversion and collagen contraction.* Exp Cell Res, 2019. **379**(1): p. 119-128.

56. Gabbiani, G., et al., *Human smooth muscle autoantibody. Its identification as antiactin antibody and a study of its binding to "nonmuscular" cells.* Am J Pathol, 1973. **72**(3): p. 473-88.

57. Skalli, O., et al., *A monoclonal antibody against alpha-smooth muscle actin: a new probe for smooth muscle differentiation.* J Cell Biol, 1986. **103**(6 Pt 2): p. 2787-96.

58. Darby, I., O. Skalli, and G. Gabbiani, *Alpha-smooth muscle actin is transiently expressed by myofibroblasts during experimental wound healing.* Lab Invest, 1990. **63**(1): p. 21-9.

59. Hinz, B., et al., *Alpha-smooth muscle actin expression upregulates fibroblast contractile activity.* Mol Biol Cell, 2001. **12**(9): p. 2730-41.

60. Hinz, B., et al., *Alpha-smooth muscle actin is crucial for focal adhesion maturation in myofibroblasts.* Mol Biol Cell, 2003. **14**(6): p. 2508-19.

61. Singer, II, et al., *In vivo co-distribution of fibronectin and actin fibers in granulation tissue: immunofluorescence and electron microscope studies of the fibronexus at the myofibroblast surface.* J Cell Biol, 1984. **98**(6): p. 2091-106.

62. Hinz, B., *The role of myofibroblasts in wound healing.* Curr Res Transl Med, 2016. **64**(4): p. 171-177.

63.   Desmoulière, A., et al., *Transforming growth factor-beta 1 induces alpha-smooth muscle actin expression in granulation tissue myofibroblasts and in quiescent and growing cultured fibroblasts.* J Cell Biol, 1993. **122**(1): p. 103-11.

64.   Gleizes, P.E., et al., *TGF-beta latency: biological significance and mechanisms of activation.* Stem Cells, 1997. **15**(3): p. 190-7.

65.   Munger, J.S., et al., *Latent transforming growth factor-beta: structural features and mechanisms of activation.* Kidney Int, 1997. **51**(5): p. 1376-82.

66.   Saharinen, J., J. Taipale, and J. Keski-Oja, *Association of the small latent transforming growth factor-beta with an eight cysteine repeat of its binding protein LTBP-1.* Embo j, 1996. **15**(2): p. 245-53.

67.   Miyazono, K., et al., *A role of the latent TGF-beta 1-binding protein in the assembly and secretion of TGF-beta 1.* Embo j, 1991. **10**(5): p. 1091-101.

68.   Taipale, J., et al., *Latent transforming growth factor-beta 1 associates to fibroblast extracellular matrix via latent TGF-beta binding protein.* J Cell Biol, 1994. **124**(1-2): p. 171-81.

69.   Dallas, S.L., et al., *Characterization and autoregulation of latent transforming growth factor beta (TGF beta) complexes in osteoblast-like cell lines. Production of a latent complex lacking the latent TGF beta-binding protein.* J Biol Chem, 1994. **269**(9): p. 6815-21.

70.   Olofsson, A., et al., *Efficient association of an amino-terminally extended form of human latent transforming growth factor-beta binding protein with the extracellular matrix.* J Biol Chem, 1995. **270**(52): p. 31294-7.

71.   Martinez-Ferrer, M., et al., *Dermal transforming growth factor-beta responsiveness mediates wound contraction and epithelial closure.* Am J Pathol, 2010. **176**(1): p. 98-107.

72.   Varga, J., J. Rosenbloom, and S.A. Jimenez, *Transforming growth factor beta (TGF beta) causes a persistent increase in steady-state amounts of type I and type III collagen and fibronectin mRNAs in normal human dermal fibroblasts.* Biochem J, 1987. **247**(3): p. 597-604.

73.   Desmoulière, A., et al., *Apoptosis mediates the decrease in cellularity during the transition between granulation tissue and scar.* Am J Pathol, 1995. **146**(1): p. 56-66.

74.   Verrecchia, F. and A. Mauviel, *Control of connective tissue gene expression by TGF beta: role of Smad proteins in fibrosis.* Curr Rheumatol Rep, 2002. **4**(2): p. 143-9.

75.   Leask, A. and D.J. Abraham, *TGF-beta signaling and the fibrotic response.* Faseb j, 2004. **18**(7): p. 816-27.

76.   Erdmann, F., et al., *International trends in the incidence of malignant melanoma 1953-2008--are recent generations at higher or lower risk?* Int J Cancer, 2013. **132**(2): p. 385-400.

77.   Whiteman, D.C., A.C. Green, and C.M. Olsen, *The Growing Burden of Invasive Melanoma: Projections of Incidence Rates and Numbers of New Cases in Six Susceptible Populations through 2031.* J Invest Dermatol, 2016. **136**(6): p. 1161-1171.

78.   D'Arcy, C. and C. Kiel, *Cell Adhesion Molecules in Normal Skin and Melanoma.* Biomolecules, 2021. **11**(8).

79.   Shain, A.H. and B.C. Bastian, *From melanocytes to melanomas.* Nat Rev Cancer, 2016. **16**(6): p. 345-58.

80.   Haass, N.K., et al., *Adhesion, migration and communication in melanocytes and melanoma.* Pigment Cell Res, 2005. **18**(3): p. 150-9.

81.   Thingnes, J., et al., *Understanding the melanocyte distribution in human epidermis: an agent-based computational model approach.* PLoS One, 2012. **7**(7): p. e40377.

82.   Lin, J.Y. and D.E. Fisher, *Melanocyte biology and skin pigmentation.* Nature, 2007. **445**(7130): p. 843-50.

83.   Fitzpatrick, T.B. and A.S. Breathnach, *[THE EPIDERMAL MELANIN UNIT SYSTEM].* Dermatol Wochenschr, 1963. **147**: p. 481-9.

84.   Jimbow, K., et al., *Some aspects of melanin biology: 1950-1975.* J Invest Dermatol, 1976. **67**(1): p. 72-89.

85.   Gray-Schopfer, V., C. Wellbrock, and R. Marais, *Melanoma biology and new targeted therapy.* Nature, 2007. **445**(7130): p. 851-7.

86.   Heistein, J.B., U. Acharya, and S.K.R. Mukkamalla, *Malignant Melanoma*, in *StatPearls*. 2022, StatPearls Publishing
        Copyright © 2022, StatPearls Publishing LLC.: Treasure Island (FL).

87.   Davis, E.J., et al., *Melanoma: What do all the mutations mean?* Cancer, 2018. **124**(17): p. 3490-3499.

88.   Davies, H., et al., *Mutations of the BRAF gene in human cancer.* Nature, 2002. **417**(6892): p. 949-54.

89.   Sini, M.C., et al., *Genetic alterations in main candidate genes during melanoma progression.* Oncotarget, 2018. **9**(9): p. 8531-8541.

90.   Ellerhorst, J.A., et al., *Clinical correlates of NRAS and BRAF mutations in primary human melanoma.* Clin Cancer Res, 2011. **17**(2): p. 229-35.

91.   Muñoz-Couselo, E., et al., *NRAS-mutant melanoma: current challenges and future prospect.* Onco Targets Ther, 2017. **10**: p. 3941-3947.

92.   Fedorenko, I.V., G.T. Gibney, and K.S. Smalley, *NRAS mutant melanoma: biological behavior and future strategies for therapeutic management.* Oncogene, 2013. **32**(25): p. 3009-18.

93.   Haluska, F.G., et al., *Genetic alterations in signaling pathways in melanoma.* Clin Cancer Res, 2006. **12**(7 Pt 2): p. 2301s-2307s.

94.   Monzon, J., et al., *CDKN2A mutations in multiple primary melanomas.* N Engl J Med, 1998. **338**(13): p. 879-87.

95.   Colombino, M., et al., *Discrepant alterations in main candidate genes among multiple primary melanomas.* J Transl Med, 2014. **12**: p. 117.

96.   Casula, M., et al., *Low Levels of Genetic Heterogeneity in Matched Lymph Node Metastases from Patients with Melanoma.* J Invest Dermatol, 2016. **136**(9): p. 1917-1920.

97.   Kong, Y., S.M. Kumar, and X. Xu, *Molecular pathogenesis of sporadic melanoma and melanoma-initiating cells.* Arch Pathol Lab Med, 2010. **134**(12): p. 1740-9.

98.   Goldstein, A.M., et al., *High-risk melanoma susceptibility genes and pancreatic cancer, neural system tumors, and uveal melanoma across GenoMEL.* Cancer Res, 2006. **66**(20): p. 9818-28.

99.   Zhou, X.P., et al., *Epigenetic PTEN silencing in malignant melanomas without PTEN mutation.* Am J Pathol, 2000. **157**(4): p. 1123-8.

100.   Birck, A., et al., *Mutation and allelic loss of the PTEN/MMAC1 gene in primary and metastatic melanoma biopsies.* J Invest Dermatol, 2000. **114**(2): p. 277-80.

101.   Hsu, M.Y., et al., *Shifts in cadherin profiles between human normal melanocytes and melanomas.* J Investig Dermatol Symp Proc, 1996. **1**(2): p. 188-94.

102.   Hodorogea, A., et al., *Epithelial-Mesenchymal Transition in Skin Cancers: A Review.* Anal Cell Pathol (Amst), 2019. **2019**: p. 3851576.

103.   Eddy, K., R. Shah, and S. Chen, *Decoding Melanoma Development and Progression: Identification of Therapeutic Vulnerabilities.* Front Oncol, 2020. **10**: p. 626129.

104.   Moro, N., C. Mauch, and P. Zigrino, *Metalloproteinases in melanoma.* Eur J Cell Biol, 2014. **93**(1-2): p. 23-9.

105.   Greene, H.S., *HETEROLOGOUS TRANSPLANTATION OF MAMMALIAN TUMORS : I. THE TRANSFER OF RABBIT TUMORS TO ALIEN SPECIES.* J Exp Med, 1941. **73**(4): p. 461-74.

106.   Folkman, J., *Tumor angiogenesis: therapeutic implications.* N Engl J Med, 1971. **285**(21): p. 1182-6.

107.   Farnsworth, R.H., et al., *Vascular remodeling in cancer.* Oncogene, 2014. **33**(27): p. 3496-505.

108.   Lugano, R., M. Ramachandran, and A. Dimberg, *Tumor angiogenesis: causes, consequences, challenges and opportunities.* Cell Mol Life Sci, 2020. **77**(9): p. 1745-1770.

109.   Tannock, I.F., *The relation between cell proliferation and the vascular system in a transplanted mouse mammary tumour.* Br J Cancer, 1968. **22**(2): p. 258-73.

110.   Holmgren, L., M.S. O'Reilly, and J. Folkman, *Dormancy of micrometastases: balanced proliferation and apoptosis in the presence of angiogenesis suppression.* Nat Med, 1995. **1**(2): p. 149-53.

111.   Brem, S., et al., *Prolonged tumor dormancy by prevention of neovascularization in the vitreous.* Cancer Res, 1976. **36**(8): p. 2807-12.

112.   Gimbrone, M.A., Jr., et al., *Tumor growth and neovascularization: an experimental model using the rabbit cornea.* J Natl Cancer Inst, 1974. **52**(2): p. 413-27.

113.   Hanahan, D., *Heritable formation of pancreatic beta-cell tumours in transgenic mice expressing recombinant insulin/simian virus 40 oncogenes.* Nature, 1985. **315**(6015): p. 115-22.

114.   Teitelman, G., S. Alpert, and D. Hanahan, *Proliferation, senescence, and neoplastic progression of beta cells in hyperplasic pancreatic islets.* Cell, 1988. **52**(1): p. 97-105.

115.   Folkman, J., et al., *Induction of angiogenesis during the transition from hyperplasia to neoplasia.* Nature, 1989. **339**(6219): p. 58-61.

116.   Folkman, J., et al., *Isolation of a tumor factor responsible for angiogenesis.* J Exp Med, 1971. **133**(2): p. 275-88.

117.   Ferrara, N. and W.J. Henzel, *Pituitary follicular cells secrete a novel heparin-binding growth factor specific for vascular endothelial cells.* Biochem Biophys Res Commun, 1989. **161**(2): p. 851-8.

118.   Senger, D.R., et al., *A highly conserved vascular permeability factor secreted by a variety of human and rodent tumor cell lines.* Cancer Res, 1986. **46**(11): p. 5629-32.

119.   Brown, L.F., et al., *Expression of vascular permeability factor (vascular endothelial growth factor) and its receptors in adenocarcinomas of the gastrointestinal tract.* Cancer Res, 1993. **53**(19): p. 4727-35.

120.   Dvorak, H.F., et al., *Distribution of vascular permeability factor (vascular endothelial growth factor) in tumors: concentration in tumor blood vessels.* J Exp Med, 1991. **174**(5): p. 1275-8.

121.   Claffey, K.P., et al., *Expression of vascular permeability factor/vascular endothelial growth factor by melanoma cells increases tumor growth, angiogenesis, and experimental metastasis.* Cancer Res, 1996. **56**(1): p. 172-81.

122.   Olofsson, B., et al., *Vascular endothelial growth factor B, a novel growth factor for endothelial cells.* Proc Natl Acad Sci U S A, 1996. **93**(6): p. 2576-81.

123. Joukov, V., et al., *A novel vascular endothelial growth factor, VEGF-C, is a ligand for the Flt4 (VEGFR-3) and KDR (VEGFR-2) receptor tyrosine kinases.* Embo j, 1996. **15**(2): p. 290-98.

124. Grimmond, S., et al., *Cloning and characterization of a novel human gene related to vascular endothelial growth factor.* Genome Res, 1996. **6**(2): p. 124-31.

125. Lee, J., et al., *Vascular endothelial growth factor-related protein: a ligand and specific activator of the tyrosine kinase receptor Flt4.* Proc Natl Acad Sci U S A, 1996. **93**(5): p. 1988-92.

126. Christofori, G. and S. Luef, *Novel forms of acidic fibroblast growth factor-1 are constitutively exported by beta tumor cell lines independent from conventional secretion and apoptosis.* Angiogenesis, 1997. **1**(1): p. 55-70.

127. Friesel, R.E. and T. Maciag, *Molecular mechanisms of angiogenesis: fibroblast growth factor signal transduction.* Faseb j, 1995. **9**(10): p. 919-25.

128. Carmeliet, P., et al., *Abnormal blood vessel development and lethality in embryos lacking a single VEGF allele.* Nature, 1996. **380**(6573): p. 435-9.

129. Ferrara, N., *Vascular endothelial growth factor.* Eur J Cancer, 1996. **32a**(14): p. 2413-22.

130. Pepper, M.S., et al., *Potent synergism between vascular endothelial growth factor and basic fibroblast growth factor in the induction of angiogenesis in vitro.* Biochem Biophys Res Commun, 1992. **189**(2): p. 824-31.

131. Montesano, R., et al., *Basic fibroblast growth factor induces angiogenesis in vitro.* Proc Natl Acad Sci U S A, 1986. **83**(19): p. 7297-301.

132. Ferrara, N., *Vascular endothelial growth factor.* Trends Cardiovasc Med, 1993. **3**(6): p. 244-50.

133. Brouty-Boyé, D. and B.R. Zetter, *Inhibition of cell motility by interferon.* Science, 1980. **208**(4443): p. 516-8.

134. Sidky, Y.A. and E.C. Borden, *Inhibition of angiogenesis by interferons: effects on tumor- and lymphocyte-induced vascular responses.* Cancer Res, 1987. **47**(19): p. 5155-61.

135. Taylor, S. and J. Folkman, *Protamine is an inhibitor of angiogenesis.* Nature, 1982. **297**(5864): p. 307-12.

136. O'Reilly, M.S., et al., *Angiostatin: a novel angiogenesis inhibitor that mediates the suppression of metastases by a Lewis lung carcinoma.* Cell, 1994. **79**(2): p. 315-28.

137. Jakobsson, L., et al., *Endothelial cells dynamically compete for the tip cell position during angiogenic sprouting.* Nat Cell Biol, 2010. **12**(10): p. 943-53.

138. Fong, G.H., et al., *Role of the Flt-1 receptor tyrosine kinase in regulating the assembly of vascular endothelium.* Nature, 1995. **376**(6535): p. 66-70.

139. Shalaby, F., et al., *Failure of blood-island formation and vasculogenesis in Flk-1-deficient mice.* Nature, 1995. **376**(6535): p. 62-6.

140. Park, J.E., et al., *Placenta growth factor. Potentiation of vascular endothelial growth factor bioactivity, in vitro and in vivo, and high affinity binding to Flt-1 but not to Flk-1/KDR.* J Biol Chem, 1994. **269**(41): p. 25646-54.

141. Jakobsson, L., K. Bentley, and H. Gerhardt, *VEGFRs and Notch: a dynamic collaboration in vascular patterning.* Biochem Soc Trans, 2009. **37**(Pt 6): p. 1233-6.

142. Lin, E.Y., et al., *Macrophages regulate the angiogenic switch in a mouse model of breast cancer.* Cancer Res, 2006. **66**(23): p. 11238-46.

143. Riabov, V., et al., *Role of tumor associated macrophages in tumor angiogenesis and lymphangiogenesis.* Front Physiol, 2014. **5**: p. 75.

144. Suchting, S., et al., *The Notch ligand Delta-like 4 negatively regulates endothelial tip cell formation and vessel branching.* Proc Natl Acad Sci U S A, 2007. **104**(9): p. 3225-30.

145. Hellström, M., et al., *Dll4 signalling through Notch1 regulates formation of tip cells during angiogenesis.* Nature, 2007. **445**(7129): p. 776-80.

146. Siekmann, A.F. and N.D. Lawson, *Notch signalling limits angiogenic cell behaviour in developing zebrafish arteries.* Nature, 2007. **445**(7129): p. 781-4.

147. Lobov, I.B., et al., *Delta-like ligand 4 (Dll4) is induced by VEGF as a negative regulator of angiogenic sprouting.* Proc Natl Acad Sci U S A, 2007. **104**(9): p. 3219-24.

148. Ma, J., et al., *Noncanonical activation of Notch1 protein by membrane type 1 matrix metalloproteinase (MT1-MMP) controls melanoma cell proliferation.* J Biol Chem, 2014. **289**(12): p. 8442-9.

149. Gerhardt, H., et al., *VEGF guides angiogenic sprouting utilizing endothelial tip cell filopodia.* J Cell Biol, 2003. **161**(6): p. 1163-77.

150. Ruhrberg, C., et al., *Spatially restricted patterning cues provided by heparin-binding VEGF-A control blood vessel branching morphogenesis.* Genes Dev, 2002. **16**(20): p. 2684-98.

151. Phng, L.K., et al., *Nrarp coordinates endothelial Notch and Wnt signaling to control vessel density in angiogenesis.* Dev Cell, 2009. **16**(1): p. 70-82.

152. Betz, C., et al., *Cell behaviors and dynamics during angiogenesis.* Development, 2016. **143**(13): p. 2249-60.

153. Daneman, R. and A. Prat, *The blood-brain barrier.* Cold Spring Harb Perspect Biol, 2015. **7**(1): p. a020412.

154. Pasqualini, R. and W. Arap, *Profiling the molecular diversity of blood vessels.* Cold Spring Harb Symp Quant Biol, 2002. **67**: p. 223-5.

155. Pasqualini, R., W. Arap, and D.M. McDonald, *Probing the structural and molecular diversity of tumor vasculature.* Trends Mol Med, 2002. **8**(12): p. 563-71.

156. Sundberg, C., et al., *Stable expression of angiopoietin-1 and other markers by cultured pericytes: phenotypic similarities to a subpopulation of cells in maturing vessels during later stages of angiogenesis in vivo.* Lab Invest, 2002. **82**(4): p. 387-401.

157. Davis, S., et al., *Isolation of angiopoietin-1, a ligand for the TIE2 receptor, by secretion-trap expression cloning.* Cell, 1996. **87**(7): p. 1161-9.

158. Dumont, D.J., et al., *Dominant-negative and targeted null mutations in the endothelial receptor tyrosine kinase, tek, reveal a critical role in vasculogenesis of the embryo.* Genes Dev, 1994. **8**(16): p. 1897-909.

159. Partanen, J., et al., *A novel endothelial cell surface receptor tyrosine kinase with extracellular epidermal growth factor homology domains.* Mol Cell Biol, 1992. **12**(4): p. 1698-707.

160. Schnürch, H. and W. Risau, *Expression of tie-2, a member of a novel family of receptor tyrosine kinases, in the endothelial cell lineage.* Development, 1993. **119**(3): p. 957-68.

161. Vikkula, M., et al., *Vascular dysmorphogenesis caused by an activating mutation in the receptor tyrosine kinase TIE2.* Cell, 1996. **87**(7): p. 1181-90.

162. Sato, T.N., et al., *Distinct roles of the receptor tyrosine kinases Tie-1 and Tie-2 in blood vessel formation.* Nature, 1995. **376**(6535): p. 70-4.

163. Suri, C., et al., *Requisite role of angiopoietin-1, a ligand for the TIE2 receptor, during embryonic angiogenesis.* Cell, 1996. **87**(7): p. 1171-80.

164. Suri, C., et al., *Increased vascularization in mice overexpressing angiopoietin-1.* Science, 1998. **282**(5388): p. 468-71.

165. Thurston, G., et al., *Angiopoietin-1 protects the adult vasculature against plasma leakage.* Nat Med, 2000. **6**(4): p. 460-3.

166. Thurston, G., et al., *Leakage-resistant blood vessels in mice transgenically overexpressing angiopoietin-1.* Science, 1999. **286**(5449): p. 2511-4.

167. Jones, N., et al., *Identification of Tek/Tie2 binding partners. Binding to a multifunctional docking site mediates cell survival and migration.* J Biol Chem, 1999. **274**(43): p. 30896-905.

168. Kim, I., et al., *Angiopoietin-1 regulates endothelial cell survival through the phosphatidylinositol 3'-Kinase/Akt signal transduction pathway.* Circ Res, 2000. **86**(1): p. 24-9.

169. Fujikawa, K., et al., *Role of PI 3-kinase in angiopoietin-1-mediated migration and attachment-dependent survival of endothelial cells.* Exp Cell Res, 1999. **253**(2): p. 663-72.

170. Papapetropoulos, A., et al., *Angiopoietin-1 inhibits endothelial cell apoptosis via the Akt/survivin pathway.* J Biol Chem, 2000. **275**(13): p. 9102-5.

171. Daly, C., et al., *Angiopoietin-1 modulates endothelial cell function and gene expression via the transcription factor FKHR (FOXO1).* Genes Dev, 2004. **18**(9): p. 1060-71.

172. Hosaka, T., et al., *Disruption of forkhead transcription factor (FOXO) family members in mice reveals their functional diversification.* Proc Natl Acad Sci U S A, 2004. **101**(9): p. 2975-80.

173. Maisonpierre, P.C., et al., *Angiopoietin-2, a natural antagonist for Tie2 that disrupts in vivo angiogenesis.* Science, 1997. **277**(5322): p. 55-60.

174. Lindahl, P., et al., *Pericyte loss and microaneurysm formation in PDGF-B-deficient mice.* Science, 1997. **277**(5323): p. 242-5.

175. Benjamin, L.E., I. Hemo, and E. Keshet, *A plasticity window for blood vessel remodelling is defined by pericyte coverage of the preformed endothelial network and is regulated by PDGF-B and VEGF.* Development, 1998. **125**(9): p. 1591-8.

176. Hellström, M., et al., *Lack of pericytes leads to endothelial hyperplasia and abnormal vascular morphogenesis.* J Cell Biol, 2001. **153**(3): p. 543-53.

177. Levéen, P., et al., *Mice deficient for PDGF B show renal, cardiovascular, and hematological abnormalities.* Genes Dev, 1994. **8**(16): p. 1875-87.

178. Soriano, P., *Abnormal kidney development and hematological disorders in PDGF beta-receptor mutant mice.* Genes Dev, 1994. **8**(16): p. 1888-96.

179. Enge, M., et al., *Endothelium-specific platelet-derived growth factor-B ablation mimics diabetic retinopathy.* Embo j, 2002. **21**(16): p. 4307-16.

180. Winkler, E.A., R.D. Bell, and B.V. Zlokovic, *Pericyte-specific expression of PDGF beta receptor in mouse models with normal and deficient PDGF beta receptor signaling.* Mol Neurodegener, 2010. **5**: p. 32.

181. Fambrough, D., et al., *Diverse signaling pathways activated by growth factor receptors induce broadly overlapping, rather than independent, sets of genes.* Cell, 1999. **97**(6): p. 727-41.

182.   Tallquist, M.D., W.J. French, and P. Soriano, *Additive effects of PDGF receptor beta signaling pathways in vascular smooth muscle cell development.* PLoS Biol, 2003. **1**(2): p. E52.

183.   Stratman, A.N., et al., *Pericyte recruitment during vasculogenic tube assembly stimulates endothelial basement membrane matrix formation.* Blood, 2009. **114**(24): p. 5091-101.

184.   Bergers, G., et al., *Benefits of targeting both pericytes and endothelial cells in the tumor vasculature with kinase inhibitors.* J Clin Invest, 2003. **111**(9): p. 1287-95.

185.   Dvorak, H.F., et al., *Identification and characterization of the blood vessels of solid tumors that are leaky to circulating macromolecules.* Am J Pathol, 1988. **133**(1): p. 95-109.

186.   Baluk, P., et al., *Abnormalities of basement membrane on blood vessels and endothelial sprouts in tumors.* Am J Pathol, 2003. **163**(5): p. 1801-15.

187.   McDonald, D.M. and P. Baluk, *Significance of blood vessel leakiness in cancer.* Cancer Res, 2002. **62**(18): p. 5381-5.

188.   Morikawa, S., et al., *Abnormalities in pericytes on blood vessels and endothelial sprouts in tumors.* Am J Pathol, 2002. **160**(3): p. 985-1000.

189.   Abramsson, A., et al., *Analysis of mural cell recruitment to tumor vessels.* Circulation, 2002. **105**(1): p. 112-7.

190.   Eberhard, A., et al., *Heterogeneity of angiogenesis and blood vessel maturation in human tumors: implications for antiangiogenic tumor therapies.* Cancer Res, 2000. **60**(5): p. 1388-93.

191.   Gee, M.S., et al., *Tumor vessel development and maturation impose limits on the effectiveness of anti-vascular therapy.* Am J Pathol, 2003. **162**(1): p. 183-93.

192.   Stratmann, A., W. Risau, and K.H. Plate, *Cell type-specific expression of angiopoietin-1 and angiopoietin-2 suggests a role in glioblastoma angiogenesis.* Am J Pathol, 1998. **153**(5): p. 1459-66.

193.   Zhang, L., et al., *Tumor-derived vascular endothelial growth factor up-regulates angiopoietin-2 in host endothelium and destabilizes host vasculature, supporting angiogenesis in ovarian cancer.* Cancer Res, 2003. **63**(12): p. 3403-12.

194.   Hammes, H.P., et al., *Angiopoietin-2 causes pericyte dropout in the normal retina: evidence for involvement in diabetic retinopathy.* Diabetes, 2004. **53**(4): p. 1104-10.

195.   Nehls, V., K. Denzer, and D. Drenckhahn, *Pericyte involvement in capillary sprouting during angiogenesis in situ.* Cell Tissue Res, 1992. **270**(3): p. 469-74.

196.   Chen, W.C., et al., *Human myocardial pericytes: multipotent mesodermal precursors exhibiting cardiac specificity.* Stem Cells, 2015. **33**(2): p. 557-73.

197.   Ozawa, M.G., et al., *Angiogenesis with pericyte abnormalities in a transgenic model of prostate carcinoma.* Cancer, 2005. **104**(10): p. 2104-15.

198.   Abramsson, A., P. Lindblom, and C. Betsholtz, *Endothelial and nonendothelial sources of PDGF-B regulate pericyte recruitment and influence vascular pattern formation in tumors.* J Clin Invest, 2003. **112**(8): p. 1142-51.

199.   Ozerdem, U., et al., *NG2 proteoglycan is expressed exclusively by mural cells during vascular morphogenesis.* Dev Dyn, 2001. **222**(2): p. 218-27.

200.   Huang, F.J., et al., *Pericyte deficiencies lead to aberrant tumor vascularizaton in the brain of the NG2 null mouse.* Dev Biol, 2010. **344**(2): p. 1035-46.

201.   Engbring, J.A. and H.K. Kleinman, *The basement membrane matrix in malignancy.* J Pathol, 2003. **200**(4): p. 465-70.

202.   Majno, G. and G.E. Palade, *Studies on inflammation. 1. The effect of histamine and serotonin on vascular permeability: an electron microscopic study.* J Biophys Biochem Cytol, 1961. **11**(3): p. 571-605.

203.   Suzuki, S., K. Sano, and H. Tanihara, *Diversity of the cadherin family: evidence for eight new cadherins in nervous tissue.* Cell Regul, 1991. **2**(4): p. 261-70.

204.   Lampugnani, M.G., et al., *A novel endothelial-specific membrane protein is a marker of cell-cell contacts.* J Cell Biol, 1992. **118**(6): p. 1511-22.

205.   Breier, G., et al., *Molecular cloning and expression of murine vascular endothelial-cadherin in early stage development of cardiovascular system.* Blood, 1996. **87**(2): p. 630-41.

206.   Vittet, D., et al., *Targeted null-mutation in the vascular endothelial-cadherin gene impairs the organization of vascular-like structures in embryoid bodies.* Proc Natl Acad Sci U S A, 1997. **94**(12): p. 6273-8.

207.   Carmeliet, P., et al., *Targeted deficiency or cytosolic truncation of the VE-cadherin gene in mice impairs VEGF-mediated endothelial survival and angiogenesis.* Cell, 1999. **98**(2): p. 147-57.

208.   Corada, M., et al., *Monoclonal antibodies directed to different regions of vascular endothelial cadherin extracellular domain affect adhesion and clustering of the protein and modulate endothelial permeability.* Blood, 2001. **97**(6): p. 1679-84.

209.   Takeichi, M., *The cadherins: cell-cell adhesion molecules controlling animal morphogenesis.* Development, 1988. **102**(4): p. 639-55.

210. Takeichi, M., *Cadherins in cancer: implications for invasion and metastasis.* Curr Opin Cell Biol, 1993. **5**(5): p. 806-11.

211. Brasch, J., et al., *Structure and binding mechanism of vascular endothelial cadherin: a divergent classical cadherin.* J Mol Biol, 2011. **408**(1): p. 57-73.

212. Navarro, P., L. Ruco, and E. Dejana, *Differential localization of VE- and N-cadherins in human endothelial cells: VE-cadherin competes with N-cadherin for junctional localization.* J Cell Biol, 1998. **140**(6): p. 1475-84.

213. Nagafuchi, A. and M. Takeichi, *Cell binding function of E-cadherin is regulated by the cytoplasmic domain.* Embo j, 1988. **7**(12): p. 3679-84.

214. Ozawa, M., H. Baribault, and R. Kemler, *The cytoplasmic domain of the cell adhesion molecule uvomorulin associates with three independent proteins structurally related in different species.* Embo j, 1989. **8**(6): p. 1711-7.

215. Lampugnani, M.G., et al., *The molecular organization of endothelial cell to cell junctions: differential association of plakoglobin, beta-catenin, and alpha-catenin with vascular endothelial cadherin (VE-cadherin).* J Cell Biol, 1995. **129**(1): p. 203-17.

216. Kowalczyk, A.P., et al., *VE-cadherin and desmoplakin are assembled into dermal microvascular endothelial intercellular junctions: a pivotal role for plakoglobin in the recruitment of desmoplakin to intercellular junctions.* J Cell Sci, 1998. **111 (Pt 20)**: p. 3045-57.

217. Wheelock, M.J. and K.R. Johnson, *Cadherin-mediated cellular signaling.* Curr Opin Cell Biol, 2003. **15**(5): p. 509-14.

218. Rajasekaran, A.K., et al., *Catenins and zonula occludens-1 form a complex during early stages in the assembly of tight junctions.* J Cell Biol, 1996. **132**(3): p. 451-63.

219. Rimm, D.L., et al., *Alpha 1(E)-catenin is an actin-binding and -bundling protein mediating the attachment of F-actin to the membrane adhesion complex.* Proc Natl Acad Sci U S A, 1995. **92**(19): p. 8813-7.

220. Nieset, J.E., et al., *Characterization of the interactions of alpha-catenin with alpha-actinin and beta-catenin/plakoglobin.* J Cell Sci, 1997. **110 (Pt 8)**: p. 1013-22.

221. Navarro, P., et al., *Catenin-dependent and -independent functions of vascular endothelial cadherin.* J Biol Chem, 1995. **270**(52): p. 30965-72.

222. Breviario, F., et al., *Functional properties of human vascular endothelial cadherin (7B4/cadherin-5), an endothelium-specific cadherin.* Arterioscler Thromb Vasc Biol, 1995. **15**(8): p. 1229-39.

223. Hashizume, H., et al., *Openings between defective endothelial cells explain tumor vessel leakiness.* Am J Pathol, 2000. **156**(4): p. 1363-80.

224. Aragon-Sanabria, V., et al., *VE-Cadherin Disassembly and Cell Contractility in the Endothelium are Necessary for Barrier Disruption Induced by Tumor Cells.* Sci Rep, 2017. **7**: p. 45835.

225. Gavard, J. and J.S. Gutkind, *VEGF controls endothelial-cell permeability by promoting the beta-arrestin-dependent endocytosis of VE-cadherin.* Nat Cell Biol, 2006. **8**(11): p. 1223-34.

226. Andriopoulou, P., et al., *Histamine induces tyrosine phosphorylation of endothelial cell-to-cell adherens junctions.* Arterioscler Thromb Vasc Biol, 1999. **19**(10): p. 2286-97.

227. Angelini, D.J., et al., *TNF-alpha increases tyrosine phosphorylation of vascular endothelial cadherin and opens the paracellular pathway through fyn activation in human lung endothelia.* Am J Physiol Lung Cell Mol Physiol, 2006. **291**(6): p. L1232-45.

228. Esser, S., et al., *Vascular endothelial growth factor induces VE-cadherin tyrosine phosphorylation in endothelial cells.* J Cell Sci, 1998. **111 (Pt 13)**: p. 1853-65.

229. Paul, R., et al., *Src deficiency or blockade of Src activity in mice provides cerebral protection following stroke.* Nat Med, 2001. **7**(2): p. 222-7.

230. Weidert, E., et al., *Actinomyosin contraction, phosphorylation of VE-cadherin, and actin remodeling enable melanoma-induced endothelial cell-cell junction disassembly.* PLoS One, 2014. **9**(9): p. e108092.

231. Peng, H.H., et al., *Involvement of phospholipase C signaling in melanoma cell-induced endothelial junction disassembly.* Front Biosci, 2005. **10**: p. 1597-606.

232. Förstermann, U., et al., *Nitric oxide synthase isozymes. Characterization, purification, molecular cloning, and functions.* Hypertension, 1994. **23**(6 Pt 2): p. 1121-31.

233. Thibeault, S., et al., *S-nitrosylation of beta-catenin by eNOS-derived NO promotes VEGF-induced endothelial cell permeability.* Mol Cell, 2010. **39**(3): p. 468-76.

234. Yang, B., et al., *Nitric Oxide Increases Arterial Endotheial Permeability through Mediating VE-Cadherin Expression during Arteriogenesis.* PLoS One, 2015. **10**(7): p. e0127931.

235. Djuric, T.Z., Maja, *Overview of MMP Biology and Gene Associations in Human Diseases.*, ed. F. Travascio. 2017: IntechOpen. 200.

236. Quintero-Fabián, S., et al., *Role of Matrix Metalloproteinases in Angiogenesis and Cancer.* Front Oncol, 2019. **9**: p. 1370.

237. Wells, J.M., A. Gaggar, and J.E. Blalock, *MMP generated matrikines.* Matrix Biol, 2015. **44-46**: p. 122-9.

238. Laronha, H., et al., *Polymerizable Matrix Metalloproteinases' Inhibitors with Potential Application for Dental Restorations.* Biomedicines, 2021. **9**(4).

239. Van Wart, H.E. and H. Birkedal-Hansen, *The cysteine switch: a principle of regulation of metalloproteinase activity with potential applicability to the entire matrix metalloproteinase gene family.* Proc Natl Acad Sci U S A, 1990. **87**(14): p. 5578-82.

240. Gomis-Rüth, F.X., *Structural aspects of the metzincin clan of metalloendopeptidases.* Mol Biotechnol, 2003. **24**(2): p. 157-202.

241. Murphy, G. and H. Nagase, *Progress in matrix metalloproteinase research.* Mol Aspects Med, 2008. **29**(5): p. 290-308.

242. Nagase, H., R. Visse, and G. Murphy, *Structure and function of matrix metalloproteinases and TIMPs.* Cardiovasc Res, 2006. **69**(3): p. 562-73.

243. Cui, N., M. Hu, and R.A. Khalil, *Biochemical and Biological Attributes of Matrix Metalloproteinases.* Prog Mol Biol Transl Sci, 2017. **147**: p. 1-73.

244. Turunen, S.P., O. Tatti-Bugaeva, and K. Lehti, *Membrane-type matrix metalloproteases as diverse effectors of cancer progression.* Biochim Biophys Acta Mol Cell Res, 2017. **1864**(11 Pt A): p. 1974-1988.

245. Chiao, Y.A., et al., *In vivo matrix metalloproteinase-7 substrates identified in the left ventricle post-myocardial infarction using proteomics.* J Proteome Res, 2010. **9**(5): p. 2649-57.

246. Van Doren, S.R., *Matrix metalloproteinase interactions with collagen and elastin.* Matrix Biol, 2015. **44-46**: p. 224-31.

247. Melander, M.C., et al., *The collagen receptor uPARAP/Endo180 in tissue degradation and cancer (Review).* Int J Oncol, 2015. **47**(4): p. 1177-88.

248. Chung, L., et al., *Collagenase unwinds triple-helical collagen prior to peptide bond hydrolysis.* Embo j, 2004. **23**(15): p. 3020-30.

249. Gross, J. and C.M. Lapiere, *Collagenolytic activity in amphibian tissues: a tissue culture assay.* Proc Natl Acad Sci U S A, 1962. **48**(6): p. 1014-22.

250. Balbín, M., et al., *Identification and enzymatic characterization of two diverging murine counterparts of human interstitial collagenase (MMP-1) expressed at sites of embryo implantation.* J Biol Chem, 2001. **276**(13): p. 10253-62.

251. Zigrino, P., et al., *Fibroblast-Derived MMP-14 Regulates Collagen Homeostasis in Adult Skin.* J Invest Dermatol, 2016. **136**(8): p. 1575-1583.

252. Holmbeck, K., et al., *MT1-MMP-deficient mice develop dwarfism, osteopenia, arthritis, and connective tissue disease due to inadequate collagen turnover.* Cell, 1999. **99**(1): p. 81-92.

253. Gutiérrez-Fernández, A., et al., *Loss of MT1-MMP causes cell senescence and nuclear defects which can be reversed by retinoic acid.* Embo j, 2015. **34**(14): p. 1875-88.

254. Puente, X.S., et al., *Molecular cloning of a novel membrane-type matrix metalloproteinase from a human breast carcinoma.* Cancer Res, 1996. **56**(5): p. 944-9.

255. Itoh, Y., et al., *Membrane type 4 matrix metalloproteinase (MT4-MMP, MMP-17) is a glycosylphosphatidylinositol-anchored proteinase.* J Biol Chem, 1999. **274**(48): p. 34260-6.

256. Pei, D. and S.J. Weiss, *Transmembrane-deletion mutants of the membrane-type matrix metalloproteinase-1 process progelatinase A and express intrinsic matrix-degrading activity.* J Biol Chem, 1996. **271**(15): p. 9135-40.

257. Mori, H., et al., *Transmembrane/cytoplasmic, rather than catalytic, domains of Mmp14 signal to MAPK activation and mammary branching morphogenesis via binding to integrin β1.* Development, 2013. **140**(2): p. 343-52.

258. Page-McCaw, A., *Remodeling the model organism: matrix metalloproteinase functions in invertebrates.* Semin Cell Dev Biol, 2008. **19**(1): p. 14-23.

259. Ra, H.J. and W.C. Parks, *Control of matrix metalloproteinase catalytic activity.* Matrix Biol, 2007. **26**(8): p. 587-96.

260. Fanjul-Fernández, M., et al., *Matrix metalloproteinases: evolution, gene regulation and functional analysis in mouse models.* Biochim Biophys Acta, 2010. **1803**(1): p. 3-19.

261. Takahashi, Y., et al., *Multiparametric in situ mRNA hybridization analysis of gastric biopsies predicts lymph node metastasis in patients with gastric carcinoma.* Jpn J Cancer Res, 2002. **93**(11): p. 1258-65.

262. Mengshol, J.A., M.P. Vincenti, and C.E. Brinckerhoff, *IL-1 induces collagenase-3 (MMP-13) promoter activity in stably transfected chondrocytic cells: requirement for Runx-2 and activation by p38 MAPK and JNK pathways.* Nucleic Acids Res, 2001. **29**(21): p. 4361-72.

263. Ortega, N., D.J. Behonick, and Z. Werb, *Matrix remodeling during endochondral ossification.* Trends Cell Biol, 2004. **14**(2): p. 86-93.

264. Thomas, G., *Furin at the cutting edge: from protein traffic to embryogenesis and disease.* Nat Rev Mol Cell Biol, 2002. **3**(10): p. 753-66.

265. Kang, T., H. Nagase, and D. Pei, *Activation of membrane-type matrix metalloproteinase 3 zymogen by the proprotein convertase furin in the trans-Golgi network.* Cancer Res, 2002. **62**(3): p. 675-81.

266. Strongin, A.Y., et al., *Mechanism of cell surface activation of 72-kDa type IV collagenase. Isolation of the activated form of the membrane metalloprotease.* J Biol Chem, 1995. **270**(10): p. 5331-8.

267. Sato, H., et al., *Cell surface binding and activation of gelatinase A induced by expression of membrane-type-1-matrix metalloproteinase (MT1-MMP).* FEBS Lett, 1996. **385**(3): p. 238-40.

268. Knäuper, V., et al., *Biochemical characterization of human collagenase-3.* J Biol Chem, 1996. **271**(3): p. 1544-50.

269. Knäuper, V., et al., *Cellular mechanisms for human procollagenase-3 (MMP-13) activation. Evidence that MT1-MMP (MMP-14) and gelatinase a (MMP-2) are able to generate active enzyme.* J Biol Chem, 1996. **271**(29): p. 17124-31.

270. Ito, A. and H. Nagase, *Evidence that human rheumatoid synovial matrix metalloproteinase 3 is an endogenous activator of procollagenase.* Arch Biochem Biophys, 1988. **267**(1): p. 211-6.

271. Imai, K., et al., *Matrix metalloproteinase 7 (matrilysin) from human rectal carcinoma cells. Activation of the precursor, interaction with other matrix metalloproteinases and enzymic properties.* J Biol Chem, 1995. **270**(12): p. 6691-7.

272. Uekita, T., et al., *Expression of membrane-type 1 matrix metalloproteinase (MT1-MMP) mRNA in trophoblast and endometrial epithelial cell populations of the synepitheliochorial placenta of goats (Capra hircus).* Arch Histol Cytol, 2001. **64**(4): p. 411-24.

273. Anilkumar, N., et al., *Palmitoylation at Cys574 is essential for MT1-MMP to promote cell migration.* Faseb j, 2005. **19**(10): p. 1326-8.

274. Yamaguchi, H., et al., *Lipid rafts and caveolin-1 are required for invadopodia formation and extracellular matrix degradation by human breast cancer cells.* Cancer Res, 2009. **69**(22): p. 8594-602.

275. Xie, Y., et al., *Nuclear matrix metalloproteinases: functions resemble the evolution from the intracellular to the extracellular compartment.* Cell Death Discov, 2017. **3**: p. 17036.

276. Kümper, M., J. Steinkamp, and P. Zigrino, *Metalloproteinases in dermal homeostasis.* Am J Physiol Cell Physiol, 2022. **323**(4): p. C1290-c1303.

277. Brew, K. and H. Nagase, *The tissue inhibitors of metalloproteinases (TIMPs): an ancient family with structural and functional diversity.* Biochim Biophys Acta, 2010. **1803**(1): p. 55-71.

278. Nagase, H., et al., *Engineering of selective TIMPs.* Ann N Y Acad Sci, 1999. **878**: p. 1-11.

279. Gomez, D.E., et al., *Tissue inhibitors of metalloproteinases: structure, regulation and biological functions.* Eur J Cell Biol, 1997. **74**(2): p. 111-22.

280. Docherty, A.J., et al., *Sequence of human tissue inhibitor of metalloproteinases and its identity to erythroid-potentiating activity.* Nature, 1985. **318**(6041): p. 66-9.

281. Stetler-Stevenson, W.G., et al., *Tissue inhibitor of metalloproteinases-2 (TIMP-2) mRNA expression in tumor cell lines and human tumor tissues.* J Biol Chem, 1990. **265**(23): p. 13933-8.

282. Pavloff, N., et al., *A new inhibitor of metalloproteinases from chicken: ChIMP-3. A third member of the TIMP family.* J Biol Chem, 1992. **267**(24): p. 17321-6.

283. Greene, J., et al., *Molecular cloning and characterization of human tissue inhibitor of metalloproteinase 4.* J Biol Chem, 1996. **271**(48): p. 30375-80.

284. Takahashi, C., et al., *Regulation of matrix metalloproteinase-9 and inhibition of tumor invasion by the membrane-anchored glycoprotein RECK.* Proc Natl Acad Sci U S A, 1998. **95**(22): p. 13221-6.

285. Oh, J., et al., *The membrane-anchored MMP inhibitor RECK is a key regulator of extracellular matrix integrity and angiogenesis.* Cell, 2001. **107**(6): p. 789-800.

286. Barrett, A.J. and P.M. Starkey, *The interaction of alpha 2-macroglobulin with proteinases. Characteristics and specificity of the reaction, and a hypothesis concerning its molecular mechanism.* Biochem J, 1973. **133**(4): p. 709-24.

287. Herman, M.P., et al., *Tissue factor pathway inhibitor-2 is a novel inhibitor of matrix metalloproteinases with implications for atherosclerosis.* J Clin Invest, 2001. **107**(9): p. 1117-26.

288. Aiken, A. and R. Khokha, *Unraveling metalloproteinase function in skeletal biology and disease using genetically altered mice.* Biochim Biophys Acta, 2010. **1803**(1): p. 121-32.

289. Oblander, S.A., et al., *Distinctive functions of membrane type 1 matrix-metalloprotease (MT1-MMP or MMP-14) in lung and submandibular gland development are independent of its role in pro-MMP-2 activation.* Dev Biol, 2005. **277**(1): p. 255-69.

290. Itoh, T., et al., *Reduced angiogenesis and tumor progression in gelatinase A-deficient mice.* Cancer Res, 1998. **58**(5): p. 1048-51.

291. van Hinsbergh, V.W. and P. Koolwijk, *Endothelial sprouting and angiogenesis: matrix metalloproteinases in the lead.* Cardiovasc Res, 2008. **78**(2): p. 203-12.

292. Gutiérrez-Fernández, A., et al., *Increased inflammation delays wound healing in mice deficient in collagenase-2 (MMP-8).* Faseb j, 2007. **21**(10): p. 2580-91.

293. Krishnaswamy, V.R., D. Mintz, and I. Sagi, *Matrix metalloproteinases: The sculptors of chronic cutaneous wounds.* Biochim Biophys Acta Mol Cell Res, 2017. **1864**(11 Pt B): p. 2220-2227.

294. Frost, J., et al., *Differential gene expression of MMP-1, TIMP-1 and HGF in clinically involved and uninvolved skin in South Africans with SSc.* Rheumatology (Oxford), 2012. **51**(6): p. 1049-52.

295. Asano, Y., et al., *Clinical significance of serum matrix metalloproteinase-13 levels in patients with localized scleroderma.* Clin Exp Rheumatol, 2006. **24**(4): p. 394-9.

296. Asano, Y., et al., *Clinical significance of serum levels of matrix metalloproteinase-13 in patients with systemic sclerosis.* Rheumatology (Oxford), 2006. **45**(3): p. 303-7.

297. Niwa, H., et al., *Decrease in matrix metalloproteinase‐3 activity in systemic sclerosis fibroblasts causes α2‐antiplasmin and extracellular matrix deposition, and contributes to fibrosis development.* Mol Med Rep, 2020. **22**(4): p. 3001-3007.

298. Waszczykowska, A., et al., *Matrix Metalloproteinases MMP-2 and MMP-9, Their Inhibitors TIMP-1 and TIMP-2, Vascular Endothelial Growth Factor and sVEGFR-2 as Predictive Markers of Ischemic Retinopathy in Patients with Systemic Sclerosis-Case Series Report.* Int J Mol Sci, 2020. **21**(22).

299. Longo, G.M., et al., *Matrix metalloproteinases 2 and 9 work in concert to produce aortic aneurysms.* J Clin Invest, 2002. **110**(5): p. 625-32.

300. Davis, V., et al., *Matrix metalloproteinase-2 production and its binding to the matrix are increased in abdominal aortic aneurysms.* Arterioscler Thromb Vasc Biol, 1998. **18**(10): p. 1625-33.

301. Thompson, R.W., et al., *Production and localization of 92-kilodalton gelatinase in abdominal aortic aneurysms. An elastolytic metalloproteinase expressed by aneurysm-infiltrating macrophages.* J Clin Invest, 1995. **96**(1): p. 318-26.

302. Matsumura, S., et al., *Targeted deletion or pharmacological inhibition of MMP-2 prevents cardiac rupture after myocardial infarction in mice.* J Clin Invest, 2005. **115**(3): p. 599-609.

303. Molloy, K.J., et al., *Unstable carotid plaques exhibit raised matrix metalloproteinase-8 activity.* Circulation, 2004. **110**(3): p. 337-43.

304. Johnson, J.L., et al., *Divergent effects of matrix metalloproteinases 3, 7, 9, and 12 on atherosclerotic plaque stability in mouse brachiocephalic arteries.* Proc Natl Acad Sci U S A, 2005. **102**(43): p. 15575-80.

305. Egeblad, M. and Z. Werb, *New functions for the matrix metalloproteinases in cancer progression.* Nat Rev Cancer, 2002. **2**(3): p. 161-74.

306. Rydlova, M., et al., *Biological activity and clinical implications of the matrix metalloproteinases.* Anticancer Res, 2008. **28**(2b): p. 1389-97.

307. Morgia, G., et al., *Matrix metalloproteinases as diagnostic (MMP-13) and prognostic (MMP-2, MMP-9) markers of prostate cancer.* Urol Res, 2005. **33**(1): p. 44-50.

308. Peng, W.J., et al., *Prognostic value of matrix metalloproteinase 9 expression in patients with non-small cell lung cancer.* Clin Chim Acta, 2012. **413**(13-14): p. 1121-6.

309. Yang, B., et al., *Matrix metalloproteinase-9 overexpression is closely related to poor prognosis in patients with colon cancer.* World J Surg Oncol, 2014. **12**: p. 24.

310. Chen, S.Z., et al., *Expression levels of matrix metalloproteinase-9 in human gastric carcinoma.* Oncol Lett, 2015. **9**(2): p. 915-919.

311. Xu, Y., et al., *The co-expression of MMP-9 and Tenascin-C is significantly associated with the progression and prognosis of pancreatic cancer.* Diagn Pathol, 2015. **10**: p. 211.

312. Weaver, A.M., *Invadopodia: specialized cell structures for cancer invasion.* Clin Exp Metastasis, 2006. **23**(2): p. 97-105.

313. Gialeli, C., A.D. Theocharis, and N.K. Karamanos, *Roles of matrix metalloproteinases in cancer progression and their pharmacological targeting.* Febs j, 2011. **278**(1): p. 16-27.

314. Vizoso, F.J., et al., *Study of matrix metalloproteinases and their inhibitors in breast cancer.* Br J Cancer, 2007. **96**(6): p. 903-11.

315. Sato, H., et al., *A matrix metalloproteinase expressed on the surface of invasive tumour cells.* Nature, 1994. **370**(6484): p. 61-5.

316. Itoh, Y.S.M., *Chapter 164 - Membrane-type Matrix Metalloproteinase 1*, in *Handbook of Proteolytic Enzymes*, N.S. Rawlings, G. , Editor. 2013, Academic Press.

317. Golubkov, V.S., et al., *Proteolysis of the membrane type-1 matrix metalloproteinase prodomain: implications for a two-step proteolytic processing and activation.* J Biol Chem, 2007. **282**(50): p. 36283-91.

318. Golubkov, V.S., et al., *Internal cleavages of the autoinhibitory prodomain are required for membrane type 1 matrix metalloproteinase activation, although furin cleavage alone generates inactive proteinase.* J Biol Chem, 2010. **285**(36): p. 27726-36.

319. Will, H., et al., *The soluble catalytic domain of membrane type 1 matrix metalloproteinase cleaves the propeptide of progelatinase A and initiates autoproteolytic activation. Regulation by TIMP-2 and TIMP-3.* J Biol Chem, 1996. **271**(29): p. 17119-23.

320. Sato, H., et al., *Activation of a recombinant membrane type 1-matrix metalloproteinase (MT1-MMP) by furin and its interaction with tissue inhibitor of metalloproteinases (TIMP)-2.* FEBS Lett, 1996. **393**(1): p. 101-4.

321. Miyagawa, T., et al., *MT1-MMP recruits the ER-Golgi SNARE Bet1 for efficient MT1-MMP transport to the plasma membrane.* J Cell Biol, 2019. **218**(10): p. 3355-3371.

322. Osenkowski, P., M. Toth, and R. Fridman, *Processing, shedding, and endocytosis of membrane type 1-matrix metalloproteinase (MT1-MMP).* J Cell Physiol, 2004. **200**(1): p. 2-10.

323. Hakulinen, J., et al., *Secretion of active membrane type 1 matrix metalloproteinase (MMP-14) into extracellular space in microvesicular exosomes.* J Cell Biochem, 2008. **105**(5): p. 1211-8.

324. Cao, J., et al., *Membrane type matrix metalloproteinase 1 activates pro-gelatinase A without furin cleavage of the N-terminal domain.* J Biol Chem, 1996. **271**(47): p. 30174-80.

325. Hernandez-Barrantes, S., et al., *Binding of active (57 kDa) membrane type 1-matrix metalloproteinase (MT1-MMP) to tissue inhibitor of metalloproteinase (TIMP)-2 regulates MT1-MMP processing and pro-MMP-2 activation.* J Biol Chem, 2000. **275**(16): p. 12080-9.

326. Itoh, Y., et al., *Homophilic complex formation of MT1-MMP facilitates proMMP-2 activation on the cell surface and promotes tumor cell invasion.* Embo j, 2001. **20**(17): p. 4782-93.

327. Butler, G.S., et al., *The TIMP2 membrane type 1 metalloproteinase "receptor" regulates the concentration and efficient activation of progelatinase A. A kinetic study.* J Biol Chem, 1998. **273**(2): p. 871-80.

328. Itoh, Y., et al., *Cell surface collagenolysis requires homodimerization of the membrane-bound collagenase MT1-MMP.* Mol Biol Cell, 2006. **17**(12): p. 5390-9.

329. d'Ortho, M.P., et al., *Membrane-type matrix metalloproteinases 1 and 2 exhibit broad-spectrum proteolytic capacities comparable to many matrix metalloproteinases.* Eur J Biochem, 1997. **250**(3): p. 751-7.

330. Ohuchi, E., et al., *Membrane type 1 matrix metalloproteinase digests interstitial collagens and other extracellular matrix macromolecules.* J Biol Chem, 1997. **272**(4): p. 2446-51.

331. Koshikawa, N., et al., *Role of cell surface metalloprotease MT1-MMP in epithelial cell migration over laminin-5.* J Cell Biol, 2000. **148**(3): p. 615-24.

332. Bini, A., et al., *Degradation of cross-linked fibrin by matrix metalloproteinase 3 (stromelysin 1): hydrolysis of the gamma Gly 404-Ala 405 peptide bond.* Biochemistry, 1996. **35**(40): p. 13056-63.

333. Bini, A., et al., *Characterization of stromelysin 1 (MMP-3), matrilysin (MMP-7), and membrane type 1 matrix metalloproteinase (MT1-MMP) derived fibrin(ogen) fragments D-dimer and D-like monomer: NH2-terminal sequences of late-stage digest fragments.* Biochemistry, 1999. **38**(42): p. 13928-36.

334. Chan, K.M., et al., *MT1-MMP inactivates ADAM9 to regulate FGFR2 signaling and calvarial osteogenesis.* Dev Cell, 2012. **22**(6): p. 1176-90.

335. Tam, E.M., et al., *Characterization of the distinct collagen binding, helicase and cleavage mechanisms of matrix metalloproteinase 2 and 14 (gelatinase A and MT1-MMP): the differential roles of the MMP hemopexin c domains and the MMP-2 fibronectin type II modules in collagen triple helicase activities.* J Biol Chem, 2004. **279**(41): p. 43336-44.

336. McQuibban, G.A., et al., *Matrix metalloproteinase activity inactivates the CXC chemokine stromal cell-derived factor-1.* J Biol Chem, 2001. **276**(47): p. 43503-8.

337. McQuibban, G.A., et al., *Matrix metalloproteinase processing of monocyte chemoattractant proteins generates CC chemokine receptor antagonists with anti-inflammatory properties in vivo.* Blood, 2002. **100**(4): p. 1160-7.

338. Kajita, M., et al., *Membrane-type 1 matrix metalloproteinase cleaves CD44 and promotes cell migration.* J Cell Biol, 2001. **153**(5): p. 893-904.

339. Sugiyama, N., et al., *EphA2 cleavage by MT1-MMP triggers single cancer cell invasion via homotypic cell repulsion.* J Cell Biol, 2013. **201**(3): p. 467-84.

340. Butler, G.S., et al., *Pharmacoproteomics of a metalloproteinase hydroxamate inhibitor in breast cancer cells: dynamics of membrane type 1 matrix metalloproteinase-mediated membrane protein shedding.* Mol Cell Biol, 2008. **28**(15): p. 4896-914.

341. Mu, D., et al., *The integrin alpha(v)beta8 mediates epithelial homeostasis through MT1-MMP-dependent activation of TGF-beta1.* J Cell Biol, 2002. **157**(3): p. 493-507.

342. Tatti, O., et al., *MT1-MMP releases latent TGF-beta1 from endothelial cell extracellular matrix via proteolytic processing of LTBP-1.* Exp Cell Res, 2008. **314**(13): p. 2501-14.

343. Barbolina, M.V. and M.S. Stack, *Membrane type 1-matrix metalloproteinase: substrate diversity in pericellular proteolysis.* Semin Cell Dev Biol, 2008. **19**(1): p. 24-33.

344. Eisenach, P.A., et al., *MT1-MMP regulates VEGF-A expression through a complex with VEGFR-2 and Src.* J Cell Sci, 2010. **123**(Pt 23): p. 4182-93.

345. Sheehy, S. and B. Annabi, *A Transcriptional Regulatory Role for the Membrane Type-1 Matrix Metalloproteinase in Carcinogen-Induced Inflammasome Gene Expression.* Gene Regul Syst Bio, 2017. **11**: p. 1177625017713996.

346. D'Alessio, S., et al., *Tissue inhibitor of metalloproteinases-2 binding to membrane-type 1 matrix metalloproteinase induces MAPK activation and cell growth by a non-proteolytic mechanism.* J Biol Chem, 2008. **283**(1): p. 87-99.

347. Sakamoto, T., D. Niiya, and M. Seiki, *Targeting the Warburg effect that arises in tumor cells expressing membrane type-1 matrix metalloproteinase.* J Biol Chem, 2011. **286**(16): p. 14691-704.

348. Kondratiev, S., et al., *Expression and prognostic role of MMP2, MMP9, MMP13, and MMP14 matrix metalloproteinases in sinonasal and oral malignant melanomas.* Hum Pathol, 2008. **39**(3): p. 337-43.

349. Hofmann, U.B., et al., *Expression and activation of matrix metalloproteinase-2 (MMP-2) and its co-localization with membrane-type 1 matrix metalloproteinase (MT1-MMP) correlate with melanoma progression.* J Pathol, 2000. **191**(3): p. 245-56.

350. Airola, K., et al., *Expression of collagenases-1 and -3 and their inhibitors TIMP-1 and -3 correlates with the level of invasion in malignant melanomas.* Br J Cancer, 1999. **80**(5-6): p. 733-43.

351. Shaverdashvili, K., et al., *MT1-MMP modulates melanoma cell dissemination and metastasis through activation of MMP2 and RAC1.* Pigment Cell Melanoma Res, 2014. **27**(2): p. 287-96.

352. Kurschat, P., et al., *Identification of activated matrix metalloproteinase-2 (MMP-2) as the main gelatinolytic enzyme in malignant melanoma by in situ zymography.* J Pathol, 2002. **197**(2): p. 179-87.

353. Durko, M., et al., *Suppression of basement membrane type IV collagen degradation and cell invasion in human melanoma cells expressing an antisense RNA for MMP-1.* Biochim Biophys Acta, 1997. **1356**(3): p. 271-80.

354. Sato, H. and T. Takino, *Coordinate action of membrane-type matrix metalloproteinase-1 (MT1-MMP) and MMP-2 enhances pericellular proteolysis and invasion.* Cancer Sci, 2010. **101**(4): p. 843-7.

355. Chung, H., et al., *Keratinocyte-derived laminin-332 promotes adhesion and migration in melanocytes and melanoma.* J Biol Chem, 2011. **286**(15): p. 13438-47.

356. Seftor, R.E., et al., *Cooperative interactions of laminin 5 gamma2 chain, matrix metalloproteinase-2, and membrane type-1-matrix/metalloproteinase are required for mimicry of embryonic vasculogenesis by aggressive melanoma.* Cancer Res, 2001. **61**(17): p. 6322-7.

357. Koshikawa, N., et al., *Membrane-type matrix metalloproteinase-1 (MT1-MMP) is a processing enzyme for human laminin gamma 2 chain.* J Biol Chem, 2005. **280**(1): p. 88-93.

358. Thakur, V. and B. Bedogni, *The membrane tethered matrix metalloproteinase MT1-MMP at the forefront of melanoma cell invasion and metastasis.* Pharmacol Res, 2016. **111**: p. 17-22.

359. Bartolomé, R.A., et al., *The chemokine receptor CXCR4 and the metalloproteinase MT1-MMP are mutually required during melanoma metastasis to lungs.* Am J Pathol, 2009. **174**(2): p. 602-12.

360. Pekkonen, P., et al., *Lymphatic endothelium stimulates melanoma metastasis and invasion via MMP14-dependent Notch3 and β1-integrin activation.* Elife, 2018. **7**.

361. Zhou, Z., et al., *Impaired endochondral ossification and angiogenesis in mice deficient in membrane-type matrix metalloproteinase I.* Proc Natl Acad Sci U S A, 2000. **97**(8): p. 4052-7.

362. Genís, L., et al., *MT1-MMP: universal or particular player in angiogenesis?* Cancer Metastasis Rev, 2006. **25**(1): p. 77-86.

363. Hiraoka, N., et al., *Matrix metalloproteinases regulate neovascularization by acting as pericellular fibrinolysins.* Cell, 1998. **95**(3): p. 365-77.

364. Gálvez, B.G., et al., *Membrane type 1-matrix metalloproteinase is activated during migration of human endothelial cells and modulates endothelial motility and matrix remodeling.* J Biol Chem, 2001. **276**(40): p. 37491-500.

365. Chun, T.H., et al., *MT1-MMP-dependent neovessel formation within the confines of the three-dimensional extracellular matrix.* J Cell Biol, 2004. **167**(4): p. 757-67.

366. Aplin, A.C., et al., *Vascular regression and survival are differentially regulated by MT1-MMP and TIMPs in the aortic ring model of angiogenesis.* Am J Physiol Cell Physiol, 2009. **297**(2): p. C471-80.

367. Han, K.Y., et al., *Proangiogenic Interactions of Vascular Endothelial MMP14 With VEGF Receptor 1 in VEGFA-Mediated Corneal Angiogenesis.* Invest Ophthalmol Vis Sci, 2016. **57**(7): p. 3313-22.

368. Devy, L., et al., *Selective inhibition of matrix metalloproteinase-14 blocks tumor growth, invasion, and angiogenesis.* Cancer Res, 2009. **69**(4): p. 1517-26.

369. Yana, I., et al., *Crosstalk between neovessels and mural cells directs the site-specific expression of MT1-MMP to endothelial tip cells.* J Cell Sci, 2007. **120**(Pt 9): p. 1607-14.

370. Hanemaaijer, R., et al., *Regulation of matrix metalloproteinase expression in human vein and microvascular endothelial cells. Effects of tumour necrosis factor alpha, interleukin 1 and phorbol ester.* Biochem J, 1993. **296 (Pt 3)**(Pt 3): p. 803-9.

371.   Seano, G., et al., *Endothelial podosome rosettes regulate vascular branching in tumour angiogenesis.* Nat Cell Biol, 2014. **16**(10): p. 931-41, 1-8.

372.   Stratman, A.N., et al., *Endothelial cell lumen and vascular guidance tunnel formation requires MT1-MMP-dependent proteolysis in 3-dimensional collagen matrices.* Blood, 2009. **114**(2): p. 237-47.

373.   Lehti, K., et al., *An MT1-MMP-PDGF receptor-beta axis regulates mural cell investment of the microvasculature.* Genes Dev, 2005. **19**(8): p. 979-91.

374.   Bahr, J.W., S, *Macrophage-Dependent Trafficking and Remodeling of the Basement Membrane-Interstitial Matrix Interface.* bioRxiv, 2018.

375.   Moses, M.A., et al., *Temporal study of the activity of matrix metalloproteinases and their endogenous inhibitors during wound healing.* J Cell Biochem, 1996. **60**(3): p. 379-86.

376.   Gilles, C., et al., *Contribution of MT1-MMP and of human laminin-5 gamma2 chain degradation to mammary epithelial cell migration.* J Cell Sci, 2001. **114**(Pt 16): p. 2967-76.

377.   Seiki, M., *The cell surface: the stage for matrix metalloproteinase regulation of migration.* Curr Opin Cell Biol, 2002. **14**(5): p. 624-32.

378.   Michopoulou, A., et al., *A novel mechanism in wound healing: Laminin 332 drives MMP9/14 activity by recruiting syndecan-1 and CD44.* Matrix Biol, 2020. **94**: p. 1-17.

379.   Mirastschijski, U., et al., *Wound healing in membrane-type-1 matrix metalloproteinase-deficient mice.* J Invest Dermatol, 2004. **123**(3): p. 600-2.

380.   Zigrino, P., et al., *Loss of epidermal MMP-14 expression interferes with angiogenesis but not with re-epithelialization.* Eur J Cell Biol, 2012. **91**(10): p. 748-56.

381.   Mori, H., et al., *New insight into the role of MMP14 in metabolic balance.* PeerJ, 2016. **4**: p. e2142.

382.   Klose, A., P. Zigrino, and C. Mauch, *Monocyte/macrophage MMP-14 modulates cell infiltration and T-cell attraction in contact dermatitis but not in murine wound healing.* Am J Pathol, 2013. **182**(3): p. 755-64.

383.   Alonso-Herranz, L., et al., *Macrophages promote endothelial-to-mesenchymal transition via MT1-MMP/TGFβ1 after myocardial infarction.* Elife, 2020. **9**.

384.   Bueno, M., et al., *ATF3 represses PINK1 gene transcription in lung epithelial cells to control mitochondrial homeostasis.* Aging Cell, 2018. **17**(2).

385.   Placido, L., et al., *Loss of MT1-MMP in Alveolar Epithelial Cells Exacerbates Pulmonary Fibrosis.* Int J Mol Sci, 2021. **22**(6).

386.   Taylor, S.H., et al., *Matrix metalloproteinase 14 is required for fibrous tissue expansion.* Elife, 2015. **4**: p. e09345.

387.   Tang, Y., et al., *MT1-MMP-dependent control of skeletal stem cell commitment via a β1-integrin/YAP/TAZ signaling axis.* Dev Cell, 2013. **25**(4): p. 402-16.

388.   Esteban, S., et al., *Endothelial MT1-MMP targeting limits intussusceptive angiogenesis and colitis via TSP1/nitric oxide axis.* EMBO Mol Med, 2020. **12**(2): p. e10862.

389.   Wong, H.L., et al., *MT1-MMP sheds LYVE-1 on lymphatic endothelial cells and suppresses VEGF-C production to inhibit lymphangiogenesis.* Nat Commun, 2016. **7**: p. 10824.

390.   Neumann, S., *The functional role of endothelial cell-derived MMP-14 in skin physiology and pathology*, in *Department of Developmental Biology*. 2014, University of Cologne. p. 82.

391.   Kümper, M., et al., *Loss of Endothelial Cell Matrix Metalloproteinase 14 Reduces Melanoma Growth and Metastasis by Increasing Tumor Vessel Stability.* J Invest Dermatol, 2022. **142**(7): p. 1923-1933.e5.

392.   Constien, R., et al., *Characterization of a novel EGFP reporter mouse to monitor Cre recombination as demonstrated by a Tie2 Cre mouse line.* Genesis, 2001. **30**(1): p. 36-44.

393.   Sonnylal, S., et al., *Postnatal induction of transforming growth factor beta signaling in fibroblasts of mice recapitulates clinical, histologic, and biochemical features of scleroderma.* Arthritis Rheum, 2007. **56**(1): p. 334-44.

394.   Zheng, B., et al., *Ligand-dependent genetic recombination in fibroblasts : a potentially powerful technique for investigating gene function in fibrosis.* Am J Pathol, 2002. **160**(5): p. 1609-17.

395.   Pach, E., et al., *Fibroblast MMP14-Dependent Collagen Processing Is Necessary for Melanoma Growth.* Cancers (Basel), 2021. **13**(8).

396.   Pach, E., et al., *Extracellular Matrix Remodeling by Fibroblast-MMP14 Regulates Melanoma Growth.* Int J Mol Sci, 2021. **22**(22).

397.   Okada, Y., H. Nagase, and E.D. Harris, Jr., *A metalloproteinase from human rheumatoid synovial fibroblasts that digests connective tissue matrix components. Purification and characterization.* J Biol Chem, 1986. **261**(30): p. 14245-55.

398.   Chin, J.R., G. Murphy, and Z. Werb, *Stromelysin, a connective tissue-degrading metalloendopeptidase secreted by stimulated rabbit synovial fibroblasts in parallel with collagenase. Biosynthesis, isolation, characterization, and substrates.* J Biol Chem, 1985. **260**(22): p. 12367-76.

399.   Sellers, A., J.J. Reynolds, and M.C. Meikle, *Neutral metallo-proteinases of rabbit bone. Separation in latent forms of distinct enzymes that when activated degrade collagen, gelatin and proteoglycans.* Biochem J, 1978. **171**(2): p. 493-6.

400.   Bejarano, P.A., et al., *Degradation of basement membranes by human matrix metalloproteinase 3 (stromelysin).* Biochem J, 1988. **256**(2): p. 413-9.

401.   Fosang, A.J., et al., *Cleavage of cartilage proteoglycan between G1 and G2 domains by stromelysins.* J Biol Chem, 1991. **266**(24): p. 15579-82.

402.   Manka, S.W., D. Bihan, and R.W. Farndale, *Structural studies of the MMP-3 interaction with triple-helical collagen introduce new roles for the enzyme in tissue remodelling.* Sci Rep, 2019. **9**(1): p. 18785.

403.   Okada, Y., et al., *Localization of matrix metalloproteinase 3 (stromelysin) in osteoarthritic cartilage and synovium.* Lab Invest, 1992. **66**(6): p. 680-90.

404.   Okada, Y., et al., *Simultaneous production of collagenase, matrix metalloproteinase 3 (stromelysin) and tissue inhibitor of metalloproteinases by rheumatoid synovial lining cells.* Matrix Suppl, 1992. **1**: p. 398-9.

405.   Murphy, G., et al., *Matrix metalloproteinase degradation of elastin, type IV collagen and proteoglycan. A quantitative comparison of the activities of 95 kDa and 72 kDa gelatinases, stromelysins-1 and -2 and punctuated metalloproteinase (PUMP).* Biochem J, 1991. **277 (Pt 1)**(Pt 1): p. 277-9.

406.   Murphy, G., et al., *Stromelysin is an activator of procollagenase. A study with natural and recombinant enzymes.* Biochem J, 1987. **248**(1): p. 265-8.

407.   Suzuki, K., et al., *Mechanisms of activation of tissue procollagenase by matrix metalloproteinase 3 (stromelysin).* Biochemistry, 1990. **29**(44): p. 10261-70.

408.   Noë, V., et al., *Release of an invasion promoter E-cadherin fragment by matrilysin and stromelysin-1.* J Cell Sci, 2001. **114**(Pt 1): p. 111-118.

409.   Maeda, S., et al., *The first stage of transforming growth factor beta1 activation is release of the large latent complex from the extracellular matrix of growth plate chondrocytes by matrix vesicle stromelysin-1 (MMP-3).* Calcif Tissue Int, 2002. **70**(1): p. 54-65.

410.   Gomis-Rüth, F.X., et al., *Mechanism of inhibition of the human matrix metalloproteinase stromelysin-1 by TIMP-1.* Nature, 1997. **389**(6646): p. 77-81.

411.   Muskett, F.W., et al., *High resolution structure of the N-terminal domain of tissue inhibitor of metalloproteinases-2 and characterization of its interaction site with matrix metalloproteinase-3.* J Biol Chem, 1998. **273**(34): p. 21736-43.

412.   Angel, P., et al., *Phorbol ester-inducible genes contain a common cis element recognized by a TPA-modulated trans-acting factor.* Cell, 1987. **49**(6): p. 729-39.

413.   Sato, H. and M. Seiki, *Regulatory mechanism of 92 kDa type IV collagenase gene expression which is associated with invasiveness of tumor cells.* Oncogene, 1993. **8**(2): p. 395-405.

414.   Benbow, U. and C.E. Brinckerhoff, *The AP-1 site and MMP gene regulation: what is all the fuss about?* Matrix Biol, 1997. **15**(8-9): p. 519-26.

415.   Bond, M., A.H. Baker, and A.C. Newby, *Nuclear factor kappaB activity is essential for matrix metalloproteinase-1 and -3 upregulation in rabbit dermal fibroblasts.* Biochem Biophys Res Commun, 1999. **264**(2): p. 561-7.

416.   Matsuno, H., et al., *Stromelysin-1 (MMP-3) in synovial fluid of patients with rheumatoid arthritis has potential to cleave membrane bound Fas ligand.* J Rheumatol, 2001. **28**(1): p. 22-8.

417.   Yoshihara, Y., et al., *Matrix metalloproteinases and tissue inhibitors of metalloproteinases in synovial fluids from patients with rheumatoid arthritis or osteoarthritis.* Ann Rheum Dis, 2000. **59**(6): p. 455-61.

418.   Blom, A.B., et al., *Crucial role of macrophages in matrix metalloproteinase-mediated cartilage destruction during experimental osteoarthritis: involvement of matrix metalloproteinase 3.* Arthritis Rheum, 2007. **56**(1): p. 147-57.

419.   Bullard, K.M., et al., *Impaired wound contraction in stromelysin-1-deficient mice.* Ann Surg, 1999. **230**(2): p. 260-5.

420.   Bullard, K.M., et al., *Stromelysin-1-deficient fibroblasts display impaired contraction in vitro.* J Surg Res, 1999. **84**(1): p. 31-4.

421.   Vaalamo, M., et al., *Patterns of matrix metalloproteinase and TIMP-1 expression in chronic and normally healing human cutaneous wounds.* Br J Dermatol, 1996. **135**(1): p. 52-9.

422.   Madlener, M., *Differential expression of matrix metalloproteinases and their physiological inhibitors in acute murine skin wounds.* Arch Dermatol Res, 1998. **290 Suppl**: p. S24-9.

423.   Madlener, M., W.C. Parks, and S. Werner, *Matrix metalloproteinases (MMPs) and their physiological inhibitors (TIMPs) are differentially expressed during excisional skin wound repair.* Exp Cell Res, 1998. **242**(1): p. 201-10.

424.   Beidler, S.K., et al., *Multiplexed analysis of matrix metalloproteinases in leg ulcer tissue of patients with chronic venous insufficiency before and after compression therapy.* Wound Repair Regen, 2008. **16**(5): p. 642-8.

425. Mudgett, J.S., et al., *Susceptibility of stromelysin 1-deficient mice to collagen-induced arthritis and cartilage destruction.* Arthritis Rheum, 1998. **41**(1): p. 110-21.

426. Rudolph-Owen, L.A., et al., *Coordinate expression of matrix metalloproteinase family members in the uterus of normal, matrilysin-deficient, and stromelysin-1-deficient mice.* Endocrinology, 1997. **138**(11): p. 4902-11.

427. Puntorieri, V., et al., *Lack of matrix metalloproteinase 3 in mouse models of lung injury ameliorates the pulmonary inflammatory response in female but not in male mice.* Exp Lung Res, 2016. **42**(7): p. 365-379.

428. Wang, M., et al., *Matrix metalloproteinase deficiencies affect contact hypersensitivity: stromelysin-1 deficiency prevents the response and gelatinase B deficiency prolongs the response.* Proc Natl Acad Sci U S A, 1999. **96**(12): p. 6885-9.

429. Choi, D.H., et al., *Matrix metalloproteinase-3 causes dopaminergic neuronal death through Nox1-regenerated oxidative stress.* PLoS One, 2014. **9**(12): p. e115954.

430. Atkinson, J.J., et al., *Membrane type 1 matrix metalloproteinase is necessary for distal airway epithelial repair and keratinocyte growth factor receptor expression after acute injury.* Am J Physiol Lung Cell Mol Physiol, 2007. **293**(3): p. L600-10.

431. Fidler, I.J., *Selection of successive tumour lines for metastasis.* Nat New Biol, 1973. **242**(118): p. 148-9.

432. Kojima, H., et al., *Detection and imaging of nitric oxide with novel fluorescent indicators: diaminofluoresceins.* Anal Chem, 1998. **70**(13): p. 2446-53.

433. Kojima, H., et al., *Development of a fluorescent indicator for nitric oxide based on the fluorescein chromophore.* Chem Pharm Bull (Tokyo), 1998. **46**(2): p. 373-5.

434. Kojima, H., et al., *Fluorescent Indicators for Imaging Nitric Oxide Production.* Angew Chem Int Ed Engl, 1999. **38**(21): p. 3209-3212.

435. Courtoy, G.E., et al., *Digital Image Analysis of Picrosirius Red Staining: A Robust Method for Multi-Organ Fibrosis Quantification and Characterization.* Biomolecules, 2020. **10**(11).

436. Vincent, S., L. Marty, and P. Fort, *S26 ribosomal protein RNA: an invariant control for gene regulation experiments in eucaryotic cells and tissues.* Nucleic Acids Res, 1993. **21**(6): p. 1498.

437. Rao, X., et al., *An improvement of the 2ˆ(-delta delta CT) method for quantitative real-time polymerase chain reaction data analysis.* Biostat Bioinforma Biomath, 2013. **3**(3): p. 71-85.

438. Bhatia, K.S., et al., *Does primary tumour volumetry performed early in the course of definitive concomitant chemoradiotherapy for head and neck squamous cell carcinoma improve prediction of primary site outcome?* Br J Radiol, 2010. **83**(995): p. 964-70.

439. Entin, I., et al., *Tumor growth retardation, cure, and induction of antitumor immunity in B16 melanoma-bearing mice by low electric field-enhanced chemotherapy.* Clin Cancer Res, 2003. **9**(8): p. 3190-7.

440. Oshimori, N., D. Oristian, and E. Fuchs, *TGF-β promotes heterogeneity and drug resistance in squamous cell carcinoma.* Cell, 2015. **160**(5): p. 963-976.

441. Zhang, H., et al., *Spontaneous lymphatic vessel formation and regression in the murine cornea.* Invest Ophthalmol Vis Sci, 2011. **52**(1): p. 334-8.

442. Seo, S., et al., *Forkhead box transcription factor FoxC1 preserves corneal transparency by regulating vascular growth.* Proc Natl Acad Sci U S A, 2012. **109**(6): p. 2015-20.

443. Tammela, T., et al., *Angiopoietin-1 promotes lymphatic sprouting and hyperplasia.* Blood, 2005. **105**(12): p. 4642-8.

444. Rezzola, S., et al., *The lymphatic vasculature: An active and dynamic player in cancer progression.* Med Res Rev, 2022. **42**(1): p. 576-614.

445. Banerji, S., et al., *LYVE-1, a new homologue of the CD44 glycoprotein, is a lymph-specific receptor for hyaluronan.* J Cell Biol, 1999. **144**(4): p. 789-801.

446. Shubik, P., *Vascularization of tumors: a review.* J Cancer Res Clin Oncol, 1982. **103**(3): p. 211-26.

447. Paduch, R., *The role of lymphangiogenesis and angiogenesis in tumor metastasis.* Cell Oncol (Dordr), 2016. **39**(5): p. 397-410.

448. Armulik, A., A. Abramsson, and C. Betsholtz, *Endothelial/pericyte interactions.* Circ Res, 2005. **97**(6): p. 512-23.

449. Kato, T., et al., *Excessive Production of Transforming Growth Factor β1 Causes Mural Cell Depletion From Cerebral Small Vessels.* Front Aging Neurosci, 2020. **12**: p. 151.

450. Eglinger, J., H. Karsjens, and E. Lammert, *Quantitative assessment of angiogenesis and pericyte coverage in human cell-derived vascular sprouts.* Inflamm Regen, 2017. **37**: p. 2.

451. Sun, Z., et al., *Reduction in pericyte coverage leads to blood-brain barrier dysfunction via endothelial transcytosis following chronic cerebral hypoperfusion.* Fluids Barriers CNS, 2021. **18**(1): p. 21.

452. Kalluri, R., *Basement membranes: structure, assembly and role in tumour angiogenesis.* Nat Rev Cancer, 2003. **3**(6): p. 422-33.

453. Taddei, A., et al., *Endothelial adherens junctions control tight junctions by VE-cadherin-mediated upregulation of claudin-5.* Nat Cell Biol, 2008. **10**(8): p. 923-34.

454. Heupel, W.M., et al., *Endothelial barrier stabilization by a cyclic tandem peptide targeting VE-cadherin transinteraction in vitro and in vivo.* J Cell Sci, 2009. **122**(Pt 10): p. 1616-25.

455. Tornavaca, O., et al., *ZO-1 controls endothelial adherens junctions, cell-cell tension, angiogenesis, and barrier formation.* J Cell Biol, 2015. **208**(6): p. 821-38.

456. Eckhard, U., et al., *Active site specificity profiling of the matrix metalloproteinase family: Proteomic identification of 4300 cleavage sites by nine MMPs explored with structural and synthetic peptide cleavage analyses.* Matrix Biol, 2016. **49**: p. 37-60.

457. Pollock, J.S., et al., *Purification and characterization of particulate endothelium-derived relaxing factor synthase from cultured and native bovine aortic endothelial cells.* Proc Natl Acad Sci U S A, 1991. **88**(23): p. 10480-4.

458. Posch, K., K. Schmidt, and W.F. Graier, *Selective stimulation of L-arginine uptake contributes to shear stress-induced formation of nitric oxide.* Life Sci, 1999. **64**(8): p. 663-70.

459. Hardy, T.A. and J.M. May, *Coordinate regulation of L-arginine uptake and nitric oxide synthase activity in cultured endothelial cells.* Free Radic Biol Med, 2002. **32**(2): p. 122-31.

460. Dutta, S. and P. Sengupta, *Men and mice: Relating their ages.* Life Sci, 2016. **152**: p. 244-8.

461. Gershenwald, J.E., et al., *Melanoma staging: Evidence-based changes in the American Joint Committee on Cancer eighth edition cancer staging manual.* CA Cancer J Clin, 2017. **67**(6): p. 472-492.

462. Maciel, L.L.F., et al., *In Vitro and In Vivo Relevant Antineoplastic Activity of Platinum(II) Complexes toward Triple-Negative MDA-MB-231 Breast Cancer Cell Line.* Pharmaceutics, 2022. **14**(10).

463. Barry, M.A., C.A. Behnke, and A. Eastman, *Activation of programmed cell death (apoptosis) by cisplatin, other anticancer drugs, toxins and hyperthermia.* Biochem Pharmacol, 1990. **40**(10): p. 2353-62.

464. Del Bello, B., et al., *Cleavage of Bcl-2 in oxidant- and cisplatin-induced apoptosis of human melanoma cells.* Oncogene, 2001. **20**(33): p. 4591-5.

465. Dahlin, J.S. and J. Hallgren, *Mast cell progenitors: origin, development and migration to tissues.* Mol Immunol, 2015. **63**(1): p. 9-17.

466. Austyn, J.M. and S. Gordon, *F4/80, a monoclonal antibody directed specifically against the mouse macrophage.* Eur J Immunol, 1981. **11**(10): p. 805-15.

467. Kuroda, K., R. Tsukifuji, and H. Shinkai, *Increased expression of heat-shock protein 47 is associated with overproduction of type I procollagen in systemic sclerosis skin fibroblasts.* J Invest Dermatol, 1998. **111**(6): p. 1023-8.

468. Junqueira, L.C., G. Bignolas, and R.R. Brentani, *Picrosirius staining plus polarization microscopy, a specific method for collagen detection in tissue sections.* Histochem J, 1979. **11**(4): p. 447-55.

469. Junquiera, L.C., L.C. Junqueira, and R.R. Brentani, *A simple and sensitive method for the quantitative estimation of collagen.* Anal Biochem, 1979. **94**(1): p. 96-9.

470. Mulholland, B., S.J. Tuft, and P.T. Khaw, *Matrix metalloproteinase distribution during early corneal wound healing.* Eye (Lond), 2005. **19**(5): p. 584-8.

471. Alhajj, M. and A. Goyal, *Physiology, Granulation Tissue*, in *StatPearls*. 2022, StatPearls Publishing Copyright © 2022, StatPearls Publishing LLC.: Treasure Island (FL).

472. Singer, A.J. and R.A. Clark, *Cutaneous wound healing.* N Engl J Med, 1999. **341**(10): p. 738-46.

473. Hunt, T.K., *The physiology of wound healing.* Ann Emerg Med, 1988. **17**(12): p. 1265-73.

474. Hinz, B. and D. Lagares, *Evasion of apoptosis by myofibroblasts: a hallmark of fibrotic diseases.* Nat Rev Rheumatol, 2020. **16**(1): p. 11-31.

475. Xing, Z., et al., *Overexpression of granulocyte-macrophage colony-stimulating factor induces pulmonary granulation tissue formation and fibrosis by induction of transforming growth factor-beta 1 and myofibroblast accumulation.* Am J Pathol, 1997. **150**(1): p. 59-66.

476. Oh, S.J., et al., *Platelet-derived growth factor-B induces transformation of fibrocytes into spindle-shaped myofibroblasts in vivo.* Histochem Cell Biol, 1998. **109**(4): p. 349-57.

477. Perl, A.K. and E. Gale, *FGF signaling is required for myofibroblast differentiation during alveolar regeneration.* Am J Physiol Lung Cell Mol Physiol, 2009. **297**(2): p. L299-308.

478. Khalil, N., et al., *Macrophage production of transforming growth factor beta and fibroblast collagen synthesis in chronic pulmonary inflammation.* J Exp Med, 1989. **170**(3): p. 727-37.

479. Rønnov-Jessen, L. and O.W. Petersen, *Induction of alpha-smooth muscle actin by transforming growth factor-beta 1 in quiescent human breast gland fibroblasts. Implications for myofibroblast generation in breast neoplasia.* Lab Invest, 1993. **68**(6): p. 696-707.

480. Goffin, J.M., et al., *Focal adhesion size controls tension-dependent recruitment of alpha-smooth muscle actin to stress fibers.* J Cell Biol, 2006. **172**(2): p. 259-68.

481. Dugina, V., et al., *Focal adhesion features during myofibroblastic differentiation are controlled by intracellular and extracellular factors.* J Cell Sci, 2001. **114**(Pt 18): p. 3285-96.

482. Eckes, B., et al., *Cell-Populated Collagen Lattice Models.* Methods Mol Biol, 2017. **1627**: p. 223-233.

483. Nakao, A., et al., *TGF-beta receptor-mediated signalling through Smad2, Smad3 and Smad4.* Embo j, 1997. **16**(17): p. 5353-62.

484. Nakao, A., et al., *Identification of Smad2, a human Mad-related protein in the transforming growth factor beta signaling pathway.* J Biol Chem, 1997. **272**(5): p. 2896-900.

485. Massagué, J., *TGFβ signalling in context.* Nat Rev Mol Cell Biol, 2012. **13**(10): p. 616-30.

486. Gustafsson, E., et al., *Tie-1-directed expression of Cre recombinase in endothelial cells of embryoid bodies and transgenic mice.* J Cell Sci, 2001. **114**(Pt 4): p. 671-6.

487. Zigrino, P., et al., *Stromal expression of MMP-13 is required for melanoma invasion and metastasis.* J Invest Dermatol, 2009. **129**(11): p. 2686-93.

488. Lafleur, M.A., et al., *Endothelial tubulogenesis within fibrin gels specifically requires the activity of membrane-type-matrix metalloproteinases (MT-MMPs).* J Cell Sci, 2002. **115**(Pt 17): p. 3427-38.

489. Kurschat, P., et al., *Tissue inhibitor of matrix metalloproteinase-2 regulates matrix metalloproteinase-2 activation by modulation of membrane-type 1 matrix metalloproteinase activity in high and low invasive melanoma cell lines.* J Biol Chem, 1999. **274**(30): p. 21056-62.

490. Hofmann, U.B., et al., *Expression of integrin alpha(v)beta(3) correlates with activation of membrane-type matrix metalloproteinase-1 (MT1-MMP) and matrix metalloproteinase-2 (MMP-2) in human melanoma cells in vitro and in vivo.* Int J Cancer, 2000. **87**(1): p. 12-9.

491. Filippov, S., et al., *MT1-matrix metalloproteinase directs arterial wall invasion and neointima formation by vascular smooth muscle cells.* J Exp Med, 2005. **202**(5): p. 663-71.

492. Warren, B., *The Vascular Morphology of Tumors.* 1st ed. 1979, CRC Press.

493. Milosevic, M.F., A.W. Fyles, and R.P. Hill, *The relationship between elevated interstitial fluid pressure and blood flow in tumors: a bioengineering analysis.* Int J Radiat Oncol Biol Phys, 1999. **43**(5): p. 1111-23.

494. Chaplin, D.J., P.L. Olive, and R.E. Durand, *Intermittent blood flow in a murine tumor: radiobiological effects.* Cancer Res, 1987. **47**(2): p. 597-601.

495. Kimura, H., et al., *Fluctuations in red cell flux in tumor microvessels can lead to transient hypoxia and reoxygenation in tumor parenchyma.* Cancer Res, 1996. **56**(23): p. 5522-8.

496. Semenza, G.L. and G.L. Wang, *A nuclear factor induced by hypoxia via de novo protein synthesis binds to the human erythropoietin gene enhancer at a site required for transcriptional activation.* Mol Cell Biol, 1992. **12**(12): p. 5447-54.

497. Liu, Y., et al., *Hypoxia regulates vascular endothelial growth factor gene expression in endothelial cells. Identification of a 5' enhancer.* Circ Res, 1995. **77**(3): p. 638-43.

498. Forsythe, J.A., et al., *Activation of vascular endothelial growth factor gene transcription by hypoxia-inducible factor 1.* Mol Cell Biol, 1996. **16**(9): p. 4604-13.

499. Levy, A.P., et al., *Transcriptional regulation of the rat vascular endothelial growth factor gene by hypoxia.* J Biol Chem, 1995. **270**(22): p. 13333-40.

500. Calvani, M., et al., *Hypoxic induction of an HIF-1alpha-dependent bFGF autocrine loop drives angiogenesis in human endothelial cells.* Blood, 2006. **107**(7): p. 2705-12.

501. Kuwabara, K., et al., *Hypoxia-mediated induction of acidic/basic fibroblast growth factor and platelet-derived growth factor in mononuclear phagocytes stimulates growth of hypoxic endothelial cells.* Proc Natl Acad Sci U S A, 1995. **92**(10): p. 4606-10.

502. Joosse, S.A., T.M. Gorges, and K. Pantel, *Biology, detection, and clinical implications of circulating tumor cells.* EMBO Mol Med, 2015. **7**(1): p. 1-11.

503. Weis, S., et al., *Endothelial barrier disruption by VEGF-mediated Src activity potentiates tumor cell extravasation and metastasis.* J Cell Biol, 2004. **167**(2): p. 223-9.

504. Chen, J., et al., *Akt1 regulates pathological angiogenesis, vascular maturation and permeability in vivo.* Nat Med, 2005. **11**(11): p. 1188-96.

505. Maes, H., et al., *Tumor vessel normalization by chloroquine independent of autophagy.* Cancer Cell, 2014. **26**(2): p. 190-206.

506. He, B., et al., *Remodeling of Metastatic Vasculature Reduces Lung Colonization and Sensitizes Overt Metastases to Immunotherapy.* Cell Rep, 2020. **30**(3): p. 714-724.e5.

507. Bjarnegård, M., et al., *Endothelium-specific ablation of PDGFB leads to pericyte loss and glomerular, cardiac and placental abnormalities.* Development, 2004. **131**(8): p. 1847-57.

508. Augustin, H.G., et al., *Control of vascular morphogenesis and homeostasis through the angiopoietin-Tie system.* Nat Rev Mol Cell Biol, 2009. **10**(3): p. 165-77.

509. Goumans, M.J., et al., *Balancing the activation state of the endothelium via two distinct TGF-beta type I receptors.* Embo j, 2002. **21**(7): p. 1743-53.

510. Cheifetz, S., et al., *Endoglin is a component of the transforming growth factor-beta receptor system in human endothelial cells.* J Biol Chem, 1992. **267**(27): p. 19027-30.

511. Lebrin, F., et al., *TGF-beta receptor function in the endothelium.* Cardiovasc Res, 2005. **65**(3): p. 599-608.

512. Alfranca, A., et al., *PGE2 induces angiogenesis via MT1-MMP-mediated activation of the TGFbeta/Alk5 signaling pathway.* Blood, 2008. **112**(4): p. 1120-8.

513. Onimaru, M., et al., *An autocrine linkage between matrix metalloproteinase-14 and Tie-2 via ectodomain shedding modulates angiopoietin-1-dependent function in endothelial cells.* Arterioscler Thromb Vasc Biol, 2010. **30**(4): p. 818-26.

514. Thamm, K., et al., *Molecular Regulation of Acute Tie2 Suppression in Sepsis.* Crit Care Med, 2018. **46**(9): p. e928-e936.

515. Idowu, T.O., et al., *Identification of specific Tie2 cleavage sites and therapeutic modulation in experimental sepsis.* Elife, 2020. **9**.

516. Sounni, N.E., et al., *Stromal regulation of vessel stability by MMP14 and TGFbeta.* Dis Model Mech, 2010. **3**(5-6): p. 317-32.

517. Schultz, G.S., et al., *Treatment of alkali-injured rabbit corneas with a synthetic inhibitor of matrix metalloproteinases.* Invest Ophthalmol Vis Sci, 1992. **33**(12): p. 3325-31.

518. Gougos, A. and M. Letarte, *Primary structure of endoglin, an RGD-containing glycoprotein of human endothelial cells.* J Biol Chem, 1990. **265**(15): p. 8361-4.

519. Gougos, A. and M. Letarte, *Identification of a human endothelial cell antigen with monoclonal antibody 44G4 produced against a pre-B leukemic cell line.* J Immunol, 1988. **141**(6): p. 1925-33.

520. Hawinkels, L.J., et al., *Matrix metalloproteinase-14 (MT1-MMP)-mediated endoglin shedding inhibits tumor angiogenesis.* Cancer Res, 2010. **70**(10): p. 4141-50.

521. Kaitu'u-Lino, T.J., et al., *MMP-14 is expressed in preeclamptic placentas and mediates release of soluble endoglin.* Am J Pathol, 2012. **180**(3): p. 888-894.

522. Stratman, A.N. and G.E. Davis, *Endothelial cell-pericyte interactions stimulate basement membrane matrix assembly: influence on vascular tube remodeling, maturation, and stabilization.* Microsc Microanal, 2012. **18**(1): p. 68-80.

523. Davis, G.E. and D.R. Senger, *Endothelial extracellular matrix: biosynthesis, remodeling, and functions during vascular morphogenesis and neovessel stabilization.* Circ Res, 2005. **97**(11): p. 1093-107.

524. Jeon, H., et al., *Pericytes from microvessel fragment produce type IV collagen and multiple laminin isoforms.* Biosci Biotechnol Biochem, 1996. **60**(5): p. 856-61.

525. Mandarino, L.J., et al., *Regulation of fibronectin and laminin synthesis by retinal capillary endothelial cells and pericytes in vitro.* Exp Eye Res, 1993. **57**(5): p. 609-21.

526. Itoh, T., et al., *Experimental metastasis is suppressed in MMP-9-deficient mice.* Clin Exp Metastasis, 1999. **17**(2): p. 177-81.

527. Hotary, K., et al., *A cancer cell metalloprotease triad regulates the basement membrane transmigration program.* Genes Dev, 2006. **20**(19): p. 2673-86.

528. Herren, B., et al., *Cleavage of beta-catenin and plakoglobin and shedding of VE-cadherin during endothelial apoptosis: evidence for a role for caspases and metalloproteinases.* Mol Biol Cell, 1998. **9**(6): p. 1589-601.

529. Huang, M., et al., *c-Met-mediated endothelial plasticity drives aberrant vascularization and chemoresistance in glioblastoma.* J Clin Invest, 2016. **126**(5): p. 1801-14.

530. Shimizu-Hirota, R., et al., *MT1-MMP regulates the PI3Kδ·Mi-2/NuRD-dependent control of macrophage immune function.* Genes Dev, 2012. **26**(4): p. 395-413.

531. Burri, P.H., R. Hlushchuk, and V. Djonov, *Intussusceptive angiogenesis: its emergence, its characteristics, and its significance.* Dev Dyn, 2004. **231**(3): p. 474-88.

532. Morbidelli, L., et al., *Nitric oxide mediates mitogenic effect of VEGF on coronary venular endothelium.* Am J Physiol, 1996. **270**(1 Pt 2): p. H411-5.

533. Noiri, E., et al., *Podokinesis in endothelial cell migration: role of nitric oxide.* Am J Physiol, 1998. **274**(1): p. C236-44.

534. Murohara, T., et al., *Nitric oxide synthase modulates angiogenesis in response to tissue ischemia.* J Clin Invest, 1998. **101**(11): p. 2567-78.

535. Murohara, T., et al., *Vascular endothelial growth factor/vascular permeability factor enhances vascular permeability via nitric oxide and prostacyclin.* Circulation, 1998. **97**(1): p. 99-107.

536. Fukumura, D., S. Kashiwagi, and R.K. Jain, *The role of nitric oxide in tumour progression.* Nat Rev Cancer, 2006. **6**(7): p. 521-34.

537. van der Zee, R., et al., *Vascular endothelial growth factor/vascular permeability factor augments nitric oxide release from quiescent rabbit and human vascular endothelium.* Circulation, 1997. **95**(4): p. 1030-7.

538. Hood, J.D., et al., *VEGF upregulates ecNOS message, protein, and NO production in human endothelial cells.* Am J Physiol, 1998. **274**(3): p. H1054-8.

539. Han, K.Y., J.H. Chang, and D.T. Azar, *MMP14-Containing Exosomes Cleave VEGFR1 and Promote VEGFA-Induced Migration and Proliferation of Vascular Endothelial Cells.* Invest Ophthalmol Vis Sci, 2019. **60**(6): p. 2321-2329.

540. Ip, Y.C., S.T. Cheung, and S.T. Fan, *Atypical localization of membrane type 1-matrix metalloproteinase in the nucleus is associated with aggressive features of hepatocellular carcinoma.* Mol Carcinog, 2007. **46**(3): p. 225-30.

541. Isenberg, J.S., et al., *Thrombospondin-1 and CD47 limit cell and tissue survival of radiation injury.* Am J Pathol, 2008. **173**(4): p. 1100-12.

542. Isenberg, J.S., D.D. Roberts, and W.A. Frazier, *CD47: a new target in cardiovascular therapy.* Arterioscler Thromb Vasc Biol, 2008. **28**(4): p. 615-21.

543. Kubes, P., I. Kurose, and D.N. Granger, *NO donors prevent integrin-induced leukocyte adhesion but not P-selectin-dependent rolling in postischemic venules.* Am J Physiol, 1994. **267**(3 Pt 2): p. H931-7.

544. De Caterina, R., et al., *Nitric oxide decreases cytokine-induced endothelial activation. Nitric oxide selectively reduces endothelial expression of adhesion molecules and proinflammatory cytokines.* J Clin Invest, 1995. **96**(1): p. 60-8.

545. Tsao, P.S., et al., *Fluid flow inhibits endothelial adhesiveness. Nitric oxide and transcriptional regulation of VCAM-1.* Circulation, 1996. **94**(7): p. 1682-9.

546. Khan, B.V., et al., *Nitric oxide regulates vascular cell adhesion molecule 1 gene expression and redox-sensitive transcriptional events in human vascular endothelial cells.* Proc Natl Acad Sci U S A, 1996. **93**(17): p. 9114-9.

547. Genís, L., et al., *Functional interplay between endothelial nitric oxide synthase and membrane type 1 matrix metalloproteinase in migrating endothelial cells.* Blood, 2007. **110**(8): p. 2916-23.

548. Liu, W.M. and C.W. Schmid, *Proposed roles for DNA methylation in Alu transcriptional repression and mutational inactivation.* Nucleic Acids Res, 1993. **21**(6): p. 1351-9.

549. Liu, W.M., et al., *Alu transcripts: cytoplasmic localisation and regulation by DNA methylation.* Nucleic Acids Res, 1994. **22**(6): p. 1087-95.

550. Bird, A.P., *DNA methylation and the frequency of CpG in animal DNA.* Nucleic Acids Res, 1980. **8**(7): p. 1499-504.

551. Prandini, M.H., et al., *The human VE-cadherin promoter is subjected to organ-specific regulation and is activated in tumour angiogenesis.* Oncogene, 2005. **24**(18): p. 2992-3001.

552. Call, G.B. and M.W. Wolfe, *Species differences in GnRH activation of the LHbeta promoter: role of Egr1 and Sp1.* Mol Cell Endocrinol, 2002. **189**(1-2): p. 85-96.

553. Palmer, G., et al., *Species-specific mechanisms control the activity of the Pit1/PIT1 phosphate transporter gene promoter in mouse and human.* Gene, 2001. **279**(1): p. 49-62.

554. Dasari, S. and P.B. Tchounwou, *Cisplatin in cancer therapy: molecular mechanisms of action.* Eur J Pharmacol, 2014. **740**: p. 364-78.

555. Sharpe, H.B., E.O. Field, and K. Hellmann, *Mode of action of the cytostatic agent "ICRF 159".* Nature, 1970. **226**(5245): p. 524-6.

556. Le Serve, A.W. and K. Hellmann, *Metastases and the normalization of tumour blood vessels by ICRF 159: a new type of drug action.* Br Med J, 1972. **1**(5800): p. 597-601.

557. Kieda, C., et al., *Stable tumor vessel normalization with pO$_2$ increase and endothelial PTEN activation by inositol trispyrophosphate brings novel tumor treatment.* J Mol Med (Berl), 2013. **91**(7): p. 883-99.

558. Calcinotto, A., et al., *Targeting TNF-α to neoangiogenic vessels enhances lymphocyte infiltration in tumors and increases the therapeutic potential of immunotherapy.* J Immunol, 2012. **188**(6): p. 2687-94.

559. Zhao, Y., et al., *Targeting Vascular Endothelial-Cadherin in Tumor-Associated Blood Vessels Promotes T-cell-Mediated Immunotherapy.* Cancer Res, 2017. **77**(16): p. 4434-4447.

560. Ager, E.I., et al., *Blockade of MMP14 activity in murine breast carcinomas: implications for macrophages, vessels, and radiotherapy.* J Natl Cancer Inst, 2015. **107**(4).

561. Mathew-Steiner, S.S., S. Roy, and C.K. Sen, *Collagen in Wound Healing.* Bioengineering (Basel), 2021. **8**(5).

562. Penn, J.W., A.O. Grobbelaar, and K.J. Rolfe, *The role of the TGF-β family in wound healing, burns and scarring: a review.* Int J Burns Trauma, 2012. **2**(1): p. 18-28.

563. Sounni, N.E., et al., *Up-regulation of vascular endothelial growth factor-A by active membrane-type 1 matrix metalloproteinase through activation of Src-tyrosine kinases.* J Biol Chem, 2004. **279**(14): p. 13564-74.

564. Saeb-Parsy, K., et al., *MT1-MMP regulates urothelial cell invasion via transcriptional regulation of Dickkopf-3.* Br J Cancer, 2008. **99**(4): p. 663-9.

565. Chase, A.J., et al., *Role of nuclear factor-kappa B activation in metalloproteinase-1, -3, and -9 secretion by human macrophages in vitro and rabbit foam cells produced in vivo.* Arterioscler Thromb Vasc Biol, 2002. **22**(5): p. 765-71.

566. Cutler, S.J., et al., *Novel STAT binding elements mediate IL-6 regulation of MMP-1 and MMP-3.* Sci Rep, 2017. **7**(1): p. 8526.

567. Sternlicht, M.D., et al., *The stromal proteinase MMP3/stromelysin-1 promotes mammary carcinogenesis.* Cell, 1999. **98**(2): p. 137-46.

568. Ha, H.Y., et al., *Overexpression of membrane-type matrix metalloproteinase-1 gene induces mammary gland abnormalities and adenocarcinoma in transgenic mice.* Cancer Res, 2001. **61**(3): p. 984-90.

569. Toriseva, M. and V.M. Kähäri, *Proteinases in cutaneous wound healing.* Cell Mol Life Sci, 2009. **66**(2): p. 203-24.

570. Ibrahim, M.M., et al., *Myofibroblasts contribute to but are not necessary for wound contraction.* Lab Invest, 2015. **95**(12): p. 1429-38.

571. McAndrews, K.M., et al., *Dermal αSMA(+) myofibroblasts orchestrate skin wound repair via β1 integrin and independent of type I collagen production.* Embo j, 2022. **41**(7): p. e109470.

572. Tassone, E., C. Valacca, and P. Mignatti, *Membrane-Type 1 Matrix Metalloproteinase Downregulates Fibroblast Growth Factor-2 Binding to the Cell Surface and Intracellular Signaling.* J Cell Physiol, 2015. **230**(2): p. 366-77.

573. Cichon, M.A. and D.C. Radisky, *Extracellular matrix as a contextual determinant of transforming growth factor-β signaling in epithelial-mesenchymal transition and in cancer.* Cell Adh Migr, 2014. **8**(6): p. 588-94.

574. Hao, H., et al., *Phenotypic modulation of intima and media smooth muscle cells in fatal cases of coronary artery lesion.* Arterioscler Thromb Vasc Biol, 2006. **26**(2): p. 326-32.

575. Stone, R.C., et al., *Epithelial-mesenchymal transition in tissue repair and fibrosis.* Cell Tissue Res, 2016. **365**(3): p. 495-506.

576. Lochter, A., et al., *Matrix metalloproteinase stromelysin-1 triggers a cascade of molecular alterations that leads to stable epithelial-to-mesenchymal conversion and a premalignant phenotype in mammary epithelial cells.* J Cell Biol, 1997. **139**(7): p. 1861-72.

577. Kuwahara, M., et al., *E-cadherin expression in wound healing of mouse skin.* J Cutan Pathol, 2001. **28**(4): p. 191-9.

578. Zhao, Y., et al., *Matrix metalloproteinase 9 induces endothelial-mesenchymal transition via Notch activation in human kidney glomerular endothelial cells.* BMC Cell Biol, 2016. **17**(1): p. 21.

579. Zeisberg, M. and R. Kalluri, *The role of epithelial-to-mesenchymal transition in renal fibrosis.* J Mol Med (Berl), 2004. **82**(3): p. 175-81.

580. Si-Tayeb, K., et al., *Matrix metalloproteinase 3 is present in the cell nucleus and is involved in apoptosis.* Am J Pathol, 2006. **169**(4): p. 1390-401.

581. Radisky, D.C., et al., *Rac1b and reactive oxygen species mediate MMP-3-induced EMT and genomic instability.* Nature, 2005. **436**(7047): p. 123-7.

582. Maquoi, E., et al., *MT1-MMP protects breast carcinoma cells against type I collagen-induced apoptosis.* Oncogene, 2012. **31**(4): p. 480-93.

583. Albrechtsen, R., et al., *ADAM12 redistributes and activates MMP-14, resulting in gelatin degradation, reduced apoptosis and increased tumor growth.* J Cell Sci, 2013. **126**(Pt 20): p. 4707-20.

584. Shu, J., et al., *Matrix metalloproteinase 3 regulates angiotensin II-induced myocardial fibrosis cell viability, migration and apoptosis.* Mol Med Rep, 2021. **23**(2).

585. Ramesh, S., G.M. Wildey, and P.H. Howe, *Transforming growth factor beta (TGFbeta)-induced apoptosis: the rise & fall of Bim.* Cell Cycle, 2009. **8**(1): p. 11-7.

586. Boström, H., et al., *PDGF-A signaling is a critical event in lung alveolar myofibroblast development and alveogenesis.* Cell, 1996. **85**(6): p. 863-73.

587. Zhang, H.Y. and S.H. Phan, *Inhibition of myofibroblast apoptosis by transforming growth factor beta(1).* Am J Respir Cell Mol Biol, 1999. **21**(6): p. 658-65.

588. Kulasekaran, P., et al., *Endothelin-1 and transforming growth factor-beta1 independently induce fibroblast resistance to apoptosis via AKT activation.* Am J Respir Cell Mol Biol, 2009. **41**(4): p. 484-93.

589. Denton, C.P., C.M. Black, and D.J. Abraham, *Mechanisms and consequences of fibrosis in systemic sclerosis.* Nat Clin Pract Rheumatol, 2006. **2**(3): p. 134-44.

590. Zeisberg, M. and R. Kalluri, *Cellular mechanisms of tissue fibrosis. 1. Common and organ-specific mechanisms associated with tissue fibrosis.* Am J Physiol Cell Physiol, 2013. **304**(3): p. C216-25.

591. Pakshir, P., et al., *The myofibroblast at a glance.* J Cell Sci, 2020. **133**(13).

Erklärung zur Dissertation
gemäß der Promotionsordnung vom 12. März 2020

Diese Erklärung muss in der Dissertation enthalten sein.
(*This version must be included in the doctoral thesis*)

„Hiermit versichere ich an Eides statt, dass ich die vorliegende Dissertation selbstständig und ohne die Benutzung anderer als der angegebenen Hilfsmittel und Literatur angefertigt habe. Alle Stellen, die wörtlich oder sinngemäß aus veröffentlichten und nicht veröffentlichten Werken dem Wortlaut oder dem Sinn nach entnommen wurden, sind als solche kenntlich gemacht. Ich versichere an Eides statt, dass diese Dissertation noch keiner anderen Fakultät oder Universität zur Prüfung vorgelegen hat; dass sie - abgesehen von unten angegebenen Teilpublikationen und eingebundenen Artikeln und Manuskripten - noch nicht veröffentlicht worden ist sowie, dass ich eine Veröffentlichung der Dissertation vor Abschluss der Promotion nicht ohne Genehmigung des Promotionsausschusses vornehmen werde. Die Bestimmungen dieser Ordnung sind mir bekannt. Darüber hinaus erkläre ich hiermit, dass ich die Ordnung zur Sicherung guter wissenschaftlicher Praxis und zum Umgang mit wissenschaftlichem Fehlverhalten der Universität zu Köln gelesen und sie bei der Durchführung der Dissertation zugrundeliegenden Arbeiten und der schriftlich verfassten Dissertation beachtet habe und verpflichte mich hiermit, die dort genannten Vorgaben bei allen wissenschaftlichen Tätigkeiten zu beachten und umzusetzen. Ich versichere, dass die eingereichte elektronische Fassung der eingereichten Druckfassung vollständig entspricht."

Teilpublikationen:

1. Kümper M, Zamek J, Steinkamp J, Pach E, Hauch C, Zigrino P; Role of MMP's and fibroblast -MMP14 in skin homeostasis and repair. Eur J Cell Biol., 2022, doi: 10.1016/j.ejcb.2022.151276.

2. Kümper M, Hessenthaler S, Zamek J, Niland S, Pach E, Hauch C, Zigrino P; Loss of endothelial cell matrix metalloproteinase 14 reduces melanoma growth and metastasis by increasing tumor vessel stability. J. Invest Dermatol. 2022 July ; 142(7)

Datum, Name und Unterschrift

2.12.2022   Maike Kümper

M. Kü

Erklärung zum Gesuch um Zulassung zur Promotion
gemäß der Promotionsordnung vom 12. März 2020

1.   Zugänglichkeit von Daten und Materialien

Die Dissertation beinhaltet die Gewinnung von Primärdaten oder die Analyse solcher Daten oder die Reproduzierbarkeit der in der Dissertation dargestellten Ergebnisse setzt die Verfügbarkeit von Datenanalysen, Versuchsprotokollen oder Probenmaterial voraus.

☐   Trifft nicht zu

☒   Trifft zu.
    In der Dissertation ist dargelegt wie diese Daten und Materialien gesichert und zugänglich sind (entsprechend den Vorgaben des Fachgebiets beziehungsweise der Betreuerin oder des Betreuers).

2.   Frühere Promotionsverfahren

    Ich habe bereits einen Doktortitel erworben oder ehrenhalber verliehen bekommen.
Oder: Für mich ist an einer anderen Fakultät oder Universität ein Promotionsverfahren eröffnet worden, aber noch nicht abgeschlossen.
Oder: Ich bin in einem Promotionsverfahren gescheitert.

☒   Trifft nicht zu

☐   Zutreffend
    Erläuterung:

3.   Straftat

    Ich bin <u>nicht</u> zu einer vorsätzlichen Straftat verurteilt worden, bei deren Vorbereitung oder Begehung der Status einer Doktorandin oder eines Doktoranden missbraucht wurde.

Ich versichere, alle Angaben wahrheitsgemäß gemacht zu haben.

2.12.2022   Maike Kümper   M. Kü

Datum   Name   Unterschrift

Curriculum Vitae

Personal Information

Name: Maike Kümper
Date of Birth: 22. September 1991
Place of Birth: Düsseldorf, Germany
Address: Weyertal 4, 50937 Köln

E-Mail: maike_1991@gmx.net

Education

Since 2018	Universität zu Köln, Doctoral Studies in Biochemistry in the Graduate School for Biological Sciences
2014-2017	Ruhr-Universität Bochum; Masterstudium in Biochemie Degree: M. Sc. Biochemistry (1,5) Title of Master Thesis: 'New cell culture models to identify new PrPC interacting proteins involved in neurotoxic and cell protective signaling'
2011-2014	Ruhr-Universität Bochum; Bachelorstudium in Biochemie Degree: B. Sc. Biochemistry (2,1) Title of Bachelor Thesis: 'Topographische Organisation der indirekten tecto-tectalen Projektion'
2002-2011	Cecilien-Gymnasium, Düsseldorf Degree: Abitur (1,4)

Work Experience

Since 10/2022	Global MSAT Specialist at Miltenyi Biotec Development and performance of customized trainings on Miltenyi Biotec Clinical instruments and protocols
08/2017-04/2022	Research Assistant at Uniklinik Köln - Organization and conduction of *in vivo* and *in vitro* experiments - Data analysis - Writing of scientific publications and proposals

Certificates

2021	Seminar Workshop "Good Scientific Conduct: Biases in Science" with Prof. Niels Gehring at the Universität zu Köln
2015	FELASA B certificate for animal handling

Studies abroad and Fellowships

2015-2016   Year abroad at the University of North Carolina in Chapel Hill, NC, USA; Graduate Program of the School of Arts and Science/Medical School, Department of Biochemistry and Neuroscience; Professor Maness

'Influence of NCAM point mutations on the Binding with Epha3'

2015-2016   DAAD Scholarship for Graduate and PhD students in North Amerika, scholarship provided by the University of North Carolina, USA; Department Cell Biology and Physiology at University of North Carolina in Chapel Hill, NC, USA; Professor Cyr

'Identification of intermediate steps of the ERQC autophagy degradation pathway of CFTR'

Publications

Kümper M, Steinkamp J, Zigrino P. Metalloproteinases in dermal homeostasis. Am J Physiol Cell Physiol. 2022 Oct 1;323(4):C1290-C1303. doi: 10.1152/ajpcell.00450.2021. Epub 2022 Sep 12. PMID: 36094433.

Kümper M, Zamek J, Steinkamp J, Pach E, Mauch C, Zigrino P. Role of MMP3 and fibroblast-MMP14 in skin homeostasis and repair. Eur J Cell Biol. 2022 Sep 23;101(4):151276. doi: 10.1016/j.ejcb.2022.151276. Epub ahead of print. PMID: 36162272.

Kümper M, Hessenthaler S, Zamek J, Niland S, Pach E, Mauch C, Zigrino P. Loss of Endothelial Cell Matrix Metalloproteinase 14 Reduces Melanoma Growth and Metastasis by Increasing Tumor Vessel Stability. J Invest Dermatol. 2022 Jul;142(7):1923-1933.e5. doi: 10.1016/j.jid.2021.12.016. Epub 2021 Dec 27. PMID: 34968503.

Pach E, Kümper M, Fromme JE, Zamek J, Metzen F, Koch M, Mauch C, Zigrino P. Extracellular Matrix Remodeling by Fibroblast-MMP14 Regulates Melanoma Growth. Int J Mol Sci. 2021 Nov 12;22(22):12276. doi: 10.3390/ijms222212276. PMID: 34830157; PMCID: PMC8625044.

Pach E, Brinckmann J, Rübsam M, Kümper M, Mauch C, Zigrino P. Fibroblast MMP14-Dependent Collagen Processing Is Necessary for Melanoma Growth. Cancers (Basel). 2021 Apr 20;13(8):1984. doi: 10.3390/cancers13081984. PMID: 33924099; PMCID: PMC8074311.

Sullivan CS, Kümper M, Temple BS, Maness PF. The Neural Cell Adhesion Molecule (NCAM) Promotes Clustering and Activation of EphA3 Receptors in GABAergic Interneurons to Induce Ras Homolog Gene Family, Member A (RhoA)/Rho-associated protein kinase (ROCK)-mediated Growth Cone Collapse. J Biol Chem. 2016 Dec 16;291(51):26262-26272. doi: 10.1074/jbc.M116.760017. Epub 2016 Nov 1. PMID: 27803162; PMCID: PMC5159490.

Oral Presentations at Conferences

09/2021 Oral presentation at the 50th Annual ESDR Meeting (virtual) titled 'Loss of endothelial cell MMP14 reduces melanoma growth and metastasis by increasing tumor vessel stability'

Poster Presentation at Conferences

European Society for Dermatological Research 2021
252, 'Loss of endothelial cell MMP14 reduces melanoma growth and metastasis by increasing tumor vessel stability'
M Kümper, S Hessenthaler, J Zamek, S Niland, E Pach, C Mauch and P Zigrino

Joint Meeting of the French and German Societies for Matrix Biology 2021 (virtual):
37, 'Role of MMP3 and MMP14 expression in fibroblast in skin repair'
Maike Kümper, Jan Zamek, Elke Pach, Yinhui Lu, Karl E. Kadler, Cornelia Mauch, Paola Zigrino

Annual Meeting of the German Society for Matrix Biology 2019
19, Endothelial cell-derived MMP-14 regulates vessel
stability and melanoma growth
Maike Kümper, Sabrina Neumann, Cornelia Mauch, Paola Zigrino

Matrix Biology Europe 2018 (MBE2018; Manchester, UK):
P94, 'Endothelial cell-derived MMP-14 is dispensable for skin formation and repair'
Sabrina Neumann, Maike Kümper, Cornelia Mauch, Paola Zigrino

Ernst Klenk Symposium 2017 (Cologne):
B-24, 'Endothelial cell-derived MMP-14 is dispensable for skin formation and repair'; S. Neumann / M. Kümper / C. Mauch / P. Zigrino

Acknowledgement